DELIVERY SYSTEMS TO ENHANCE NEURAL REGENERATION IN THE CENTRAL NERVOUS SYSTEM

TAISA REGINA STUMPF DA SILVA

Thesis submitted to the University of Ottawa

in partial fulfillment of the requirements for

Doctorate in Philosophy in Chemical Engineering

Department of Chemical and Biological Engineering

Faculty of Engineering

University of Ottawa

DELIVERY SYSTEMS TO ENHANCE NEURAL REGENERATION IN THE CENTRAL NERVOUS SYSTEM

Taisa Regina Stumpf da Silva, 2019

Department of Chemical and Biological Engineering, University of Ottawa

ABSTRACT

The central nervous system (CNS) is susceptible to several disorders that can affect the structure or function of the brain or spinal cord, such as stroke and spinal cord injury (SCI). CNS disorders are complex, frequently causing failure of cognitive, motor and sensory functions. Unfortunately, there are only a few care alternatives for patients with CNS disorders, due to the limited capacity of the CNS to spontaneously regenerate; what expresses the need to develop innovative solutions, such as scaffolds that also could act as drug delivery systems to promote tissue and functional repairs in the CNS. To achieve this goal, three main projects were developed in this thesis. In the first project, a novel drug releasing duraplasty that can be applied as part of decompressive craniectomy (DC) was designed and tested. While DC can significantly reduce the risk of death, this procedure does not reverse the stroke damage. Thus, biosynthesized cellulose (BC) was used to produce a new duraplasty loaded with growth factors. The *in vivo* animal studies revealed that our duraplasty had excellent biocompatibility when implanted onto rodents' brains. In the second project, BC tubes were prepared and nerve growth factor was incorporated into the tubes to be used as potential nerve guides to assist with the reconstitution of nerve tissues across SCI lesion. Physical and mechanical properties of the drug delivery systems produced were evaluated and compared to the neural native tissue. In

addition, cell cultures demonstrated that growth factors released from both drug delivery systems were bioactive for over 7 days. In the third project, linear and 2-branched peptides were synthesized as potential bioactive molecules to improve tissue regeneration. These peptides, containing the RGDS sequence, were synthesized through Solid Phase Peptide Synthesis and characterized by mass spectrometry, high-performance liquid chromatography, and their conformational structures were analyzed by an energy minimized 3D model. In summary, this thesis explores the use of BC as drug releasing systems, which are promising and clinically relevant strategies to enhance nerve regeneration for many patients facing physical, mental and financial strains due to stroke, SCI or other difficult-to-cure injuries to the CNS.

Keywords: *biosynthesized cellulose; stroke; duraplasty; spinal cord injury; nerve guidance tube; PC12; NSPC; branched peptides; RGDS*

STATEMENT OF CONTRIBUTIONS

This thesis was written entirely by the author. All figures and tables were created by the author unless otherwise mentioned in the caption. The author designed, produced and fully characterized the drug delivery systems as well as the peptides presented here. The result analyses were largely performed by the author. The *in vitro* and *in vivo* tests, presented at Chapter 3, were lead mainly by Ryan V. Sandarage and Tongda Li, respectively. The H&E images in Chapter 3 were analyzed by others. The scientific guidance throughout the thesis and editorial comments for the written work were provided by Dr. Xudong Cao.

ACKNOWLEDGEMENTS

First of all, I would like express my sincere gratitude to my supervisor, Dr. Xudong Cao, for the opportunity to work on his research group, for his guidance, support, and enthusiasm throughout my PhD. Thank you for the discussions, encouragements and pushing me to challenge myself when it was necessary. Definitely, I am not the same researcher and person who started this journey.

I would like to thank the members of my defence committee, Dr. Alison McGuigan, Dr. Ajoy Basak, Dr. Jean-Philippe St-Pierre and Dr. Sidney Omelon, for taking the time to read and for the important contributions in my thesis.

I would like to thank my current and past lab colleagues: Danny, Hesham Elkhadem, Shuying Li, Tongda Li, Xingkai Hao, Dimitri, Jian Tang, Qi Chu, Yubo Qin, Yuqian Jiang, Zizhen Li, for their support. Particularly, Holly McCulloch for her friendship and countless coffee breaks that helped me to pass through the hard times. In addition, I would like to thank you Linda Tang, Patrick Fournier, Ryan Sandarage and Ahmad Galuta for their help with this work. Linda, Patrick and Qi, it was a pleasure guiding you throughout your projects, I learned a lot with you.

I also would like to thank the professors and faculty members of my department for their assistance. In special for the administration support of Francine Pétrin, Frantz Célestin and Sylvie Saindon. And for the technical support of Louis Tremblay, Franco Ziroldo, Gérard Nina and James MacDermid. I would also like to acknowledge Dr. Ajoy Basak, Dr. Eve Tsai and Dr. Katlyn Kirkwood for sharing their lab facilities.

I would like to acknowledge and appreciate the National Council for Scientific and Technological Development (CNPq, Brazil), the Ontario Graduate Scholarship (OGS) program, the University of Ottawa and my supervisor, Dr. Cao, for financial support.

People were born, people passed away, bonds were broken, birthdays were missed, weddings were missed, family lunches on Sundays were missed, card games night were missed, but love never was missed, it was always there! I am grateful for the experiences that I had during my PhD journey, but without the love of these special people, that would not be possible:

My parents, Cladis and Eurenio, it is always because of you and for you. *Amo e admiro vocês!*

My brother and sister-in-law, Marcos and Dayha, because I know that you will always be there for me.

My sisters by choice, Aline, Rosiana and Sabrina. It has been almost two decades of friendship and most of that time we lived apart, and that was never an excuse to not be a part of each other lives. You were there practically to all my ups and downs in life, and for that I am thankful. Rosiana, you are "my person", you were there in all the moments! *Amo-te!*

My dear Canadian family, "*Mafia*", Andrea, Adriana, Danilo, Diego, Edlene, Gabriel, Hellen, Jerry, Juliana, Julio, Leo, Marina, Patricia, Tereza and Tiago. You made this journey lighter, funnier and a little more alcoholic too! Andrea, I am so grateful that we sucked in English in 2013. You are the older sister that I never had!

The children that bring light in my life Donatella, Giovanna, Marco Antonio and Melissa. In special, my godsons, Leonardo and Oliver, you are the purest love in my life. *A dinda ama vocês e sente saudades sempre!* You all inspired me to be a better person and fight for a better world.

My in-law family, Rosangela, Rafael, Fabi, Vo Geraldo, Vo Lindinha and all the others. If I could choose my husband's family, I would pick each and every one of you.

My best friend and love, Danilo. No words can express how much I appreciate your support during all these years; without you this would not happen. Thank you! Thank you! Thank you! In the biomedical engineering context, if I were a cell you would be a biomaterial, however no modifications would be necessary because our cell–biomaterial interactions are already everything that I need. *Te amo muito, meu feinho!*

TABLE OF CONTENT

LIST OF NOMENCLATURE, ABBREVIATIONS, SYMBOLS AND GLOSSARY

Nomenclature

CO_2	Carbon dioxide
Na_2HPO_4	Disodium hydrogen phosphate
NaOH	Sodium hydroxide
-C(=O)OH	Carboxyl group
$-NH_2$	Amine group
-SH	Thiol group

Abbreviations

3D	Three dimensional
Acm	Acetamidomethyl
Adoa	8-Amino-3,6-dioxaoctanoic acid
ANOVA	Analysis of variance
ATCC	American type culture collection
BBB	Blood–brain barrier
BBC	Blended biosynthesized cellulose
BBC5GF	Blended biosynthesized cellulose 5 loaded with growth factors
BSCB	Blood–spinal cord barrier
BC	Biosynthesized cellulose
BCT	Biosynthesized cellulose tubes
BrdU	5-Bromo-2'-deoxyuridine,
CNS	Central nervous system

CSF	Cerebrospinal fluid
DAPI	4’,6-Diamidino-2-phenylindole
DC	Decompressive craniectomy
DMF	Dimethylformamide
ECM	Extracellular matrix
EGF	Epidermal growth factor
ELISA	Enzyme-linked immunosorbent assay
FBS	Fetal bovine serum
FDA	Food and Drug Administration
FGF2	Fibroblast growth factor-2
Fmoc	9-Fluorenylmethoxycarbonyl
GF	Growth factor
GFAP	Glial fibrillary acidic protein
GFM	Growth factor matched media
HATU	O-(7-Azabenzotriazol-1-yl)-N,N,N’,N’-tetramethyluronium hexafluorophosphate
HBTU	O-(Benzotriazol-1-yl)-N,N,N’,N’-tetramethyluronium hexafluorophosphate
HPLC	High performance liquid chromatography
MAP	Multiple antigen peptide
MALDI-MS	Matrix-assisted laser desorption/ionization - mass spectrum
MS	Mass spectrometry
MTT	3-(4,5-Dimethylthiazol-2-yl)-2,5-diphenyltetrazolium bromide

NGF	Nerve growth factor
NSPC	Neural stem/progenitor cell
NTSCI	Non-traumatic spinal cord injury
O4	Oligodendrocyte marker O4 antibody
OtBu	Tert-butyloxy
Pbf	2,2,4,6,7-Pentamethyldihydrobenzofuran-5-sulfonyl
PBS	Phosphate buffered saline
PC12	Rat adrenal gland cell line
PPG	Permanent protecting group
RGD	Arginine–glycine–aspartic acid
RGDS	Arginine–glycine–aspartic acid–serine
RP-HPLC	Reverse phase - high performance liquid chromatography
RR	Rehydration Ratio
SCI	Spinal cord injury
SEM	Scanning electron microscopy
SFM	Serum-free media
Sox2	Sex determining region Y-box 2
SPPS	Solid-phase peptide synthesis
SR	Swelling ratio
SVZ	Subventricular zone
tBu	Tert-butyl
TE	Tissue engineering
TFA	Trifluoroacetic acid

TG	TentaGel amide resin
TPG	Temporary protecting group
Trt	Trityl
TSCI	Traumatic spinal cord injury
WHO	World Health Organization

Symbols

%	Percentage
rpm	Revolutions per minute
~	Approximately
M	Molar concentration
°C	Degree Celsius
g/L	Gram per liter
g	Gram
h	Hour
µm	Micrometer
mm	Millimeter
CFU/mL	Colony forming unit per milliliter

Glossary

Biomaterial	Material (synthetic or natural) that has been designed to be applied in biological systems to treat, increase or substitute body parts and allow recovery of biological functions from diseases or accidents.

Biocompatible	Ability of a biomaterial or medical device to perform its intended function, with the desired degree of incorporation in the host, without eliciting any undesirable local or systemic effects in that host.
Biofunctional	Having a biological functional (molecule, device, etc.)
Bioactive molecule	A molecule that has an effect on a living organism
Biomolecule	Or biological molecule are molecules that are produced or presented in living organisms, essential to some typically biological process.

LIST OF TABLES

LIST OF FIGURES

CHAPTER 1 – INTRODUCTION & HYPOTHESIS

1.1. General Introduction

The central nervous system (CNS) has a reduced capacity to spontaneously regenerate after disease or injury, demanding innovative approaches to promote tissue and functional repairs [1]. Providing a tissue engineering scaffold that also acts as a drug delivery system has a great potential to increase nerve regeneration and enhance functional recoveries in the CNS. Therefore, in this thesis, projects were developed focusing on the production and characterization of two different drug delivery systems based on biosynthesized cellulose (BC) for stroke and spinal cord injury (SCI) regeneration and on the synthesis and optimization of linear and two-branched "RGDS" peptides as potential molecules to enhance cell−biomaterial interaction.

Tissue engineering devices, particularly those to be used as implantable scaffolds, are generally made from biomaterials that offer a variety of structures and properties. To this end, many biomaterials – both synthetic and naturally occurring – have been used for CNS applications, where additional modifications to the scaffold material are usually required. One approach that is well recognized for that is anchoring biologically active entities into the biomaterial, such as growth factors (GFs) and peptides. Recently, naturally occurring materials such as cellulose, chitosan, hyaluronic acid, and collagen have attracted significant interests as potential biomaterials for applications in tissue engineering (TE) [2]. Among these materials, cellulose is perhaps the most common naturally occurring polymer on earth. It is an important structural component found in cell walls of green plants, algae, oomycetes and some cellulose-producing strains (i.e. biosynthesized cellulose, BC) in biofilm form [3]. While it is necessary to employ different chemical treatments to obtain pure cellulose from plants [4], BC is readily produced more pure than plant cellulose and does not contain any other compound present in the plant pulp or from animal origin [5].

In the first project, presented in Chapter 3, a novel BC-based drug releasing duraplasty that can be applied as part of decompressive craniectomy (DC) after stroke was designed and tested (**Figure 1.1**). Stroke is a CNS disorder consisting of the sudden death of brain cells due to a lack of oxygen and nutrients [6]. It is the second leading cause of death [7] and the third leading cause of disability [8] around the world. In Canada, between 2012–2013, there were 741,800 stroke survivors [9]. Unfortunately, the treatment options for stroke are very limited and the neurological damage cannot be completely repaired [10-12]. Usually, after a stroke, extensive portions of the brain are damaged, causing significant brain swelling. DC is a standard surgical procedure performed on stroke patients to alleviate the increased intracranial pressure by temporarily removing a portion of the skull, opening the dura and then applying a duraplasty (i.e. membrane patch) onto the exposed brain [13-15]. While DC can significantly reduce the risk of death, this procedure with the duraplasty implantation does not reverse the stroke damage [13, 16]. Thus, BC was used to produce the new duraplasty, and GFs were loaded into the membrane. The use of GFs have shown promising results to stimulate neural stem/progenitor cells (NSPCs) proliferation and migration from the subventricular zone (SVZ) to the injury site and consequently tissue regeneration [17, 18]. **Figure 1.1** shows a schematic representation of this process. Physical and mechanical properties of the resulting duraplasty were studied. In addition, the bioactivity of the GFs released from the BC-based duraplasty were evaluated in primary rodent NSPCs for 1 and 2 weeks. Lastly, the *in vivo* biocompatibility of the drug releasing BC duraplasty was demonstrated in animal models and inflammatory changes associated with the biomaterial were evaluated.

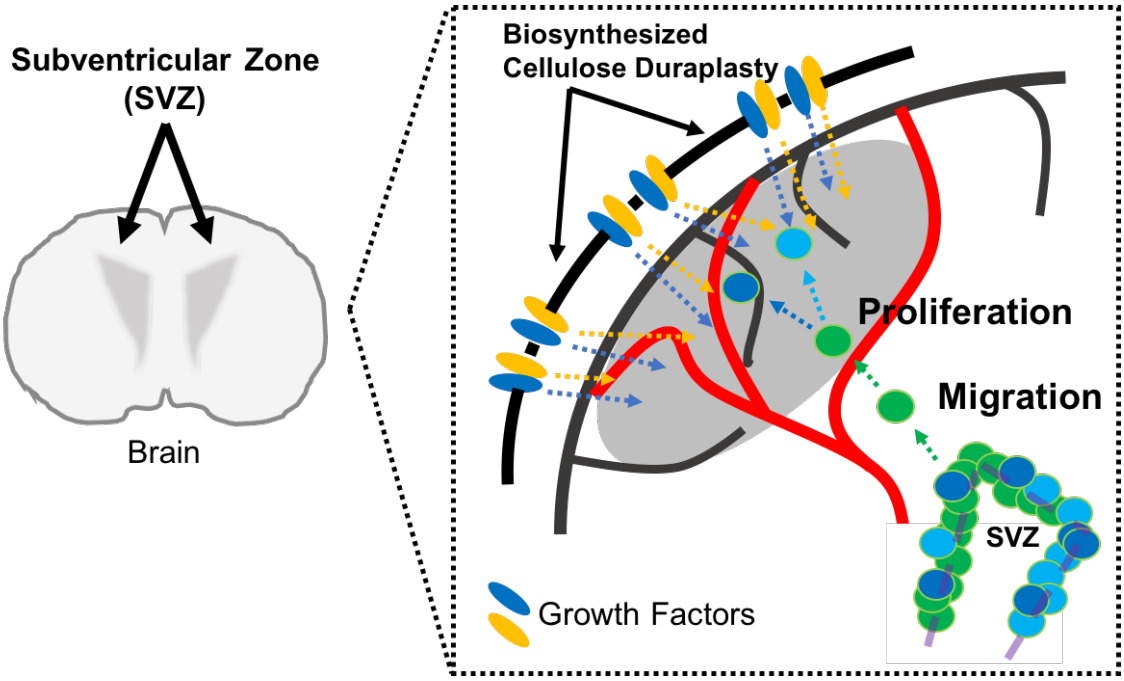

Figure 1.1 – Schematic representation of biosynthesised cellulose (BC)-based duraplasty application. The growth factors loaded BC duraplasty is locally implanted onto the brain after decompressive craniectomy (DC) after stroke. The growth factors are released and stimulated the migration and proliferation of post-stroke neural stem/progenitor cells (NSPCs) from the subventricular zone (SVZ) to the injury site to promote tissue repair.

In the second project, presented in Chapter 4, BC hydrogels were produced in tube-shape and nerve growth factor (NGF) was incorporated into the BC tubes as a potential nerve guidance tubes to assist with the reconnection of nerve tissues across SCI lesion. **Figure 1.2** shows a schematic representation of the NGF-enriched (i.e. NGF-loaded) nerve guidance tube for application in SCI. The SCI is another CNS disorder that can result in permanent motor and sensory damage due to a severed communication pathway [19]. Functional repair of SCI thus remains one of the most challenging clinical problems. The World Health Organization (WHO) estimates that every year, between 250,000 and 500,000 people sustain a SCI [20]. In Canada, it is estimated that there are 4,500 new cases of SCI each year [21].

Recently, TE based approaches have used biomaterials for SCI regeneration [22]. Among the biomaterial approaches, hydrogel tubes can be used as nerve guidance tubes to reconnect injury gaps by providing structural orientation for the nerve tissue and as vehicles

for the delivery of bioactive molecules to promote cell growth at the site of the injury [22]. One of the most frequently used bioactive molecule for release into a SCI is NGF, which is well known to improve neuronal outgrowth and has been applied as a chemo-attractant to promote axon guidance [23, 24]. In this study, *Gluconacetobacter hansenii* was cultivated during several time points in a specific bioreactor to produce biosynthesized cellulose tubes (BCTs). Different cultivation parameters were measured, BCTs physical and mechanical properties were evaluated and compared to the native tissue. In addition, the drug delivery behavior of the enriched nerve guidance tube was studied, as well as the NGF bioactivity against PC12 cells.

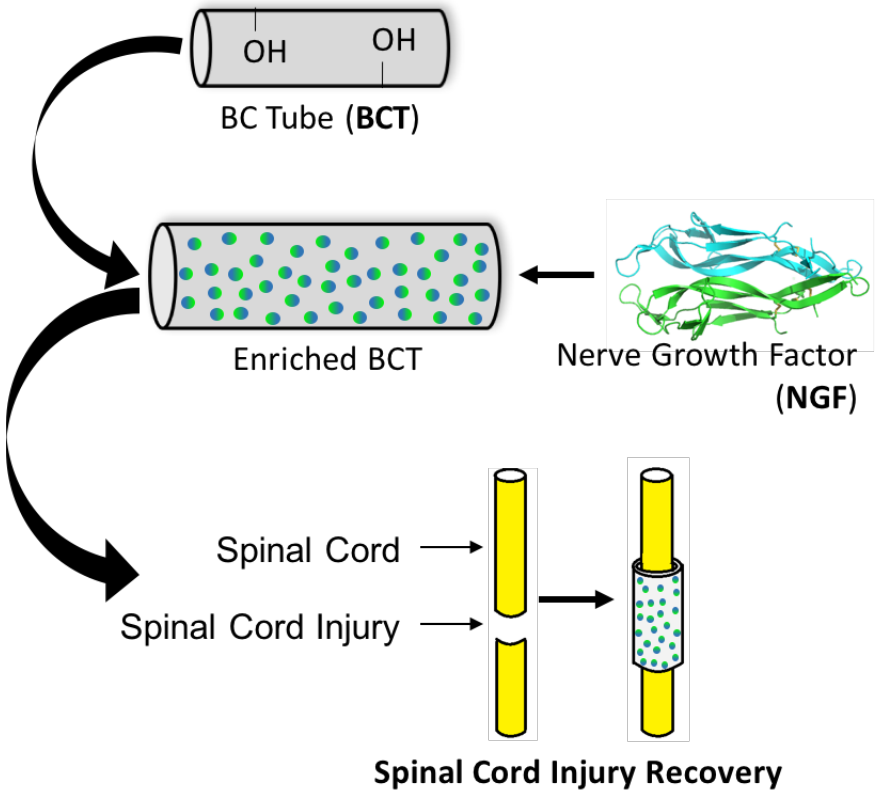

Figure 1.2 – Schematic representation of biosynthesized cellulose tubes (BCTs) for SCI application. BCTs were produced and enriched with nerve growth factor (NGF) to serve as nerve guidance tubes for SCI regeneration.

As third project, Chapter 5, linear and 2-branched peptides were synthesized as potential bioactive molecules to improve tissue regeneration. Peptides are involved on a variety of physiological functions and biochemical processes. Specially, the tetrapeptide arginine-glycine-aspartic acid-serine (RGDS) is the most efficient and most often used peptide moiety to stimulate cell adhesion on synthetic surfaces, due to its ability to address more than one cell adhesion receptor and its biological impact on cell anchoring, behavior and survival [25]. In addition, the building of branched peptides (i.e. multiple antigen peptide (MAP) system) containing RGDS moiety and the immobilization of such peptides in biomaterials has represented an attractive approach to improve cell-biomaterial interactions in TE [26-31]. MAPs have shown higher cellular uptake than their similar linear counterparts, since they present higher density of functional binding sites and consequently much lower concentrations can be used [32-39]. Therefore, Chapter 5, linear and 2-branched peptides containing the RGDS sequence were synthesized through solid-phase peptide synthesis and characterized by mass spectrometry, high-performance liquid chromatography, and their conformational structures were analyzed by a theoretical energy-minimized 3D model. Peptides synthesized can be loaded into drug delivery systems, such as the BCT systems, to improve cell–biomaterial interactions.

1.2. Hypothesis

- It is hypothesized that blending the original biosynthesized cellulose is an effective approach to produce duraplasty membranes and to modify its properties, such as cellulose mass, swelling capacity and mechanical. In addition, it is believed that using this fabrication technique the duraplasty could easily be loaded with bioactive

molecules and that delivered would be effective to stimulate neural stem/progenitor cell migration, proliferation and differentiation.

- It is hypothesized that culturing *G. Hansenii* for different time length in a bioreactor containing a silicone tubing would produce biosynthesized cellulose tubes with different cellulose mass and thickness and that would influence in the tubes properties. Besides, it is hypnotized that these tubes could be used as drug delivery systems to stimulate PC12 cells differentiation.
- It is hypothesized that using Solid Phase Peptide Synthesis chemistry peptides containing the RGDS peptide moiety with different configurations, e.g. linear and branch, could be synthesized. And, the peptides chemical structures could be confirmed by HPLC and MALDI.

1.3. Specific Aims

i. Produce blended biosynthesized cellulose (BBC) for drug releasing duraplasty applications in stroke;
ii. Generate biosynthesized cellulose tubes (BCTs) as nerve guidance delivery systems;
iii. Characterize physically and mechanically the two drug delivery systems (BCT and BBC);
iv. Enrich both systems with growth factors;
v. Evaluate the drug delivery profile of enriched-BBC and BCT;
vi. Analyse the *in vitro* activity and effect of the growth factors delivered from the systems;
vii. Determine the *in vivo* biocompatibility of BBC duraplasty;

viii. Synthesize and characterize different peptides with RGDS sequence in linear or branched configurations.

1.4. Thesis Overview

This thesis contains 8 chapters. **Chapter 1** introduces the research, its main hypothesis, specific objectives and the thesis structure. **Chapter 2** provides a review of the current literature on central nervous system (CNS), biosynthesized cellulose (BC), peptides and describes the state-of-the-art biomaterials available for CNS disorders, specifically for stroke and spinal cord injury. **Chapter 3** of this thesis describes the development and analysis of a novel BC-based drug releasing duraplasty for stroke application. In **Chapter 4** is demonstrated the production and *in vitro* study of a BC-based nerve guidance drug delivery tube for spinal cord injury treatment. **Chapter 5** shows the synthesis and characterization of peptides as potential therapeutic molecules. **Chapter 6** of this thesis, provides a general discussion of the results obtained in this thesis. In **Chapter 7** an overall summary and final conclusions on the work contained in this thesis are presented. Finally, the recommendations for further work based on this thesis are discussed in **Chapter 8**.

1.5. Statement of Novelty

In this thesis, for the first time, a blending fabrication technique was used to produce biosynthesized cellulose-based duraplasties as drug delivery systems to be applied as part of a standard decompressive craniectomy after stroke. In addition, several biosynthesized cellulose tubes were prepared and their physical and mechanical characteristics evaluated and compared. These tubes were enriched with nerve growth factor and their activity was tested for the first time as potential nerve guidance drug delivery systems for SCI.

1.6. References

[1] Y.C. Wang, H. Tan, X.H. Hui, Biomaterial Scaffolds in Regenerative Therapy of the Central Nervous System, Biomed Res Int (2018).

[2] D. Ozdil, H.M. Aydin, Polymers for medical and tissue engineering applications, J Chem Technol Biot 89(12) (2014) 1793-1810.

[3] D. Klemm, B. Heublein, H.P. Fink, A. Bohn, Cellulose: Fascinating biopolymer and sustainable raw material, Angew Chem Int Edit 44(22) (2005) 3358-3393.

[4] K. Keegstra, Plant Cell Walls, Plant Physiol 154(2) (2010) 483-486.

[5] A.F. Jozala, L.C. de Lencastre-Novaes, A.M. Lopes, V.D. Santos-Ebinuma, P.G. Mazzola, A. Pessoa, D. Grotto, M. Gerenutti, M.V. Chaud, Bacterial nanocellulose production and application: a 10-year overview, Appl Microbiol Biot 100(5) (2016) 2063-2072.

[6] Mozaffarian, Heart Disease and Stroke Statistics-2016 Update: A Report From the American Heart Association (vol 133, pg e38, 2016), Circulation 133(15) (2016) E599-E599.

[7] Global Health Estimates 2016: Deaths by Cause, Age, Sex, by Country and by Region, 2000-2016. Geneva, World Health Organization, 2018. http://www.who.int/healthinfo/global_burden_disease/estimates/en/. (Accessed May 7th 2019).

[8] Global Health Estimates 2015: Disease burden by Cause, Age, Sex, by Country and by Region, 2000-2015. Geneva, World Health Organization, 2016. http://www.who.int/healthinfo/global_burden_disease/estimates/en/index1.html. (Accessed May 7th 2019).

[9] Public Health Agency of Canada, Stroke in Canada : highlights from the Canadian Chronic Disease Surveillance System. http://publications.gc.ca/collections/collection_2018/aspc-phac/HP35-88-2017-eng.pdf.

[10] R.Y. Tam, T. Fuehrmann, N. Mitrousis, M.S. Shoichet, Regenerative therapies for central nervous system diseases: a biomaterials approach, Neuropsychopharmacology 39(1) (2014) 169-88.

[11] A. Rogalewski, A. Schneider, E.B. Ringelstein, W.R. Schabitz, Toward a multimodal neuroprotective treatment of stroke, Stroke 37(4) (2006) 1129-36.

[12] P. Sensharma, G. Madhumathi, R.D. Jayant, A.K. Jaiswal, Biomaterials and cells for neural tissue engineering: Current choices, Mater Sci Eng C Mater Biol Appl 77 (2017) 1302-1315.

[13] D. Staykov, R. Gupta, Hemicraniectomy in malignant middle cerebral artery infarction, Stroke 42(2) (2011) 513-6.

[14] O.M. Arnaout, S.G. Aoun, H.H. Batjer, B.R. Bendok, Decompressive hemicraniectomy after malignant middle cerebral artery infarction: rationale and controversies, Neurosurg Focus 30(6) (2011) E18.

[15] E. Juttler, A. Unterberg, J. Woitzik, J. Bosel, H. Amiri, O.W. Sakowitz, M. Gondan, P. Schiller, R. Limprecht, S. Luntz, H. Schneider, T. Pinzer, C. Hobohm, J. Meixensberger, W. Hacke, D.I. Investigators, Hemicraniectomy in older patients with extensive middle-cerebral-artery stroke, N Engl J Med 370(12) (2014) 1091-100.

[16] X. Lu, B. Huang, J. Zheng, Y. Tao, W. Yu, L. Tang, R. Zhu, S. Li, L. Li, Decompressive craniectomy for the treatment of malignant infarction of the middle cerebral artery, Sci Rep 4 (2014) 7070.

[17] Y. Wang, M.J. Cooke, N. Sachewsky, C.M. Morshead, M.S. Shoichet, Bioengineered sequential growth factor delivery stimulates brain tissue regeneration after stroke, J Control Release 172(1) (2013) 1-11.

[18] M.J. Robertson, P. Gip, D.V. Schaffer, Neural stem cell engineering- directed differentiation of adult and embryonic stem cells into neurons, Frontiers in Bioscience 13 (2008) 21-50.

[19] R.C. Assuncao-Silva, E.D. Gomes, N. Sousa, N.A. Silva, A.J. Salgado, Hydrogels and Cell Based Therapies in Spinal Cord Injury Regeneration, Stem Cells Int (2015).

[20] International Perspectives on Spinal Cord Injury. 2013. Geneva, World Health Organization, 2013. https://www.who.int/disabilities/policies/spinal_cord_injury/report/en/. (Accessed February 11th 2019).

[21] J. Bickenbach, A. Officer, T. Shakespeare, P. von Groote, W.H. Organization, T.I.S.C. Society, International perspectives on spinal cord injury in: J. Bickenbach (Ed.) 1.Spinal cord injuries – history. 2.Spinal cord injuries – epidemiology. 3.Spinal cord injuries – prevention and control. 4.Spinal cord injuries – rehabilitation. 5.Delivery of health care. 6.Disabled persons - psychology., World Health Organization (WHO), 2013.

[22] S. Kubinova, New trends in spinal cord tissue engineering, Futur Neurol 10(2) (2015) 129-145.

[23] X. Cao, M.S. Shoichet, Investigating the synergistic effect of combined neurotrophic factor concentration gradients to guide axonal growth, Neuroscience 122(2) (2003) 381-389.

[24] A. Singh, S. Asikainen, A.K. Teotia, P.A. Shiekh, E. Huotilainen, I. Qayoom, J. Partanen, J. Seppala, A. Kumar, Biomimetic Photocurable Three-Dimensional Printed Nerve Guidance Channels with Aligned Cryomatrix Lumen for Peripheral Nerve Regeneration, Acs Appl Mater Inter 10(50) (2018) 43327-43342.

[25] F.K. Andrade, S.M.G. Moreira, L. Domingues, F.M.P. Gama, Improving the affinity of fibroblasts for bacterial cellulose using carbohydrate-binding modules fused to RGD, J Biomed Mater Res A 92A(1) (2010) 9-17.

[26] J.H. Collier, Modular self-assembling biomaterials for directing cellular responses, Soft Matter 4(12) (2008) 2310-2315.

[27] M. Zhou, A.M. Smith, A.K. Das, N.W. Hodson, R.F. Collins, R.V. Ulijn, J.E. Gough, Self-assembled peptide-based hydrogels as scaffolds for anchorage-dependent cells, Biomaterials 30(13) (2009) 2523-2530.

[28] C.A. Goubko, S. Majumdar, A. Basak, X.D. Cao, Hydrogel cell patterning incorporating photocaged RGDS peptides, Biomed Microdevices 12(3) (2010) 555-568.

[29] C.A. Goubko, A. Basak, S. Majumdar, X.D. Cao, Dynamic cell patterning of photoresponsive hyaluronic acid hydrogels, J Biomed Mater Res A 102(2) (2014) 381-391.

[30] C.A. Goubko, A. Basak, S. Majumdar, H. Jarrell, N.H. Khieu, X.D. Cao, Comparative analysis of photocaged RGDS peptides for cell patterning, J Biomed Mater Res A 101(3) (2013) 787-796.

[31] R.A. Plenderleith, C.J. Pateman, C. Rodenburg, J.W. Haycock, F. Claeyssens, C. Sammond, S. Rimmer, Arginine-glycine-aspartic acid functional branched semi-interpenetrating hydrogels, Soft Matter 11(38) (2015) 7567-7578.

[32] I.A. Monreal, Q. Liu, K. Tyson, T. Bland, D.S. Dalisay, E.V. Adams, G.A. Wayman, H.C. Aguilar, J.P. Saludes, Branched dimerization of Tat peptide improves permeability to HeLa and hippocampal neuronal cells, Chem Commun 51(25) (2015) 5463-5466.

[33] W.L. Zhu, S.Y. Shin, Effects of dimerization of the cell-penetrating peptide Tat analog on antimicrobial activity and mechanism of bactericidal action, J Pept Sci 15(5) (2009) 345-352.

[34] F.S. Hassane, G.D. Ivanova, E. Bolewska-Pedyczak, R. Abes, A.A. Arzumanov, M.J. Gait, B. Lebleu, J. Gariepy, A Peptide-Based Dendrimer That Enhances the Splice-Redirecting Activity of PNA Conjugates in Cells, Bioconjugate Chem 20(8) (2009) 1523-1530.

[35] A.M. Angeles-Boza, A. Erazo-Oliveras, Y.J. Lee, J.P. Pellois, Generation of Endosomolytic Reagents by Branching of Cell-Penetrating Peptides: Tools for the Delivery of Bioactive Compounds to Live Cells in Cis or Trans, Bioconjugate Chem 21(12) (2010) 2164-2167.

[36] G.A. Eggimann, S. Buschor, T. Darbre, J.L. Reymond, Convergent synthesis and cellular uptake of multivalent cell penetrating peptides derived from Tat, Antp, pVEC, TP10 and SAP, Org Biomol Chem 11(39) (2013) 6717-6733.

[37] G.A. Eggimann, E. Blattes, S. Buschor, R. Biswas, S.M. Kammer, T. Darbre, J.L. Reymond, Designed cell penetrating peptide dendrimers efficiently internalize cargo into cells, Chem Commun 50(55) (2014) 7254-7257.

[38] S.H. Park, J. Doh, S.I. Park, J.Y. Lim, S.M. Kim, J.I. Youn, H.T. Jin, S.H. Seo, M.Y. Song, S.Y. Sung, M. Kim, S.J. Hwang, J.M. Choi, S.K. Lee, H.Y. Lee, C.L. Lim, Y.J. Chung, D. Yang, H.N. Kim, Z.H. Lee, K.Y. Choi, S.S. Jeun, Y.C. Sung, Branched oligomerization of cell-permeable peptides markedly enhances the transduction efficiency of adenovirus into mesenchymal stem cells, Gene Ther 17(8) (2010) 1052-1061.

[39] J. Hoyer, U. Schatzschneider, M. Schulz-Siegmund, I. Neundorf, Dimerization of a cell-penetrating peptide leads to enhanced cellular uptake and drug delivery, Beilstein J Org Chem 8 (2012) 1788-1797.

CHAPTER 2 – LITERATURE REVIEW

2.1. Central Nervous System (CNS)

The brain and spinal cord are what anatomically make up the central nervous system (CNS). The CNS along with the peripheral system (nerves and ganglia) form the nervous system, which has an essential function in the body control. The CNS receives the information related to the senses (sight, hearing, taste, smell, and touch) and sends out orders to move muscles and control glands.

The CNS is susceptible to various diseases, also known as central nervous system disorders. These disorders can affect the structure or function of the brain or spinal cord and can be caused by several different origins including diseases and traumas. Among the many CNS disorders, this thesis will focus on stroke (*Section 2.2*) and spinal cord injury (SCI, *Section 2.3*). CNS disorders are complicated, often resulting in the loss of motor, sensory, and cognitive functions. Unfortunately, there are few treatment options for patients with CNS disorders, due to the limited capacity of the CNS to spontaneously regenerate [1]. This lack of regeneration capability is due to the absence of growth factors (GFs) and extracellular matrix (ECM) proteins that can promote the axon growth, the presence of molecules that inhibit the axonal growth, and the formation of a glial scar - a chemical and physical barrier - at and around the injury area [2]. Research is ongoing to improve the CNS regeneration ability by delivering bioactive molecules to the CNS through a variety of different methodologies. The aim of these molecules is to stimulate neuroprotection and promote the proliferation and migration of endogenous neural stem/progenitor cells (NSPCs) to the lesion site [3]. Furthermore, the blood–brain and spinal cord barriers (BBB and BSCB, respectively) are protective barriers in the CNS, protecting the brain and the spinal cord against harmful and

hazard agents, but also impeding the efficacy of systemic drug delivery methods (i.e. oral and intravenous) [4].

Considering the special structure of the BBB/BSCB, new therapeutic designs or the elaborations of efficient delivery methods are required for CNS drug delivery [5]. Most drugs used to treat CNS disorders are administrated intravenously or orally; however only a few bioactive molecules can bypass the BBB/BSCB and achieve the injured tissue in efficacious doses [6, 7]. Therefore, for the effective drug amount to reach the target site, it is necessary to increase the drug dose or to extend the administration time, which increases the risk of toxicity. In the case of SCI, serial injections or continuous osmotic mini-pump infusion have been used to deliver high concentrations of molecules to the spinal cord intrathecal space. However, these methods present several limitations, such as uneven distribution of the released molecule (with serial injection) or increased risk of infection or obstruction of the used device (with external minipump infusion) [4]. To bypass the BBB, intraventricular injection into the brain has been used, but this technique is very invasive and can result in substantial tissue damage due to the insertion of a catheter through the brain tissue [8]. Therefore, approaches involving biomaterials and bioactive molecules have been proposed to both improve cell survival and enhance drug concentration at the injured site [9, 10].

2.2. Stroke

Cerebrovascular accident or stroke is a CNS disorder and it is the sudden death of brain cells due to a lack of oxygen and nutrients, usually because of a blood vessel burst (hemorrhagic stroke) or blockage (ischemic stroke, 87 % of all strokes) [11]. Roughly 10 % of ischemic strokes are classified as malignant or massive because of the presence of space-occupying cerebral edema that is severe enough to produce brain tissue shifts and herniation. Patients

with this syndrome have a mortality rate as high as 78 %. The most common symptoms of a stroke include loss of sensation or weakness on one side of the body, confusion, difficulty in speaking, seeing and/or walking, headaches, dizziness and/or fainting. Generally, these symptoms are abrupt and may vary depending on the gravity of the brain injury. When the brain injury is very severe it can be fatal. Worldwide, stroke is the second leading cause of death [12] and the third leading cause of disability [13]. 15 million people experience stroke every year, among those, 5 million die and 5 million are permanently disabled. Canadian data shows that between 2012–2013 there were 741,800 stroke survivors aged 20+ -- an increased of ~41 % in 10 years -- and the number of deaths was 57,000 [14]. Unfortunately, treatment options for stroke are very limited and the neurological damage cannot be completely repaired [10, 15, 16].

2.2.1. Overview of Treatment Strategies

After a stroke, the current clinical therapy is limited in promoting circulation, restoring perfusion of the occluded vessels (normally includes surgical clot retrieval or thrombolytic treatment), and protecting ischemic cells from death. It has been shown that the administration of intravenous thrombolysis within 4.5 hours from a stroke event can significantly improve patients' outcome [17]. However, only a minority of patients (up to 25% in well-organized stroke centers) receive intravenous thrombolysis, and its benefit in large vessel occlusion is limited by an overall low recanalization rate of approximately 20 % [17].

Recent research has focused on developing strategies to stimulate endogenous neurogenesis. Usually, post-stroke NSPCs proliferate in a higher rate in the subventricular zone (SVZ), and some precursor cells are redirected to the damaged site [18, 19]. For *in vitro* studies, the activation time of NSPCs ranges from 5 to 7 days after ischemic injury [20], and

2 to 6 weeks after middle cerebral artery occlusion (MCAO) injury [21]. Because of the absence of ECM and the occurrence of cytotoxic factors, many of the new NSPCs do not survive long enough to mature and to incorporate into the neural system. In fact, it is estimated that only 0.2 % of NSPCs became mature neurons in MCAO models [22], showing the limited repair ability of the damaged tissue [22-25].

NSPCs are multipotent cells and can proliferate and create multiple cell lineages, such as oligodendrocytes, neurons, and astrocytes both *in vitro* and *in vivo*. The use of GFs to stimulate NSPCs proliferation and migration to the injury region and consequently tissue regeneration has shown promising results with an enhanced efficacy when two combined GFs are applied [26, 27] (see Figure 1.1 above). Epidermal growth factor (EGF), fibroblast growth factor-2 (FGF2), erythropoietin (EPO), vascular endothelial growth factor (VEGF), brain-derived neurotrophic factor (BDNF), and others have been shown, in pre-clinical studies, to stimulate axonal propagation, neurogenesis, and other features of neural repair [3, 28-32]. Specifically EGF, a neural regeneration factor that enhances neural stem cell growth by acting as a mitogen for NSPCs [33], and FGF2 have been shown to promote neurogenesis by increasing adult NSPC proliferation [28, 34]. The use of EGF and FGF2 together have resulted in increased NSPC proliferation [26] and therefore were used in the study presented in Chapter 3.

2.2.1.1. Decompressive Craniectomy (DC) and Duraplasty

Strokes frequently damage large portions of the brain, causing significant brain swelling with secondary injuries in the surrounding brain tissue. Medication is often not effective to relieve

the intracranial pressure and therefore surgical procedures are often required. Decompressive craniectomy (DC) is a typical surgical procedure performed on stroke patients when cerebral ischemia leads to cerebral edema and increased intracranial pressure. Two main groups of stroke patients may benefit from craniectomy: (1) patients with large cerebellar infarction and subsequent suboccipital craniectomy; (2) patients with large infarction of the middle cerebral artery territory, also called malignant middle cerebral artery infarction [17]. It is estimated that from the ischemic stroke patients only 0.3 % are potentially eligible for a DC procedure [35]. Patients with middle cerebral artery infarction who are eligible for DC should receive surgery within 48 h from symptom onset [17].

The DC alleviates the increased intracranial pressure by temporarily removing a portion of the skull and opening the dura as shown in **Figure 2.1** [36-38]. A duraplasty material is then applied onto the exposed brain [38]. Despite documented invasiveness of this procedure, randomized controlled trials have shown that the DC significantly reduces mortality in patients suffering from acute ischemic stroke [38-40]. Unfortunately, the DC procedure with the duraplasty implantation does not lead to any improvement in brain function [36, 41].

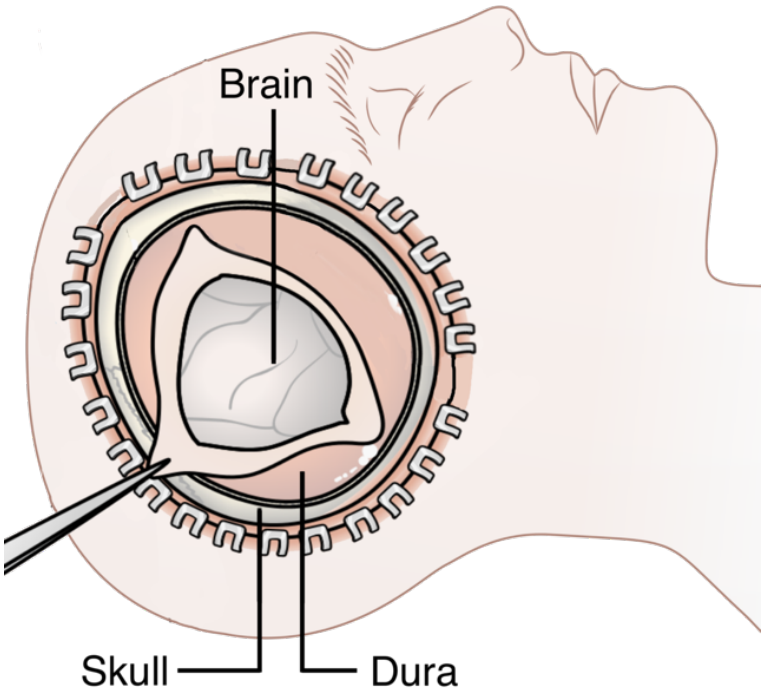

Figure 2.1 – Decompressive craniectomy (DC) procedure, where a portion of the skull is temporarily removed and the dura is opened to exposure the brain. *Adapted from an image by Cancer Research UK; license: CC BY-SA 4.0.*

Several types of plain duraplasty options have been developed for implantation during DC procedure over the years. For example, Codman Duraform® Dural Graft (Johnson & Johnson, New Brunswick, NJ) is a currently commercially available duraplasty. It is composed of type I collagen [42]. It has been shown to cause no inflammatory reaction, exhibits manageable handling qualities, and prevents cerebrospinal fluid (CSF) leakage [42]. Some other examples of duraplasties on the market are: NeoDura™ based on poly(L-lactic acid) (PLA) and porcine gelatin from Medprin Biotech GmbH (Frankfurt, Germany) [43]; TissuePatchDural™ from Tissuemed, composed of poly(lactide-co-glycolide) (Leeds, UK) [44]; DuraGen®Plus made of collagen by Integra LifeSciences Corporation (Plainsboro, NJ, USA) [45]; Gelfoam® made from porcine skin gelatin (Pfizer, New York, NY, USA) [46].

Another example of a commercial duraplasty is SyntheCel® Dura Replacement (DePuySynthes – Johnsons&Johnsons, New Brunswick, NJ) based on naturally occurring biosynthesized cellulose (BC). Rosen et al. studied SyntheCel in a human controlled trial for 6 months and compared it with other commercially available duraplasties including Duraform®, DuraGen®, and Preclude® (product was discontinued) [47]. Using a noninferiority design, the authors concluded that the safety and efficacy of the BC duraplasty were comparable to the other commercial products [47]. However, SyntheCel Dura Replacement has not been loaded with any therapeutic ingredients, likely due to the difficulty in incorporating bioactive molecules into the duraplasty fabrication process while maintaining sterility. As a result, while proven clinically important in saving patient lives, none of the current commercially available duraplasties lead to any improvement in functional outcome.

2.3. Spinal Cord Injury (SCI)

The spinal column consists of 33 vertebrae stacked one on top of the other, which together with the supporting muscles, exert functions of balance and movement. In the center of the vertebrae there is a spinal canal whose function is to accommodate and protect the spinal cord. The spinal cord is a bundle of nerve tissue situated within the spinal canal (**Figure 2.2**) [48]. It measures about 45 cm in an adult human and extends from the brain to the second lumbar vertebra (L1-L2) and ends tapering and forming a tail (*cauda equina* or "horse's tail"). The spinal cord makes connections between the brain and the body, and from it come the spinal nerves, which have the function of conducting sensory and motor nerve impulses, and are responsible for innervations of the trunk, arms, legs and part of the head.

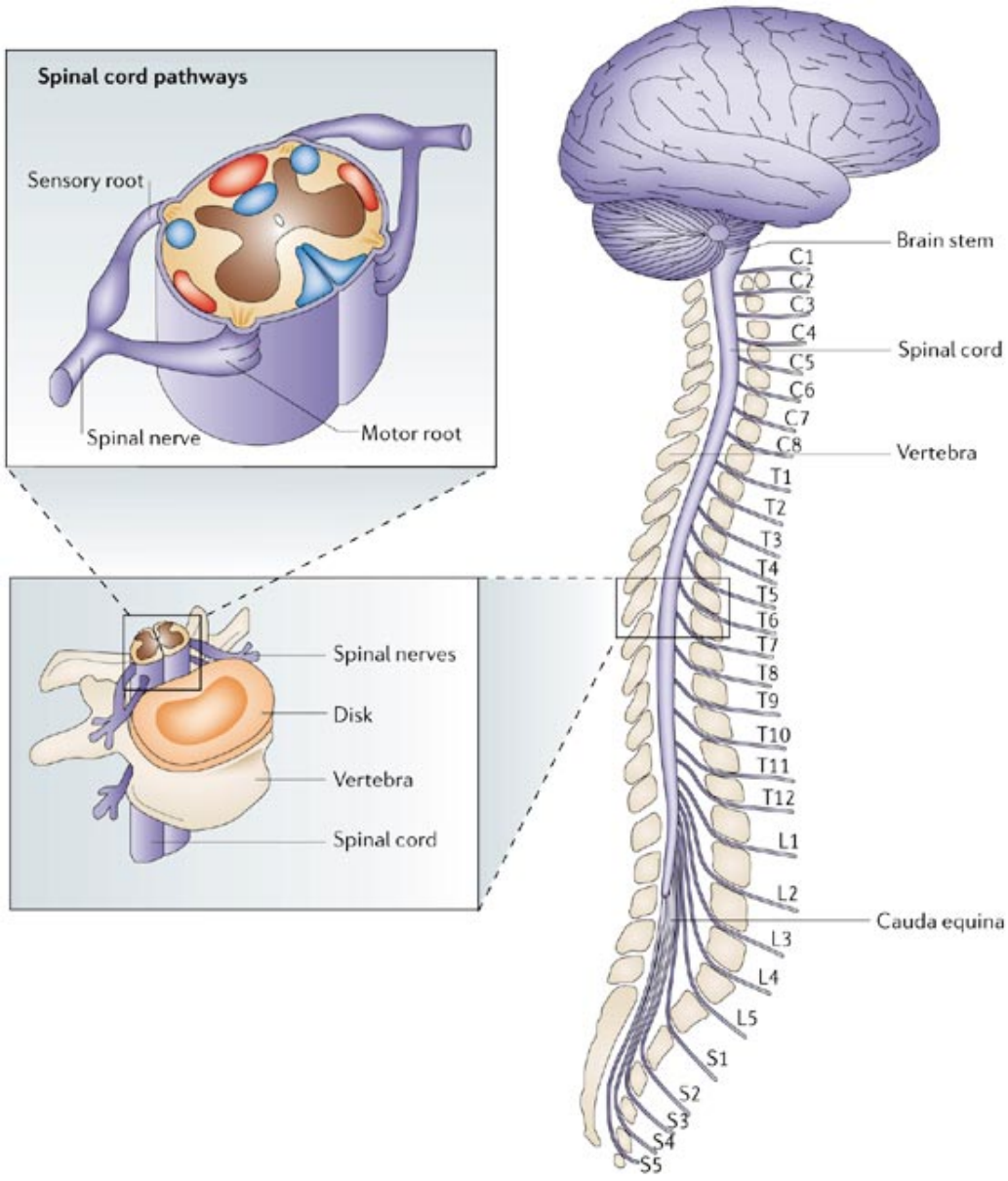

Figure 2.2 – Organization of the spinal column and the spinal cord pathways [46]. *Reproduced with permission from Springer Nature.*

When the spinal cord is damaged, there are symptoms depending on the extent and location of the injury: they can include loss of sensory or motor control and loss of involuntary regulation of the body. The effects and level of the injury are determined by the neurological segmental level, e.g. a lesion in the eighth thoracic vertebra undertakes from the ninth thoracic nerve root. Usually, the higher up to the spinal cord the lesion occurs, the greater the loss of

sensory or motor control will be. A spinal cord injury (SCI) can be classified according to the extent and severity of the sensory-motor impairment, which depends on whether the spinal cord is partially or fully affected. It can be classified as complete if there is no motor or sensory function at the sacral segment (S4-S5) and incomplete if some motor and/or sensory functions are preserved below the level of injury.

SCI presents a great complexity of factors and can occur at various levels [49]. Tetraplegia or a cervical SCI indicates that there is sensory and motor loss in the four limbs of the body. Paraplegia or a thoracic SCI commonly causes sensory and/or motor loss in the trunk and legs. The cause of the damage to the spinal cord can be non-traumatic (NTSCI) or traumatic (TSCI). NTSCI usually involves a pathology – including infectious diseases, tumors, musculoskeletal diseases, and congenital problems. TSCI, on the other hand, can result from many different causes – such as traffic accidents, injury with weapons (sharp objects and fire arms), falls, and sports injuries. Canadian data shows that 85,500 people were living with SCI in 2010, and 44,000 of those cases were from a TSCI. Estimates of age-specific cases of SCI in Canada indicate that TSCI is mostly observed in younger populations, while NTSCI is typically diagnosed in older age groups. In addition, there are an estimated of 4,529 new cases of SCI each year in Canada [50]. While extensive studies are being done to overcome the SCI, there is still no widely accepted therapeutic modality bearing positive neurological outcome [48, 51].

2.3.1. Overview of Treatment Strategies

SCI is a medical condition necessitating urgent treatment to decrease the long-term effects. No two injuries are the same and an injury could occur to anyone, at any time. SCI neurological

deficits can be very debilitating as they are caused by damaging nerve fibers (axons) and cells that allow the transmission of signals along the spinal cord. The conventional clinical therapy is based on stabilization, controlling the inflammation, preventing secondary cell death, rehabilitation, and medication to treat complications, which are largely ineffective in tissue regeneration and restitution of function [52]. To this end, new therapeutic approaches have been developed, including neuroprotection to minimize the loss of secondary tissue after the injury [53, 54], stimulation of axonal regeneration by administration of GFs or various types of stem and progenitor cells [55, 56], neutralization of axonal growth inhibitory factors [49, 57], and providing alternative paths for the regeneration [58, 59].

2.4. Biomaterials

The study of cell–biomaterial interactions is of the upmost importance to determine the biological properties of a future implant. The diversity of cellular responses to different materials demonstrates the capacity of cells to chemically recognize and to adapt or not to a biomaterial [60]. Biomaterials can be defined as "materials (synthetic or natural; solid or liquid) applied in or as medical devices in contact with biological systems" [61] or as "part of a system which treat, increase or substitute any tissue, organ or body function" [62]. In other words, biomaterials are materials designed to substitute body parts and allow recovery of biological functions from diseases or accidents. To encourage regeneration, overall, an ideal biomaterial should be biocompatible, biofunctional, sterile, permeable and porous. The permeability is important for the transport of nutrients and gas exchange and the porosity to allow cell penetration and tissue formation. In addition, the biomaterial should promote the production of ECM, and allow the transport and transmission of biomolecular signals [63, 64].

In addition, an ideal biomaterial should encourage cell adhesion, growth and differentiation as well as having suitable mechanical properties comparable to the native tissue.

For example, collagen and chitosan are biodegradable biomaterials and have been shown to be biocompatible; however, their application is limited because of their poor mechanical characteristics [1, 65]. The choice of biomaterial is based on the different regeneration strategies between using a non-degradable *versus* a biodegradable implant. A balance must be achieved between the rate of degradation and regeneration; fast degradation can lead to a loss of stability, distortion and loss of tissue and therefore a lack of regeneration. It is also crucial to understand the toxicity of the degradation products. From the application point of view, many natural or naturally derived polymers, such as fibrin, collagen, chitosan, hyaluronic acid, hyaluronan–methylcellulose (HAMC) blend, alginate, and agarose have been studied to deliver molecules to the CNS [10, 15, 28, 66-75].

Among the numerous categories of biomaterials, hydrogels have shown potential because of their porosity and their inherent flexibility [76]. Hydrogels can be easily adjusted to be as malleable as soft neural tissue, minimizing the possibility of irritation of the surrounding native tissue after the implantation in the CNS and they can also be molded easily into different shapes [77]. In addition, hydrogel biomaterials are preferable to solid biomaterials since they allow for sufficient permeability to transport oxygen and other nutrients in a soluble state [78]. Hydrogels have naturally high porosity and have been shown to lead to increased cellular viability compared to solid biomaterials [78]. Lately, investigators have designed more complex hydrogels that address characteristics such as topography, mechanical strength, cell adhesion, and degradation [68, 79, 80]. Some examples of hydrogels that have been applied for tissue engineering (TE) are alginate, collagen, hyaluronic acid,

chitosan, agarose, and BC [10]. Several reports have suggested that hydrogels can promote cell adhesion and axon regeneration in CNS injury both *in vitro* and *in vivo* [1, 79, 81].

Due to the lack of biofunctionality of some hydrogels, additional surface modifications may be necessary to provide an environment that more efficiently promotes cell regeneration. Because of the complexity of CNS injuries, the appropriate drug incorporation technique and release profile depend on the injured tissue. To promote cell adhesion and proliferation, cell adhesion peptides derived from fibronectin or laminin have been incorporated into hydrogels [82]. For example, since its discovery, in 1984, arginine–glycine–aspartate (RGD) tripeptide sequence was immobilized into different hydrogels, e.g. gellan-gum [83], agarose [84], hyaluronan [85], methylcellulose [86], hyaluronic acid [87], poly-N-(2-hydroxypropyl) methacrylamide (pHPMA) [88, 89], and have shown to improve adhesion and proliferation of NSPCs.

Biomaterials, such as polymer-based hydrogels, may provide a useful medium through which bioactive molecules can be delivered directly into the CNS injury site, as they have a 3D network of hydrophilic polymers that allows diffusion of molecules out of the system while maintaining physical structure [15, 69, 81]. The incorporation of bioactive molecules, such as GFs, into hydrogels have provided successful neural regeneration systems [90]. There are various reasons why hydrogel based systems are ideal GFs release platforms for repair of neural tissue. First, this technique does not involve living tissue, thereby decreasing the chances for rejections and adverse responses. Second, drug delivery systems made of hydrogels normally eliminate the use of devices that can fail, such as catheters and pumps. Furthermore, hydrogels can provide local specific delivery of one or more bioactive molecules, which is advantageous due to the short *in vivo* half-time of GFs [10, 90]. In addition, the properties of hydrogels can be modified to adjust the release rate of the GF into the desired

location. Finally, GFs can be incorporated into hydrogels through different techniques, e.g. directly during manufacturing, covalently attached, or encapsulated into microspheres [91]. These reasons allow hydrogels to play important roles as drug delivery systems. However, their great potential has been hampered by two major challenges: the difficulty to produce hydrogels with adequate mechanical properties [10, 15, 92] and the sterilization process of hydrogels [93] without affecting the bioactivity of incorporated drugs.

The GFs are endogenous proteins capable of motivating the differentiation and proliferation of cells, due to their ability to direct cellular activities and to bind to cell receptors [94]. Integrating GFs into biomaterials may ensure cellular viability, adhesion and stimulation of neurite growth [95, 96]. Some examples of GFs that have been incorporated into drug delivery hydrogels with their respective CNS applications are shown in **Table 2.1**. Also, the flexibility of hydrogels has allowed the production of different shapes of drug loaded-hydrogels, which can be injected or implanted at the injury site. Injectable hydrogels are normally applied to chemically support axonal regeneration through the delivery of GFs, however this technique fails to hold the GFs at the lesion site and the GFs may rapidly degrade after injection. On the other hand, using implanted hydrogels as exogenous GF vehicles it may be advantageous to also physically support cellular function and growing axons at a specific local [97].

Table 2.1 – Exogenous growth factors (GFs) used to enrich (load) different types of hydrogels (natural and synthetic) for central nervous system (CNS) applications (spinal cord injury (SCI) and stroke) and technique of implantation.

Growth Factor	Biomaterial	Type	SCI	Stroke
BDNF	Agarose	Natural	Injectable [98]	
	Hyaluronic acid	Natural	Multi-channels [99]	
	Hyaluronic acid / collagen	Natural		Injectable [31]
BDNF	Hyaluronic acid / collagen	Natural		Injectable [100]
BDNF and GDNF	Poly-ε-caprolactone (PCL)	Synthetic	Injectable [101]	
	Polyethylene glycol (PEG) / poly(lactic-co-glycolic acid) (PLGA) microparticles	Synthetic	Membrane [102]	Injectable [103, 104]
GDNF	Alginate	Natural	Injectable [105]	
NGF	PLGA / fibronectin / lipoplexes	Mixture	Multi-channels [106]	
	Collagen / Matrigel	Natural	Tube [107]	
	Agarose / collagen / laminin	Natural	Cylinder [108]	
	Agarose	Natural	Cylinder [109]	
	Poly(2-hydroxyethyl methacrylate) (HEMA) / methyl methacrylate (MMA)	Synthetic	Multi-channels [110]	
	PEG / Polylactic acid (PLA)	Synthetic	Cylinder [111]	
	Mesoporous silica nanoparticles / collagen	Mixture	Injectable [112]	

	PLGA / ethylene-vinyl acetate (EVA)	Synthetic		Epi-cortical implants [113]
NGF and BDNF	Hyaluronic acid / laminin / retinoic acid	Mixture	Multi-channels [114]	
NGF, BDNF and NT-3	Fibronectin	Natural	Membrane [115]	
	EVA	Synthetic	Cylinder [116]	
NGF and NT-3	HEMA / poly(L-lysine) (PLL)	Synthetic	Cylinder [117, 118]	
NT-3	Collagen	Natural	Injectable [119]	
	Collagen / Chitosan microparticles	Natural		Injectable [120]
	Gelatin	Natural	Tube [121]	
	PLGA	Synthetic	Cylinder [122, 123]	
	PEG / PLA	Synthetic	Tube [124]	
NT-3 and FGF1	HEMA / MMA	Synthetic	Multi-channels [125]	
EGF and FGF1	Collagen	Natural	Injectable [126, 127]	
EGF	HAMC / PEG	Synthetic		Epi-cortical (injectable) [26, 28, 128]
	Chitosan / chitin / PLGA microspheres	Mixture	Multi-channels [129]	
FGF2	Collagen	Natural	Injectable [130]	

	Gelatin	Natural	Injectable [131]	
	HEMA / [2-(methacryloyloxy)ethyl] trimethylammonium chloride (MOETACL)	Synthetic	Injectable [132]	
VEGF and BDNF	Hyaluronic acid / PLGA microspheres	Synthetic	Multi-channels [133]	Injectable [75]
VEGF	Alginate	Natural	Injectable [134]	Injectable [135]
	Poly(dimethylsiloxane–tetraethoxysilane) (PDMS-TEOS)	Synthetic		Injectable [136, 137]
VEGF and Ang1	Hyaluronic acid / PLGA microspheres	Mixture		Epi-cortical implant [138]
rPDGF-A	Hyaluronan / methylcellulose	Natural	Injectable [139, 140]	
PDGF-BB and IGF-1	Methylcellulose / collagen / laminin	Mixture	Tube [141]	
IGF-1 and HGF	Gelatin microspheres	Natural		Injectable [142]

Abbreviations. BDNF: brain-derived neurotrophic factor; GDNF: glial derived neurotrophic factor; NGF: nerve growth factor; NT-3: neurotrophin-3; FGF1: fibroblast growth factor1; EGF: epidermal growth factor; FGF2: fibroblast growth factor2; VEGF: vascular endothelial growth factor; Ang1: angiopoietin-1; rPDGF-A: recombinant rat platelet-derived growth factor-A; PDGF- BB: platelet derived growth factor-BB; IGF-1: insulin-like growth factor-1; HGF: hepatocyte growth factor.

2.4.1. Biomaterials for Stroke

The brain tissue is very delicate and soft, with a Young's Modulus (i.e. elastic modulus) between 1–14 kPa in humans [143], and 0.1–500 Pa in rodents [144]. The brain is heterogeneous and its physical and mechanical properties vary depending on the region and within the same anatomical structure as well [145]. For example, the stiffness and the diffusion

parameters of the brain tissue will depend on the cellular composition of the tissue. The brain is mainly constituted by ECM, which consists primarily of hyaluronic acid, collagen type IV, laminin, fibronectin, and proteoglycans [146]. The injury response in the brain ECM is different from most tissues of the body; in the brain the glial scar is softer than the surrounding healthy tissue, while the scar tissue in other parts of the body is usually stiffer than the healthy tissue. This may be partially due to the lack of fibrous collagen type I in the brain [147].

When designing a biomaterial for brain application it is important to consider the delicate brain tissue and the restricted space of the skull. The exceptional set of design principles for biomaterial depend on the therapeutic approach; however, some characteristics are universal. Some of the characteristics of biomaterials that are significant to consider after injury are the porosity, chemical composition and mechanical properties. The porosity is important to stabilize the damaged tissue by permitting the diffusion of nutrients. Porosity also affects the biomaterial swelling behaviour. Due to the restricted space of the skull the biomaterial must also have a low swelling capacity to avoid increasing intracranial pressure and compressing the brain tissue. Biomaterial interaction with brain tissue is also dependent of the biomaterial' chemical and mechanical compatibility. Mechanically, biomaterials with similar mechanical properties to surrounding environment have been the most successful, showing greater biocompatibility since they are able to mimic the native brain tissue [148-150]. Biomaterials stiffer than the brain tissue stimulated gliosis, while softer ones lead to reduced material stability [68, 151]. Since finding a crude biomaterial with all these desired properties is challenging, physical, mechanical and chemical properties of the biomaterial can be modified to achieved that.

Biomaterials can be fabricated from both natural and synthetic materials. Natural polymers have improved biocompatibility due to similarities with ECM in the body [152].

Naturally derived polymers can have intrinsic bioactivity, eliminating the necessity for biofunctionalization. However, due to their biological origins, natural polymers are also vulnerable to biodegradation, which may compromise the physical and mechanical stability. The most used natural polymers in neural TE are collagen, hyaluronic acid, fibrin, laminin, methylcellulose, chitosan, and alginate [28, 71, 74, 75, 153]. Typically, synthetic biomaterials are biologically inert and consequently have weak cell adherence. However, synthetic biomaterials are generally chemically stable and can easily be adjusted (e.g. mechanical properties) for stroke applications. Several synthetic biomaterials for the brain have been studied, such as pHPMA, pHEMA, PEG, PLA, polyglycolic acid (PGA), PLGA, poly(d-lysine), and PCL [69, 154].

Overall, biomaterials can be used in stroke treatments to: (1) bypass the BBB, (2) provide localized and controlled drug delivery, (3) increase drug stability, (4) support and protect NSPCs, and (5) create a suitable environment for new neural tissue formation. Several strategies have been investigated involving the direct delivery of drugs, mainly GFs, and the development of drug carriers, such as biomaterials, to promote neural regeneration after stroke [30, 155]. The two main strategies for the drug delivery to the brain are the intracranial and epi-cortical direct delivery (**Figure 2.3**). In order to bypass the BBB, in the intracranial or intracerebroventricular delivery a needle is used to inject the drug delivery biomaterial directly or closer to the brain injury site (**Figure 2.3A**). While by the intracranial injection a higher concentration of molecules can be reached, this approach is limited by the risk of infections and further tissue damage due to the insertion of needles, catheters and minipumps. Meanwhile, epi-cortical delivery has been investigated as an alternative strategy to delivery drugs to the brain [28, 156]. To avoid further tissue damage, in the epi-cortical delivery a drug-loaded biomaterial is inserted or injected onto the surface of the brain (**Figure 2.3B**). The

biomaterial would release the drugs, which would diffuse through the brain tissue to reach the NSPCs located in the SVZ. One possible limitation of this strategy is the limited range of the bioactive molecule penetration into the brain tissue [157, 158]. However, some studies have shown that drugs delivered epi-cortically were able to penetrate the post-stroke area and stimulate NSPC proliferation [26, 156]. Some examples of biomaterials used for direct delivery of bioactive molecules into the brain are shown on **Table 2.1** (above).

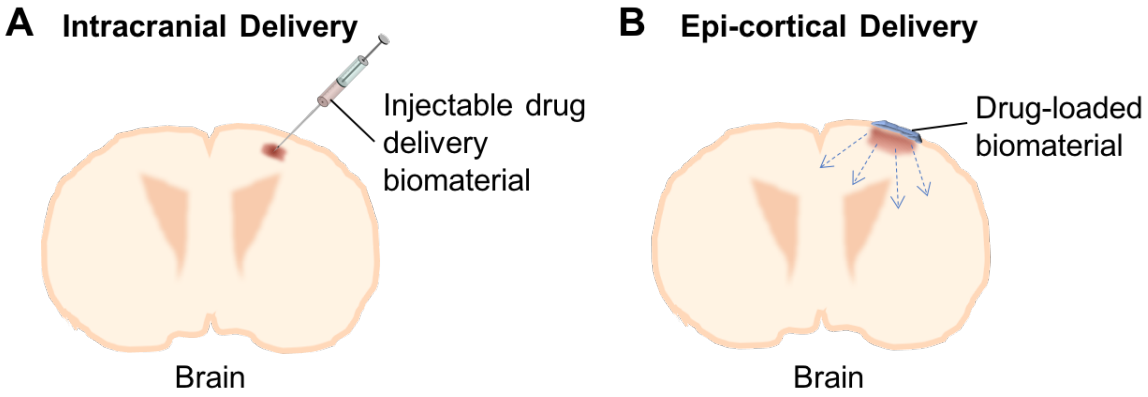

Figure 2.3 – Two techniques to delivery drug to the brain: intracranial delivery (**A**) and epi-cortical delivery (**B**).

Ju et al. recently reported local delivery of vascular endothelial growth factor (VEGF) and angiopoietin-1 (Ang1) incorporated into PLGA microspheres, that were mixed with modified hyaluronic acid (HA) hydrogel [138]. The HA hydrogel was further modified by binding with the antibody of Nogo receptor (NgR-Ab) to promote neural regeneration. The modified hydrogel containing the GFs-loaded microspheres presented good responses for the survival and proliferation of human umbilical artery endothelial cells (HUAECs) and NSPCs, when cultivated *in vitro*. In addition, when the drug-loaded biomaterial was implanted in mouse stroke model showed to have good biocompatibility, promoted angiogenesis, and inhibited gliosis and inflammation [138].

In another study to delivery drugs to the NSPC site, Cook et al. produced hyaluronan and methylcellulose (HAMC) hydrogels and incorporated EGF or modified poly(ethylene glycol)-modified EGF (PEG-EGF) into the hydrogels. The loaded hydrogel was epi-cortically implanted on mouse brains after stroke. Interestingly, the EGF modified with PEG showed a higher tissue penetration depth, while maintaining bioactivity, relative to EGF alone [28, 128]. Moreover, Cooke et al. and Wang et al. demonstrated that EGF [28] and EPO [159], respectively, were able to penetrate brain tissue, to stimulate NSPCs proliferation and migration, and to promote tissue regeneration in stroke animal models. In a similar strategy, PEG-EGF and EPO were first encapsulated in PLGA nanoparticles and then EPO-PLGA was coated with poly(sebacic acid). These enriched particles were incorporated in HAMC hydrogel and were able to sequential delivery the EGF-PEG and EPO, which promoted tissue repair in a mouse stroke model [26]. These minimally-invasive systems for the epi-cortically delivery of drugs to the brain show the potential of biomaterial-based local drug delivery systems to bypass the BBB and provide sustained delivery to the SVZ in the brain.

2.4.1. Biomaterials for Spinal Cord Injury (SCI)

Even with recent advances in medicine, spinal trauma remains one of the most tragic traumatic injuries [48]. Lately, several biomaterials, natural and synthetic, both degradable and non-degradable, were explored for supporting the repair of SCI [59, 160]. The most researched natural biomaterials include agarose, alginate, chitosan, collagen, fibrin, fibronectin, gellan-gum, hyaluronan, hyaluronic acid, matrigel, methylcellulose and other proteins derived from the ECM [161]. Common synthetic polymers include calcium sulfate cement,

oligo[poly(ethylene glycol) fumarate] (OPF), PCL, PEG, poly-*b*-hydroxybutyrate (PHB), poly(2-hydroxyethyl methacrylate) (pHEMA), pHPMA, PLA, PLGA, PGA [59, 82, 162, 163], degradable copolymer of PHEMA-*b*-PLA [164], and self-assembling peptides (SAPs) [165].

The effectiveness of the biomaterial implantation at the SCI site is a great challenge due to the complex geometry. In a complete SCI, neural cells encounter an inhibitory environment as well as a physical gap. For the development of implanted hydrogels (i.e. nerve guidance scaffolds) different morphologies have been used, including tubes, channels and cylinders in shapes **Figure 2.4**. While the nerve guidance tubes are hollow tubular bridging scaffolds, the nerve guidance channels are tubes consisting of internal multi-channels, and the nerve guidance cylinders are solid filled cylinders, as can be seen in **Figure 2.4**. Specifically, nerve guidance tubes are used to provide physical support and orientation for the reconnection of the nerve tissue across the lesion. Several different natural and synthetic polymers have been used to prepare neve guidance tubes such as poly(acrylonitrile)(PAN)-poly(vinyl chloride)(PVC) [166], PHEMA [167, 168], poly(α-hydroxy acids) [169], chitosan [170-173], collagen [174, 175], alginate [176], agarose [177], PHB [178, 179], polyvinylidene fluoride (PVDF) [180], and polypyrrole (PP) [181, 182].

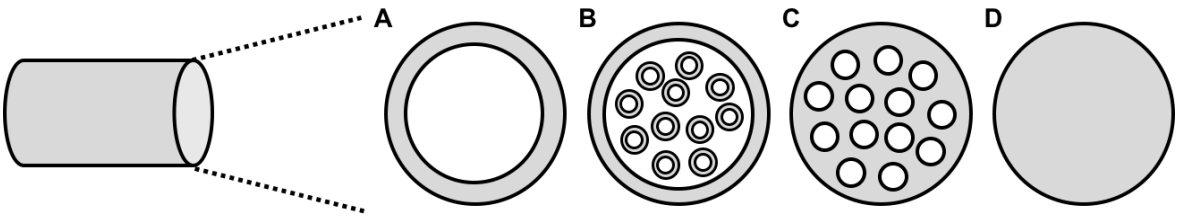

Figure 2.4 – Schematic representation of the cross-section of nerve guidance scaffolds. **A)** Nerve guidance tubes. **B)** and **C)** Nerve guidance channels. **D)** Nerve guidance cylinder.

The physical and chemical structure of these biomaterials affects the regenerative capacity of the implant. Several materials based on type I collagen (NeuroMatrix™, Neuroflex™, NeuraGen® and NeuraWrap™ Nerve Protector), PGA (GEM Neurotube®), poly(L-lactide-co-ε-caprolactone) (PLCL) (Neurolac®), and poly-vinyl alcohol hydrogel (SaluBridge™, nondegradable) have already been approved by the US Food and Drug Administration (FDA) for use in short gap nerve repair [183]. The main application of these materials is in human peripheral nerves, however that increased the interest to apply these nerve guidance tubes to CNS nerve regeneration such as SCI repair [65, 111, 116]. Nonetheless, there is a large necessity for new biomaterials, since no specific biomaterial has established itself as a perfect choice for nervous system regeneration.

Frequently, after a SCI occurs there is a significant loss of neural tissue. Nerve guidance scaffolds can serve as a vehicle for the delivery of cells and other bioactive molecules [52]. For example, the use of exogenous GFs by direct administration or by delivery from scaffolds have been previously studied [184, 185]. Another strategy is the direct implantation of cells to the injury site. The big disadvantages of this strategy are the low cell survival, the uncontrolled differentiation and the short permanency of the cells at the lesion site since they prefer to migrate to neighboring sites [163]. Therefore, a promising strategy to promote neural regeneration after a SCI is the implantation of nerve guidance scaffolds enriched (i.e. loaded) with GFs to promote cell growth at the site of the injury. The most frequently used bioactive molecules for release into a SCI include chondroitinase ABC [186], neurotrophins (BDNF, NT-3, and NGF), and the anti-inflammatory drugs dexamethasone and methylprednisolone [91, 97].

NGF is well known to improve neuronal outgrowth and has been applied as a chemo-attractant to promote axon growth [94, 187]. For example, Lee et al. incorporated NGF into mesoporous silica nanoparticles, which was then combined into collagen hydrogel as an injectable biomaterial. The NGF release was sustained over one week and improved neurite outgrowth of PC12 cells, confirming the effectiveness for neural tissue engineering [112]. Using a different approach, Stokols et al. synthesized nerve guidance cylinders of agarose containing NGF. The system was characterized and the release and bioactive of NGF were studied. NGF was bioactive and stimulated neurite outgrowth of PC12 cells [109, 177]. In both cases, NGF interacted with the biomaterials mainly through electrostatic interactions. In another study, nerve guidance tube made of collagen and Matrigel was loaded with NGF and covered by living dorsal root ganglia (DRG) axons. The scaffold was implanted in a rodent SCI model and after 4 weeks the DRG axons extended out of the scaffold into the host spinal cord tissue [107]. These studies demonstrate the promise of biomaterials constructs containing NGF to promote neural outgrowth and axon guidance for SCI applications; and it was the approached studied in Chapter 4.

Many papers have addressed TE strategies and offered a comprehensive list of biomaterials for SCI repair [52, 77, 160, 162, 188-192] even clinical trial studies [193, 194]; however there have been no reports in the literature about the application of GF-loaded biosynthesized cellulose tubes (BCTs) for the treatment of SCI as can be seen in **Table 2.1** (above).

2.4.1. Drug Delivery Mechanisms for Hydrogels

Hydrogels are soft tissue biocompatible polymers and may provide a valuable vehicle for drug delivery since bioactive molecules can be easily dispersed within the hydrogel network [15,

69, 81]. Drug delivery systems can be engineered and studied in a variety of mechanisms. Langer et al. categorized the mechanisms of the drug delivery systems into diffusion-controlled, chemically controlled, and swelling-controlled [195]. Among these, diffusion-controlled and swelling-controlled systems have been widely studied experimentally and also mathematically. However, significantly absent from most of the models is the ability to predict burst release [196].

Burst release is a nonstady-state and high-rate release of molecules that mostly is seen at the beginning of the controlled release process, immediately upon placement in the release media [197]. Burst release has been attributed to a variety of physical, chemical and processing parameters. Some of the reasons that can cause burst release are: desorption of the drugs entrapped on the surface of gels [198], poor distribution of drugs within the hydrogel network during formation, drying, or storage [199], heterogeneous nature of polymer network [200] or percolation-limited diffusion of entrapped materials [201].

Because burst release happens in a very short time compared to the entire release, it has not been specifically investigated in most published results, and it has been ignored in most mathematical models. The burst effect can be viewed from two perspectives: it is often considered as a negative phenomenon due to the initial high release rates that may lead to toxicity or tissue irritation in the human body [197, 202] or, in certain situations, rapid release or high initial rates of delivery may be desirable. Huang and Brazel have shown that dry samples can magnified burst effects, but prolonged the release process [197]. Zero order sustained release is often the target of drug delivery and many researchers have taken novel methods to design drug delivery vehicles in order to achieve the sustained release profile [203, 204].

Zero order model [204]: Defines the process of constant drug release from a drug

delivery system and drug level in the media. It investigates the concentration-independent drug release rate from the formulation. Zero order model can be represented by the equations:

$$Q_0 - Q_t = K_0 t \quad (1)$$

$$Q_t = Q_0 + K_0 t \quad (2)$$

Q_t is the amount of drug released at time t,

Q_0 is the initial amount of drug in solution, usually equal zero,

K_0 is the zero order release constant.

In diffusion-controlled systems, a substance is released from a device by permeation from its interior to the surrounding medium [205]. In these systems of polymeric matrices drug diffusion is the rate-limiting step. A variety of models have been developed to predict release profiles in these systems [195, 205]. Release behavior from monolithic dispersion systems consisting of dispersed solid release agent was modeled by Higuchi [206-208].

Higuchi model [206, 207]: This simple and classic model is considered one of the widely used and the most well-known controlled-release equation, but the burst stage is usually not explicitly defined. The classical basic Higuchi equation is represented by

$$Q = A\sqrt{D(2C_0 - C_s)C_s t} \quad (3)$$

where Q is the cumulative amount of drug released in time t per unit area, C_0 is the initial drug concentration, C_S is the drug solubility in the matrix and D is the diffusion coefficient of the drug molecule in the matrix.

This relation is valid until total depletion of the drug in the dosage form is achieved. To study the dissolution from a planar heterogeneous matrix system, where the drug concentration in the matrix is lower than its solubility and the release occurs through porous system, the expression can be given by equation (4).

$$Q = \sqrt{(D\delta/\tau)(2C - \delta C_s)C_s t} \quad (4)$$

where D is the diffusion coefficient of the drug molecule in the solvent; δ is the porosity of the matrix; τ is the tortuosity of the matrix and Q, A, C_s and t have the meaning described above.

Tortuosity is defined as the dimensions of radius and branching of the pores and canals in the matrix. After simplifying the above equation, Higuchi equation can be represented in the simplified form

$$Q = K_H t^{1/2} \quad (5)$$

where, K_H is the Higuchi dissolution constant.

Higuchi model is used to investigate the drug release from the matrix based on Fickian diffusion. It is important to note that a few assumptions are made in this Higuchi model. These assumptions are:

i. The initial drug concentration in the system is much higher than the matrix solubility
ii. Perfect sink conditions are maintained
iii. The diffusivity of the drug is constant
iv. The swelling of the polymer is negligible.

In the strictest interpretations for diffusion-controlled systems, most models assume that the polymeric membranes or matrices do not change during the release process. However, for the swelling-controlled systems, absorption of solvent (water) leads to polymer expansion and thus different release kinetics [205], where convective transport of water is combined with Fickian diffusion to determine the overall release profile. The release rate is determined by the rate of diffusion of fluid in the polymer and its macromolecular relaxation [209]. The drug release in a swelling-controlled system is typically non-Fickian in nature, which is frequently expressed by the classic equation for fractional release, Korsmeyer-Peppas model, Eq. (6)

[210-213]. The value of n in this equation describes the relative importance of Fickian, a value of n < 0.5/0.45/0.43 for a slab/cylinder/sphere indicates a diffusion controlled drug release. When n > 1/0.89/0.85 for a slab/cylinder/sphere, the drug release behavior is called case-II transport. In contrast, when 0.5/0.45/0.43 < n < 1/0.89/0.85, the drug release behavior is classified as a combination of both phenomenon and is referred to anomalous transport. However, current models for swelling controlled release are not capable of accounting for burst release beyond simplistic equations.

Korsmeyer-Peppas model [212, 213]: A simple relationship which described the drug release from a polymeric system follow which type of dissolution and it is represented by the equation:

$$\frac{M_t}{M_\infty} = K_{kp} t^n \quad (6)$$

M_t/M_∞ is a fraction of drug released at time t,

M_t is the amount of drug released in time t,

M_∞ is the amount of drug released after time ∞,

n is the diffusional exponent or drug release exponent,

K_{kp} is the Korsmeyer release rate constant.

2.5. Biosynthesized Cellulose (BC)

The following section mainly consists of parts of the review paper entitled "*In Situ* and *Ex Situ* Modifications of Bacterial Cellulose for Applications in Tissue Engineering" by Stumpf et al. [214], published in Materials Science and Engineering: C. Formatting, updates (e.g. **Figure 2.6**) and minor modifications (such as figure numbers and labels) were made. A new section (*2.5.2.1. In Situ Modification of Biosynthesized Cellulose – 3D Structures*) was added to provide relevant information to this thesis.

Cellulose $(C_6H_{10}O_5)_n$ is a naturally occurring homopolysaccharide formed by a linear chain of monosaccharide β-D-glucose linked by β(1→4) bond. The repeating unit is cellobiose formed by the union of two glucose molecules (**Figure 2.5A**). Cellulose is the most widespread naturally occurring material on earth, with a biomass production estimated to be about 1.5×10^{12} tons annually [215]. It is an important structural component found in cell walls of green plants and some species of bacteria also produce cellulose (i.e. biosynthesized cellulose or bacterial cellulose, BC) in the form of biofilm [215]. While it is necessary to employ different chemical treatments to obtain pure cellulose from plants [216], BC is readily produced in pure form and does not contain any other compound present in the plant pulp or from animal origin [217].

BC was originally discovered in the 1880s by A. J. Brown [218, 219] and it is produced by a few genus of bacteria, such as *Agrobacterium*, *Alcaligenes*, *Pseudomonas*, *Rhizobium*, *Sarcina,* and *Gluconacetobacter* [217, 220]. The bacteria secret the cellulose chains outside of the cells, which form elementary sub-fibers, subsequently the sub-fibers are then linked together by hydrogen bonding to form microfibrils. Ultimately microfibrils are organized together to form ribbons [221]. BC biosynthesis has been extensively documented by Ross et al., who presented an account on BC synthesis "machinery", genetics and its regulatory mechanism in a model organism (*Acetobacter xylinum*), a non-pathogenic bacteria [222, 223]. Recently, many other publications provided overviews of genetic modifications of cellulose producing bacteria, focusing mainly on BC production yields [221, 224-226]; interested readers are referred to consult other excellent studies for examples of genetic engineering approaches to produce BC [227-232].

BC membrane is formed in a structure with asymmetrical layers at the air/liquid interface, resulting in a denser surface where it is in contact with air and a more gelatinous network on the other side where it is in contact with the liquid as illustrate in **Figure 2.5B** [233-237]. After BC synthesis, the membrane is further processed to remove bacterial cells, organic acids, salts as well as residual sugars and other components of the culture media, which could be integrated within the cellulose network. This purification process can be accomplished by various methods, including washing, centrifugation, filtration, and chemical extraction. Among these methods, washing BC with hot and diluted sodium hydroxide solution, rinsing with distilled water, and finally sterilizing the BC by autoclaving is commonly used [234, 238-240]. **Figure 2.5C** shows a BC membrane obtained by washing with 0.1M NaOH at 50 °C followed by extensive washing with distilled water. It should be noted that there are no reports in the literature concerning the presence of pathogen-associated molecular patterns in the purified BC; in fact, it will become clear later in this thesis that BC has been shown to be biocompatible. It is believed that bacteria produce cellulose biofilms in order to protect the organisms from ultraviolet radiation and other chemical or mechanical insults to the bacteria [222], as well as to improve nutrient transport [241].

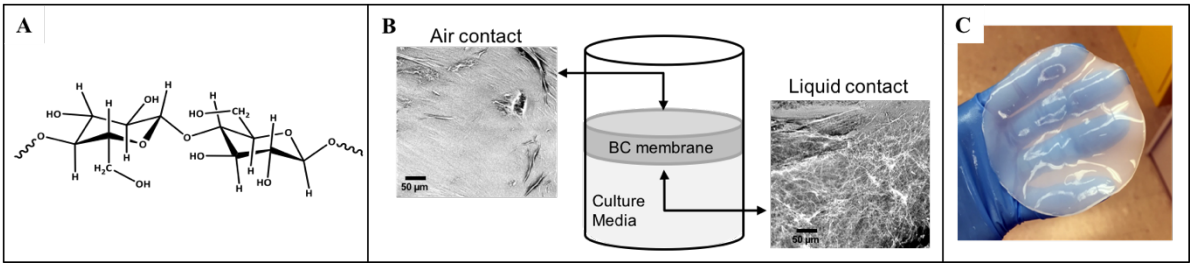

Figure 2.5 – Biosynthesized cellulose **(**BC) structure and morphology. **A)** Chemical structure of cellulose. **B)** SEM micrographs of BC membrane showing the difference of fibers density depending on surface contact (e.g. air or liquid). **C)** Photograph of a BC membrane after purification. *From personal files and [214].*

Unmodified BC has unique physical and mechanical properties not displayed by other biomaterials, such as high purity, ultrafine fibrous network structure with a variable pore geometry [242, 243], high water holding capacity (absorbing over 100 times of its own weight in water) [244-246], high degree of crystallinity (i.e. 84-89%) [247], broad chemical and physical modifying ability [248, 249], and the ability to be molded into different structures [250]. Moreover, BC membranes and fibers have Young's modulus of 15-18 GPa and 78 GPa, respectively [241, 251].

2.5.1. Biosynthesized Cellulose in Tissue Engineering

The first documented BC applications in biomedical were reported by a Brazilian company in 1986, 1989, and 1990 in a series of patents (see patents WO 08602095, WO 08908148 and US 4912049) that discussed the applications of Biofill® in different TE applications, such as skin substitutes for burns and ulcers [252]. In parallel, Johnson & Johnson explored the use of BC as a liquid loaded pad for wound care in 1986 and 1987 (see patents US 4588400 and US 4655758). Subsequent studies investigated biocompatibilities of BC using L929 cells (mouse fibroblasts cells) [253] and in rats [234]. Recently more extensive studies on BC have been conducted, and its full potentials in TE applications have started to be gradually realised [254-256]. However, its potential as a biomaterial in TE applications has not yet been fully explored. As shown in **Figure 2.6**, there is a significant difference between the number of annual publications when "bacterial cellulose" was used as a keyword and those when "bacterial cellulose" + "tissue engineering" were used (data obtained from Web of Science in February 2019). A closer look at the publications of BC with TE applications reveals that the majority of these papers mainly deal with investigations to modify BC scaffold porosities, introducing

functional groups and/or antimicrobial molecules, increasing BC degradation rates, and enhancing BC biocompatibilities.

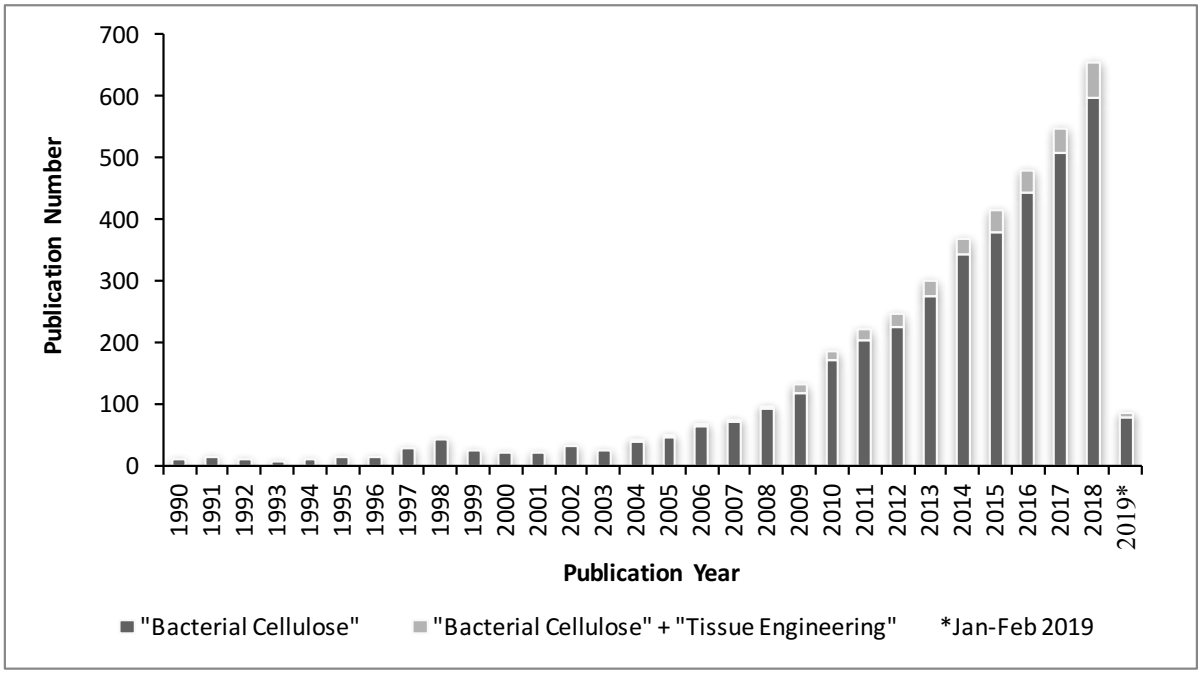

Figure 2.6 – Annual publications on biosynthesized cellulose (BC) and BC with tissue engineering applications from 1990 to February 2019. Search engine used Web of Science™, search term "bacterial cellulose" and "bacterial cellulose" with refined topic "tissue engineering". *Adapted from [214].*

Due to its structural similarities to ECM components, BC has been reported to show good biocompatibilities. For example, using MTT assay and confocal imaging, Recouvreux et al. showed that human vein endothelial cells proliferated and migrated vertically into a BC hydrogel [250]. In addition, Zang et al. studied the differentiation of human adipose-derived mesenchymal stem cells (HASCs) cultured on BC, and showed that the HASCs were successfully differentiated into osteoblasts and formed a consistent layer of osteoblasts on the BC [257]. Moreover, BC scaffolds seeded with the HASCs were implanted into ulna defects of rabbits, and significant mineralization was observed in the defects after 8 weeks when

compared with the control group; the researchers also noted that there were no signs of any inflammation responses [257].

Furthermore, BC has been used in many other *in vivo* studies. In a meticulously designed study, Helenius et al. subcutaneously implanted BC membranes on the back of Wistar rats, and subsequently evaluated host responses to the implanted BC material in terms of foreign body reactions, chronic inflammation, angiogenesis, and cell growth for a period of 12 weeks. The study showed that BC was fully integrated within the host tissue and did not induce any inflammation or rejection during the course of the study. **Table A.1** (Appendix A) summarizes findings described above. Indeed, many studies have demonstrated that BC can be well integrated with host tissues for many different TE applications, as can be seen in **Table A.2** (Appendix A). **Figure 2.7** shows the applications of BC biomaterials as soft and hard tissues.

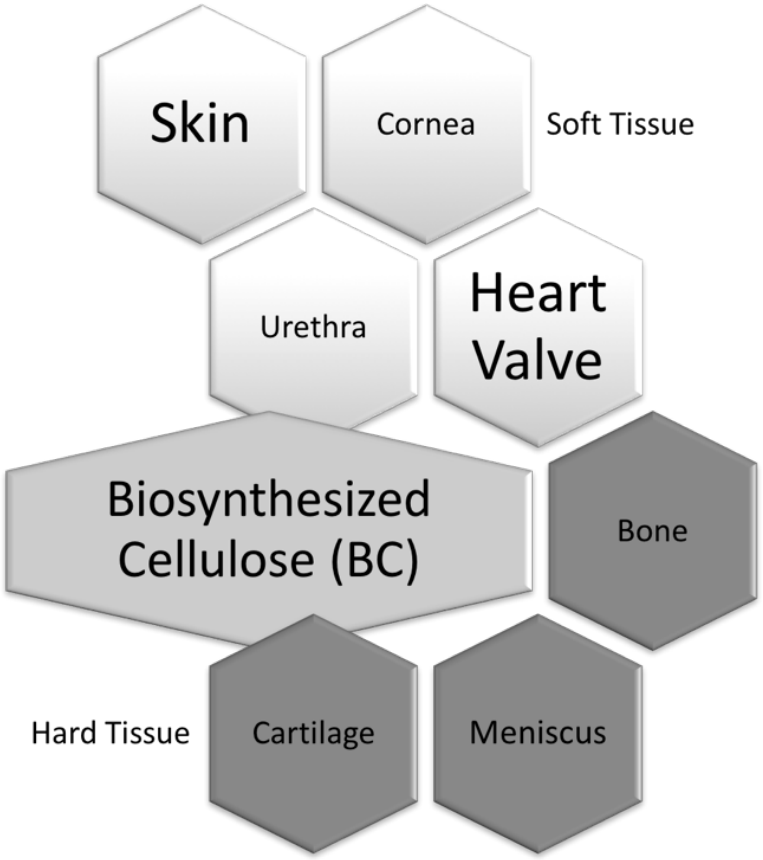

Figure 2.7 – Examples of tissue engineering applications of biosynthesized cellulose (BC) biomaterials as both hard (dark grey) and soft tissues (light grey).

2.5.2. Modified Biosynthesized Cellulose for Applications in Tissue Engineering

Despite recent advances, there are still many challenges to overcome before the full potentials of BC can be completely realized as a choice of material in TE applications. These challenges include optimizing culture conditions to control porosities of BC scaffold, introducing functional groups to BC matrix, and increasing BC degradation rate for specific applications [258-260]. To achieve these goals, BC has been modified using different methods, such as chemical modifications: modification of the chemical structures and functionalities, and physical modifications: modification of the 3D structures, porosities, crystallinities, and fiber densities. In general, there are two main strategies to implement these modifications: *in situ*

and *ex situ* methods (**Figure 2.8**). *In situ* modification is to modify BC during bacterial cell culture by varying the culture conditions (e.g. static or agitated condition), adding additional materials such as additives or reinforcement materials to the culture, or changing the carbon source and fermentation containers, which may or may not cause chemical changes in the resulting BC (see **Figure 2.8A**). In contrast, *ex situ* modification of BC is carried out after the BC has been formed, and it is done by either chemical or physical methods (see **Figure 2.8B**).

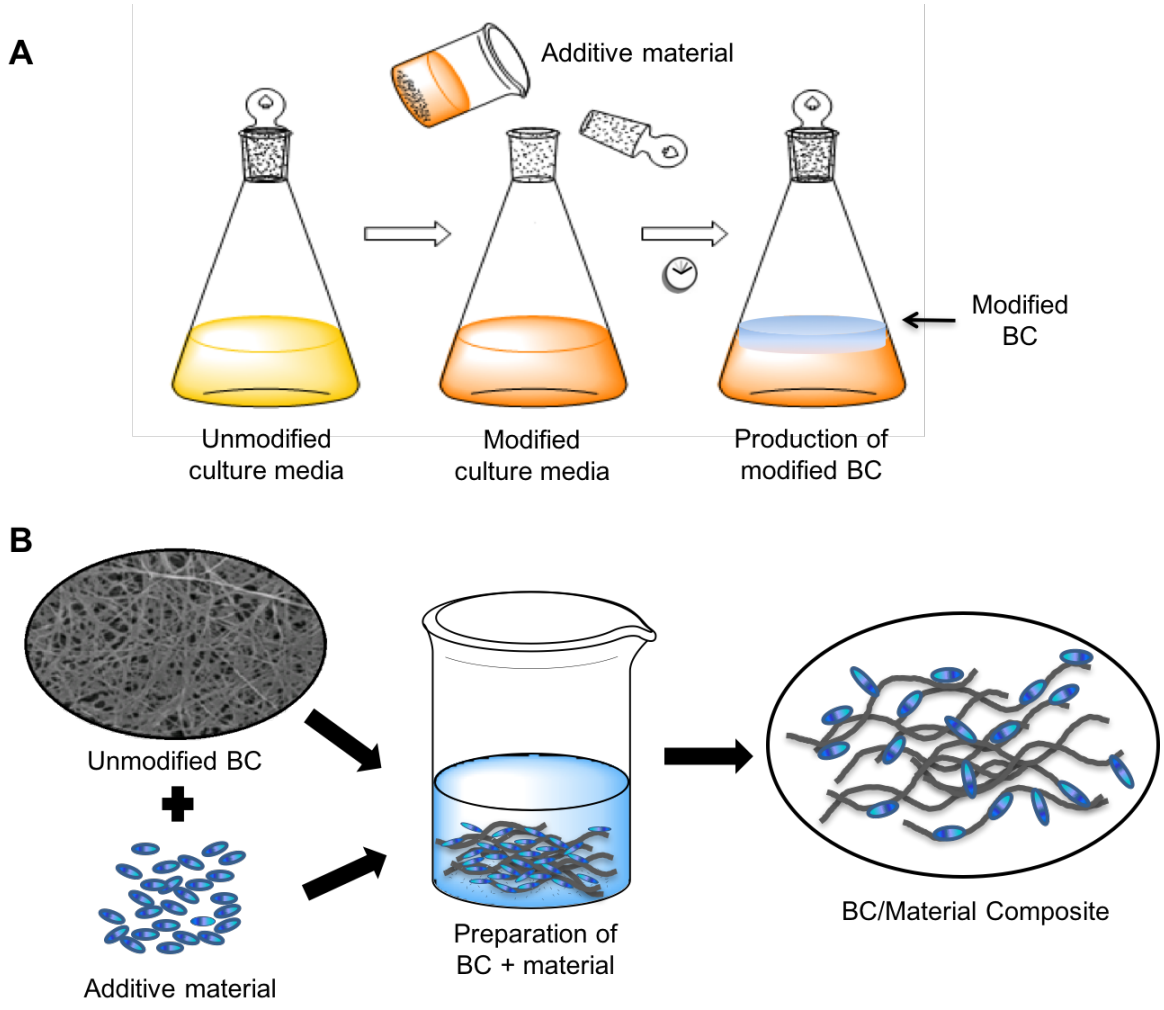

Figure 2.8 – Schematic representation of biosynthesized cellulose (BC) modification methods. **A)** *In situ* modification of BC, in which the culture media composition is changed, usually with the addition of other materials, i.e. additive/reinforcement material. **B)** *Ex situ* modification, in which BC is modified by chemical treatment or absorption of others materials after the BC membrane has been formed in culture. *From [214]*.

There are many studies describing *in situ* [246, 261-265] and *ex situ* [246, 247, 266-278] modifications of BC; however there are few research focusing on TE applications of these new composites. In the following sections, *in situ* modifications for preparation of different 3D structures and *ex situ* modification by physical methods for applications in TE are discussed.

2.5.2.1. *In Situ* Modification of Biosynthesized Cellulose – 3D Structures

In situ modification represents a common and important modification method of BC. This modification method can change mechanical properties as well as micro- and macro-structures, which are influenced by bacterial culture conditions [221, 279-282]. BC is traditionally produced in static culture using cellulose-producing strains, which produce a cellulose membrane on the media surface as shown in **Figure 2.5** (above). The production process is simple, inexpensive, and widely used [283, 284]. BC produced in static culture has various biomedical applications, such as in the regeneration of periodontal tissues [285], in the repair of abdominal defects [286], as a replacement for dura mater [287], and in the treatment of chronic wounds and burns [252, 288].

Biosynthesized cellulose can be produced in different shapes and molded into 3D structures during *in vitro* culture, depending on the production method chosen (e.g. static culture, agitated culture or airlift reactor) [235, 250, 289, 290]. For example, when the cellulose-producing bacteria is cultivated under agitated conditions, it produces a network of cellulose fibers with different characteristics and forms compared to those produced under

static conditions [291-293]. Furthermore, when cultivated statically the BC membrane (**Figure 2.9A**) is accumulated on the surface of the culture media (**Figure 2.5B**, above), otherwise when in agitated culture 3D BC structures are formed inside the media, probably result from the shear force produced during agitation culture, which cause the intertwine of cellulose ribbons [258, 294, 295]. Examples of forms obtained in the agitated culture are the spherical (**Figure 2.9B**) [294, 296] and cocoons – large 3D hydrogels of BC (**Figure 2.9C**) [250, 297].

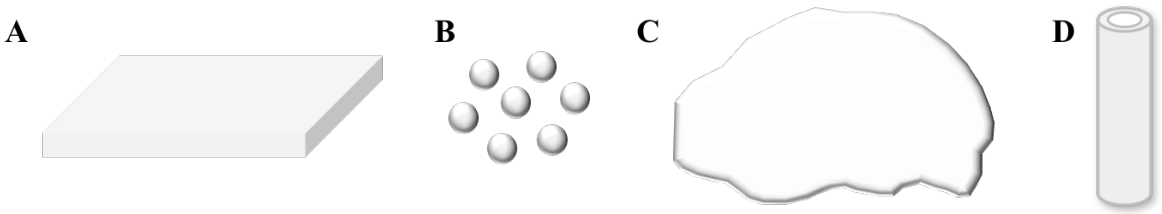

Figure 2.9 – Different shapes of biosynthesized cellulose (BC). **A**) BC membrane. **B**) Spherical BC. **C**) BC cocoon-like – large 3D hydrogel of BC. **D**) BC tube (BCT).

Another structural modification of BC which has been studied for biomedical applications is the tubular form (biosynthesized cellulose tubes – BCTs, **Figure 2.9D**). This form has been suggested for use as a blood vessel substitute [234, 298, 299], vascular grafts [300-304], biofiltration [305], and nerve regeneration [215, 306, 307]. For the formation of BCT, Bodin et al. developed a vertical bioreactor where silicone tubing was used as a shape template [302, 308]. The silicone tubing allows for oxygen diffusion to the bacteria inside the media. Studies of the structure revealed that the outer side of BCT was more porous than the inner side, and the cross-section revealed that the biomaterial was composed of layers. The number of BCT layers and the cellulose yield increased with an increase in the concentration of oxygen in the media. In addition, Bodin et al. studied the *in vitro* biocompatibility of BCTs with endothelial cells, which formed a confluent layer on the surface of the tube after 7 cultivation days [302]. In another study, BCTs have shown good biocompatibility when they

were cultured with primary Schwann cells and were implanted in a sciatic nerve injury model in Sprague Dawley rats for 6 weeks [307]. Moreover, to evaluate BCT as a potential substitute for small-diameter blood vessels, BCTs were used to replace carotid arteries in Texel sheep for a period of 12 weeks [298]. It was observed that a confluent endothelial cell layer without any signs of inflammation was formed along the BCTs and that vascular smooth muscle cells migrated into the BCT matrix [298]. Similar results were also observed in a study by Kowalska-Ludwicka et al. who used BCTs for peripheral nerve regeneration for a period of 6 months [306].

2.5.2.1. *Ex Situ* Modification of Biosynthesized Cellulose – Physical Modification

Biosynthesized cellulose is a biopolymer that can be subjected to almost all techniques used for polymer modifications [280]. In *ex situ* modifications, BC polymer matrix is impregnated with different materials to modify BC membranes (**Figure 2.9A**, above), and this usually happens after the BC purification process. Physical *ex situ* modification is commonly done through physical absorption – porous BC matrix can be filled with solutions or particle suspensions – the presence of hydroxyl groups in the cellulose chains often results in strong hydrogen bonding between the BC molecules and absorbed molecules [221]. The *ex situ* modification through absorption is much simpler and more versatile than the *in situ* modification method [249].

In order to enhance BC cell–biomaterial interactions, BC and silk fibroin (SF) were prepared using a physical *ex situ* modification method by Barud et al. [309]. More specifically, BC membranes were soaked into different SF solutions of 25 %, 50 %, and 75 %, after 24 h

the BC composites were removed and freeze-dried. SEM results revealed a well inter-connected porous network structure. The best result achieved was with 50 % fibroin content (BC/SF50), where the equal ratio offered a synergistic effect while preserving individual properties of BC and SF. It was further demonstrated that BC/SF50 scaffolds improved cell adhesion and proliferation in comparison with pure BC. Furthermore, cytotoxicity and genotoxicity tests showed that the BC/SF50 composite was non-cytotoxic and non-genotoxic, suggesting its potential applications in biomedical applications [309]. Similarly, Gao et al. investigated poly(ethylene glycol) 400 (PEG400) absorbed into BC sponge [310]. The resulting sponge exhibited high surface area, high porosity, and excellent biocompatibility as shown by MTT assays with mesenchymal stem cells [310].

To incorporate antibacterial properties into BC, sodium alginate (SA) and silver sulfadiazine (AgSD) were used to prepare BC films [311]. Biosynthesized cellulose was synthesized in a static *Acetobacter xylinum* culture. Subsequently, the BC membranes were sliced and compressed to form BC slurry. The BC/SA was prepared by mixing BC slurry with SA solution (2.0 %, w/v), to which AgSD was added; finally, the mixture was crosslinked by calcium chloride ($CaCl_2$). The resulting BC/SA–AgSD composites showed excellent antimicrobial performances against *Escherichia coli*, *Staphylococcus aureus* and *Candida albicans* while MTT assays suggested good biocompatibility with human embryonic kidney cells. These results demonstrated that BC/SA–AgSD composites could potentially be used as a wound dressing material [311]. Similarly, benzalkonium chloride [312] and polyvinyl alcohol (PVA) with potassium sorbate [313] were absorbed into BC film to introduce antimicrobial activities to BC [312]. In another study, PVA was used to produce BC/PVA composite, which was used to further produce an antimicrobial composite comprising potassium sorbate. The antimicrobial properties of the composite was tested against

Escherichia coli and showed antimicrobial activities that positively correlated to the concentration of potassium sorbate used in the BC composite [313].

Nanostructures of BC membranes can act as a template in the synthesis of a variety of nanomaterials, such as silver nanoparticles (AgNPs), which have been known to introduce antimicrobial properties to BC through *ex situ* modifications. These nanostructures of BC membranes play a crucial role in the formation of AgNPs by acting as both nano-reactors for nanoparticle nucleation/growth and particle-size restrictor to limit out-of-control growth of the particles, producing small size nanoparticles with a well-controlled narrow particle size distribution. For example, Yang et al. prepared a BC membrane impregnated with AgNPs (BC/AgNPs) by initially immersing the BC membrane in silver nitrate ($AgNO_3$) solution after which the impregnated silver ions (Ag^{+1}) were reduced to Ag^0 particles [314]. Antimicrobial properties of the BC/AgNPs was tested against *Escherichia coli* and *Staphylococcus aureus*. The results showed that the BC/AgNPs composite exhibited clear inhibition zones against both model bacteria tested (i.e. 2 mm for *E. coli*. and 9 mm for *S. aureus*), while no inhibition zone was observed for native BC [314]. Similar methods were described in others studies which showed comparable antimicrobial results [315-317].

In order to better disperse nanoparticles inside of 3D BC matrix, ultrasonic sound has recently been used to assist BC *ex situ* modifications. For example, ultrasound has been used to prepare zinc oxide (ZnO) nanoparticle loaded BC nanocomposite for antimicrobial applications [318, 319]. In a study by Katepetch and colleagues, ZnO nanoparticles were synthesized and simultaneously incorporated into a 3D BC matrix by ultrasound treatement that was believed to deliver activation energy to convert zinc ion precursor (i.e. $Zn(OH)_2$) to ZnO nanoparticles [318]. In a separate study, Jebel et al. used ultrasound to evenly and more effectively incorporate ZnO nanoparticle dispersion into BC membranes [319]. While this

study was mainly targeted for BC application in packaging industry, similar methodology could have been used to prepare BC scaffold with antimicrobial properties for TE applications. In fact, Luan et al. used ultrasonication-assisted process to synthesize silver sulfadiazine impregnated BC membrane, in an attempt to prepare an antimicrobial dressing material for wound treatment [320].

Growth factors have also been incorporated into BC scaffolds. In an interesting study to promote bone regeneration, Shi et al. loaded BC scaffold with bone morphogenetic protein-2 (BMP-2) to study the possibility of using BC scaffold as a localized GF delivery system for bone TE [321]. The data showed that BC scaffolds loaded with BMP-2 induced *in vitro* differentiation of mouse fibroblast-like C2C12 cells into osteoblasts and that the osteogenic activity of induced osteoblasts was positively correlated to BMP-2 concentrations used to prepare the BC scaffolds, as demonstrated by alkaline phosphatase (ALP) activity assays. In addition, *in vivo* data further suggested that BC scaffolds with BMP-2 showed more bone formation and higher calcium concentration than blank BC scaffolds 2 and 4 weeks post implantations [321]. Similarly, attachment of RGD-containing peptides to BC hydrogels have shown to greatly improve endothelial cell adhesion and growth in tissue scaffolding applications [285, 322-329]. These studies suggest that once properly designed, BC scaffolds can also be used as drug delivery vehicles for GFs and peptides in TE applications.

2.6. Peptides

Peptides are molecules that contain two to tens of amino acids. A large diversity of biochemical processes and physiological functions depend on them. Synthetic peptides are used to mimic the biological functions of natural peptides, which are short chains of amino acid monomers

(i.e. non-repeating unit) linked by peptide bonds. The carboxyl group (-C(=O)OH) of one amino acid (**1**) reacts with the amine group ($-NH_2$) of another amino acid (**2**) forming a covalent chemical bond called peptide bond (**3**) (**Figure 2.10**). The 20 different amino acids differ in their side-chain functionalities and own different polarities that are essential for their biological function [330].

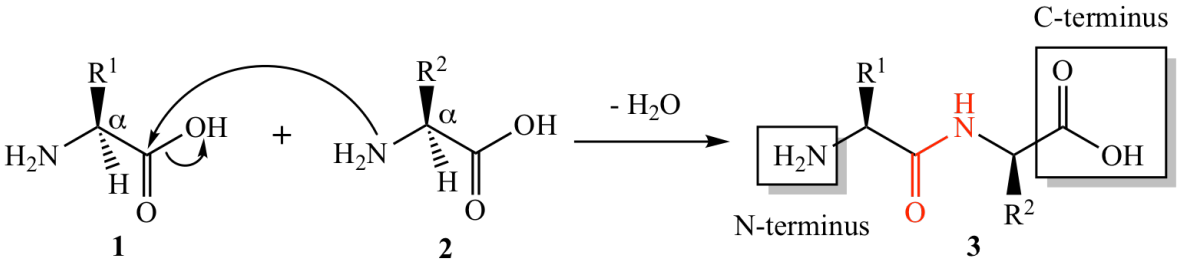

Figure 2.10 – Formation of a peptide (**3**). Reaction of the carboxyl group of amino acid (**1**) with the amine group of amino acid (**2**) resulting in a peptide bond (in red, **3**).

Peptides have diverse biological functions, one of which is cell signaling role aiming to deliver and translate the biochemical "message" that activates molecular, structural, cellular, and biological outcomes. Many peptides act as hormones and neurotransmitters, while others act as neuropeptides, toxins, or as natural antibiotics [331]. These peptides have a large variety of sizes, for example, the neurotransmitter leu-enkephalin has 5 amino acids residues, the antibiotic gomesin 18 and the hormone calcitonin has 32 residues, what characterize the extensive variety of functions of peptides. Because the broad range of functions, peptides are promising biomolecules for the medicinal market [332]. In fact, several endogenous peptides are commonly used as therapeutics, for example: insulin (diabetes treatment), oxytocin (labor and lactation induction) and calcitonin (osteoporosis and hypercalcaemia).

In 1963, Merrifield [333] developed a novel solid phase peptide synthesis technique, which was based on the employment of coupling reagents as well as the mixture of temporary protecting groups (TPGs) and permanent protecting groups (PPGs) to control the peptide

formation. Each peptide sequence was generated in steps on an insoluble polymeric solid support, called resin, involving the sequential addition of protected amino acids [334]. When an amino acid is incorporated into a peptide for the formation of the peptide bond the amino acid releases either a hydrogen ion from the amine end, or a hydroxyl ion from the carboxyl end, or both together as a water molecule. This method was called Solid Phase Peptide Synthesis (SPPS), since the peptide is synthesized in two phases, an insoluble solid support and liquid soluble reagents. **Table 2.2** shows the amino acids and their respective protective groups that were used in Chapter 5.

Table 2.2 – Chemical structures, codes and side chain protection groups of amino acids.

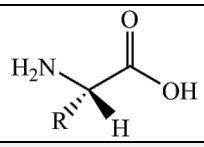

Amino acid	Three-letter code	One-letter code	Side-chain (R)	Permanent protecting group (PPG)	Temporary protecting group (TPG)
Glycine	Gly	G	H-	-	Fmoc
Aspartic Acid	Asp	D	HOOC-CH_2-	O*t*Bu	
Lysine	Lys	K	H_2N-$CH_2CH_2CH_2CH_2$-	Fmoc	
Arginine	Arg	R	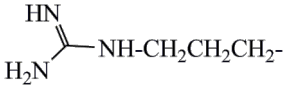	Pbf	
Serine	Ser	S	HO-CH_2-	*t*Bu	
Cysteine	Cys	C	HS-CH_2-	Trt or Acm	
β-Alanine	β-Ala	βA	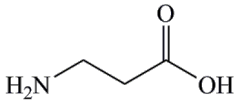	-	
8-Amino-3,6-dioxaoctanoic acid[1]	Adoa	-	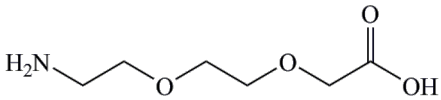	-	

The stereochemistry of all α-amino acids is L-form. [1]Unnatural amino acid. O*t*Bu = *tert*-butyloxycarbonyl, Fmoc = 9-fluorenylmethoxycarbonyl, Pbf = 2,2,4,6,7-pentamethyldihydrobenzofuran-5-sulfonyl, *t*Bu = *tert*-butyl, Trt = trityl, Acm = acetamidomethyl.

The principles of SPPS are illustrated in **Figure 2.11**. The amine group of one amino acid (**1**) is linked to the carboxyl group of the other (**2**). However, a single product can be formed only if one amine group and one carboxyl group are available for reaction. Therefore, it is necessary to protect some groups and activate others to avoid undesirable reactions [333]. The carboxyl group of the amino acid (**1**) is activated by a reaction with a coupling reagent, and then is coupled to a resin - polymer particles that protects the amino acid C-terminus from side reactions. The α-amine group of the amino acid (**1**) is protected by a temporary protecting group (TPG_1) that can be easily removed, and its side-chain functional groups must be masked with permanent protecting groups (PPG_1), which are stable under the reaction conditions used during peptide synthesis. The TPG_1 of the amino acid (**1**) is removed, then the free amine group attacks the activated carboxyl group of the other amino acid (**2**), leading to a peptide bond. After coupling, the excess reactants are removed through filtration and washings. These processes (deprotection, activation and coupling) are repeated until the desired peptide chain is obtained. In a final step, the peptide is released from the resin and the side-chain PPG is removed [333]. The SPPS approach is advantageous due to the use of a solid phase (resin), which can be washed several times after each reaction step removing any impurity or reagent excess. The crude product can be purified using standard analytical methods such as chromatographic techniques, and can be identified using mass spectrometry (MS) [330, 335].

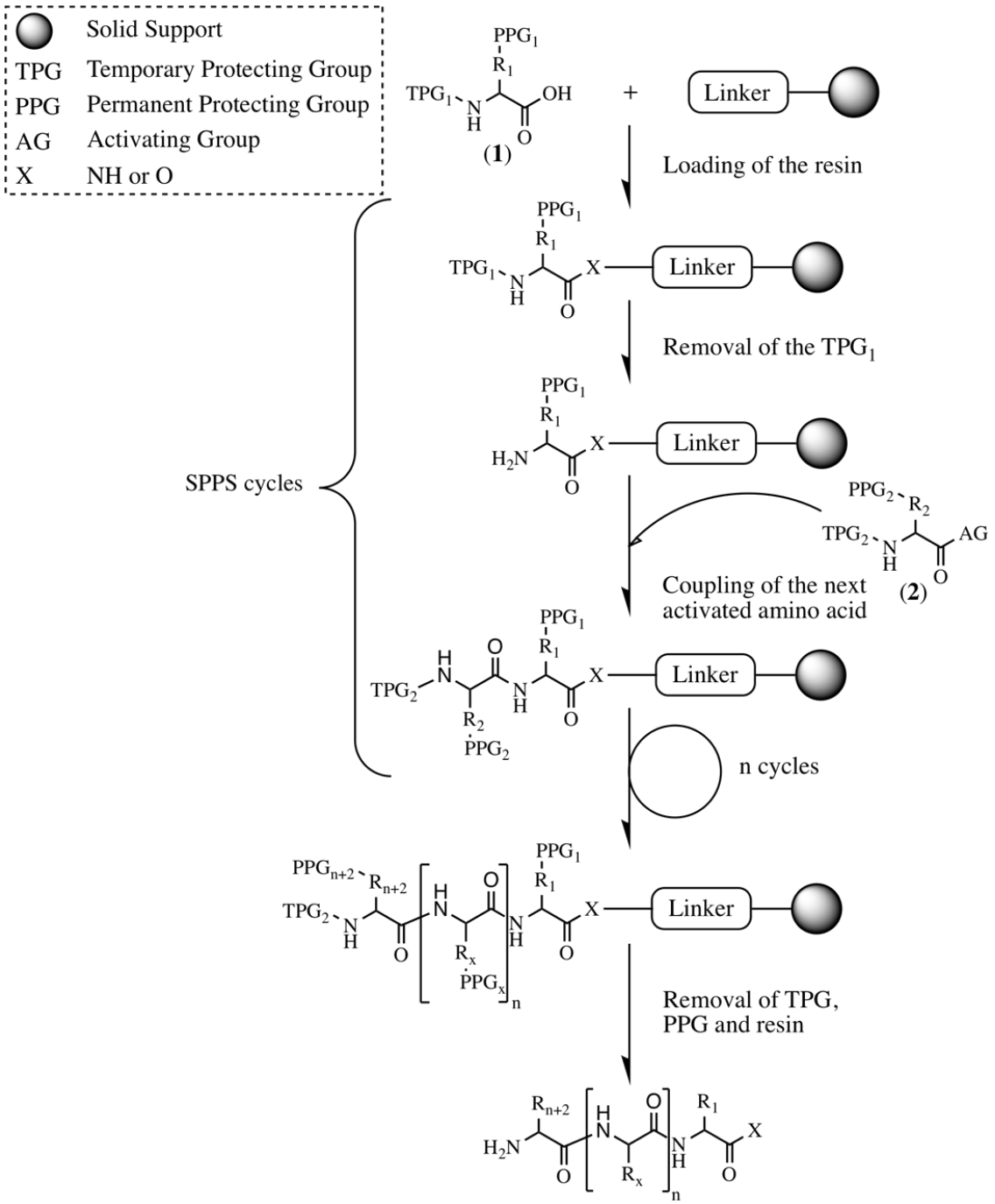

Figure 2.11 – Schematic diagram showing general principles of Solid Phase Peptide Synthesis (SPPS). *Inspired by [314].*

2.6.1. Branched Peptides

The building of multi-substituted chemical identities (branched peptides) has attracted interest in modern biomedicine since they imitate the conformational structures of functional protein

domains involved in biological molecular detection, such as antigen–antibody, ligand–receptor, substrate–enzyme, and others protein–protein interactions. Branched peptides were introduced by J. P. Tam in the 1980s [306] and have been found to be useful for the development of new therapeutic agents, such as vaccines, antibodies, and antimicrobial and antitumor drugs [252, 287, 293, 298, 300, 336]. The peptide conformation is fundamental to its binding with the corresponding integrin receptor. Therefore, branched peptides have been immobilized into biomaterial surfaces to improve cell–biomaterial interactions [337]. Currently, most branched peptides are based on the multiple antigen peptide (MAP) system, with the configuration shown in **Figure 2.12**. MAPs are a cascade-type peptide dendrimer with a wide size distribution. Lysine (Lys, K) is the most commonly used amino acid in the core matrix, because it has two ends, the α- and ε-amine side chain groups, available for branching reactions onto which epitope peptide sequences can be attached [338, 339].

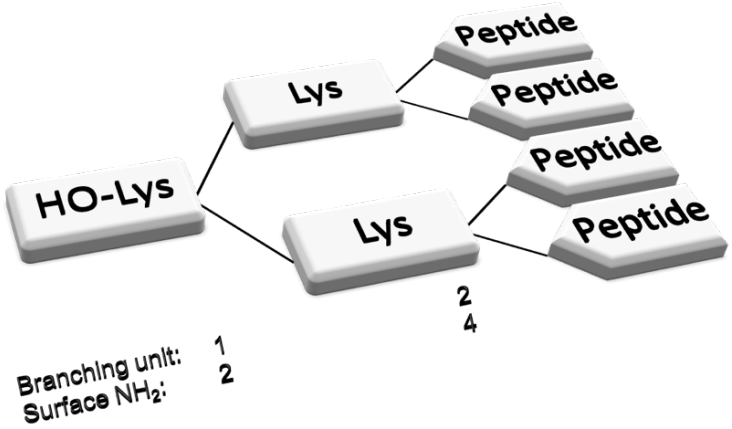

Figure 2.12 – Representation of a multiple antigen peptide (MAP). MAP incorporating four peptide monomers. An increase in the number of Lysine (Lys) branching units increases the number of surface amine groups. *Inspired by [339].*

A variety of synthetic methods have been described for the formulation of branched peptides. The standard approach is to employ the selective protection and deprotection on the

side-chain acid or on the amine group of the branch-site amino acid, then to couple them to a N-terminus amine or C-terminus acid of another protected peptide [340], for this SPPS is extensively applied [299, 341].

2.6.1. Branched versus Linear Peptides

The detection of a target molecule is the foundation of biological processes. However, it is not necessary to synthesize the entire molecule, the use of pharmacophore molecules (i.e. part of a molecule that is bioactive) can have the desired activity [342, 343]. Peptides can imitate the specific conformational binding site of natural proteins and therefore represent a promising approach for the study of protein structure and function [344]. The reduced immunogenicity of short peptides requires a conjugation of transporter proteins or highly branched ligands to obtain strong immune response and to improve the binding affinity.

MAPs are well-defined, hyper branched polymers with a high density of functional binding sites. They consist of a lysine central core with surface functional groups and branching units linked to it [345, 346]. MAPs have shown great promise compared to their similar linear proteins in different biomedical fields, such as hepatitis A [347], antimicrobial activity [348, 349], and antigenicity [350], etc. It is important to note that multi-branched peptides have shown higher cellular uptake compared to their parent monomers [351-358]. Due to the improved uptake of the branched designs much lower concentrations can be used [351].

2.6.2. RGD-Containing Peptides

The most common amino acid sequences used to mimic the *in vivo* environment are the cell–adhesive domains derived from laminin (IKVAV, RGD, YIGSR), collagen (DGEA, RGD), and fibronectin (REDV, RGDS) [359]. In particular, arginine-glycine-aspartic acid (RGD)-

containing peptides are often used peptides to enhance cell adhesion on biomaterial surfaces. This is due to their use throughout the organism, their ability to address more than one cell adhesion receptor, and their biological impact on cell anchoring, behavior and survival [325]. Therefore, developing biomaterials modified with RGD-containing peptides represents an attractive research avenue to optimize cell–biomaterial interactions in TE [360-367]. For example, RGD was immobilized into elastin hydrogels and showed to affect the *in vitro* neurite outgrowth from dorsal root ganglia. The authors reported that increasing the density of RGD increased the length and density of neurites [368]. Silva et al. functionalized a modified gellan gum hydrogel with the glycine-arginine-glycine-aspartic acid-serine (GRGDS) peptide, which demonstrated superior cell adhesion and viability of NSPCs when co-cultured *in vitro.* The researchers suggested that the GRGDS-modified hydrogel may have therapeutic benefits for SCI treatment. [83]. In another study, arginine-glycine-aspartic acid-serine (RGDS) peptides were bonded to a titanium surface. The surface modification showed to improve osteoblasts attachment and survival, having the potential to promote osseointegration *in vivo* [369]. These studies showed the relevance of incorporating RGD-containing peptides into biomaterials to improve cell–biomaterial interactions and neural outcomes.

Improve cell–biomaterial interactions through the incorporations of RGD or RGDS sequences into biomaterial surfaces is known to change the epitope density [370]. MAP systems containing such peptides moieties can increase the density and accessibility of binding sites on the biomaterial surface and therefore influencing cell behavior [370-375]. It is suggested that RGD-containing branched-peptides would have more conformational flexibility than linear peptides, what would improve the accessibility and, potentially, its recognition by integrin. Therefore, MAP systems containing RGDS moieties were synthesized in the study presented in Chapter 5.

2.7. References

[1] Y.C. Wang, H. Tan, X.H. Hui, Biomaterial Scaffolds in Regenerative Therapy of the Central Nervous System, Biomed Res Int (2018).

[2] M.T. Fitch, J. Silver, CNS injury, glial scars, and inflammation: Inhibitory extracellular matrices and regeneration failure, Experimental Neurology 209(2) (2008) 294-301.

[3] P. Dibajnia, C.M. Morshead, Role of neural precursor cells in promoting repair following stroke, Acta Pharmacol Sin 34(1) (2013) 78-90.

[4] C.T. Lu, Y.Z. Zhao, H.L. Wong, J. Cai, L. Peng, X.Q. Tian, Current approaches to enhance CNS delivery of drugs across the brain barriers, Int J Nanomedicine 9 (2014) 2241-57.

[5] W.M. Pardridge, Drug transport across the blood-brain barrier, J Cerebr Blood F Met 32(11) (2012) 1959-1972.

[6] J. Wu, S.H. Yoon, W.M. Wu, N. Bodor, Synthesis and biological evaluations of brain-targeted chemical delivery systems of [Nva2]-TRH, The Journal of pharmacy and pharmacology 54(7) (2002) 945-50.

[7] J. Brownlees, C.H. Williams, Peptidases, peptides, and the mammalian blood-brain barrier, Journal of neurochemistry 60(3) (1993) 793-803.

[8] P.P. Wang, J. Frazier, H. Brem, Local drug delivery to the brain, Adv Drug Deliver Rev 54(7) (2002) 987-1013.

[9] M.M. Pakulska, B.G. Ballios, M.S. Shoichet, Injectable hydrogels for central nervous system therapy, Biomed Mater 7(2) (2012).

[10] P. Sensharma, G. Madhumathi, R.D. Jayant, A.K. Jaiswal, Biomaterials and cells for neural tissue engineering: Current choices, Mater Sci Eng C Mater Biol Appl 77 (2017) 1302-1315.

[11] Mozaffarian, Heart Disease and Stroke Statistics-2016 Update: A Report From the American Heart Association (vol 133, pg e38, 2016), Circulation 133(15) (2016) E599-E599.

[12] Global Health Estimates 2016: Deaths by Cause, Age, Sex, by Country and by Region, 2000-2016. Geneva, World Health Organization, 2018. http://www.who.int/healthinfo/global_burden_disease/estimates/en/. (Accessed May 7th 2019).

[13] Global Health Estimates 2015: Disease burden by Cause, Age, Sex, by Country and by Region, 2000-2015. Geneva, World Health Organization, 2016. http://www.who.int/healthinfo/global_burden_disease/estimates/en/index1.html. (Accessed May 7th 2019).

[14] Public Health Agency of Canada, Stroke in Canada : highlights from the Canadian Chronic Disease Surveillance System. http://publications.gc.ca/collections/collection_2018/aspc-phac/HP35-88-2017-eng.pdf.

[15] R.Y. Tam, T. Fuehrmann, N. Mitrousis, M.S. Shoichet, Regenerative therapies for central nervous system diseases: a biomaterials approach, Neuropsychopharmacology 39(1) (2014) 169-88.

[16] A. Rogalewski, A. Schneider, E.B. Ringelstein, W.R. Schabitz, Toward a multimodal neuroprotective treatment of stroke, Stroke 37(4) (2006) 1129-36.

[17] L.P. Pallesen, K. Barlinn, V. Puetz, Role of Decompressive Craniectomy in Ischemic Stroke, Front Neurol 9 (2018) 1119.

[18] V. Pencea, K.D. Bingaman, L.J. Freedman, M.B. Luskin, Neurogenesis in the subventricular zone and rostral migratory stream of the neonatal and adult primate forebrain, Exp Neurol 172(1) (2001) 1-16.

[19] S.G. Kernie, J.M. Parent, Forebrain neurogenesis after focal Ischemic and traumatic brain injury, Neurobiol Dis 37(2) (2010) 267-74.

[20] T. Ikeda, M. Iwai, T. Hayashi, I. Nagano, M. Shogi, T. Ikenoue, K. Abe, Limited differentiation to neurons and astroglia from neural stem cells in the cortex and striatum after ischemia/hypoxia in the neonatal rat brain, Am J Obstet Gynecol 193(3 Pt 1) (2005) 849-56.

[21] L. Li, K.M. Harms, P.B. Ventura, D.C. Lagace, A.J. Eisch, L.A. Cunningham, Focal Cerebral Ischemia Induces a Multi lineage Cytogenic Response from Adult Subventricular Zone that is Predominantly Gliogenic, Glia 58(13) (2010) 1610-1619.

[22] A. Arvidsson, T. Collin, D. Kirik, Z. Kokaia, O. Lindvall, Neuronal replacement from endogenous precursors in the adult brain after stroke, Nat Med 8(9) (2002) 963-70.

[23] K. Jin, X. Wang, L. Xie, X.O. Mao, W. Zhu, Y. Wang, J. Shen, Y. Mao, S. Banwait, D.A. Greenberg, Evidence for stroke-induced neurogenesis in the human brain, Proc Natl Acad Sci U S A 103(35) (2006) 13198-202.

[24] F.R. J., L.S. W., Enhanced neurogenesis following stroke, Journal of Neuroscience Research 73(3) (2003) 277-283.

[25] J. Lu, A. Manaenko, Q. Hu, Targeting Adult Neurogenesis for Poststroke Therapy, Stem Cells Int 2017 (2017) 5868632.

[26] Y. Wang, M.J. Cooke, N. Sachewsky, C.M. Morshead, M.S. Shoichet, Bioengineered sequential growth factor delivery stimulates brain tissue regeneration after stroke, J Control Release 172(1) (2013) 1-11.

[27] M.J. Robertson, P. Gip, D.V. Schaffer, Neural stem cell engineering- directed differentiation of adult and embryonic stem cells into neurons, Frontiers in Bioscience 13 (2008) 21-50.

[28] M.J. Cooke, Y. Wang, C.M. Morshead, M.S. Shoichet, Controlled epi-cortical delivery of epidermal growth factor for the stimulation of endogenous neural stem cell proliferation in stroke-injured brain, Biomaterials 32(24) (2011) 5688-97.

[29] T. Rhim, D.Y. Lee, M. Lee, Drug delivery systems for the treatment of ischemic stroke, Pharm Res 30(10) (2013) 2429-44.

[30] S. Lanfranconi, F. Locatelli, S. Corti, L. Candelise, G.P. Comi, P.L. Baron, S. Strazzer, N. Bresolin, A. Bersano, Growth factors in ischemic stroke, J Cell Mol Med 15(8) (2011) 1645-87.

[31] D.J. Cook, C. Nguyen, H.N. Chun, L.L. I, A.S. Chiu, M. Machnicki, T.I. Zarembinski, S.T. Carmichael, Hydrogel-delivered brain-derived neurotrophic factor promotes tissue repair and recovery after stroke, J Cereb Blood Flow Metab 37(3) (2017) 1030-1045.

[32] K. Jin, Y. Zhu, Y. Sun, X.O. Mao, L. Xie, D.A. Greenberg, Vascular endothelial growth factor (VEGF) stimulates neurogenesis in vitro and in vivo, Proc Natl Acad Sci U S A 99(18) (2002) 11946-50.

[33] T. Teramoto, J. Qiu, J.-C. Plumier, M.A. Moskowitz, EGF amplifies the replacement of parvalbumin-expressing striatal interneurons after ischemia, Journal of Clinical Investigation 111(8) (2003) 1125-1132.

[34] W.A. Wolf, J.L. Martin, G.L. Kartje, R.G. Farrer, Evidence for fibroblast growth factor-2 as a mediator of amphetamine-enhanced motor improvement following stroke, PLoS One 9(9) (2014) e108031.

[35] R. Rahme, R. Curry, D. Kleindorfer, J.C. Khoury, A.J. Ringer, B.M. Kissela, K. Alwell, C.J. Moomaw, M.L. Flaherty, P. Khatri, How often are patients with ischemic stroke eligible for decompressive hemicraniectomy?, Stroke 43(2) (2012) 550-552.

[36] D. Staykov, R. Gupta, Hemicraniectomy in malignant middle cerebral artery infarction, Stroke 42(2) (2011) 513-6.

[37] O.M. Arnaout, S.G. Aoun, H.H. Batjer, B.R. Bendok, Decompressive hemicraniectomy after malignant middle cerebral artery infarction: rationale and controversies, Neurosurg Focus 30(6) (2011) E18.

[38] E. Juttler, A. Unterberg, J. Woitzik, J. Bosel, H. Amiri, O.W. Sakowitz, M. Gondan, P. Schiller, R. Limprecht, S. Luntz, H. Schneider, T. Pinzer, C. Hobohm, J. Meixensberger, W. Hacke, D.I. Investigators, Hemicraniectomy in older patients with extensive middle-cerebral-artery stroke, N Engl J Med 370(12) (2014) 1091-100.

[39] K. Vahedi, J. Hofmeijer, E. Juettler, E. Vicaut, B. George, A. Algra, G.J. Amelink, P. Schmiedeck, S. Schwab, P.M. Rothwell, M.G. Bousser, H.B. van der Worp, W. Hacke, D. Decimal, H. investigators, Early decompressive surgery in malignant infarction of the middle cerebral artery: a pooled analysis of three randomised controlled trials, Lancet Neurol 6(3) (2007) 215-22.

[40] M. Geurts, H.B. van der Worp, L.J. Kappelle, G.J. Amelink, A. Algra, J. Hofmeijer, H.S. Committee, Surgical decompression for space-occupying cerebral infarction: outcomes at 3 years in the randomized HAMLET trial, Stroke 44(9) (2013) 2506-8.

[41] X. Lu, B. Huang, J. Zheng, Y. Tao, W. Yu, L. Tang, R. Zhu, S. Li, L. Li, Decompressive craniectomy for the treatment of malignant infarction of the middle cerebral artery, Sci Rep 4 (2014) 7070.

[42] B. Sommerich, A. Barnick, M. Barakat, M. Ward, In vivo tissue reaction, resorption, safety, and efficacy of a collagen dural substitute in an animal model, Codman & Shurtleff, Inc., Rayham, MA, 2005.

[43] Z. Shi, T. Xu, Y. Yuan, K. Deng, M. Liu, Y. Ke, C. Luo, T. Yuan, A. Ayyad, A New Absorbable Synthetic Substitute With Biomimetic Design for Dural Tissue Repair, Artif Organs 40(4) (2016) 403-13.

[44] M. Schiariti, F. Acerbi, M. Broggi, G. Tringali, A. Raggi, G. Broggi, P. Ferroli, Two alternative dural sealing techniques in posterior fossa surgery: (Polylactide-co-glycolide) self-adhesive resorbable membrane versus polyethylene glycol hydrogel, Surg Neurol Int 5 (2014) 171.

[45] L. Rabinowitz, H. Monnerie, S. Shashidhara, P.D. Le Roux, Growth of rat cortical neurons on DuraGen, a collagen-based dural graft matrix, Neurol Res 27(8) (2005) 887-894.

[46] G.T. Knowlson, Gel-foam granuloma in the brain, J Neurol Neurosurg Psychiatry 37(8) (1974) 971-3.

[47] C.L. Rosen, G.K. Steinberg, F. DeMonte, J.B. Delashaw, S.B. Lewis, M.E. Shaffrey, K. Aziz, J. Hantel, F.F. Marciano, Results of the Prospective, Randomized, Multicenter Clinical Trial Evaluating a Biosynthesized Cellulose Graft for Repair of Dural Defects, Neurosurgery 69(5) (2011) 1093-1103.

[48] E.J. Bradbury, S.B. McMahon, Opinion - Spinal cord repair strategies: why do they work?, Nat Rev Neurosci 7(8) (2006) 644-653.

[49] D.C. Baptiste, M.G. Fehlings, Update on the treatment of spinal cord injury, Prog Brain Res 161 (2007) 217-233.

[50] J. Bickenbach, A. Officer, T. Shakespeare, P. von Groote, W.H. Organization, T.I.S.C. Society, International perspectives on spinal cord injury in: J. Bickenbach (Ed.) 1.Spinal cord injuries – history. 2.Spinal cord injuries – epidemiology. 3.Spinal cord injuries – prevention and control. 4.Spinal cord injuries – rehabilitation. 5.Delivery of health care. 6.Disabled persons - psychology., World Health Organization (WHO), 2013.

[51] A.K. Varma, A. Das, G. Wallace, J. Barry, A.A. Vertegel, S.K. Ray, N.L. Banik, Spinal Cord Injury: A Review of Current Therapy, Future Treatments, and Basic Science Frontiers, Neurochemical Research 38(5) (2013) 895-905.

[52] S. Kubinova, New trends in spinal cord tissue engineering, Futur Neurol 10(2) (2015) 129-145.

[53] B.K. Kwon, C.G. Fisher, M.F. Dvorak, W. Tetzlaff, Strategies to promote neural repair and regeneration after spinal cord injury, Spine 30(17) (2005) S3-S13.

[54] E.C. Tsai, A.V. Krassioukov, C.H. Tator, Corticospinal regeneration into lumbar grey matter correlates with locomotor recovery after complete spinal cord transection and repair with peripheral nerve grafts, fibroblast growth factor 1 fibrin glue, and spinal fusion, J Neuropath Exp Neur 64(3) (2005) 230-244.

[55] Y.D. Teng, W.L. Liao, H. Choi, D. Konya, S. Sabbarwal, R. Langer, R.L. Sidman, E.Y. Synder, W.R. Frontera, Physical activity-mediated functional recovery after spinal cord injury: potential roles of neural stem cells, Regenerative Medicine 1(6) (2006) 763-776.

[56] E.C. Tsai, C.H. Tator, Neuroprotection and regeneration strategies for spinal cord repair, Curr Pharm Design 11(10) (2005) 1211-1222.

[57] M.E. Schwab, Nogo and axon regeneration, Curr Opin Neurobiol 14(1) (2004) 118-124.

[58] M. Wintzer, M. Mladinic, D. Lazarevic, C. Casseler, A. Cattaneo, J. Nicholls, Strategies for identifying genes that play a role in spinal cord regeneration, Journal of Anatomy 204(1) (2004) 3-11.

[59] E.C. Tsai, P.D. Dalton, M.S. Shoichet, C.H. Tator, Synthetic hydrogel guidance channels facilitate regeneration of adult rat brainstem motor axons after complete spinal cord transection, J Neurotraum 21(6) (2004) 789-804.

[60] K. Anselme, Osteoblast adhesion on biomaterials, Biomaterials 21(7) (2000) 667-681.

[61] B.D. Ratner, Biomaterials science : an introduction to materials in medicine, 2nd ed., Elsevier Academic Press, Amsterdam ; Boston, 2004.

[62] M.N. Helmus, J.A. Hubbell, Materials Selection, Cardiovasc Pathol 2(3) (1993) S53-S71.

[63] B. Palsson, S. Bhatia, Tissue engineering, Pearson Prentice Hall, Upper Saddle River, N.J., 2004.

[64] S.F. Yang, K.F. Leong, Z.H. Du, C.K. Chua, The design of scaffolds for use in tissue engineering. Part 1. Traditional factors, Tissue Eng 7(6) (2001) 679-689.

[65] K.S. Straley, C.W.P. Foo, S.C. Heilshorn, Biomaterial Design Strategies for the Treatment of Spinal Cord Injuries, J Neurotraum 27(1) (2010) 1-19.

[66] P.B. Malafaya, G.A. Silva, R.L. Reis, Natural-origin polymers as carriers and scaffolds for biomolecules and cell delivery in tissue engineering applications, Adv Drug Deliv Rev 59(4-5) (2007) 207-33.

[67] P. Jendelová, Š. Kubinová, I. Sandvig, S. Erceg, A. Sandvig, E. Syková, Current developments in cell- and biomaterial-based approaches for stroke repair, Expert Opinion on Biological Therapy 16(1) (2015) 43-56.

[68] P. Moshayedi, L.R. Nih, I.L. Llorente, A.R. Berg, J. Cinkornpumin, W.E. Lowry, T. Segura, S.T. Carmichael, Systematic optimization of an engineered hydrogel allows for selective control of human neural stem cell survival and differentiation after transplantation in the stroke brain, Biomaterials 105 (2016) 145-55.

[69] Z.Z. Khaing, R.C. Thomas, S.A. Geissler, C.E. Schmidt, Advanced biomaterials for repairing the nervous system: what can hydrogels do for the brain?, Materials Today 17(7) (2014) 332-340.

[70] Z. Yang, H. Duan, L. Mo, H. Qiao, X. Li, The effect of the dosage of NT-3/chitosan carriers on the proliferation and differentiation of neural stem cells, Biomaterials 31(18) (2010) 4846-54.

[71] J.W. Austin, C.E. Kang, M.D. Baumann, L. DiDiodato, K. Satkunendrarajah, J.R. Wilson, G.J. Stanisz, M.S. Shoichet, M.G. Fehlings, The effects of intrathecal injection of a hyaluronan-based hydrogel on inflammation, scarring and neurobehavioural outcomes in a rat model of severe spinal cord injury associated with arachnoiditis, Biomaterials 33(18) (2012) 4555-64.

[72] P.J. Johnson, A. Tatara, D.A. McCreedy, A. Shiu, S.E. Sakiyama-Elbert, Tissue-engineered fibrin scaffolds containing neural progenitors enhance functional recovery in a subacute model of SCI, Soft Matter 6(20) (2010) 5127-5137.

[73] W.M. Tian, C.L. Zhang, S.P. Hou, X. Yu, F.Z. Cui, Q.Y. Xu, S.L. Sheng, H. Cui, H.D. Li, Hyaluronic acid hydrogel as Nogo-66 receptor antibody delivery system for the repairing of injured rat brain: in vitro, Journal of Controlled Release 102(1) (2005) 13-22.

[74] R.K. Mittapalli, X.L. Liu, C.E. Adkins, M.I. Nounou, K.A. Bohn, T.B. Terrell, H.S. Qhattal, W.J. Geldenhuys, D. Palmieri, P.S. Steeg, Q.R. Smith, P.R. Lockman, Paclitaxel-Hyaluronic NanoConjugates Prolong Overall Survival in a Preclinical Brain Metastases of Breast Cancer Model, Mol Cancer Ther 12(11) (2013) 2389-2399.

[75] Y. Wang, Y.T. Wei, Z.H. Zu, R.K. Ju, M.Y. Guo, X.M. Wang, Q.Y. Xu, F.Z. Cui, Combination of Hyaluronic Acid Hydrogel Scaffold and PLGA Microspheres for Supporting Survival of Neural Stem Cells, Pharm Res-Dordr 28(6) (2011) 1406-1414.

[76] A. Acarregui, J.L. Pedraz, F.J. Blanco, R.M. Hernandez, G. Orive, Hydrogel-Based Scaffolds for Enclosing Encapsulated Therapeutic Cells, Biomacromolecules 14(2) (2013) 322-330.

[77] R.C. Assuncao-Silva, E.D. Gomes, N. Sousa, N.A. Silva, A.J. Salgado, Hydrogels and Cell Based Therapies in Spinal Cord Injury Regeneration, Stem Cells Int (2015).

[78] J.L. Drury, D.J. Mooney, Hydrogels for tissue engineering: scaffold design variables and applications, Biomaterials 24(24) (2003) 4337-4351.

[79] A. Acarregui, E. Herran, M. Igartua, F.J. Blanco, J.L. Pedraz, G. Orive, R.M. Hernandez, Multifunctional hydrogel-based scaffold for improving the functionality of encapsulated therapeutic cells and reducing inflammatory response, Acta Biomater 10(10) (2014) 4206-4216.

[80] C. Chircov, A.M. Grumezescu, L.E. Bejenaru, Hyaluronic acid-based scaffolds for tissue engineering, Rom J Morphol Embryo 59(1) (2018) 71-76.

[81] O.A. Carballo-Molina, I. Velasco, Hydrogels as scaffolds and delivery systems to enhance axonal regeneration after injuries, Front Cell Neurosci 9 (2015) 13.

[82] A. Hejcl, P. Lesny, M. Pradny, J. Michalek, P. Jendelova, J. Stulik, E. Sykova, Biocompatible Hydrogels in Spinal Cord Injury Repair, Physiol Res 57 (2008) S121-S132.

[83] N.A. Silva, M.J. Cooke, R.Y. Tam, N. Sousa, A.J. Salgado, R.L. Reis, M.S. Shoichet, The effects of peptide modified gellan gum and olfactory ensheathing glia cells on neural stem/progenitor cell fate, Biomaterials 33(27) (2012) 6345-6354.

[84] I. Caron, F. Rossi, S. Papa, R. Aloe, M. Sculco, E. Mauri, A. Sacchetti, E. Erba, N. Panini, V. Parazzi, M. Barilani, G. Forloni, G. Perale, L. Lazzari, P. Veglianese, A new three dimensional biomimetic hydrogel to deliver factors secreted by human mesenchymal stem cells in spinal cord injury, Biomaterials 75 (2016) 135-147.

[85] P. Musoke-Zawedde, M.S. Shoichet, Anisotropic three-dimensional peptide channels guide neurite outgrowth within a biodegradable hydrogel matrix, Biomed Mater 1(3) (2006) 162-169.

[86] T. Fuhrmann, R.Y. Tam, B. Ballarin, B. Coles, I.E. Donaghue, D. van der Kooy, A. Nagy, C.H. Tator, C.M. Morshead, M.S. Shoichet, Injectable hydrogel promotes early survival of induced pluripotent stem cell-derived oligodendrocytes and attenuates longterm teratoma formation in a spinal cord injury model, Biomaterials 83 (2016) 23-36.

[87] F.Z. Cui, W.M. Tian, S.P. Hou, Q.Y. Xu, I.S. Lee, Hyaluronic acid hydrogel immobilized with RGD peptides for brain tissue engineering, J Mater Sci-Mater M 17(12) (2006) 1393-1401.

[88] S. Woerly, E. Pinet, L. de Robertis, D. Van Diep, M. Bousmina, Spinal cord repair with PHPMA hydrogel containing RGD peptides (NeuroGel (TM)), Biomaterials 22(10) (2001) 1095-1111.

[89] A. Hejcl, J. Sedy, M. Kapcalova, D.A. Toro, T. Amemori, P. Lesny, K. Likavcanova-Masinova, E. Krumbholcova, M. Pradny, J. Michalek, M. Burian, M. Hajek, P. Jendelova, E. Sykova, HPMA-RGD Hydrogels Seeded with Mesenchymal Stem Cells Improve Functional Outcome in Chronic Spinal Cord Injury, Stem Cells Dev 19(10) (2010) 1535-1546.

[90] Z.M. Wang, Z.F. Wang, W.W. Lu, W.X. Zhen, D.Z. Yang, S.L. Peng, Novel biomaterial strategies for controlled growth factor delivery for biomedical applications, Npg Asia Mater 9 (2017).

[91] S.M. Willerth, S.E. Sakiyama-Elbert, Approaches to neural tissue engineering using scaffolds for drug delivery, Adv Drug Deliver Rev 59(4-5) (2007) 325-338.

[92] S. Yao, X. Liu, X. Wang, A. Merolli, X. Chen, F. Cui, Directing neural stem cell fate with biomaterial parameters for injured brain regeneration, Progress in Natural Science: Materials International 23(2) (2013) 103-112.

[93] Z. Dai, J. Ronholm, Y. Tian, B. Sethi, X. Cao, Sterilization techniques for biodegradable scaffolds in tissue engineering applications, J Tissue Eng 7 (2016) 2041731416648810.

[94] Y.Q. Wu, Z.G. Wang, P.T. Cai, T. Jiang, Y.Y. Li, Y. Yuan, R. Li, Y.F. Lu, J. Wang, D.Q. Chen, Q.Q. Zeng, S.N. Khor, R.S. Zhong, H.Y. Zhang, Y. Lin, X.K. Li, J. Xiao, Dual Delivery of bFGF-and NGF-Binding Coacervate Confers Neuroprotection by Promoting Neuronal Proliferation, Cellular Physiology and Biochemistry 47(3) (2018) 948-956.

[95] E.G. Fine, I. Decosterd, M. Papaloizos, A.D. Zurn, P. Aebischer, GDNF and NGF released by synthetic guidance channels support sciatic nerve regeneration across a long gap, Eur J Neurosci 15(4) (2002) 589-601.

[96] I.P. Clements, J.M. Munson, R.V. Bellamkonda, Chapter II.6.14 - Neuronal Tissue Engineering, in: B.D. Ratner, A.S. Hoffman, F.J. Schoen, J.E. Lemons (Eds.), Biomaterials Science (Third Edition), Academic Press2013, pp. 1291-1306.

[97] J.S. Katz, J.A. Burdick, Hydrogel mediated delivery of trophic factors for neural repair, Wires Nanomed Nanobi 1(1) (2009) 128-139.

[98] A. Jain, Y.T. Kim, R.J. McKeon, R.V. Bellamkonda, In situ gelling hydrogels for conformal repair of spinal cord defects, and local delivery of BDNF after spinal cord injury, Biomaterials 27(3) (2006) 497-504.

[99] M.Y. Gao, P. Lu, B. Bednark, D. Lynam, J.M. Conner, J. Sakamoto, M.H. Tuszynski, Templated agarose scaffolds for the support of motor axon regeneration into sites of complete spinal cord transection, Biomaterials 34(5) (2013) 1529-1536.

[100] A.N. Clarkson, K. Parker, M. Nilsson, F.R. Walker, E.K. Gowing, Combined ampakine and BDNF treatments enhance poststroke functional recovery in aged mice via AKT-CREB signaling, J Cerebr Blood F Met 35(8) (2015) 1272-1279.

[101] T. Fuhrmann, J. Obermeyer, C.H. Tator, M.S. Shoichet, Click-crosslinked injectable hyaluronic acid hydrogel is safe and biocompatible in the intrathecal space for ultimate use in regenerative strategies of the injured spinal cord, Methods 84 (2015) 60-69.

[102] M.K. Horne, D.R. Nisbet, J.S. Forsythe, C.L. Parish, Three-Dimensional Nanofibrous Scaffolds Incorporating Immobilized BDNF Promote Proliferation and Differentiation of Cortical Neural Stem Cells, Stem Cells Dev 19(6) (2010) 843-852.

[103] K.J. Lampe, D.S. Kern, M.J. Mahoney, K.B. Bjugstad, The administration of BDNF and GDNF to the brain via PLGA microparticles patterned within a degradable PEG-based hydrogel: Protein distribution and the glial response, J Biomed Mater Res A 96a(3) (2011) 595-607.

[104] K.B. Bjugstad, K. Lampe, D.S. Kern, M. Mahoney, Biocompatibility of poly(ethylene glycol)-based hydrogels in the brain: An analysis of the glial response across space and time, J Biomed Mater Res A 95a(1) (2010) 79-91.

[105] E. Ansorena, P. De Berdt, B. Ucakar, T. Simon-Yarza, D. Jacobs, O. Schakman, A. Jankovski, R. Deumens, M.J. Blanco-Prieto, V. Preat, A. des Rieux, Injectable alginate hydrogel loaded with GDNF promotes functional recovery in a hemisection model of spinal cord injury, Int J Pharm 455(1-2) (2013) 148-158.

[106] L. De Laporte, A. Huang, M.M. Ducommun, M.L. Zelivyanska, M.O. Aviles, A.F. Adler, L.D. Shea, Patterned transgene expression in multiple-channel bridges after spinal cord injury, Acta Biomater 6(8) (2010) 2889-2897.

[107] A. Iwata, K.D. Browne, B.J. Pfister, J.A. Gruner, D.H. Smith, Long-term survival and outgrowth of mechanically engineered nervous tissue constructs implanted into spinal cord lesions, Tissue Eng 12(1) (2006) 101-110.

[108] X.J. Yu, G.P. Dillon, R.V. Bellamkonda, A laminin and nerve growth factor-laden three-dimensional scaffold for enhanced neurite extension, Tissue Eng 5(4) (1999) 291-304.

[109] S. Stokols, M.H. Tuszynski, The fabrication and characterization of linearly oriented nerve guidance scaffolds for spinal cord injury, Biomaterials 25(27) (2004) 5839-5846.

[110] A. Piotrowicz, M.S. Shoichet, Nerve guidance channels as drug delivery vehicles, Biomaterials 27(9) (2006) 2018-2027.

[111] J.O. Winter, S.F. Cogan, J.F. Rizzo, Neurotrophin-eluting hydrogel coatings for neural stimulating electrodes, J Biomed Mater Res B 81b(2) (2007) 551-563.

[112] J.H. Lee, J.H. Park, M. Eltohamy, R. Perez, E.J. Lee, H.W. Kim, Collagen gel combined with mesoporous nanoparticles loading nerve growth factor as a feasible therapeutic three-dimensional depot for neural tissue engineering, Rsc Adv 3(46) (2013) 24202-24214.

[113] W.M. Saltzman, M.W. Mak, M.J. Mahoney, E.T. Duenas, J.L. Cleland, Intracranial delivery of recombinant nerve growth factor: Release kinetics and protein distribution for three delivery systems, Pharm Res-Dordr 16(2) (1999) 232-240.

[114] S. Rochkind, A. Shahar, D. Fliss, D. El-Ani, L. Astachov, T. Hayon, M. Alon, R. Zamostiano, O. Ayalon, I. Biton, Y. Cohen, R. Halperin, D. Schneider, A. Oron, Z. Nevo, Development of a tissue-engineered composite implant for treating traumatic paraplegia in rats, Eur Spine J 15(2) (2006) 234-245.

[115] V.R. King, M. Henseler, R.A. Brown, J.V. Priestley, Mats made from fibronectin support oriented growth of axons in the damaged spinal cord of the adult rat, Experimental Neurology 182(2) (2003) 383-398.

[116] J. Bloch, E.G. Fine, N. Bouche, A.D. Zurn, P. Aebischer, Nerve growth factor- and neurotrophin-3-releasing guidance channels promote regeneration of the transected rat dorsal root, Experimental Neurology 172(2) (2001) 425-432.

[117] T.A. Kapur, M.S. Shoichet, Immobilized concentration gradients of nerve growth factor guide neurite outgrowth, J Biomed Mater Res A 68a(2) (2004) 235-243.

[118] K. Moore, M. Macsween, M. Shoichet, Immobilized concentration gradients of neurotrophic factors guide neurite outgrowth of primary neurons in macroporous scaffolds, Tissue Eng 12(2) (2006) 267-278.

[119] D.A. Houweling, A.J. Lankhorst, W.H. Gispen, P.R. Bar, E.A.J. Joosten, Collagen containing neurotrophin-3 (NT-3) attracts regrowing injured corticospinal axons in the adult rat spinal cord and promotes partial functional recovery, Experimental Neurology 153(1) (1998) 49-59.

[120] L.H. Mo, Z.Y. Yang, A.F. Zhang, X.G. Li, The repair of the injured adult rat hippocampus with NT-3-chitosan carriers, Biomaterials 31(8) (2010) 2184-2192.

[121] H.M. Duan, W.H. Ge, A.F. Zhang, Y. Xi, Z.H. Chen, D.D. Luo, Y. Cheng, K.S. Fan, S. Horvath, M.V. Sofroniew, L.M. Cheng, Z.Y. Yang, Y.E. Sun, X.G. Li, Transcriptome analyses reveal molecular mechanisms underlying functional recovery after spinal cord injury, P Natl Acad Sci USA 112(43) (2015) 13360-13365.

[122] B.L. Du, X. Zeng, Y.H. Ma, B.Q. Lai, J.M. Wang, E.A. Ling, J.L. Wu, Y.S. Zeng, Graft of the gelatin sponge scaffold containing genetically-modified neural stem cells promotes cell differentiation, axon regeneration, and functional recovery in rat with spinal cord transection, J Biomed Mater Res A 103(4) (2015) 1533-1545.

[123] K. Zhang, Z. Liu, G. Li, B.Q. Lai, L.N. Qin, Y. Ding, J.W. Ruan, S.X. Zhang, Y.S. Zeng, Electro-Acupuncture Promotes the Survival and Differentiation of Transplanted Bone Marrow Mesenchymal Stem Cells Pre-Induced with Neurotrophin-3 and Retinoic Acid in Gelatin Sponge Scaffold after Rat Spinal Cord Transection, Stem Cell Rev Rep 10(4) (2014) 612-625.

[124] J. Fan, H. Zhang, J. He, Z. Xiao, B. Chen, J. Xiaodan, J. Dai, R. Xu, Neural regrowth induced by PLGA nerve conduits and neurotrophin-3 in rats with complete spinal cord transection, J Biomed Mater Res B Appl Biomater 97(2) (2011) 271-7.

[125] E.C. Tsai, P.D. Dalton, M.S. Shoichet, C.H. Tator, Matrix inclusion within synthetic hydrogel guidance channels improves specific supraspinal and local axonal regeneration after complete spinal cord transection, Biomaterials 27(3) (2006) 519-533.

[126] M.C.J. Hamann, C.H. Tator, M.S. Shoichet, Injectable intrathecal delivery system for localized administration of EGF and FGF-2 to the injured rat spinal cord, Experimental Neurology 194(1) (2005) 106-119.

[127] M.C.J. Hamann, E.C. Tsai, C.H. Tator, M.S. Shoichet, Novel intrathecal delivery system for treatment of spinal cord injury, Experimental Neurology 182(2) (2003) 300-309.

[128] Y.F. Wang, M.J. Cooke, Y. Lapitsky, R.G. Wylie, N. Sachewsky, D. Corbett, C.M. Morshead, M.S. Shoichet, Transport of epidermal growth factor in the stroke-injured brain, Journal of Controlled Release 149(3) (2011) 225-235.

[129] A. Goraltchouk, V. Scanga, C.M. Morshead, M.S. Shoichet, Incorporation of protein-eluting microspheres into biodegradable nerve guidance channels for controlled release, Journal of Controlled Release 110(2) (2006) 400-407.

[130] D.J. Macaya, K. Hayakawa, K. Arai, M. Spector, Astrocyte infiltration into injectable collagen-based hydrogels containing FGF-2 to treat spinal cord injury, Biomaterials 34(14) (2013) 3591-3602.

[131] T. Furuya, M. Hashimoto, M. Koda, A. Murata, A. Okawa, M. Dezawa, D. Matsuse, Y. Tabata, K. Takahashi, M. Yamazaki, Treatment with basic fibroblast growth factor-incorporated gelatin hydrogel does not exacerbate mechanical allodynia after spinal cord contusion injury in rats, J Spinal Cord Med 36(2) (2013) 134-139.

[132] B. Chen, J.Y. He, H. Yang, Q. Zhang, L.L. Zhang, X. Zhang, E. Xie, C.C. Liu, R. Zhang, Y. Wang, L.H. Huang, D.J. Hao, Repair of spinal cord injury by implantation of bFGF-incorporated HEMA-MOETACL hydrogel in rats, Sci Rep-Uk 5 (2015).

[133] Y.J. Wen, S.K. Yu, Y.H. Wu, R.K. Ju, H. Wang, Y.J. Liu, Y. Wang, Q.Y. Xu, Spinal cord injury repair by implantation of structured hyaluronic acid scaffold with PLGA microspheres in the rat, Cell and Tissue Research 364(1) (2016) 17-28.

[134] A. des Rieux, P. De Berdt, E. Ansorena, B. Ucakar, D. Jacobs, O. Schakman, E. Audouard, C. Bouzin, D. Auhl, T. Simon-Yarza, O. Feron, M.J. Blanco-Prieto, P. Carmeliet, C. Bailly, F. Clotman, V. Preat, Vascular endothelial growth factor-loaded injectable hydrogel enhances plasticity in the injured spinal cord, J Biomed Mater Res A 102(7) (2014) 2345-2355.

[135] D.F. Emerich, E. Silva, O. Ali, D. Mooney, W. Bell, S.J. Yu, Y. Kaneko, C. Borlongan, Injectable VEGF Hydrogels Produce Near Complete Neurological and Anatomical Protection Following Cerebral Ischemia in Rats, Cell Transplant 19(9) (2010) 1063-1071.

[136] T. Yamashita, H.Z. Zhang, K. Deguchi, K. Oota, A. Tuchiya, V. Lukic, S. Nagotani, T. Kamiya, K. Abe, Vascular endothelial growth factor promotes brain tissue regeneration with a biomaterial polydimethylsiloxane-tetraethoxysilane, Neuroscience Research 61 (2008) S133-S133.

[137] H.Z. Zhang, T. Hayashi, K. Tsuru, K. Deguchi, M. Nagdhara, S. Hayakawa, M. Nagai, T. Kamiya, A. Osaka, K. Abe, Vascular endothelial growth factor promotes brain tissue regeneration with a novel biomaterial polydimethylsiloxane-tetraethoxysilane, Brain Res 1132(1) (2007) 29-35.

[138] R.K. Ju, Y.J. Wen, R.B. Gou, Y. Wang, Q.Y. Xu, The Experimental Therapy on Brain Ischemia by Improvement of Local Angiogenesis With Tissue Engineering in the Mouse, Cell Transplant 23 (2014) S83-S95.

[139] A.J. Mothe, R.Y. Tam, T. Zahir, C.H. Tator, M.S. Shoichet, Repair of the injured spinal cord by transplantation of neural stem cells in a hyaluronan-based hydrogel, Biomaterials 34(15) (2013) 3775-3783.

[140] R.Y. Tam, M.J. Cooke, M.S. Shoichet, A covalently modified hydrogel blend of hyaluronan-methyl cellulose with peptides and growth factors influences neural stem/progenitor cell fate, J Mater Chem 22(37) (2012) 19402-19411.

[141] M.R. Wells, K. Kraus, D.K. Batter, D.G. Blunt, J. Weremowitz, S.E. Lynch, H.N. Antoniades, H.A. Hansson, Gel matrix vehicles for growth factor application in nerve gap injuries repaired with tubes: A comparison of biomatrix, collagen, and methylcellulose, Experimental Neurology 146(2) (1997) 395-402.

[142] K. Nakaguchi, H. Jinnou, N. Kaneko, M. Sawada, T. Hikita, S. Saitoh, Y. Tabata, K. Sawamoto, Growth Factors Released from Gelatin Hydrogel Microspheres Increase New Neurons in the Adult Mouse Brain, Stem Cells International (2012).

[143] L.V. Hiscox, C.L. Johnson, E. Barnhill, M.D.J. McGarry, J. Huston, E.J.R. van Beek, J.M. Starr, N. Roberts, Magnetic resonance elastography (MRE) of the human brain: technique, findings and clinical applications, Phys Med Biol 61(24) (2016) R401-R437.

[144] A.F. Christ, K. Franze, H. Gautier, P. Moshayedi, J. Fawcett, R.J.M. Franklin, R.T. Karadottir, J. Guck, Mechanical difference between white and gray matter in the rat cerebellum measured by scanning force microscopy, Journal of Biomechanics 43(15) (2010) 2986-2992.

[145] B.S. Elkin, E.U. Azeloglu, K.D. Costa, B. Morrison, Mechanical heterogeneity of the rat hippocampus measured by atomic force microscope indentation, J Neurotraum 24(5) (2007) 812-822.

[146] L.W. Lau, R. Cua, M.B. Keough, S. Haylock-Jacobs, V.W. Yong, OPINION Pathophysiology of the brain extracellular matrix: a new target for remyelination, Nat Rev Neurosci 14(10) (2013) 722-729.

[147] E. Moeendarbary, I.P. Weber, G.K. Sheridan, D.E. Koser, S. Soleman, B. Haenzi, E.J. Bradbury, J. Fawcett, K. Franze, The soft mechanical signature of glial scars in the central nervous system, Nat Commun 8 (2017).

[148] N. Annabi, J.W. Nichol, X. Zhong, C.D. Ji, S. Koshy, A. Khademhosseini, F. Dehghani, Controlling the Porosity and Microarchitecture of Hydrogels for Tissue Engineering, Tissue Eng Part B-Re 16(4) (2010) 371-383.

[149] K. Whang, K.E. Healy, D.R. Elenz, E.K. Nam, D.C. Tsai, C.H. Thomas, G.W. Nuber, F.H. Glorieux, R. Travers, S.M. Sprague, Engineering bone regeneration with bioabsorbable scaffolds with novel microarchitecture, Tissue Eng 5(1) (1999) 35-51.

[150] R.J. Wade, J.A. Burdick, Engineering ECM signals into biomaterials, Materials Today 15(10) (2012) 454-459.

[151] K.C. Spencer, J.C. Sy, K.B. Ramadi, A.M. Graybiel, R. Langer, M.J. Cima, Characterization of Mechanically Matched Hydrogel Coatings to Improve the Biocompatibility of Neural Implants (vol 7, 1952, 2017), Sci Rep-Uk 7 (2017).

[152] M.D. Baumann, C.E. Kang, J.C. Stanwick, Y.F. Wang, H. Kim, Y. Lapitsky, M.S. Shoichet, An injectable drug delivery platform for sustained combination therapy, Journal of Controlled Release 138(3) (2009) 205-213.

[153] M.J. Caicco, T. Zahir, A.J. Mothe, B.G. Ballios, A.J. Kihm, C.H. Tator, M.S. Shoichet, Characterization of hyaluronan-methylcellulose hydrogels for cell delivery to the injured spinal cord, J Biomed Mater Res A 101(5) (2013) 1472-1477.

[154] A. Tuladhar, S.L. Payne, M.S. Shoichet, Harnessing the Potential of Biomaterials for Brain Repair after Stroke, Front Mater 5 (2018).

[155] P. Jendelova, S. Kubinova, I. Sandvig, S. Erceg, A. Sandvig, E. Sykova, Current developments in cell- and biomaterial-based approaches for stroke repair, Expert Opin Biol Ther 16(1) (2016) 43-56.

[156] A. Tuladhar, C.M. Morshead, M.S. Shoichet, Circumventing the blood-brain barrier: Local delivery of cyclosporin A stimulates stem cells in stroke-injured rat brain, Journal of Controlled Release 215 (2015) 1-11.

[157] C.E. Brown, K. Aminoltejari, H. Erb, I.R. Winship, T.H. Murphy, In Vivo Voltage-Sensitive Dye Imaging in Adult Mice Reveals That Somatosensory Maps Lost to Stroke Are Replaced over Weeks by New Structural and Functional Circuits with Prolonged Modes of Activation within Both the Peri-Infarct Zone and Distant Sites, Journal of Neuroscience 29(6) (2009) 1719-1734.

[158] S.T. Carmichael, I. Archibeque, L. Luke, T. Nolan, J. Momiy, S.L. Li, Growth-associated gene expression after stroke: Evidence for a growth-promoting region in peri-infarct cortex, Experimental Neurology 193(2) (2005) 291-311.

[159] Y.F. Wang, M.J. Cooke, C.M. Morshead, M.S. Shoichet, Hydrogel delivery of erythropoietin to the brain for endogenous stem cell stimulation after stroke injury, Biomaterials 33(9) (2012) 2681-2692.

[160] A.E. Haggerty, M. Oudega, Biomaterials for spinal cord repair, Neurosci Bull 29(4) (2013) 445-459.

[161] T.D. Merson, J.A. Bourne, Endogenous neurogenesis following ischaemic brain injury: Insights for therapeutic strategies, Int J Biochem Cell B 56 (2014) 4-19.

[162] S. Kubinova, E. Sykova, Biomaterials combined with cell therapy for treatment of spinal cord injury, Regen Med 7(2) (2012) 207-24.

[163] S.W. Liu, T. Schackel, N. Weidner, R. Puttagunta, Biomaterial-Supported Cell Transplantation Treatments for Spinal Cord Injury: Challenges and Perspectives, Frontiers in Cellular Neuroscience 11 (2018).

[164] V. Pertici, T. Trimaille, J. Laurin, M.S. Felix, T. Marqueste, B. Pettmann, J.P. Chauvin, D. Gigmes, P. Decherchi, Repair of the injured spinal cord by implantation of a synthetic degradable block copolymer in rat, Biomaterials 35(24) (2014) 6248-6258.

[165] H. Nomura, C.H. Tator, M.S. Shoichet, Bioengineered strategies for spinal cord repair, J Neurotraum 23(3-4) (2006) 496-507.

[166] L.D. Moon, J.L. Leasure, F.H. Gage, M.B. Bunge, Motor enrichment sustains hindlimb movement recovered after spinal cord injury and glial transplantation, Restor Neurol Neurosci 24(3) (2006) 147-61.

[167] P.D. Dalton, L. Flynn, M.S. Shoichet, Manufacture of poly(2-hydroxyethyl methacrylate-co-methyl methacrylate) hydrogel tubes for use as nerve guidance channels, Biomaterials 23(18) (2002) 3843-51.

[168] A. Hejcl, J. Ruzicka, M. Kapcalova, K. Turnovcova, E. Krumbholcova, M. Pradny, J. Michalek, J. Cihlar, P. Jendelova, E. Sykova, Adjusting the Chemical and Physical Properties of Hydrogels Leads to Improved Stem Cell Survival and Tissue Ingrowth in Spinal Cord Injury Reconstruction: A Comparative Study of Four Methacrylate Hydrogels, Stem Cells Dev 22(20) (2013) 2794-2805.

[169] Y. Xiong, J.X. Zhu, Z.Y. Fang, C.G. Zeng, C. Zhang, G.L. Qi, M.H. Li, W. Zhang, D.P. Quan, J. Wan, Coseeded Schwann cells myelinate neurites from differentiated neural stem cells in neurotrophin-3-loaded PLGA carriers, Int J Nanomedicine 7 (2012) 1977-89.

[170] T. Freier, H.S. Koh, K. Kazazian, M.S. Shoichet, Controlling cell adhesion and degradation of chitosan films by N-acetylation, Biomaterials 26(29) (2005) 5872-8.

[171] H. Nomura, T. Zahir, H. Kim, Y. Katayama, I. Kulbatski, C.M. Morshead, M.S. Shoichet, C.H. Tator, Extramedullary chitosan channels promote survival of transplanted neural stem and progenitor cells and create a tissue bridge after complete spinal cord transection, Tissue Eng Part A 14(5) (2008) 649-65.

[172] H. Nomura, B. Baladie, Y. Katayama, C.M. Morshead, M.S. Shoichet, C.H. Tator, Delayed implantation of intramedullary chitosan channels containing nerve grafts promotes extensive axonal regeneration after spinal cord injury, Neurosurgery 63(1) (2008) 127-41; discussion 141-3.

[173] X. Li, Z. Yang, A. Zhang, The effect of neurotrophin-3/chitosan carriers on the proliferation and differentiation of neural stem cells, Biomaterials 30(28) (2009) 4978-85.

[174] X.R. Li, Z.F. Xiao, J. Han, L. Chen, H.S. Xiao, F.K. Ma, X.L. Hou, X. Li, J. Sun, W.Y. Ding, Y.N. Zhao, B. Chen, J.W. Dai, Promotion of neuronal differentiation of neural progenitor cells by using EGFR antibody functionalized collagen scaffolds for spinal cord injury repair, Biomaterials 34(21) (2013) 5107-5116.

[175] L. Yao, W. Daly, B. Newland, S. Yao, W. Wang, B.K.K. Chen, N. Madigan, A. Windebank, A. Pandit, Improved axonal regeneration of transected spinal cord mediated by multichannel collagen conduits functionalized with neurotrophin-3 gene, Gene Ther 20(12) (2013) 1149-1157.

[176] P. Prang, R. Muller, A. Eljaouhari, K. Heckmann, W. Kunz, T. Weber, C. Faber, M. Vroemen, U. Bogdahn, N. Weidner, The promotion of oriented axonal regrowth in the injured spinal cord by alginate-based anisotropic capillary hydrogels, Biomaterials 27(19) (2006) 3560-3569.

[177] S. Stokols, M.H. Tuszynski, Freeze-dried agarose scaffolds with uniaxial channels stimulate and guide linear axonal growth following spinal cord injury, Biomaterials 27(3) (2006) 443-451.

[178] L.N. Novikova, J. Pettersson, M. Brohlin, M. Wiberg, L.N. Novikov, Biodegradable poly-beta-hydroxybutyrate scaffold seeded with Schwann cells to promote spinal cord repair, Biomaterials 29(9) (2008) 1198-1206.

[179] S. Ribeiro-Samy, N.A. Silva, V.M. Correlo, J.S. Fraga, L. Pinto, A. Teixeira-Castro, H. Leite-Almeida, A. Almeida, J.M. Gimble, N. Sousa, A.J. Salgado, R.L. Reis, Development and Characterization of a PHB-HV-based 3D Scaffold for a Tissue Engineering and Cell-therapy Combinatorial Approach for Spinal Cord Injury Regeneration, Macromol Biosci 13(11) (2013) 1576-1592.

[180] C.H. Hung, Y.L. Lin, T.H. Young, The effect of chitosan and PVDF substrates on the behavior of embryonic rat cerebral cortical stem cells, Biomaterials 27(25) (2006) 4461-4469.

[181] Y. Wan, A.X. Yu, H. Wu, Z.X. Wang, D.J. Wen, Porous-conductive chitosan scaffolds for tissue engineering II. in vitro and in vivo degradation, J Mater Sci-Mater M 16(11) (2005) 1017-1028.

[182] J.Y. Lee, C.A. Bashur, A.S. Goldstein, C.E. Schmidt, Polypyrrole-coated electrospun PLGA nanofibers for neural tissue applications, Biomaterials 30(26) (2009) 4325-4335.

[183] B. Schlosshauer, L. Dreesmann, H.E. Schaller, N. Sinis, Synthetic nerve guide implants in humans: A comprehensive survey, Neurosurgery 59(4) (2006) 740-747.

[184] T. Limongi, A. Rocchi, F. Cesca, H. Tan, E. Miele, A. Giugni, M. Orlando, M.P. Donnorso, G. Perozziello, F. Benfenati, E. Di Fabrizio, Delivery of Brain-Derived Neurotrophic Factor by 3D Biocompatible Polymeric Scaffolds for Neural Tissue Engineering and Neuronal Regeneration, Mol Neurobiol 55(12) (2018) 8788-8798.

[185] N. Haney, P. Akula, A. Reddy, T. Ninh, G. Pema, S. Talwar, B. Rezk, L. Alzweri, Z. Heidari, A. Abdel-Mageed, V. John, W. Hellstrom, The Effect of Insulin- Like Growth Factor-1 (Igf-1) Delivered Via Polymeric Plga Microspheres on Erectile Function after Bilateral Cavernous Nerve Injury in the Rat, J Urology 199(4) (2018) E1175-E1175.

[186] H. Lee, R.J. McKeon, R.V. Bellamkonda, Sustained delivery of thermostabilized chABC enhances axonal sprouting and functional recovery after spinal cord injury, P Natl Acad Sci USA 107(8) (2010) 3340-3345.

[187] X. Cao, M.S. Shoichet, Investigating the synergistic effect of combined neurotrophic factor concentration gradients to guide axonal growth, Neuroscience 122(2) (2003) 381-389.

[188] M.D. Wang, P. Zhai, X.B. Chen, D.J. Schreyer, X.D. Sun, F.Z. Cui, Bioengineered Scaffolds for Spinal Cord Repair, Tissue Eng Part B-Re 17(3) (2011) 177-194.

[189] A.P. Pego, S. Kubinova, D. Cizkova, I. Vanicky, F.M. Mar, M.M. Sousa, E. Sykova, Regenerative medicine for the treatment of spinal cord injury: more than just promises?, J Cell Mol Med 16(11) (2012) 2564-82.

[190] V. Krishna, S. Konakondla, J. Nicholas, A. Varma, M. Kindy, X.J. Wen, Biomaterial-based interventions for neuronal regeneration and functional recovery in rodent model of spinal cord injury: A systematic review, J Spinal Cord Med 36(3) (2013) 174-190.

[191] N.A. Silva, N. Sousa, R.L. Reis, A.J. Salgado, From basics to clinical: A comprehensive review on spinal cord injury, Prog Neurobiol 114 (2014) 25-57.

[192] W.C. Ji, S.Y. Hu, J. Zhou, G. Wang, K.Z. Wang, Y.L. Zhang, Tissue engineering is a promising method for the repair of spinal cord injuries (Review), Exp Ther Med 7(3) (2014) 523-528.

[193] J.R. Siebert, A. Eade, D.J. Osterhout, Biomaterial Approaches to Enhancing Neurorestoration after Spinal Cord Injury: Strategies for Overcoming Inherent Biological Obstacles, Biomed Res Int (2015).

[194] Z. Xiao, F. Tang, J. Tang, H. Yang, Y. Zhao, B. Chen, S. Han, N. Wang, X. Li, S. Cheng, G. Han, C. Zhao, X. Yang, Y. Chen, Q. Shi, S. Hou, S. Zhang, J. Dai, One-year clinical study of NeuroRegen scaffold implantation following scar resection in complete chronic spinal cord injury patients, Sci China Life Sci 59(7) (2016) 647-55.

[195] R. Langer, Polymeric Delivery Systems for Controlled Drug Release, Chem Eng Commun 6(1-3) (1980) 1-48.

[196] H. Hezaveh, I.I. Muhamad, Controlled drug release via minimization of burst release in pH-response kappa-carrageenan/polyvinyl alcohol hydrogels, Chem Eng Res Des 91(3) (2013) 508-519.

[197] X. Huang, C.S. Brazel, Analysis of burst release of proxyphylline from poly(vinyl alcohol) hydrogels, Chem Eng Commun 190(4) (2003) 519-532.

[198] K.J. Pekarek, J.S. Jacob, E. Mathiowitz, Double-Walled Microspheres for Drug-Delivery, Mater Res Soc Symp P 331 (1994) 97-101.

[199] S.K. Mallapragada, N.A. Peppas, P. Colombo, Crystal dissolution-controlled release systems .2. Metronidazole release from semicrystalline poly(vinyl alcohol) systems, J Biomed Mater Res 36(1) (1997) 125-130.

[200] N.S. Patil, J.S. Dordick, D.G. Rethwisch, Macroporous poly(sucrose acrylate) hydrogel for controlled release of macromolecules, Biomaterials 17(24) (1996) 2343-2350.

[201] A.R. Tzafriri, Mathematical modeling of diffusion-mediated release from bulk degrading matrices, Journal of Controlled Release 63(1-2) (2000) 69-79.

[202] A. Kishida, K. Murakami, H. Goto, M. Akashi, H. Kubota, T. Endo, Polymer drugs and polymeric drugs X: Slow release of 5-fluorouracil from biodegradable poly(gamma-glutamic acid) and its benzyl ester matrices, J Bioact Compat Pol 13(4) (1998) 270-278.

[203] C.S. Brazel, N.A. Peppas, Mechanisms of solute and drug transport in relaxing, swellable, hydrophilic glassy polymers, Polymer 40(12) (1999) 3383-3398.

[204] S. Dash, P.N. Murthy, L. Nath, P. Chowdhury, Kinetic Modeling on Drug Release from Controlled Drug Delivery Systems, Acta Pol Pharm 67(3) (2010) 217-223.

[205] X. Huang, C.S. Brazel, On the importance and mechanisms of burst release in matrix-controlled drug delivery systems, J Control Release 73(2-3) (2001) 121-36.

[206] T. Higuchi, Rate of Release of Medicaments from Ointment Bases Containing Drugs in Suspension, J Pharm Sci-Us 50(10) (1961) 874-&.

[207] T. Higuchi, Mechanism of Sustained-Action Medication - Theoretical Analysis of Rate of Release of Solid Drugs Dispersed in Solid Matrices, J Pharm Sci-Us 52(12) (1963) 1145-&.

[208] J. Siepmann, N.A. Peppas, Higuchi equation: derivation, applications, use and misuse, Int J Pharm 418(1) (2011) 6-12.

[209] R.S. Harland, A. Gazzaniga, M.E. Sangalli, P. Colombo, N.A. Peppas, Drug Polymer Matrix Swelling and Dissolution, Pharm Res-Dordr 5(8) (1988) 488-494.

[210] P. Colombo, P.L. Catellani, N.A. Peppas, L. Maggi, U. Conte, Swelling Characteristics of Hydrophilic Matrices for Controlled Release New Dimensionless Number to Describe the Swelling and Release Behavior, Int J Pharm 88(1-3) (1992) 99-109.

[211] N.A. Peppas, P. Colombo, Analysis of drug release behavior from swellable polymer carriers using the dimensionality index, Journal of Controlled Release 45(1) (1997) 35-40.

[212] N.A. Peppas, N.M. Franson, The Swelling Interface Number as a Criterion for Prediction of Diffusional Solute Release Mechanisms in Swellable Polymers, J Polym Sci Pol Phys 21(6) (1983) 983-997.

[213] R.W. Korsmeyer, E. Vonmeerwall, N.A. Peppas, Solute and Penetrant Diffusion in Swellable Polymers .2. Verification of Theoretical-Models, J Polym Sci Pol Phys 24(2) (1986) 409-434.

[214] T.R. Stumpf, X.Y. Yang, J.C. Zhang, X.D. Cao, In situ and ex situ modifications of bacterial cellulose for applications in tissue engineering, Mat Sci Eng C-Mater 82 (2018) 372-383.

[215] D. Klemm, B. Heublein, H.P. Fink, A. Bohn, Cellulose: Fascinating biopolymer and sustainable raw material, Angew Chem Int Edit 44(22) (2005) 3358-3393.

[216] K. Keegstra, Plant Cell Walls, Plant Physiol 154(2) (2010) 483-486.

[217] A.F. Jozala, L.C. de Lencastre-Novaes, A.M. Lopes, V.D. Santos-Ebinuma, P.G. Mazzola, A. Pessoa, D. Grotto, M. Gerenutti, M.V. Chaud, Bacterial nanocellulose production and application: a 10-year overview, Appl Microbiol Biot 100(5) (2016) 2063-2072.

[218] A.J. Brown, On an acetic ferment which forms cellulose, Journal of the Chemical Society 49 (1886) 432-439.

[219] A.J. Brown, The chemical action of pure cultivation of Bacterium aceti, Journal Of Chemical Society 49 (1886) 172–186.

[220] H. El-Saied, A.H. Basta, R.H. Gobran, Research progress in friendly environmental technology for the production of cellulose products (bacterial cellulose and its application), Polym-Plast Technol 43(3) (2004) 797-820.

[221] S.-P. Lin, I. Loira Calvar, J. Catchmark, J.-R. Liu, A. Demirci, K.-C. Cheng, Biosynthesis, production and applications of bacterial cellulose, Cellulose 20(5) (2013) 2191-2219.

[222] P. Ross, R. Mayer, M. Benziman, Cellulose biosynthesis and function in bacteria, Microbiol Rev 55(1) (1991) 35-58.

[223] P. Ross, H. Weinhouse, Y. Aloni, D. Michaeli, P. Weinbergerohana, R. Mayer, S. Braun, E. Devroom, G.A. Vandermarel, J.H. Vanboom, M. Benziman, Regulation of Cellulose Synthesis in Acetobacter-Xylinum by Cyclic Diguanylic Acid, Nature 325(6101) (1987) 279-281.

[224] Z.J. Shi, Y. Zhang, G.O. Phillips, G. Yang, Utilization of bacterial cellulose in food, Food Hydrocolloid 35 (2014) 539-545.

[225] C. Campano, A. Balea, A. Blanco, C. Negro, Enhancement of the fermentation process and properties of bacterial cellulose: a review, Cellulose 23(1) (2016) 57-91.

[226] K.Y. Lee, G. Buldum, A. Mantalaris, A. Bismarck, More Than Meets the Eye in Bacterial Cellulose: Biosynthesis, Bioprocessing, and Applications in Advanced Fiber Composites, Macromol Biosci 14(1) (2014) 10-32.

[227] V. Yadav, B.J. Paniliatis, H. Shi, K. Lee, P. Cebe, D.L. Kaplan, Novel In Vivo-Degradable Cellulose-Chitin Copolymer from Metabolically Engineered Gluconacetobacter xylinus, Appl Environ Microb 76(18) (2010) 6257-6265.

[228] Y. Yamada, P. Yukphan, T.L.V. Huong, Y. Muramatsu, D. Ochaikul, S. Tanasupawat, Y. Nakagawa, Description of Komagataeibacter gen. nov., with proposals of new combinations (Acetobacteraceae), J Gen Appl Microbiol 58(5) (2012) 397-404.

[229] M. Florea, H. Hagemann, G. Santosa, J. Abbott, C.N. Micklem, X. Spencer-Milnes, L.D. Garcia, D. Paschou, C. Lazenbatt, D.Z. Kong, H. Chughtai, K. Jensen, P.S. Freemont, R. Kitney, B. Reeve, T. Ellis, Engineering control of bacterial cellulose production using a genetic toolkit and a new cellulose-producing strain, P Natl Acad Sci USA 113(24) (2016) E3431-E3440.

[230] A. Suwanposri, P. Yukphan, Y. Yamada, D. Ochaikul, Identification and biocellulose production of Gluconacetobacter strains isolated from tropical fruits in Thailand, Maejo Int J Sci Tech 7(1) (2013) 70-82.

[231] J. Fang, S. Kawano, K. Tajima, T. Kondo, In Vivo Curdlan/Cellulose Bionanocomposite Synthesis by Genetically Modified Gluconacetobacter xylinus, Biomacromolecules 16(10) (2015) 3154-3160.

[232] M. Florea, B. Reeve, J. Abbott, P.S. Freemont, T. Ellis, Genome sequence and plasmid transformation of the model high-yield bacterial cellulose producer Gluconacetobacter hansenii ATCC 53582, Sci Rep-Uk 6 (2016).

[233] H. Backdahl, G. Helenius, A. Bodin, U. Nannmark, B.R. Johansson, B. Risberg, P. Gatenholm, Mechanical properties of bacterial cellulose and interactions with smooth muscle cells, Biomaterials 27(9) (2006) 2141-2149.

[234] D. Klemm, D. Schumann, U. Udhardt, S. Marsch, Bacterial synthesized cellulose - artificial blood vessels for microsurgery, Prog Polym Sci 26(9) (2001) 1561-1603.

[235] J.A. Camarero, B.J. Hackel, J.J. de Yoreo, A.R. Mitchell, A new method for the preparation of peptide C-terminal alpha-thioesters compatible with Fmoc-solid-phase peptide synthesis, Peptide Revolution: Genomics, Proteomics & Therapeutics (2004) 111-112.

[236] P. White, R. Steinauer, S. Barthelemy, B. Dorner, Pseudoproline Dipeptides in Fmoc-Solid Phase Peptide Synthesis, J Pept Sci 10 (2004) 151-151.

[237] F.V. Berti, C.R. Rambo, P.F. Dias, L.M. Porto, Nanofiber density determines endothelial cell behavior on hydrogel matrix, Materials Science and Engineering: C 33(8) (2013) 4684-4691.

[238] S. Gea, C.T. Reynolds, N. Roohpour, B. Wirjosentono, N. Soykeabkaew, E. Bilotti, T. Peijs, Investigation into the structural, morphological, mechanical and thermal behaviour of bacterial cellulose after a two-step purification process, Bioresource Technol 102(19) (2011) 9105-9110.

[239] A. Meftahi, R. Khajavi, A. Rashidi, M.K. Rahimi, A. Bahador, Effect of Purification on Nano Microbial Cellulose Pellicle Properties, Proc Mat Sci 11 (2015) 206-211.

[240] B.A. McKenna, D. Mikkelsen, J.B. Wehr, M.J. Gidley, N.W. Menzies, Mechanical and structural properties of native and alkali-treated bacterial cellulose produced by Gluconacetobacter xylinus strain ATCC 53524, Cellulose 16(6) (2009) 1047-1055.

[241] M. Iguchi, S. Yamanaka, A. Budhiono, Bacterial cellulose - a masterpiece of nature's arts, J Mater Sci 35(2) (2000) 261-270.

[242] A.M. Sokolnicki, R.J. Fisher, T.P. Harrah, D.L. Kaplan, Permeability of bacterial cellulose membranes, J Membrane Sci 272(1-2) (2006) 15-27.

[243] A.R.Y. Marzieh Moosavi-Nasab, Investigation of Physicochemical Properties of the Bacterial Cellulose Produced by Gluconacetobacter xylinus from Date Syrup, World Academy of Science, Engineering and Technology, 2010, pp. 1248-1253.

[244] S.B. Lin, C.P. Hsu, L.C. Chen, H.H. Chen, Adding enzymatically modified gelatin to enhance the rehydration abilities and mechanical properties of bacterial cellulose, Food Hydrocolloid 23(8) (2009) 2195-2203.

[245] C.N. Choi, H.J. Song, M.J. Kim, M.H. Chang, S.J. Kim, Properties of bacterial cellulose produced in a pilot-scale spherical type bubble column bioreactor, Korean J Chem Eng 26(1) (2009) 136-140.

[246] M. Ul-Islam, T. Khan, J.K. Park, Water holding and release properties of bacterial cellulose obtained by in situ and ex situ modification, Carbohyd Polym 88(2) (2012) 596-603.

[247] H.S. Barud, J.L. Souza, D.B. Santos, M.S. Crespi, C.A. Ribeiro, Y. Messaddeq, S.J.L. Ribeiro, Bacterial cellulose/poly(3-hydroxybutyrate) composite membranes, Carbohyd Polym 83(3) (2011) 1279-1284.

[248] N. Shah, M. Ul-Islam, W.A. Khattak, J.K. Park, Overview of bacterial cellulose composites: A multipurpose advanced material, Carbohyd Polym 98(2) (2013) 1585-1598.

[249] W.L. Hu, S.Y. Chen, J.X. Yang, Z. Li, H.P. Wang, Functionalized bacterial cellulose derivatives and nanocomposites, Carbohydrate Polymers 101 (2014) 1043-1060.

[250] D.O.S. Recouvreux, C.R. Rambo, F.V. Berti, C.A. Carminatti, R.V. Antonio, L.M. Porto, Novel three-dimensional cocoon-like hydrogels for soft tissue regeneration, Mat Sci Eng C-Mater 31(2) (2011) 151-157.

[251] G. Guhados, W.K. Wan, J.L. Hutter, Measurement of the elastic modulus of single bacterial cellulose fibers using atomic force microscopy, Langmuir 21(14) (2005) 6642-6646.

[252] J.D. Fontana, A.M. Desouza, C.K. Fontana, I.L. Torriani, J.C. Moreschi, B.J. Gallotti, S.J. Desouza, G.P. Narcisco, J.A. Bichara, L.F.X. Farah, Acetobacter Cellulose Pellicle as a Temporary Skin Substitute, Appl Biochem Biotech 24-5 (1990) 253-264.

[253] K. Watanabe, Y. Eto, S. Takano, S. Nakamori, H. Shibai, S. Yamanaka, A New Bacterial Cellulose Substrate for Mammalian-Cell Culture - a New Bacterial Cellulose Substrate, Cytotechnology 13(2) (1993) 107-114.

[254] E. Fragal, T.S.P. Cellet, V.H. Fragal, M.V.P. Companhoni, T. Ueda-Nakamura, E.C. Muniz, R. Silva, A.F. Rubira, Hybrid materials for bone tissue engineering from biomimetic growth of hydroxiapatite on cellulose nanowhiskers, Carbohyd Polym 152 (2016) 734-746.

[255] H.L. Luo, D.H. Ji, W. Li, J. Xiao, C.Z. Li, G.Y. Xiong, Y. Zhu, Y.Z. Wan, Constructing a highly bioactive 3D nanofibrous bioglass scaffold via bacterial cellulose-templated sol-gel approach, Materials Chemistry and Physics 176 (2016) 1-5.

[256] E. Akaraonye, J. Filip, M. Safarikova, V. Salih, T. Keshavarz, J.C. Knowles, I. Roy, Composite scaffolds for cartilage tissue engineering based on natural polymers of bacterial origin, thermoplastic poly(3-hydroxybutyrate) and micro-fibrillated bacterial cellulose, Polym Int 65(7) (2016) 780-791.

[257] S.S. Zang, Q. Zhuo, X. Chang, G.X. Qiu, Z.H. Wu, G. Yang, Study of osteogenic differentiation of human adipose-derived stem cells (HASCs) on bacterial cellulose, Carbohyd Polym 104 (2014) 158-165.

[258] W.K. Czaja, D.J. Young, M. Kawecki, R.M. Brown, The future prospects of microbial cellulose in biomedical applications, Biomacromolecules 8(1) (2007) 1-12.

[259] E.J. Vandamme, S. De Baets, A. Vanbaelen, K. Joris, P. De Wulf, Improved production of bacterial cellulose and its application potential, Polym Degrad Stabil 59(1-3) (1998) 93-99.

[260] A. Semlali, K. Killer, H. Alanazi, W. Chmielewski, M. Rouabhia, Cigarette smoke condensate increases C. albicans adhesion, growth, biofilm formation, and EAP1, HWP1 and SAP2 gene expression, Bmc Microbiol 14 (2014).

[261] G.F. Perotti, H.S. Barud, Y. Messaddeq, S.J.L. Ribeiro, V.R.L. Constantino, Bacterial cellulose-laponite clay nanocomposites, Polymer 52(1) (2011) 157-163.

[262] Y. Hu, J.M. Catchmark, Formation and Characterization of Spherelike Bacterial Cellulose Particles Produced by Acetobacter xylinum JCM 9730 Strain, Biomacromolecules 11(7) (2010) 1727-1734.

[263] H.C. Huang, L.C. Chen, S.B. Lin, H.H. Chen, Nano-biomaterials application In situ modification of bacterial cellulose structure by adding HPMC during fermentation, Carbohyd Polym 83(2) (2011) 979-987.

[264] O.A. Saibuatong, M. Phisalaphong, Novo aloe vera-bacterial cellulose composite film from biosynthesis, Carbohyd Polym 79(2) (2010) 455-460.

[265] H.C. Huang, L.C. Chen, S.B. Lin, C.P. Hsu, H.H. Chen, In situ modification of bacterial cellulose network structure by adding interfering substances during fermentation, Bioresource Technol 101(15) (2010) 6084-6091.

[266] Y.Y. Feng, X.Q. Zhang, Y.T. Shen, K. Yoshino, W. Feng, A mechanically strong, flexible and conductive film based on bacterial cellulose/graphene nanocomposite, Carbohyd Polym 87(1) (2012) 644-649.

[267] A.L. Buyanov, I.V. Gofman, L.G. Revel'skaya, A.K. Khripunov, A.A. Tkachenko, Anisotropic swelling and mechanical behavior of composite bacterial cellulose-poly(acrylamide or acrylamide-sodium acrylate) hydrogels, J Mech Behav Biomed 3(1) (2010) 102-111.

[268] J. George, K.V. Ramana, A.S. Bawa, Siddaramaiah, Bacterial cellulose nanocrystals exhibiting high thermal stability and their polymer nanocomposites, Int J Biol Macromol 48(1) (2011) 50-57.

[269] H.S. Barud, J.M.A. Caiut, J. Dexpert-Ghys, Y. Messaddeq, S.J.L. Ribeiro, Transparent Bacterial Cellulose-Boehmite-epoxi-Siloxane Nanocomposites, Composites Part A: Applied Science and Manufacturing (0) (2012).

[270] S. Gea, E. Bilotti, C.T. Reynolds, N. Soykeabkeaw, T. Peijs, Bacterial cellulose-poly(vinyl alcohol) nanocomposites prepared by an in-situ process, Mater Lett 64(8) (2010) 901-904.

[271] M.A. Woehl, C.D. Canestraro, A. Mikowski, M.R. Sierakowski, L.P. Ramos, F. Wypych, Bionanocomposites of thermoplastic starch reinforced with bacterial cellulose nanofibres: Effect of enzymatic treatment on mechanical properties, Carbohyd Polym 80(3) (2010) 866-873.

[272] D. Muller, C.R. Rambo, D.O.S. Recouvreux, L.M. Porto, G.M.O. Barra, Chemical in situ polymerization of polypyrrole on bacterial cellulose nanofibers, Synthetic Met 161(1-2) (2011) 106-111.

[273] M. Sakaguchi, T. Ohura, T. Iwata, Diblock copolymer of bacterial cellulose and poly(methyl methacrylate) initiated by chain-end-type radicals produced by mechanical scission of glycosidic linkages of bacterial cellulose, Abstr Pap Am Chem S 241 (2011).

[274] S.T. Chang, L.C. Chen, S.B. Lin, H.H. Chen, Nano-biomaterials application: Morphology and physical properties of bacterial cellulose/gelatin composites via crosslinking, Food Hydrocolloid 27(1) (2012) 137-144.

[275] E. Trovatti, L. Oliveira, C.S.R. Freire, A.J.D. Silvestre, C.P. Neto, J.J.C.C. Pinto, A. Gandini, Novel bacterial cellulose-acrylic resin nanocomposites, Compos Sci Technol 70(7) (2010) 1148-1153.

[276] Z.J. Cai, G. Yang, Optical nanocomposites prepared by incorporating bacterial cellulose nanofibrils into poly(3-hydroxybutyrate), Mater Lett 65(2) (2011) 182-184.

[277] T. Oshima, S. Taguchi, K. Ohe, Y. Baba, Phosphorylated bacterial cellulose for adsorption of proteins, Carbohyd Polym 83(2) (2011) 953-958.

[278] D. Tsalagkas, R. Lagana, I. Poljansek, P. Oven, L. Csoka, Fabrication of bacterial cellulose thin films self-assembled from sonochemically prepared nanofibrils and its characterization, Ultrason Sonochem 28 (2016) 136-143.

[279] K.V. Ramana, A. Tomar, L. Singh, Effect of various carbon and nitrogen sources on cellulose synthesis by Acetobacter xylinum, World J Microb Biot 16(3) (2000) 245-248.

[280] N.I. Tkacheva, S.V. Morozov, I.A. Grigor'ev, D.M. Mognonov, N.A. Kolchanov, Modification of cellulose as a promising direction in the design of new materials, Polymer Science Series B 55(7-8) (2013) 409-429.

[281] D.R. Ruka, G.P. Simon, K.M. Dean, Altering the growth conditions of Gluconacetobacter xylinus to maximize the yield of bacterial cellulose, Carbohyd Polym 89(2) (2012) 613-622.

[282] W.H. Tang, S.R. Jia, Y.Y. Jia, H.J. Yang, The influence of fermentation conditions and post-treatment methods on porosity of bacterial cellulose membrane, World J Microb Biot 26(1) (2010) 125-131.

[283] S. Masaoka, T. Ohe, N. Sakota, Production of Cellulose from Glucose by Acetobacter-Xylinum, J Ferment Bioeng 75(1) (1993) 18-22.

[284] R. Jonas, L.F. Farah, Production and application of microbial cellulose, Polym Degrad Stabil 59(1–3) (1998) 101-106.

[285] A.B. Novaes Jr, A.B. Novaes, Bone formation over a TiAl6V4(IMZ) implant placed into an extraction socket in association with membrane therapy (Gengiflex), Clinical Oral Implants Research 4(2) (1993) 106-110.

[286] S.C. Falcao, J.E. Neto, A.R.D.B. Coelho, Incorporation by host tissue of two biomaterials used as repair of defects produced in abdominal wall of rats, Acta Cir Bras 23(1) (2008) 78-83.

[287] L.R. Mello, L.T. Feltrin, P.T.F. Neto, F.A.P. Ferraz, Duraplasty with biosynthetic cellulose: An experimental study, J Neurosurg 86(1) (1997) 143-150.

[288] W. Czaja, A. Krystynowicz, S. Bielecki, R.M. Brown, Microbial cellulose - the natural power to heal wounds, Biomaterials 27(2) (2006) 145-151.

[289] J.W. Lee, F. Deng, W.G. Yeomans, A.L. Allen, R.A. Gross, D.L. Kaplan, Direct incorporation of glucosamine and N-acetylglucosamine into exopolymers by Gluconacetobacter xylinus (=Acetobacter xylinum) ATCC 10245: Production of chitosan-cellulose and chitin-cellulose exopolymers, Appl Environ Microb 67(9) (2001) 3970-3975.

[290] D. Ciechanska, Multifunctional bacterial cellulose/chitosan composite materials for medical applications, Fibres Text East Eur 12(4) (2004) 69-72.

[291] W.F. Dudman, Cellulose production by Acetobacter actigenum in defined medium, J Gen Microbiol 21 (1959) 327-37.

[292] M. Schramm, S. Hestrin, Factors Affecting Production of Cellulose at the Air Liquid Interface of a Culture of Acetobacter-Xylinum, Journal of General Microbiology 11(1) (1954) 123-&.

[293] F. Yoshinaga, N. Tonouchi, K. Watanabe, Research progress in production of bacterial cellulose by aeration and agitation culture and its application as a new industrial material, Biosci Biotech Bioch 61(2) (1997) 219-224.

[294] W. Czaja, D. Romanovicz, R.M. Brown, Structural investigations of microbial cellulose produced in stationary and agitated culture, Cellulose 11(3-4) (2004) 403-411.

[295] M. Schramm, Z. Gromet, S. Hestrin, Synthesis of Cellulose by Acetobacter-Xylinum .3. Substrates and Inhibitors, Biochem J 67 (1957) 669-679.

[296] H.X. Zhu, S.R. Jia, H.J. Yang, Y.Y. Jia, L. Yan, J. Li, Preparation and Application of Bacterial Cellulose Sphere: A Novel Biomaterial, Biotechnol Biotec Eq 25(1) (2011) 2233-2236.

[297] D.O.S. Recouvreux, Desenvolvimento de novos biomateriais baseados em celulose bacteriana para aplicações biomédicas e de engenharia de tecidos, Programa de Pós-Graduação em Engenharia Química, Universidade Federal de Santa Catarina, Florianópolis, 2008, p. 124.

[298] M. Scherner, S. Reutter, D. Klemm, A. Sterner-Kock, M. Guschlbauer, T. Richter, G. Langebartels, N. Madershahian, T. Wahlers, J. Wippermann, In vivo application of tissue-engineered blood vessels of bacterial cellulose as small arterial substitutes: proof of concept?, J Surg Res 189(2) (2014) 340-347.

[299] S.S. Zang, R. Zhang, H. Chen, Y.D. Lu, J.H. Zhou, X. Chang, G.X. Qiu, Z.H. Wu, G. Yang, Investigation on artificial blood vessels prepared from bacterial cellulose, Mat Sci Eng C-Mater 46 (2015) 111-117.

[300] D.A. Schumann, J. Wippermann, D.O. Klemm, F. Kramer, D. Koth, H. Kosmehl, T. Wahlers, S. Salehi-Gelani, Artificial vascular implants from bacterial cellulose: preliminary results of small arterial substitutes, Cellulose 16(5) (2009) 877-885.

[301] J. Wippermann, D. Schumann, D. Klemm, H. Kosmehl, S. Satehi-Gelani, T. Wahlers, Preliminary Results of Small Arterial Substitute Performed with a New Cylindrical Biomaterial Composed of Bacterial Cellulose, Eur J Vasc Endovasc 37(5) (2009) 592-596.

[302] A. Bodin, H. Backdahl, H. Fink, L. Gustafsson, B. Risberg, P. Gatenholm, Influence of cultivation conditions on mechanical and morphological properties of bacterial cellulose tubes, Biotechnol Bioeng 97(2) (2007) 425-434.

[303] H. Backdahl, B. Risberg, P. Gatenholm, Observations on bacterial cellulose tube formation for application as vascular graft, Mat Sci Eng C-Mater 31(1) (2011) 14-21.

[304] F. Hong, B. Wei, L. Chen, Preliminary Study on Biosynthesis of Bacterial Nanocellulose Tubes in a Novel Double-Silicone-Tube Bioreactor for Potential Vascular Prosthesis, Biomed Res Int (2015).

[305] H. Orelma, L.O. Morales, L.S. Johansson, I.C. Hoeger, I. Filpponen, C. Castro, O.J. Rojas, J. Laine, Affibody conjugation onto bacterial cellulose tubes and bioseparation of human serum albumin, Rsc Adv 4(93) (2014) 51440-51450.

[306] K. Kowalska-Ludwicka, J. Cala, B. Grobelski, D. Sygut, D. Jesionek-Kupnicka, M. Kolodziejczyk, S. Bielecki, Z. Pasieka, Modified bacterial cellulose tubes for regeneration of damaged peripheral nerves, Arch Med Sci 9(3) (2013) 527-534.

[307] C.L. Zhu, F. Li, X.Y. Zhou, L. Lin, T.Y. Zhang, Kombucha-synthesized bacterial cellulose: Preparation, characterization, and biocompatibility evaluation, J Biomed Mater Res A 102(5) (2014) 1548-1557.

[308] A. Bodin, H. BÄCKDAHL, P. Gatenholm, L. Gustafsson, B. Risberg, Bacterial cellulose tubes, Google Patents, 2012.

[309] H.G.O. Barud, H.D. Barud, M. Cavicchioli, T.S. do Amaral, O.B. de Oliveira, D.M. Santos, A.L.D.A. Petersen, F. Celes, V.M. Borges, C.I. de Oliveira, P.F. de Oliveira, R.A. Furtado, D.C. Tavares, S.J.L. Ribeiro, Preparation and characterization of a bacterial cellulose/silk fibroin sponge scaffold for tissue regeneration, Carbohyd Polym 128 (2015) 41-51.

[310] C.A. Gao, Y.Z. Wan, C.X. Yang, K.R. Dai, T.T. Tang, H.L. Luo, J.H. Wang, Preparation and characterization of bacterial cellulose sponge with hierarchical pore structure as tissue engineering scaffold, J Porous Mat 18(2) (2011) 139-145.

[311] W. Shao, H. Liu, X.F. Liu, S.X. Wang, J.M. Wu, R. Zhang, H.H. Min, M. Huang, Development of silver sulfadiazine loaded bacterial cellulose/sodium alginate composite films with enhanced antibacterial property, Carbohyd Polym 132 (2015) 351-358.

[312] B. Wei, G.A. Yang, F. Hong, Preparation and evaluation of a kind of bacterial cellulose dry films with antibacterial properties, Carbohyd Polym 84(1) (2011) 533-538.

[313] I.M. Jipa, L. Dobre, M. Stroescu, A. Stoica-Guzun, S. Jinga, T. Dobre, Preparation and characterization of bacterial cellulose-poly(vinyl alcohol) films with antimicrobial properties, Mater Lett 66(1) (2012) 125-127.

[314] G. Yang, J.J. Xie, F. Hong, Z.J. Cao, X.X. Yang, Antimicrobial activity of silver nanoparticle impregnated bacterial cellulose membrane: Effect of fermentation carbon sources of bacterial cellulose, Carbohyd Polym 87(1) (2012) 839-845.

[315] L.C.S. Maria, A.L.C. Santos, P.C. Oliveira, A.S.S. Valle, H.S. Barud, Y. Messaddeq, S.J.L. Ribeiro, Preparation and Antibacterial Activity of Silver Nanoparticles Impregnated in Bacterial Cellulose, Polimeros 20(1) (2010) 72-77.

[316] H.S. Barud, C.A. Ribeiro, J.M.V. Capela, M.S. Crespi, S.J.L. Ribeiro, Y. Messadeq, Kinetic parameters for thermal decomposition of microcrystalline, vegetal, and bacterial cellulose, J Therm Anal Calorim 105(2) (2011) 421-426.

[317] M. Sureshkumar, D.Y. Siswanto, C.K. Lee, Magnetic antimicrobial nanocomposite based on bacterial cellulose and silver nanoparticles, J Mater Chem 20(33) (2010) 6948-6955.

[318] C. Katepetch, R. Rujiravanit, H. Tamura, Formation of nanocrystalline ZnO particles into bacterial cellulose pellicle by ultrasonic-assisted in situ synthesis, Cellulose 20(3) (2013) 1275-1292.

[319] F.S. Jebel, H. Almasi, Morphological, physical, antimicrobial and release properties of ZnO nanoparticles-loaded bacterial cellulose films, Carbohyd Polym 149 (2016) 8-19.

[320] J.B. Luan, J. Wu, Y.D. Zheng, W.H. Song, G.J. Wang, J. Guo, X. Ding, Impregnation of silver sulfadiazine into bacterial cellulose for antimicrobial and biocompatible wound dressing, Biomed Mater 7(6) (2012).

[321] Q. Shi, Y. Li, J. Sun, H. Zhang, L. Chen, B. Chen, H.L. Yang, Z.X. Wang, The osteogenesis of bacterial cellulose scaffold loaded with bone morphogenetic protein-2, Biomaterials 33(28) (2012) 6644-6649.

[322] A. Svensson, E. Nicklasson, T. Harrah, B. Panilaitis, D.L. Kaplan, M. Brittberg, P. Gatenholm, Bacterial cellulose as a potential scaffold for tissue engineering of cartilage, Biomaterials 26(4) (2005) 419-431.

[323] F.K. Andrade, J.P. Silva, M. Carvalho, E.M.S. Castanheira, R. Soares, M. Gama, Studies on the hemocompatibility of bacterial cellulose, J Biomed Mater Res A 98A(4) (2011) 554-566.

[324] F.K. Andrade, R. Costa, L. Domingues, R. Soares, M. Gama, Improving bacterial cellulose for blood vessel replacement: Functionalization with a chimeric protein containing a cellulose-binding module and an adhesion peptide, Acta Biomater 6(10) (2010) 4034-4041.

[325] F.K. Andrade, S.M.G. Moreira, L. Domingues, F.M.P. Gama, Improving the affinity of fibroblasts for bacterial cellulose using carbohydrate-binding modules fused to RGD, J Biomed Mater Res A 92A(1) (2010) 9-17.

[326] H. Fink, L. Ahrenstedt, A. Bodin, H. Brumer, P. Gatenholm, A. Krettek, B. Risberg, Bacterial cellulose modified with xyloglucan bearing the adhesion peptide RGD promotes endothelial cell adhesion and metabolism - a promising modification for vascular grafts, J Tissue Eng Regen M 5(6) (2011) 454-463.

[327] A. Bodin, L. Ahrenstedt, H. Fink, H. Brumer, B. Risberg, P. Gatenholm, Modification of nanocellulose with a xyloglucan-RGD conjugate enhances adhesion and proliferation of endothelial cells: Implications for tissue engineering, Biomacromolecules 8(12) (2007) 3697-3704.

[328] M. Rouabhia, J. Asselin, N. Tazi, Y. Messaddeq, D. Levinson, Z. Zhang, Production of biocompatible and antimicrobial bacterial cellulose polymers functionalized by RGDC grafting groups and gentamicin, ACS Appl Mater Interfaces 6(3) (2014) 1439-46.

[329] R. Pertile, S. Moreira, F. Andrade, L. Domingues, M. Gama, Bacterial cellulose modified using recombinant proteins to improve neuronal and mesenchymal cell adhesion, Biotechnol Prog (2011).

[330] V. Made, S. Els-Heindl, A.G. Beck-Sickinger, Automated solid-phase peptide synthesis to obtain therapeutic peptides, Beilstein J Org Chem 10 (2014) 1197-1212.

[331] D.J. Craik, D.P. Fairlie, S. Liras, D. Price, The Future of Peptide-based Drugs, Chem Biol Drug Des 81(1) (2013) 136-147.

[332] T. Uhlig, T. Kyprianou, F.G. Martinelli, C.A. Oppici, D. Heiligers, D. Hills, X.R. Calvo, P. Verhaert, The emergence of peptides in the pharmaceutical business: From exploration to exploitation, EuPA Open Proteomics 4 (2014) 58-69.

[333] R.B. Merrifield, Solid Phase Peptide Synthesis. I. The Synthesis of a Tetrapeptide, Journal of the American Chemical Society 85(14) (1963) 2149-2154.

[334] R.B. Merrifield, Solid-Phase Synthesis (Nobel Lecture), Angewandte Chemie-International Edition in English 24(10) (1985) 799-810.

[335] M. Amblard, J.A. Fehrentz, J. Martinez, G. Subra, Methods and Protocols of modern solid phase peptide synthesis, Mol Biotechnol 33(3) (2006) 239-254.

[336] V. Haridas, S. Sadanandan, P.Y. Collart-Dutilleul, S. Gronthos, N.H. Voelcker, Lysine-Appended Polydiacetylene Scaffolds for Human Mesenchymal Stem Cells, Biomacromolecules 15(2) (2014) 582-590.

[337] R.A. Plenderleith, C.J. Pateman, C. Rodenburg, J.W. Haycock, F. Claeyssens, C. Sammond, S. Rimmer, Arginine-glycine-aspartic acid functional branched semi-interpenetrating hydrogels, Soft Matter 11(38) (2015) 7567-7578.

[338] S. Ramesh, P. Cherkupally, T. Govender, H.G. Kruger, F. Albericio, B.G. de la Torre, 6-(Bromomaleimido)hexanoic Acid as a Connector for the Construction of Multiple Branched Peptide Platforms, Org Lett 17(3) (2015) 464-467.

[339] K. Sadler, J.P. Tam, Peptide dendrimers: applications and synthesis, Journal of Biotechnology 90(3-4) (2002) 195-229.

[340] J. Lu, X.-B. Tian, W. Huang, A new strategy for synthesis of branched cyclic peptide by Asn side-chain hydrazide ligation, Chinese Chemical Letters (0).

[341] W. Chan, P. White, Fmoc Solid Phase Peptide Synthesis: A Practical Approach, OUP Oxford2000.

[342] K.S. Lam, S.E. Salmon, E.M. Hersh, V.J. Hruby, W.M. Kazmierski, R.J. Knapp, A New Type of Synthetic Peptide Library for Identifying Ligand-Binding Activity, Nature 354(6348) (1991) 82-84.

[343] R. Franke, T. Hirsch, J. Eichler, A rationally designed synthetic mimic of the discontinuous CD4-binding site of HIV-1 gp120, J Recept Sig Transd 26(5-6) (2006) 453-460.

[344] J. Eichler, Synthetic peptide arrays and peptide combinatorial libraries for the exploration of protein-ligand interactions and the design of protein inhibitors, Comb Chem High T Scr 8(2) (2005) 135-143.

[345] K. Sadler, J.P. Tam, Peptide dendrimers: applications and synthesis, Reviews in Molecular Biotechnology 90(3–4) (2002) 195-229.

[346] J.P. Tam, Recent advances in multiple antigen peptides, J Immunol Methods 196(1) (1996) 17-32.

[347] M.J. Gomara, S. Riedemann, I. Vega, H. Ibarra, G. Ercilla, I. Haro, Use of linear and multiple antigenic peptides in the immunodiagnosis of acute hepatitis A virus infection, J Immunol Methods 234(1-2) (2000) 23-34.

[348] I. Kim, H.H. Jeong, Y.J. Kim, N.E. Lee, K.M. Huh, C.S. Lee, G.H. Kim, E. Lee, A "Light-up" 1D supramolecular nanoprobe for silver ions based on assembly of pyrene-labeled peptide amphiphiles: cell-imaging and antimicrobial activity, J Mater Chem B 2(38) (2014) 6478-6486.

[349] J.G. Li, S.P. Liu, R. Lakshminarayanan, Y. Bai, K. Pervushin, C. Verma, R.W. Beuerman, Molecular simulations suggest how a branched antimicrobial peptide perturbs a bacterial membrane and enhances permeability, Bba-Biomembranes 1828(3) (2013) 1112-1121.

[350] P. Kim, C.P. Pau, Comparing tandem repeats and multiple antigenic peptides as the antigens to detect antibodies by enzyme immunoassay, J Immunol Methods 257(1-2) (2001) 51-54.

[351] I.A. Monreal, Q. Liu, K. Tyson, T. Bland, D.S. Dalisay, E.V. Adams, G.A. Wayman, H.C. Aguilar, J.P. Saludes, Branched dimerization of Tat peptide improves permeability to HeLa and hippocampal neuronal cells, Chem Commun 51(25) (2015) 5463-5466.

[352] W.L. Zhu, S.Y. Shin, Effects of dimerization of the cell-penetrating peptide Tat analog on antimicrobial activity and mechanism of bactericidal action, J Pept Sci 15(5) (2009) 345-352.

[353] F.S. Hassane, G.D. Ivanova, E. Bolewska-Pedyczak, R. Abes, A.A. Arzumanov, M.J. Gait, B. Lebleu, J. Gariepy, A Peptide-Based Dendrimer That Enhances the Splice-Redirecting Activity of PNA Conjugates in Cells, Bioconjugate Chem 20(8) (2009) 1523-1530.

[354] A.M. Angeles-Boza, A. Erazo-Oliveras, Y.J. Lee, J.P. Pellois, Generation of Endosomolytic Reagents by Branching of Cell-Penetrating Peptides: Tools for the Delivery of Bioactive Compounds to Live Cells in Cis or Trans, Bioconjugate Chem 21(12) (2010) 2164-2167.

[355] G.A. Eggimann, S. Buschor, T. Darbre, J.L. Reymond, Convergent synthesis and cellular uptake of multivalent cell penetrating peptides derived from Tat, Antp, pVEC, TP10 and SAP, Org Biomol Chem 11(39) (2013) 6717-6733.

[356] G.A. Eggimann, E. Blattes, S. Buschor, R. Biswas, S.M. Kammer, T. Darbre, J.L. Reymond, Designed cell penetrating peptide dendrimers efficiently internalize cargo into cells, Chem Commun 50(55) (2014) 7254-7257.

[357] S.H. Park, J. Doh, S.I. Park, J.Y. Lim, S.M. Kim, J.I. Youn, H.T. Jin, S.H. Seo, M.Y. Song, S.Y. Sung, M. Kim, S.J. Hwang, J.M. Choi, S.K. Lee, H.Y. Lee, C.L. Lim, Y.J. Chung, D. Yang, H.N. Kim, Z.H. Lee, K.Y. Choi, S.S. Jeun, Y.C. Sung, Branched oligomerization of cell-permeable peptides markedly enhances the transduction efficiency of adenovirus into mesenchymal stem cells, Gene Ther 17(8) (2010) 1052-1061.

[358] J. Hoyer, U. Schatzschneider, M. Schulz-Siegmund, I. Neundorf, Dimerization of a cell-penetrating peptide leads to enhanced cellular uptake and drug delivery, Beilstein J Org Chem 8 (2012) 1788-1797.

[359] K.J. Lampe, S.C. Heilshorn, Building stem cell niches from the molecule up through engineered peptide materials, Neurosci Lett 519(2) (2012) 138-146.

[360] J.H. Collier, Modular self-assembling biomaterials for directing cellular responses, Soft Matter 4(12) (2008) 2310-2315.

[361] M. Zhou, A.M. Smith, A.K. Das, N.W. Hodson, R.F. Collins, R.V. Ulijn, J.E. Gough, Self-assembled peptide-based hydrogels as scaffolds for anchorage-dependent cells, Biomaterials 30(13) (2009) 2523-2530.

[362] C.A. Goubko, S. Majumdar, A. Basak, X.D. Cao, Hydrogel cell patterning incorporating photocaged RGDS peptides, Biomed Microdevices 12(3) (2010) 555-568.

[363] C.A. Goubko, A. Basak, S. Majumdar, X.D. Cao, Dynamic cell patterning of photoresponsive hyaluronic acid hydrogels, J Biomed Mater Res A 102(2) (2014) 381-391.

[364] C.A. Goubko, A. Basak, S. Majumdar, H. Jarrell, N.H. Khieu, X.D. Cao, Comparative analysis of photocaged RGDS peptides for cell patterning, J Biomed Mater Res A 101(3) (2013) 787-796.

[365] T.Y. Kang, J.H. Lee, B.J. Kim, J.A. Kang, J.M. Hong, B.S. Kim, H.J. Cha, J.W. Rhie, D.W. Cho, In vivo endothelization of tubular vascular grafts through in situ recruitment of endothelial and endothelial progenitor cells by RGD-fused mussel adhesive proteins, Biofabrication 7(1) (2015).

[366] K.M. Lee, G.S. Jung, J.K. Park, S.K. Choi, W.B. Jeon, Effects of Arg-Gly-Asp-modified elastin-like polypeptide on pseudoislet formation via up-regulation of cell adhesion molecules and extracellular matrix proteins, Acta Biomater 9(3) (2013) 5600-5608.

[367] C. Tao, J.B. Huang, Y. Lu, H. Zou, X.Y. He, Y. Chen, Y.Q. Zhong, Development and characterization of GRGDSPC-modified poly(lactide-co-glycolide acid) porous microspheres incorporated with protein-loaded chitosan microspheres for bone tissue engineering, Colloid Surface B 122 (2014) 439-446.

[368] K.J. Lampe, A.L. Antaris, S.C. Heilshorn, Design of three-dimensional engineered protein hydrogels for tailored control of neurite growth, Acta Biomater 9(3) (2013) 5590-5599.

[369] A.G. Secchi, V. Grigoriou, I.M. Shapiro, E.A. Cavalcanti-Adam, R.J. Composto, P. Ducheyne, C.S. Adams, RGDS peptides immobilized on titanium alloy stimulate bone cell attachment, differentiation and confer resistance to apoptosis, J Biomed Mater Res A 83a(3) (2007) 577-584.

[370] M.O. Guler, L. Hsu, S. Soukasene, D.A. Harrington, J.F. Hulvat, S.I. Stupp, Presentation of RGDS epitopes on self-assembled nanofibers of branched peptide amphiphiles, Biomacromolecules 7(6) (2006) 1855-1863.

[371] K.L. Niece, J.D. Hartgerink, J.J.J.M. Donners, S.I. Stupp, Self-assembly combining two bioactive peptide-amphiphile molecules into nanofibers by electrostatic attraction, Journal of the American Chemical Society 125(24) (2003) 7146-7147.

[372] S.R. Bull, M.O. Guler, R.E. Bras, T.J. Meade, S.I. Stupp, Self-assembled peptide amphiphile nanofibers conjugated to MRI contrast agents, Nano Letters 5(1) (2005) 1-4.

[373] P. Simpson, B.C. Merrifield, Real-Time Signal-Processing Applications of a Distributed Array Processor, Comput Phys Commun 37(1-3) (1985) 133-140.

[374] D.A. Harrington, E.Y. Cheng, M.O. Guler, L.K. Lee, J.L. Donovan, R.C. Claussen, S.I. Stupp, Branched peptide-amphiphiles as self-assembling coatings for tissue engineering scaffolds, J Biomed Mater Res A 78A(1) (2006) 157-167.

[375] H. Storrie, M.O. Guler, S.N. Abu-Amara, T. Volberg, M. Rao, B. Geiger, S.I. Stupp, Supramolecular crafting of cell adhesion, Biomaterials 28(31) (2007) 4608-4618.

CHAPTER 3 – DESIGN AND EVALUATION OF BIOSYNTHESIZED CELLULOSE DURAPLASTY TO STIMULATE NEURAL STEM CELL PROLIFERATION

3.1. Introduction

A cerebrovascular accident or stroke, occurs as the result of lack of perfusion to regions of the brain leading to death of the brain cells. Strokes are classified into two types: hemorrhagic, caused by a ruptured vessel, and ischemic, caused by blockage of an artery due to a thrombus. Worldwide, stroke is the second leading cause of death [1] and the third leading cause of disability [2]. Every year, there are fifteen million new stroke patients, of whom five million die and five million are permanently disabled. Unfortunately, the options to treat stroke are very limited, and the neurological damage cannot be completely repaired [3]. Decompressive craniectomy (DC) is typically performed in stroke patients where cerebral ischemia leads to cerebral edema and increased intracranial pressure. The DC alleviates the increased intracranial pressure by removing a portion of the skull and opening the dura. A duraplasty material will then be applied onto the exposed brain [4]. Despite the relative invasiveness of this procedure, randomized controlled trials have shown that the use of DC significantly reduces mortality in patients suffering from acute ischemic stroke [4, 5]. Unfortunately, the DC procedure with the duraplasty implantation does not lead to significant improvement in brain functional recovery [6].

Several types of plain duraplasty options have been developed for this purpose over the years. For example, Codman Duraform® Dural Graft (Johnson & Johnson, New Brunswick, NJ) is a currently commercially available duraplasty that is composed of type I collagen [7]. It has shown to cause a minimal inflammatory reaction, having manageable handling qualities, and was able to prevent cerebrospinal fluid (CSF) leakage [7]. Another example of a commercial duraplasty is SyntheCel® Dura Replacement (DePuySynthes – Johnsons&Johnsons, New Brunswick, NJ) made of biosynthesized cellulose (BC). Rosen et

al. studied SyntheCel in a human controlled trial for 6 months and compared it with other commercially available duraplasties including Duraform®, DuraGen®, and Preclude® (product was discontinued) [8]. Using a noninferiority design, the authors concluded that the safety and efficacy of the BC duraplasty were comparable to the other commercial products on the market [8]. However, SyntheCel Dura Replacement is not loaded with any therapeutic ingredients, likely because the loading of bioactive molecules into the duraplasty cannot be easily incorporated into the duraplasty fabrication process. As a result, while proven clinically important in saving patient lives, none of the current commercially available duraplasties will lead to any improvement in functional outcome.

Biosynthesized cellulose (BC) can be produced by *Gluconoacetobacter hansenii* and has several remarkable properties, such as high purity and unique morphology, characterized by an ultrafine nanofibrous network structure [9]. Due to its porosity and hydrophilicity, BC has high swelling capacity [10, 11] and permeability [12]. In addition, BC is a biocompatible material, not showing chronic inflammatory reactions when implanted subcutaneously in rats [13] and exhibiting low foreign body reactions, absence of cortical adhesion, as well as the property of malleability when implanted in the brain of mongrel dogs [14] – one of the few reports showing BC as a suitable substitute for dura mater in animal studies. Other advantage of BC is that its physical structure (e.g. thickness, homogeneity, and density of the network) may be readily modified according to the desired application [15, 16]. Moreover, BC can be sterilized by heat treatment (e.g. steam sterilization), an effective, fast, and simple technique, leaving no toxic residues [17]. These valuable qualities make BC an attractive biomaterial for the fabrication of a drug releasing duraplasty.

Growth factors (GFs) can be loaded into a BC duraplasty to improve the ability of the implant to promote post-stroke neurogenesis and eventually functional neurological recovery. Recently, GFs have been demonstrated to stimulate endogenous neural stem/progenitor cells (NSPCs) proliferation and migration to the site of injury thus resulting in enhanced tissue regeneration and functional neurological recovery [18-21]. It is known that post-stroke endogenous NSPCs proliferate at a higher rate in the subventricular zone (SVZ), and some precursor cells migrate to the injury site; unfortunately most of the endogenous NSPCs do not survive long enough to mature and incorporate into the nervous system, making the repair of the damaged tissue very limited [22, 23]. In pre-clinical studies, GFs such as epidermal growth factor (EGF), fibroblast growth factor-2 (FGF2), erythropoietin, and vascular endothelial growth factor, have shown to stimulate axonal re-growth, neurogenesis, and other features of neural repair [18-20]. Particularly, EGF is a neural regeneration factor that enhances neural stem cell growth by acting as a mitogen for NSPCs [19] and FGF2 promotes neurogenesis by increasing adult NSPCs proliferation [24]. Moreover, the combination of some GFs showed synergistic effects by enhancing tissue regeneration [21]. Specifically, the incorporation of both EGF and FGF2 has been demonstrated to increase NSPC proliferation [25] and EGF has been shown to have these beneficial effects after stroke when applied topically [21].

Therefore, in this study, EGF and FGF2 were selected to be loaded into the biosynthesized cellulose (BC) based duraplasty. BC was physically modified and drug releasing duraplasties at several cellulose ratios were produced. The GFs-enriched BC drug releasing duraplasty can be applied as permanent implant during DC procedure in patients with severe stroke, preventing the necessity for a second intervention. After fabrication, the physical and mechanical characterization of the drug releasing duraplasty were performed to investigate the structure, strength, and elasticity of the new duraplasty. In addition, by using the fabrication

technique proposed here, GFs were sterilely incorporated into the BC duraplasty in a reliable and effective way. Swelling and *in vitro* drug release were studied to evaluate the overall potential of our material as a drug releasing duraplasty. Lastly, as proof of concept, the novel drug releasing duraplasty was tested *in vitro*, where NSPCs proliferation and differentiation were analyzed, and *in vivo* biocompatibility was evaluated.

3.2. Materials and Methods

3.2.1. Materials

Biosynthesized cellulose producing bacteria *G. hansenii* were obtained from American Type Culture Collection (ATCC®) (Manassas, VA). Recombinant human fibroblast growth factor-2 (FGF2), recombinant human epidermal growth factor (EGF), and ELISA detection kits for FGF2 and EGF were obtained from PeproTech Inc. (Rocky Hill, NJ). All other chemicals were purchased from Sigma-Aldrich (St. Louis, MO) and used as received unless indicated otherwise.

3.2.1.1. Production of Blended Biosynthesized Cellulose (BBC) Membranes

Biosynthesized cellulose (BC) was obtained from *Gluconacetobacter hansenii* cultures in a modified Hestrin-Schramm culture media containing glucose (20.0 g/L), peptone (5.0 g/L), yeast extract (5.0 g/L), disodium phosphate (2.7 g/L), and citric acid (1.5 g/L) [26]. Original BC membranes were produced in a static cell culture at 26 °C for 7 days, after which the membranes were collected, washed with 0.1 M NaOH at 50 °C under agitation for 24 h, and extensively rinsed with distilled water. To produce blended BC membranes (BBC), never-

dried BC membranes were blended (Oster®, Brampton, ON) to produce a homogenous pulp. The resulting pulp was subsequently filtered using a Buchner fritted disc filter (Rockwood, TN) to form a thin paper-like membrane (i.e. BBC membrane), which was subsequently lyophilized. Five different types of BBC membranes in order of dry cellulose mass were prepared, with BBC1 group containing the lowest amount of cellulose while BBC5 group containing the highest. All resulting BBC membranes were sterilized by autoclave before further use [17].

3.2.2. Characterization of Blended Biosynthesized Cellulose (BBC) Membranes

3.2.2.1. Swelling Ratio (SR)

The swelling ratio (SR) of BBC was determined by a gravimetric method. In brief, dried BBC membranes were weighed (W_{dry}) and subsequently immersed into PBS (pH 7.4) at 37 °C for 96 hours; subsequently the swollen membranes were retrieved and weighed again (W_{swo}). The SR of the BBC membranes was determined by the following equation.

$$SR\ (\%) = \frac{W_{swo} - W_{dry}}{W_{dry}} \times 100$$

3.2.2.2. Mechanical Properties

To characterize the mechanical properties of the BBC membranes, tensile tests were conducted on swollen BBC membranes. The measurements were carried out at 25 ± 2 °C and relative humidity of 45 ± 5 % on Instron ElectroPuls™ E3000 All-Electric Dynamic Test Instrument (Norwood, MA) equipped with Instron® Bluehill® Software (Norwood, MA). Rectangular BBC membranes (15 mm × 10 mm) were used in the tensile test. The crosshead speed was set

at 5 mm/min and a load cell dynamic rating of ± 250 N was used. The samples were tested for Young's modulus and ultimate tensile strength (UTS).

3.2.2.3. Scanning Electron Microscope (SEM) Analysis

To study the microstructures of the resulting BBCs, a Phenom Pro scanning electron microscope (SEM) (Phoenix, AZ) was used. Both dry BBC1 and BBC5 membranes were investigated.

3.2.3. Drug Delivery Study

Recombinant human fibroblast growth factor-2 (FGF2) and recombinant human epidermal growth factor (EGF) were used as model drugs to be delivered, and BBC5 membrane was studied as the drug delivery system. The dried BBC5 membrane was cut into the shape of a rat cerebral hemisphere. Subsequently, dried and autoclaved BBC5 was added in a 24-well plate, and 70 µL FGF2 and EGF sterile solution was pipetted on the top of the membrane (referred to as BBC5GF). The membrane was kept static for 2 hours until the FGF2/EGF solution was completely absorbed by the membrane. To study the drug delivery performance of the membrane, the resulting BBC5GF was completely submerged in 2 mL of PBS (pH 7.4) at 37 °C; at predetermined time intervals, 0.32 mL of the releasing buffer was collected and replenished with the same volume of fresh buffer. Concentrations of both FGF2 and EGF from the collected samples were determined by both FGF2 and EGF ELISAs using vendor's protocols.

3.2.4. In Vitro Analyses

All animal studies were performed in strict compliance with the Guide to the Care and Use of Experimental Animals prepared by the Canadian Council of Animal Care and protocols approved by the Animal Care Committee of the Ottawa Hospital Research Institute. For the harvesting of human spinal cord tissue, ethics approval for the study was obtained from the Ottawa Health Science Network Research Ethics Board and from the Trillium-Gift of Life Foundation which oversees organ donation in Ontario. Informed written consent was obtained from the family of the deceased organ donor.

3.2.4.1. Primary Neural Stem/Progenitor Cell Culture

To analyze whether the growth factors delivered by the BBC5 drug releasing duraplasty could stimulate proliferation of NSPCs, primary NSPCs from the SVZ of SD rats were isolated and cultured as previously described [27]. Specifically, the cells were seeded into 6-well plates (ultra-low attachment, BD Biosciences Inc., Franklin Lakes, NJ) at a concentration of 20,000 cells/mL and cultured at 37 °C, 5 % CO_2, and 20 % O_2 (normoxia). The NSPCs were cultured in serum-free medium (SFM) consisting of DMEM/F-12 (1:1) and supplemented with B27 neural supplement, 2 mM L-glutamine, and 100 µg/mL penicillin-streptomycin (Invitrogen Inc., Waltham, MA). To deliver the GFs to the cell culture, BBC5GF membranes were placed in PET inserts, pore size of 0.4 µm (EMD Millipore, Burlington, MA), that in turn were placed inside of the NSPC cell culture containing the SFM media for up to two weeks. Neurospheres were photograph Nikon Ti-Eclipse microscope (Mississauga, ON) and their neurosphere diameters, cross-section area and quantities were examined using ImageJ software. Additionally, NSPCs were cultured in pure SFM media and with nude BBC5, as negative controls. As positive control, NSPCs were also cultured in the growth factor matched media (GFM) constituted of SFM supplemented with 110 ng/mL EGF and 110 ng/mL FGF2.

To test the multipotency of the NSPCs treated with BBC5GF, individual neurospheres collected from BBC5GF treated cultures (as described above) were transferred into the wells of 96-well plates pre-coated with Matrigel and the cells were induced to differentiate for 7 days by adding 1 % FBS into the SFM. In addition, BrdU (4μg/mL, EMD Millipore, Burlington, MA) was used in the cell culture media from Day 1 to track cell proliferation. Finally, the cells were fixed with 4 % paraformaldehyde after 7 days of culture and were immunostained as described below. In parallel, neurospheres treated with GFM were also similarly processed for comparison.

3.2.4.2. Immunostaining

To identify cell differentiation, the cells that were processed as described above were immunostained for markers of NSPCs and differentiated progeny. Briefly, the fixed cells were blocked with 10 % normal goat serum (NGS) and permeabilized with 0.3 % Triton-X 100 (Invitrogen Inc., Waltham, MA) for 1 hour at room temperature, and subsequently incubated with the primary antibody in 10 % NGS at 4 °C overnight. The following primary antibodies were used: Nestin (1∶500) (Santa Cruz Biotechnology, Dallas, TX) for neural progenitor cells; BrdU (1∶300) (EMD Millipore, Burlington, MA) for proliferating cells; Sox2 (1∶200) (EMD Millipore, Burlington, MA) for neural stem cells; O4 (1∶300) for oligodendrocytes; glial fibrillary acidic protein (GFAP) (1∶500) (EMD Millipore, Burlington, MA) for astrocytes; and βIII-tubulin (1∶300) (Santa Cruz Biotechnology, Dallas, TX) for neurons. After extensive washes with PBS (pH 7.4), the samples were incubated with appropriate Alexa 488 or Alexa 568 labelled secondary antibodies (Invitrogen Inc., Waltham, MA) in 2 % NGS at room

temperature for 2 hours, washed again with PBS (pH 7.4) and finally counterstained with Hoechst (1:2000).

3.2.5. Blended Biosynthesized Cellulose (BBC) Membrane as Duraplasty

To investigate the feasibility of the BBC membrane as duraplasty, growth factor loaded BBC5GF membranes were implanted in a rodent as part of a DC procedure. In brief, adult female SD rats, 9-10 weeks of age (Charles River Laboratories, Senneville, QC) were anesthetized by isoflurane inhalation, and the right cerebral hemisphere was surgically decompressed by craniectomy, where the posterior third of the frontal, parietal and anterior third of the occipital bone were removed and the dura mater was finely resected and excised. Subsequently, the BBC5GF membrane was applied onto the surface of the craniectomy, and skin was stapled closed on top. After the procedure the animals received a single dose of Ceftriaxone 2 g/kg (Sandoz, Boucherville, QC), as antibiotic prophylaxis, for the first 24 hours. Also, to maintain analgesia for 72 hours post-DC, 1 mg/kg of Buprenorphine (Champion Alstoe, Whitby, ON) was administered. Rats were sacrificed 1 week and 4 weeks after the DC and the brains were carefully dissected, fixed in 4 % paraformaldehyde for 24 hours, and subsequently cryoprotected in 30 % sucrose. The prepared tissues were embedded in paraffin and coronally sectioned into 5 μm sections for H&E staining. Finally, the H&E stained sections were mounted on coverslips using Permount (Fisher Scientific, Waltham, MA) and analyzed by Nikon Ti-Eclipse microscope. Additionally, as controls, three groups of SD rats were allocated to the implantation of nude BBC5, to the no surgical group, and to decompression alone for each time point.

3.2.6. Statistical Analysis

All statistical analyses were carried out using one-way and two-way ANOVA, followed by post hoc Tukey's analysis, using GraphPad Prism 6 Data (GraphPad Software, La Jolla, CA). *P* values < 0.05 were considered statistically significant.

3.3. Results

3.3.1. Production and Characterization of Blended Biosynthesized Cellulose (BBC) Membranes

This study investigated the potential of BBC duraplasty as drug delivery systems to stimulate brain tissue regeneration after stroke. As shown in **Figure 3.1**, BBC membranes were produced by blending BC membranes originally obtained from bacterial cultures. To investigate the characteristics of BBC samples, five different initial cellulose pulp concentrations were used to obtain five different BBCs in crescent order of cellulose mass: BBC1, BBC2, BBC3, BBC4 and BBC5 (see **Figure 3.1D**). As shown in **Figure 3.1E** and **Figure 3.1F**, from BBC1 to BBC5, there was a descending trend for SR with BBC1 exhibiting the highest SR while BBC5 the lowest among all samples. It should be mentioned that the SR for all BBC membranes rapidly increased within 5 hours and remained roughly constant after 48 hours.

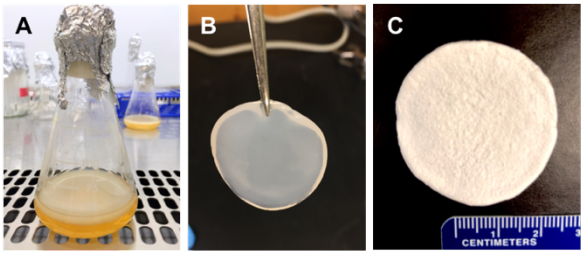

D

Sample	Cellulose Pulp (g/L)	Dry Cellulose (g)
BBC1	1.6348 ± 0.0096****	0.1243 ± 0.0008****
BBC2	2.6050 ± 0.0112****	0.1775 ± 0.0008****
BBC3	3.4064 ± 0.0006****	0.2130 ± 0.0005****
BBC4	3.9141 ± 0.1571***	0.2413 ± 0.0005****
BBC5	4.6452 ± 0.1883	0.3058 ± 0.0056

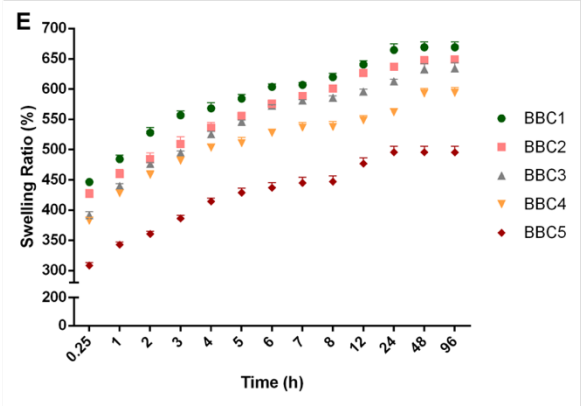

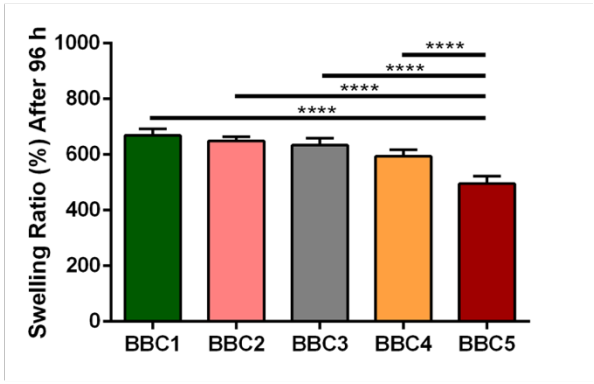

Figure 3.1 – Production and physical properties of the resulting BBC membranes. **(A)** Flask of inoculum containing a BC membrane. **(B)** Original BC membrane after purification. **(C)** BBC membrane after filtration and lyophilization. **(D)** Table showing the different concentrations of the initial cellulose pulp used to produce BBC1-5 membranes and their respective dry cellulose mass; n = 6. **(E)** Swelling ratios of BBC1-5 in PBS at 37 °C in different time points, n = 7. **(F)** Swelling ratios after 96 hours. *(One-way ANOVA followed by multiple-comparisons test (Tukey's) were performed for statistical analysis. Data obtained from two independent experiments and presented as mean ± s.e.m.; **p < 0.01; ***p < 0.001; ****p < 0.0001 from BBC5).*

The mechanical properties of the BBCs were studied. As shown in **Figure 3.2**, BBC5, the membrane prepared with the highest cellulose content, exhibited greater Young's Modulus and tensile strength when compared to those with lesser mass (i.e. BBC1-4). Specifically, the BBC5 demonstrated a Young's modulus of 0.37 ± 0.02 MPa and an ultimate tensile strength (UTS) of 0.96 ± 0.02 MPa, values that are respectively about 9 and 6 times higher than BBC1 (**Figure 3.2B** and **Figure 3.2C**, respectively).

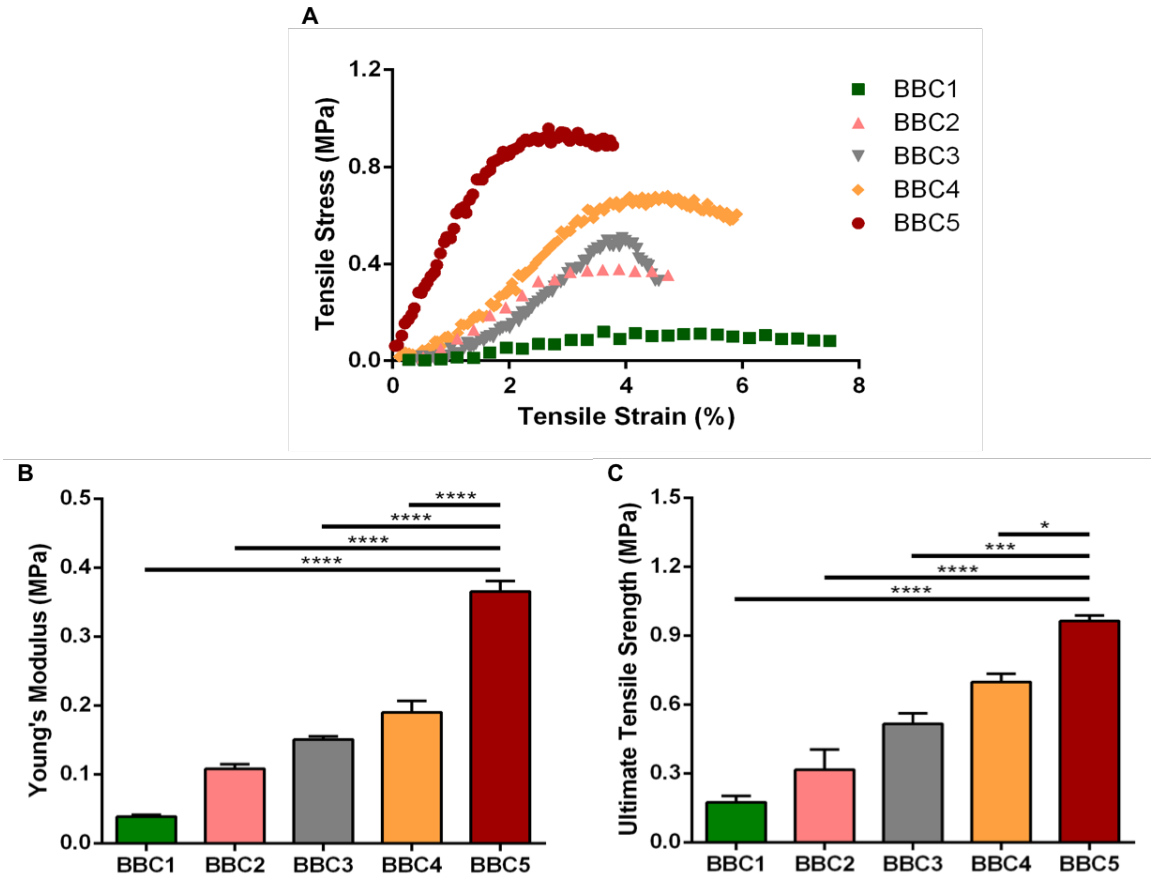

Figure 3.2 – Mechanical properties of blended biosynthesized cellulose (BBC) membranes. **(A)** Representative stress-strain curves for BBC1-5; **(B)** Young's Modulus of different BBC membranes; **(C)** Ultimate tensile strength (UTS). The mechanical properties were measured using swollen BBC membranes. *(One-way ANOVA followed by a multiple-comparisons test (Tukey's) were used for statistical analysis. Data obtained from two independent experiments in triplicate and is presented as mean ± s.e.m. *p < 0.05, ***p < 0.001, ****p < 0.0001 from BBC5).*

In addition, the microstructures of the prepared BBC1 and BBC5 membranes were evaluated using SEM for comparison, as shown in **Figure 3.3**. When the cellulose-producing bacteria are statically cultured, they produce BC biomass as a heterogeneous membrane at the air-liquid interface, as shown in **Figure 3.1A**. This original biomass membrane is composed of highly entangled cellulose fibers networks, which are denser at the membrane/air interface (**Figure 3.3A**) than at the membrane/liquid interface on the opposite side, as shown in **Figure 3.3A** and **Figure 3.3D**. For the BBC membranes, SEM images show that the increased in cellulose content, BBC1 (**Figure 3.3B, Figure 3.3E** and **Figure 3.3H)** to BBC5 (**Figure 3.3C,**

Figure 3.3F and **Figure 3.3I)**, resulted in a denser fiber network and less porous microstructure on both sides of the membranes, and thicker but less entangled inner layers.

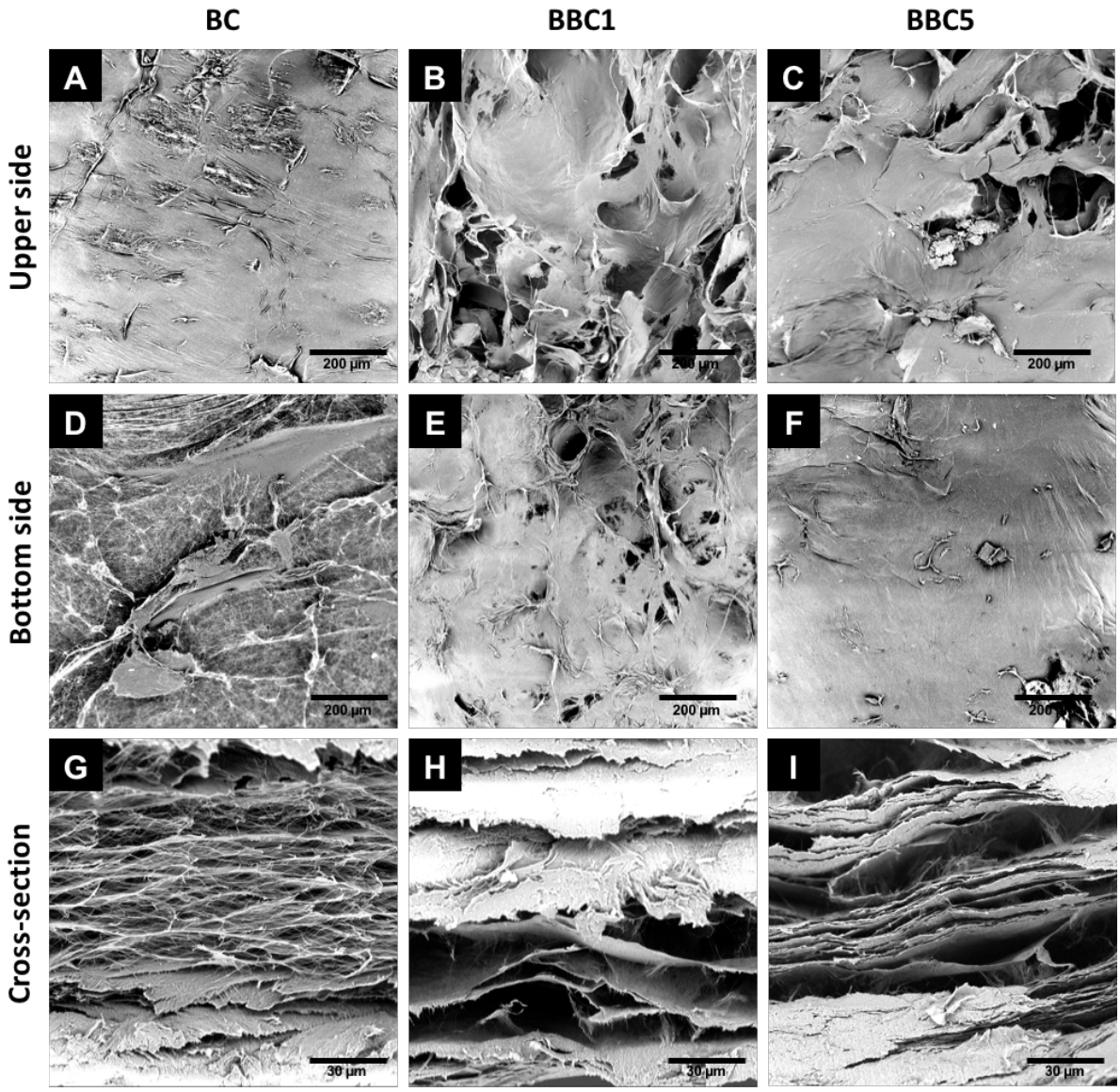

Figure 3.3 – Scanning electron microscopy micrographs of dried biosynthesized cellulose (BC, original), blended biosynthesized cellulose (BBC1, membrane with lowest dry cellulose mass), and BBC5 (membrane with highest dry cellulose mass): upper side (air contact), bottom side (liquid contact for BC and filter contact for BBC) with 300× magnification, and cross-section views with 2000× magnification. Three samples were assayed in duplicate by SEM analysis.

3.3.2. Drug Delivery Studies

The blended biosynthesized cellulose samples form malleable membranes that can be loaded with drugs and applied to the apical of the brain during DC surgery. Because of the structural and mechanical properties, BBC5 was selected to be used for the rest of the studies unless indicated otherwise. The membranes were cut into shape and size to cover the craniotomy defect overlying the rat cerebral hemisphere (length of 12.5 ± 0.1 mm, width of 8.0 ± 0.1 mm, and weight of 22.1 ± 0.1 mg) as shown in **Figure 3.4A** and **Figure 3.4B**. The thickness of BBC5 increased from 0.57 ± 0.01 mm to 1.11 ± 0.18 mm after being fully rehydrated. It is also noted that the GFs were successfully loaded into BBC5, where the average FGF2/EGF entrapment efficiency was 99.5 %. As shown in **Figure 3.4C**, the BBC5GF drug releasing duraplasty had a similar sustained release for both FGF2 and EGF, featuring an initial burst release at the first 8 hours and an almost linear release until Day 10, after which the amount of drug in solution did not changed significantly (**Figure 3.4C**). It is noted that after ten days of release, the cumulative amount released of FGF2 was 397.4 ± 6.9 ng and for EGF was 393.6 ± 9.2 ng, 94 % of the total amount of growth factors that were initially loaded in the membranes.

A

Mass		
	Dry cellulose (mg)	22.1 ± 0.1
Dimensions		
	Dry thickness (mm)	0.57 ± 0.01
	Wet thickness (mm)	1.11 ± 0.18
	Length (mm)	12.5 ± 0.1
	Width (mm)	8.0 ± 0.1
Drug Release Characteristic		
	FGF2	**EGF**
	Entrapment efficiency (%)	99.5 ± 0.5	99.6 ± 0.3

B

C

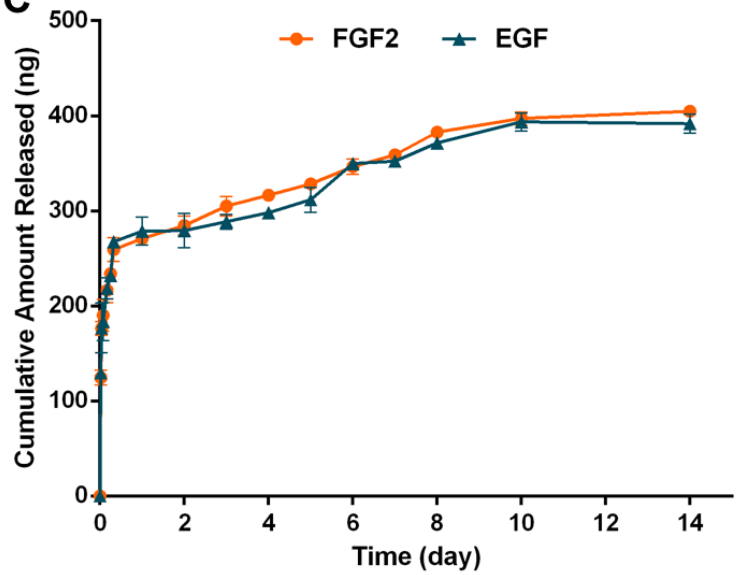

Figure 3.4 – FGF2 and EGF release profile from BBC5GF. **(A)** Table of physical characteristics and drug entrapment efficiency of BBC5GF. **(B)** Image of the final BBC5GF - rat cerebral hemisphere**. (C)** Cumulative amount of FGF2 (orange) and EGF (dark blue) over 14 days as determined by ELISA. (*Two-way ANOVA was used for statistical analysis.* Values are presented as mean ± *s.e.m.*, n = 5).

3.3.3. Blended Biosynthesized Cellulose (BBC) as a Drug Delivery Vehicle for Growth Factors

The bioactivities of the growth factors released from the BBC5GF were evaluated by culturing NSPCs derived from SVZ of rodent brains. As shown in **Figure 3.5A**, NSPCs formed

neurospheres when they were co-cultured with BBC5GF membranes, a similar performance as when they were cultured in cell culture media containing EGF and FGF2 (i.e. GFM). It is also evident from **Figure 3.5B** that in the first week of culture, the number of NSPCs neurospheres when co-cultured with BBC5GF was significantly higher than that of neurospheres when co-cultured with SFM and BBC5, the two negative controls ($p < 0.01$). Interestingly, no significant difference in the number of neurosphere was observed between BBC5GF and the positive control GFM after one week of culture, demonstrating that growth factors released from the BBC5GF were bioactive. Despite both BBC5GF and GFM had formed more neurospheres in comparison with the negative controls (**Figure 3.5B**), the diameter and estimated cross-section area of the formed neurospheres were not statistically different amongst all samples after one week (**Figure 3.5C** and **Figure 3.5D**). In the second week, the general trend among the samples was similar as the first week; however GFM culture produced significantly more neurospheres than BBC5GF ($p < 0.05$; **Figure 3.5B**), and the neurosphere diameters were also statistically larger than those from the BBC5GF culture ($p < 0.01$; **Figure 3.5C**). Besides, after two weeks, the diameter of BBC5GF formed neurospheres was statistically different from SFM ($p < 0.05$; **Figure 3.5C**), however there was no statistical difference for the estimated cross-section area of formed neurospheres at Week 2 (**Figure 3.5D**).

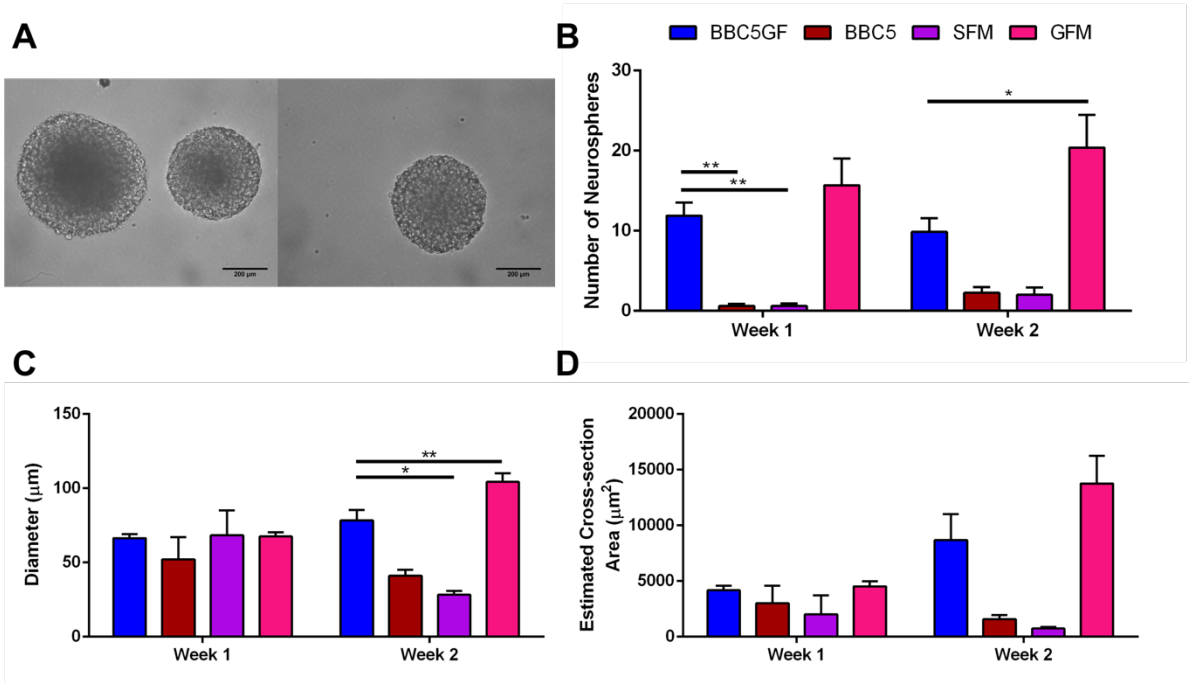

Figure 3.5 – BBC5GF stimulates rodent SVZ neural stem/progenitor cell proliferation for a period of one week. **(A)** Images of neurospheres taken at 20× magnification. Left image: BBC5GF neurospheres; right image: GFM neurospheres; after 2 weeks. NSPCs were treated for one and two weeks and assessed for **(B)** the number of neurospheres formed, **(C)** the diameter of neurospheres, and **(D)** their estimated cross-section area. Estimated cross-section area of neurospheres were calculated using measured diameters. *(Two-way ANOVA followed by a multiple-comparisons test (Tukey's) in (B), (C) and (D) were used for statistical analysis. Values are presented as mean ± s.e.m; n =10. Only comparisons related to BBC5GF are shown, *p<0.05, **p<0.01).*

To elucidate whether cells from the growth factor treated neurospheres were multipotent, individual neurospheres were transferred onto an adherent substrate and allowed to differentiate in the presence of 1% FBS. It was observed that the proliferative capacity of BBC5GF and positive control derived neurospheres was the same over one and two weeks of respective treatments (**Figure 3.6A**). In particular, it is noted that after one and two weeks of treatments, the percentage of Sox2 and Nestin cells remained ~40-60 %, strongly suggesting the presence of stem and progenitor cells **(Figure 3.6B, Figure 3.6C** and **Figure 3.6D)** in the neurospheres that were initially treated with either BBC5GF and the positive control (i.e. GFM). To further assess whether NSPCs derived from the BBC5GF were capable of differentiating into three main lineages of the CNS: oligodendrocytes, astrocytes and neurons,

immunostaining was used. Fluorescent microscopy showed cells stained positive for: O4 for oligodendrocytes (**Figure 3.7A**), GFAP for astrocytes (**Figure 3.7B**), and βIII-tubulin for neurons (**Figure 3.7C**). It was observed that the differentiated NSPCs favored astrogenesis over neurogenesis and oligodendrogenesis and that no statistically significant differences were observed in the percentage of each differentiated cell type between BBC5GF and positive control (GFM) treatments for either one or two weeks (**Figure 3.7**). Altogether, it was observed that NSPCs treated with BBC5GF were multipotent and that the duraplasty biomaterial did not alter NSPC differentiation behavior *in vitro*.

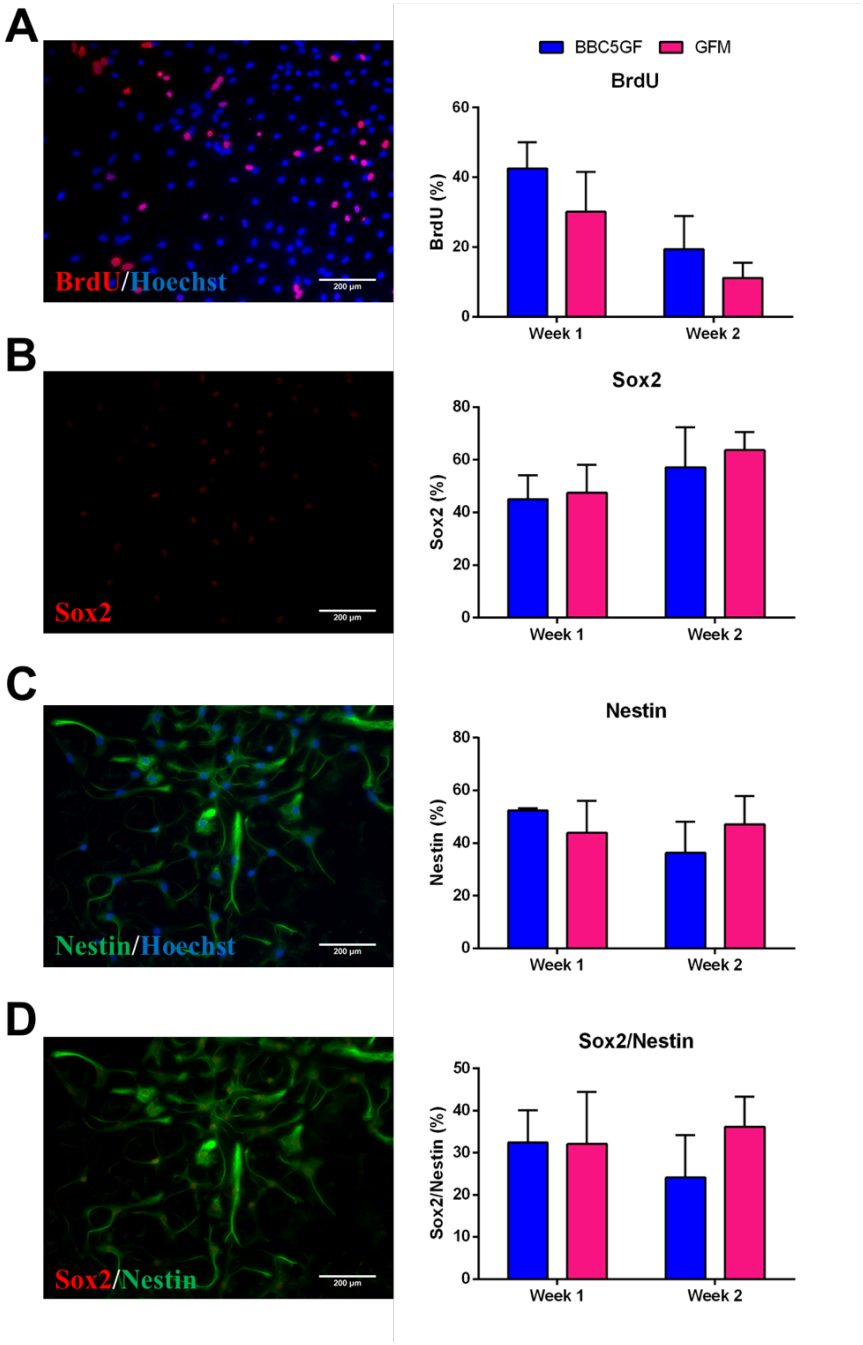

Figure 3.6 – Multipotent analysis of neural stem/progenitor cells derived from Week 1 and Week 2; neurospheres have proliferative capacity and maintain stemness after one week under differentiation conditions. On the left column, representative fluorescent images of BBC5GF stained cells from Week 1. On the right column, quantitative comparison for BBC5GF (blue), and GFM (pink) treatments. **(A)** Left: BrdU (red) is expressed in nuclei of dividing cells and Hoechst (blue). Right: quantitative results for levels of BrdU. **(B)** Left: Sox2 (red) is expressed in nuclei of neural precursor cells. Right: graph showing the levels of Sox2. **(C)** Left: Nestin (green) is expressed in cytoskeleton of neural stem/progenitor cells and Hoechst (blue). Right: graph showing the levels of Nestin. **(D)** Left: Overlay of Sox2 (red) and Nestin (green) expression in differentiated cells. Right: graph showing the co-expression levels of Sox2 and Nestin. *(Two-way ANOVA was used for statistical analysis. Data presented as mean ± s.e.m., n = 4.)*

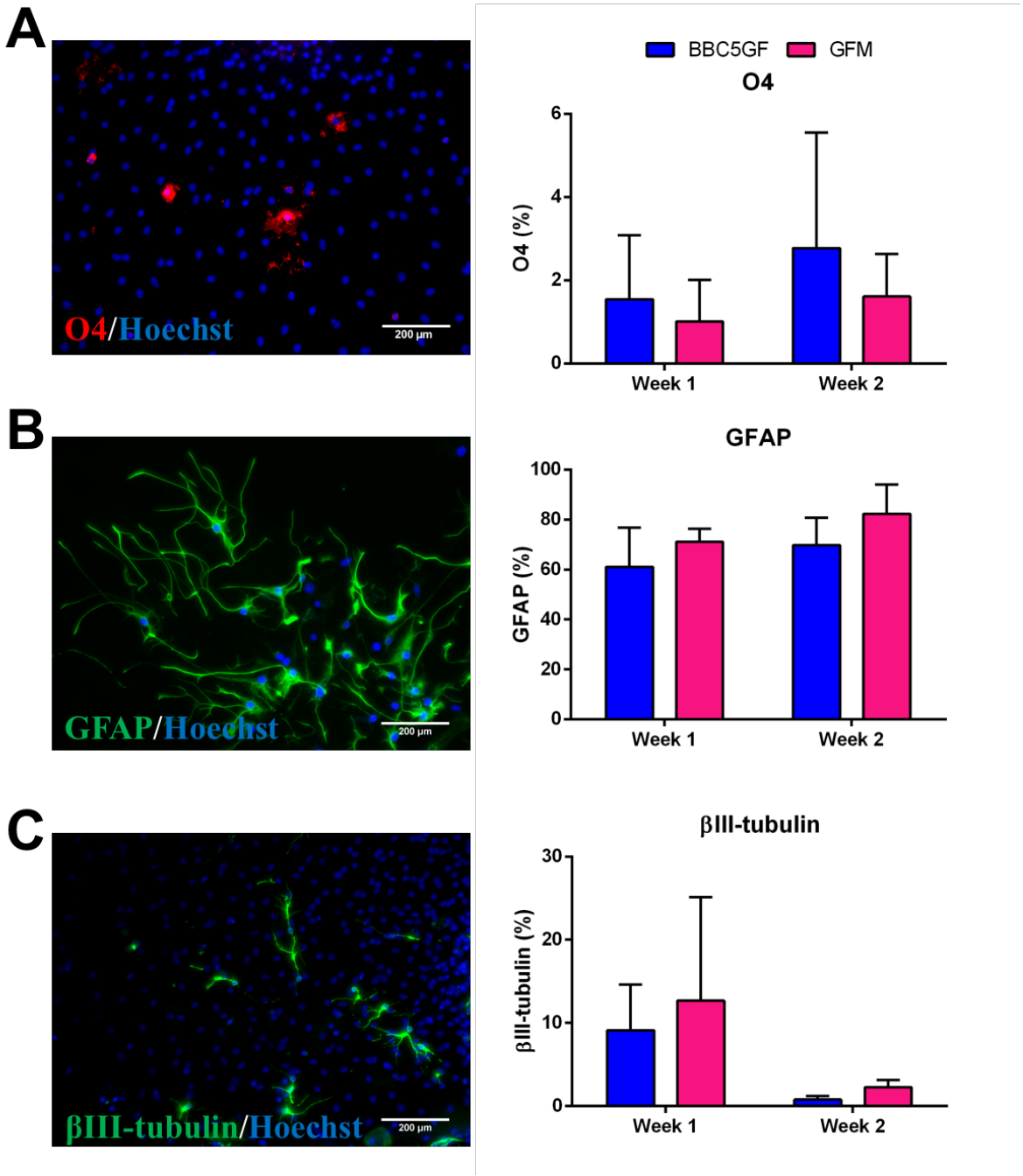

Figure 3.7 – Neural stem/progenitor cells derived from Week 1 and 2; neurospheres differentiate into oligodendrocytes, astrocytes and neurons. On the left column, representative images of stained BBC5GF differentiated cells from Week 1. On the right column, quantitative comparison showing no significant different between BBC5GF (blue) and GFM (pink) treatments. (**A)** Left: O4 (red) is expressed on the cell surface of oligodendrocytes. Right: expression levels of O4. **(B)** Left: GFAP (green) is expressed in the cytoskeleton of astrocytes. Right: expression levels of GFAP. **(C)** Left: βIII-tubulin (green) is expressed in the cytoskeleton of neurons. Right: expression levels of βIII-tubulin over one or two weeks. All nuclei were counter stained with Hoechst (blue). *(Two-way ANOVA was used for statistical analysis. Data presented as mean ± s.e.m., n = 4.)*

3.3.4. Biocompatibility of Growth Factor-Enriched Blended Biosynthesized Cellulose (BBC5GF) as a Duraplasty

To test BBC5GF drug releasing duraplasty biocompatibility, BBC5GF membranes were placed over the decompressed brains and inflammatory changes associated with the biomaterial were evaluated by H&E staining. Representative coronal sections are shown in **Figure 3.8**. As shown in **Figure 3.8A** and **Figure 3.8B,** samples from no surgery and DC only demonstrated normal histology of the brain, as expected. In the brains where BBC5GF and BBC5 membranes were implanted, at 1 week and 4 weeks there were no signs of macrophage invasion at the apical surface of the brain (**Figure 3.8C** and **Figure 3.8D**). Furthermore, there were no evidences of neutrophils or eosinophils, suggesting that there were no infection, abscess or foreign body response (**Figure 3.8C** and **Figure 3.8D**). Finally, no laminar necrosis or cortical atrophy were observed in the specimens (**Figure 3.8C** and **Figure 3.8D**). All the above findings suggest that BBC5GF drug releasing duraplasty is biocompatible *in vivo*.

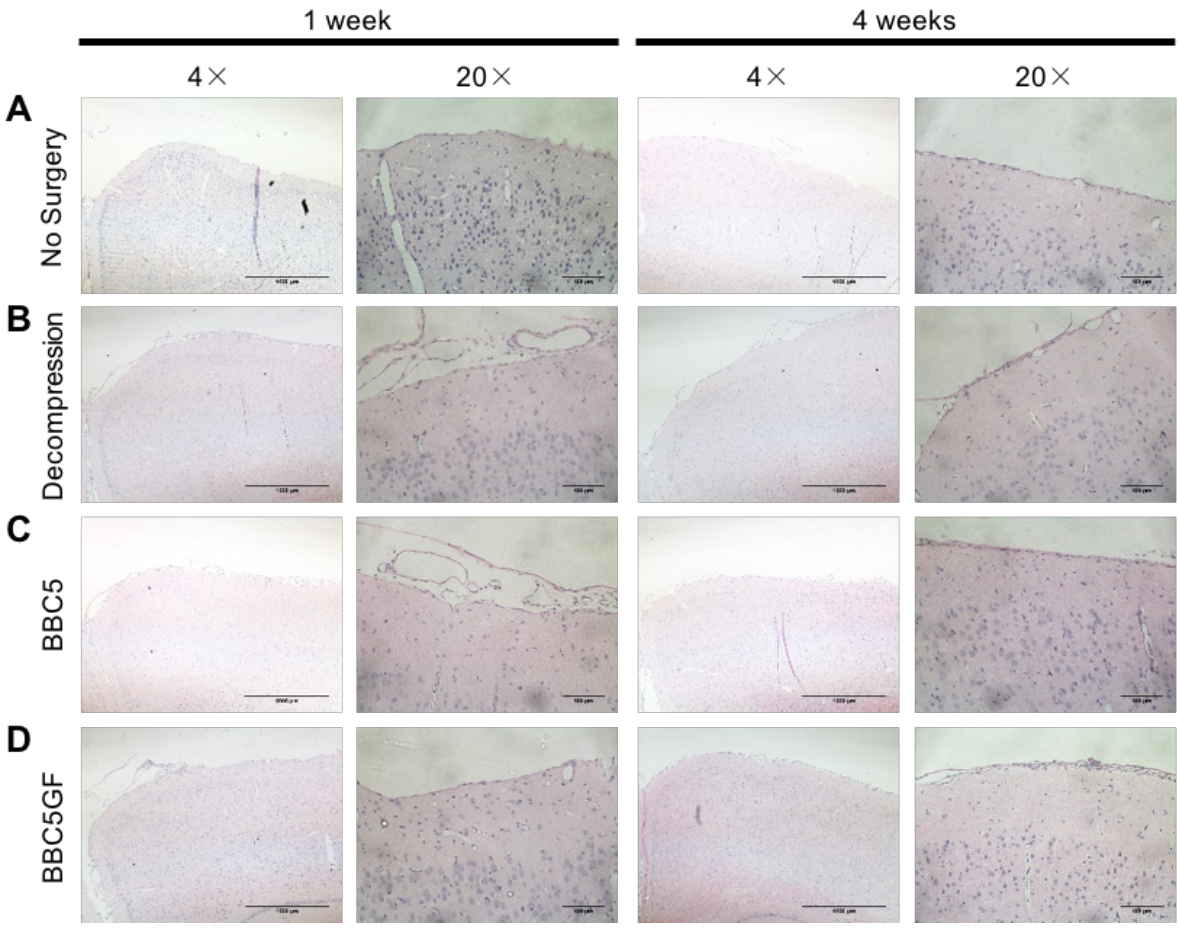

Figure 3.8 – Biocompatibility study of BBC5GF. Hematoxylin and eosin staining of representative coronal brain sections over the decompression region and BBC5GF duraplasty (if applicable) after one and four weeks. Sprague-Dawley brain with **(A)** no surgery, **(B)** decompressive craniectomy, **(C)** nude BBC5 implanted, and **(D)** BBC5GF implanted. Two left columns: 4× and 20× magnification images of rat brains after 1week of surgery (n = 5). Two right columns: 4× and 20× magnification images of rat brains from 4 weeks post-surgery (n = 5).

3.4. Discussion

The standard methods of dura mater repair consist of the application of sealants and the use of dura mater replacement materials (duraplasty) to expand or replace the resected dura mater during a neurosurgical procedure [4, 6]. An ideal duraplasty biomaterial for brain repair should have a combination of biophysical and biochemical characteristics, including: (1) be readily available and sterilized without compromising its properties; (2) appropriate size -- it should fit the defected area; (3) suitable mechanical properties for easy implantation and suturability

(i.e. suitable for suture); (4) perform as a drug delivery vehicle, and (5) good *in vivo* biocompatibility without causing inflammation [17, 28, 29]. In this study, BC-based drug delivery system to be used as duraplasty for DC were produced and characterized. Unlike conventional hydrogel fabrication methods [30] BBC production method is free of organic solvents or any other additives, resulting in a highly purified cellulose membrane in an approach that protects the essential biocompatibility of the material. In addition, this fabrication method gives the possibility to control/modify BC physical characteristics, such as fiber density, porosity, SR and mechanical properties. The blending protocol appeared to have reduced the difference between upper and bottom surfaces seen in the original BC (**Figure 3.3**); besides being a reproducible fabrication process batch-to-batch. What is important for drug delivery applications so that the release is both consistent and predictable [31, 32]. Furthermore, the fabrication technique allowed a much easier incorporation of therapeutic drugs into the membranes, as the prepared BBC can simply be sterilized by autoclaving, in comparison with other BC-based drug delivery systems, where the incorporation of additives makes the sterilization process a challenge [15, 17].

The thickness and SR were both tested to ensure that the BBC had the potential to perform the role of duraplasty while demonstrating a suitable drug release profile. The duraplasty is implanted into the brain post-DC; therefore, the duraplasty thickness must not cause increased pressure in the area it is important that it cause no further damage to an already injured area. Besides BBC5 thickness doubled after being fully rehydrated still significant less thick than the commercially available Duraform® (4.02 ± 0.07 mm, $p < 0.0001$) and within the range of human dura mater in different locations of 0.53 to 1.88 mm [33]. Therefore, the thickness of the BBC5 should not cause any complications when this duraplasty is implanted.

The SR of a biomaterial is important as it impacts on the release behavior [31, 34]. The faster a biomaterial swells and allows liquid into the matrix, the faster the drug can diffuse out [35]. The biomaterial SR is based primarily on its pore size and the formation of hydrogen bonds between the material and the water molecules [10]. The SR for the five samples decreased with the increased in the dry cellulose mass, where BBC5 presented the lowest SR (**Figure 3.1E** and **Figure 3.1F**) among the samples. The increase in the dry cellulose mass resulted in the construction of a more rigid structure with lower porosity as shown on SEM micrographs (**Figure 3.3**), which impeded the penetration of water molecules. Consequently, the percentage of water absorbed decreased, which led to a reduction in the SR [10]. These results demonstrated that BBC samples after sterilization kept their ability to reabsorb water, showing that this procedure did not affect the samples' physical structure. In addition, it is possible that the increased dry cellulose mass resulted in an increase in the number of hydrogen bonds formed within the membrane, resulting in a denser membrane and lower influx of water. This suggests that the higher the cellulose mass in the membranes, the lower it would be the initial drug burst. Therefore, BBC5 was considered being the best candidate to be used as duraplasty. In addition, BBC5' SR (496 ± 27 %) was 13 times lower than to the commercial available duraplastly Duraform® (6500 ± 146 %), what indicates that Duraform® was not designed as a drug delivery system and probably would present a high initial drug burst.

An ideal duraplasty should be moldable so that it is able to conform to the shape of the brain, but strong enough to withstand the surgical procedures for implantation [36]. For the BBC samples, the higher cellulose mass BBC (BBC5) presented a higher UTS and Young's Modulus than the lower cellulose mass BBC (BBC1). This is expected since an increased amount of cellulose means a higher number of hydrogen bonds and that results in a higher

strength and stiffness. The UTS and Young's modulus for BBC5 were 0.96 ± 0.02 MPa and 0.37 ± 0.02 MPa (**Figure 3.2**), in comparison to Duraform® they were 0.020 ± 0.003 MP and 0.034 ± 0.004 MPa, respectively, suggesting that BBC5 membranes are mechanically stronger than the commercial product.

To improve the regenerative potential of our new BBC duraplasty, EGF and FGF2 were incorporated into the BBC5 membranes (BBC5GF), and their release profiles were studied. In this work, FGF2 and EGF were loaded directly on the top of the BBC5 samples by physical adsorption which resulted in a high entrapment efficiency (**Figure 3.4A**). The *in vitro* drug release profiles demonstrated an initial burst release in the first 8 hours, which was likely due to the presence GFs on the surface of the membranes (**Figure 3.4C**). This initial release phase was followed by a more gradual and almost linear release until ten days, due to the diffusion of GFs. The maximum cumulative percentage released of FGF2 (94.3 ± 3.7 %) and EGF (93.4 ± 3.1 %) from BBC5GF was achieved in ten days, period that it's consider essential for the activation time of NSPCs after injury [37].

To further evaluate the potential of BBC5GF duraplasty, NSPC culture was used to investigate if BBC5GF will enhance the proliferation of the NSPCs. Our results showed that there was an increase in the number of neurospheres after one week of cultivation when BBC5GF was used (**Figure 3.5**), strongly suggesting that BBC5GF was able to stimulate NSPC proliferation. Similar results were observed for porcine brain cells **(Figure B.1** in Appendix B) and for human spinal cord cells (**Figure B.2** in Appendix B). It should be noted that while these human cells were collected from a single human spinal cord donor, given the difficulty of the procuring such tissue and obtaining suitable donors, the data from these *in vitro* studies significantly strengthens the arguments for the clinical relevance of the BBC5GF.

NSPCs have been previously shown to differentiate to neurons, oligodendrocytes and astrocytes when cultured in 1% FBS supplemented media [38]. To ensure that NSPCs maintain this differentiation capacity when cultured with BBC5GF, the cells were characterized by immunohistochemistry after one and two weeks of culture. BBC5GF impacts neither the differentiation capacity of NSPCs to neurons, astrocytes and oligodendrocytes, nor the presence of the precursor population (**Figure 3.6** and **Figure 3.7**). It was observed that NSPCs derived from the BBC5GF treatment group were indeed multipotent (**Figure 3.6**) and displayed a dominant astrocyte phenotype upon differentiation for one and two weeks, similarly as the positive control (**Figure 3.7**). In addition, as shown in **Figure 3.6**, the percentage of Sox2 and Nestin of NSPCs grown in GFM media and BBC5GF were similar and high. This is consistent with previous studies that showed EGF/FGF2 promoted proliferation of precursor cells *vs.* differentiation [19, 24]. Further, the H&E staining confirmed the biocompatibility of the BBC5GF (**Figure 3.8**).

3.5. Conclusion

We presented a novel BC-based drug releasing duraplasty that can be applied as part of decompression craniectomy procedure in stroke patients to stimulate neural stem cell proliferation. By using a new fabrication technique as proposed herein, drug releasing duraplasties with different cellulose amounts were produced, and we showed that the BBC5 (i.e. highest cellulose mass) demonstrated the lowest swelling ratio capacity, mechanically stronger and a promising candidate as drug releasing duraplasty. In addition, EGF/FGF2 were sterilely incorporated into the BBC5 duraplasty in a reliable and effective way. The *in vitro* drug release study of the growth factors-enriched BBC5 (BBC5GF) suggests that BBC5GF could be exploited as scaffold in a controlled delivery system for protein-based drugs to the

brain. The dosage of growth factors proved sufficient to stimulate primary rodent neural stem/progenitor cell (NSPC) proliferation *in vitro* for a period of one week. This trend of NSPC proliferation continued into the second week, but this effect was only moderate. The BBC5GF did not affect the differentiation profile and capacity of NSPCs to oligodendrocytes, astrocytes and neurons, nor the presence of the precursor population. Indeed, the NSPCs derived from the BBC5GF treatment were multipotent and displayed a dominant astrocyte phenotype upon differentiation for one and two weeks. Finally, the *in vivo* post-decompression implantation of BBC5GF in adult rats demonstrated BBC5GF excellent biocompatibility. These findings indicate that a BBC loaded with growth factors is a promising and clinically relevant drug releasing duraplasty to stimulate neural stem cell proliferation for treatment of acute ischemic stroke and other central nervous disorders such as spinal cord injury.

3.6. References

[1] Global Health Estimates 2016: Deaths by Cause, Age, Sex, by Country and by Region, 2000-2016. Geneva, World Health Organization, 2018. http://www.who.int/healthinfo/global_burden_disease/estimates/en/. (Accessed May 7th 2019).

[2] Global Health Estimates 2015: Disease burden by Cause, Age, Sex, by Country and by Region, 2000-2015. Geneva, World Health Organization, 2016. http://www.who.int/healthinfo/global_burden_disease/estimates/en/index1.html. (Accessed May 7th 2019).

[3] A. Rogalewski, A. Schneider, E.B. Ringelstein, W.R. Schabitz, Toward a multimodal neuroprotective treatment of stroke, Stroke 37(4) (2006) 1129-36.

[4] E. Juttler, A. Unterberg, J. Woitzik, J. Bosel, H. Amiri, O.W. Sakowitz, M. Gondan, P. Schiller, R. Limprecht, S. Luntz, H. Schneider, T. Pinzer, C. Hobohm, J. Meixensberger, W. Hacke, D.I. Investigators, Hemicraniectomy in older patients with extensive middle-cerebral-artery stroke, N Engl J Med 370(12) (2014) 1091-100.

[5] M. Geurts, H.B. van der Worp, L.J. Kappelle, G.J. Amelink, A. Algra, J. Hofmeijer, H.S. Committee, Surgical decompression for space-occupying cerebral infarction: outcomes at 3 years in the randomized HAMLET trial, Stroke 44(9) (2013) 2506-8.

[6] D. Staykov, R. Gupta, Hemicraniectomy in malignant middle cerebral artery infarction, Stroke 42(2) (2011) 513-6.

[7] B. Sommerich, A. Barnick, M. Barakat, M. Ward, In vivo tissue reaction, resorption, safety, and efficacy of a collagen dural substitute in an animal model, Codman & Shurtleff, Inc., Rayham, MA, 2005.

[8] C.L. Rosen, G.K. Steinberg, F. DeMonte, J.B. Delashaw, S.B. Lewis, M.E. Shaffrey, K. Aziz, J. Hantel, F.F. Marciano, Results of the Prospective, Randomized, Multicenter Clinical Trial Evaluating a Biosynthesized Cellulose Graft for Repair of Dural Defects, Neurosurgery 69(5) (2011) 1093-1103.

[9] A.R.Y. Marzieh Moosavi-Nasab, Investigation of Physicochemical Properties of the Bacterial Cellulose Produced by Gluconacetobacter xylinus from Date Syrup, World Academy of Science, Engineering and Technology, 2010, pp. 1248-1253.

[10] M. Ul-Islam, T. Khan, J.K. Park, Water holding and release properties of bacterial cellulose obtained by in situ and ex situ modification, Carbohyd Polym 88(2) (2012) 596-603.

[11] T.R. Stumpf, R.A.N. Pertile, C.R. Rambo, L.M. Porto, Enriched glucose and dextrin mannitol-based media modulates fibroblast behavior on bacterial cellulose membranes, Mat Sci Eng C-Mater 33(8) (2013) 4739-4745.

[12] A. Meftahi, R. Khajavi, A. Rashidi, M. Sattari, M.E. Yazdanshenas, M. Torabi, The effects of cotton gauze coating with microbial cellulose, Cellulose 17(1) (2010) 199-204.

[13] G. Helenius, H. Backdahl, A. Bodin, U. Nannmark, P. Gatenholm, B. Risberg, In vivo biocompatibility of bacterial cellulose, J Biomed Mater Res A 76A(2) (2006) 431-438.

[14] L.R. Mello, L.T. Feltrin, P.T.F. Neto, F.A.P. Ferraz, Duraplasty with biosynthetic cellulose: An experimental study, J Neurosurg 86(1) (1997) 143-150.

[15] T.R. Stumpf, X.Y. Yang, J.C. Zhang, X.D. Cao, In situ and ex situ modifications of bacterial cellulose for applications in tissue engineering, Mat Sci Eng C-Mater 82 (2018) 372-383.

[16] H. Ullah, F. Wahid, H.A. Santos, T. Khan, Advances in biomedical and pharmaceutical applications of functional bacterial cellulose-based nanocomposites, Carbohydr Polym 150 (2016) 330-52.

[17] Z. Dai, J. Ronholm, Y. Tian, B. Sethi, X. Cao, Sterilization techniques for biodegradable scaffolds in tissue engineering applications, J Tissue Eng 7 (2016) 2041731416648810.

[18] D.J. Cook, C. Nguyen, H.N. Chun, L.L. I, A.S. Chiu, M. Machnicki, T.I. Zarembinski, S.T. Carmichael, Hydrogel-delivered brain-derived neurotrophic factor promotes tissue repair and recovery after stroke, J Cereb Blood Flow Metab 37(3) (2017) 1030-1045.

[19] M.J. Cooke, Y. Wang, C.M. Morshead, M.S. Shoichet, Controlled epi-cortical delivery of epidermal growth factor for the stimulation of endogenous neural stem cell proliferation in stroke-injured brain, Biomaterials 32(24) (2011) 5688-97.

[20] P. Dibajnia, C.M. Morshead, Role of neural precursor cells in promoting repair following stroke, Acta Pharmacol Sin 34(1) (2013) 78-90.

[21] Y. Wang, M.J. Cooke, N. Sachewsky, C.M. Morshead, M.S. Shoichet, Bioengineered sequential growth factor delivery stimulates brain tissue regeneration after stroke, J Control Release 172(1) (2013) 1-11.

[22] A. Arvidsson, T. Collin, D. Kirik, Z. Kokaia, O. Lindvall, Neuronal replacement from endogenous precursors in the adult brain after stroke, Nat Med 8(9) (2002) 963-70.

[23] J. Lu, A. Manaenko, Q. Hu, Targeting Adult Neurogenesis for Poststroke Therapy, Stem Cells Int 2017 (2017) 5868632.

[24] W.A. Wolf, J.L. Martin, G.L. Kartje, R.G. Farrer, Evidence for fibroblast growth factor-2 as a mediator of amphetamine-enhanced motor improvement following stroke, PLoS One 9(9) (2014) e108031.

[25] F. Hu, X. Wang, G. Liang, L. Lv, Y. Zhu, B. Sun, Z. Xiao, Effects of epidermal growth factor and basic fibroblast growth factor on the proliferation and osteogenic and neural differentiation of adipose-derived stem cells, Cell Reprogram 15(3) (2013) 224-32.

[26] M. Schramm, S. Hestrin, Factors Affecting Production of Cellulose at the Air Liquid Interface of a Culture of Acetobacter-Xylinum, Journal of General Microbiology 11(1) (1954) 123-&.

[27] W.X. Guo, N.E. Patzlaff, E.M. Jobe, X.Y. Zhao, Isolation of multipotent neural stem or progenitor cells from both the dentate gyrus and subventricular zone of a single adult mouse, Nat Protoc 7(11) (2012) 2005-2012.

[28] P. Jendelová, Š. Kubinová, I. Sandvig, S. Erceg, A. Sandvig, E. Syková, Current developments in cell- and biomaterial-based approaches for stroke repair, Expert Opinion on Biological Therapy 16(1) (2015) 43-56.

[29] S. Yao, X. Liu, X. Wang, A. Merolli, X. Chen, F. Cui, Directing neural stem cell fate with biomaterial parameters for injured brain regeneration, Progress in Natural Science: Materials International 23(2) (2013) 103-112.

[30] E.M. Ahmed, Hydrogel: Preparation, characterization, and applications: A review, J Adv Res 6(2) (2015) 105-121.

[31] J. Li, D.J. Mooney, Designing hydrogels for controlled drug delivery, Nat Rev Mater 1(12) (2016).

[32] Z.M. Wang, Z.F. Wang, W.W. Lu, W.X. Zhen, D.Z. Yang, S.L. Peng, Novel biomaterial strategies for controlled growth factor delivery for biomedical applications, Npg Asia Mater 9 (2017).

[33] D. De Kegel, J. Vastmans, H. Fehervary, B. Depreitere, J. Vander Sloten, N. Famaey, Biomechanical characterization of human dura mater, J Mech Behav Biomed 79 (2018) 122-134.

[34] M.C.I.M. Amin, N. Ahmad, N. Halib, I. Ahmad, Synthesis and characterization of thermo- and pH-responsive bacterial cellulose/acrylic acid hydrogels for drug delivery, Carbohyd Polym 88(2) (2012) 465-473.

[35] R. Zarzycki, Z. Modrzejewska, K. Nawrotek, Drug Release from Hydrogel Matrices, Ecol Chem Eng S 17(2) (2010) 9-28.

[36] S.F. Danish, A. Samdani, A. Hanna, P. Storm, L. Sutton, Experience with acellular human dura and bovine collagen matrix for duraplasty after posterior fossa decompression for Chiari malformations, J Neurosurg 104(1) (2006) 16-20.

[37] T. Ikeda, M. Iwai, T. Hayashi, I. Nagano, M. Shogi, T. Ikenoue, K. Abe, Limited differentiation to neurons and astroglia from neural stem cells in the cortex and striatum after ischemia/hypoxia in the neonatal rat brain, Am J Obstet Gynecol 193(3 Pt 1) (2005) 849-56.

[38] T. Zahir, Y.F. Chen, J.F. MacDonald, N. Leipzig, C.H. Tator, M.S. Shoichet, Neural Stem/Progenitor Cells Differentiate In Vitro to Neurons by the Combined Action of Dibutyryl cAMP and Interferon-gamma, Stem Cells Dev 18(10) (2009) 1423-1432.

CHAPTER 4 – PRODUCTION AND EVALUATION OF BIOSYNTHESIZED CELLULOSE TUBE (BCT) AS PROMISING NERVE GUIDANCE DRUG DELIVERY TUBE FOR SPINAL CORD INJURIES TREATMENT

4.1. Introduction

Spinal cord injury (SCI) is a central nervous system (CNS) condition that often results in permanent sensory and motor dysfunctions. The restricted ability of the CNS to regenerate is mostly attributed to the hostile inhibitory environment across the injury site and to the growth of scar tissue that prejudice axonal regeneration and recovery of spinal cord [1]. As a result, functional recovery after SCI remains one of the most perplexing clinical problems. Currently, clinical treatments of the SCI are usually limited to the decrease of swelling and pain and the prevention of secondary injuries through the administration of anti-inflammatory drugs [2].

Although there have been great efforts to explore the optimal combination of strategies necessary for effective repair of the spinal cord, new factors that affect this repair continue to be identified [3-5]. SCI is a multifaceted clinical condition and in recent years, regenerative medicine and tissue engineering based approaches have been proposed as options for SCI repair [6], especially those using biomaterials [7]. Biomaterials can be designed to bridge extensive damage, to provide physical, directional and mechanical support for axonal regrowth, to inhibit scar tissue formation and potentially to facilitate repair by serving as a local release system for growth factors (GFs). Tube-shaped biomaterials, i.e. guidance tubes, are porous hollow fiber tubes that can be implanted where bridging is necessary [8-11]. Implanted nerve guidance tubes for repair of SCI must stay open long enough for axonal regeneration (protecting against compression), whether degradable or non-degradable.

Biomaterials selected for construction of nerve guidance tubes for spinal cord repair should have the following characteristics: proper suturability and swelling properties; mechanical properties (specifically Young's modulus) matching to that of the spinal cord; biocompatibility with the host tissue; and allow for cell adhesion and axonal regrowth [12, 13].

Integrating GFs into the biomaterial selected ensures cellular viability, adhesion and stimulates neurite growth [14, 15]. GFs are proteins capable of motivating the differentiation and proliferation of cells, due to their ability to direct cellular activities and to bind to cell receptors [16]. Among various GFs found in the body, nerve growth factor (NGF) is well recognized for stimulating the differentiation and survival of sensory and sympathetic neurons in the CNS. The NGF has been showed to improve neuronal outgrowth and has been applied as a chemo-attractant to promote axon guidance [17, 18].

In recent years, progress has been made to design biomaterials as nerve guidance tubes using natural and/or synthetic polymers such as polyglycolic acid (PGA), type I collagen, polyvinyl alcohol (PVA), and poly-DL-lactide-co-caprolactone (PLCL) [19-22]. Despite the fact that some of these materials are approved by the FDA, the clinical reality is that these biomaterials fail to repair and completely recover the spinal cord function after injury [23]. Therefore, here we proposed the use of biosynthesized cellulose (BC) as a nerve guidance tube for the regeneration of SCI. BC is produced by various bacterial species, including *Gluconacetobacter*, which is an excellent renewable source of pure cellulose. BC was discovered in the 1880s, however only in the 20th century its biomedical applicability has been gradually recognized [24, 25]. BC has exceptional properties such as high stability, high mechanical strength, high porosity, high crystallinity, low toxicity, and good biocompatibility [26]. Additionally, since the BC is produced only in aerobic condition, their assembly can be guided to form different shapes depending on the air–liquid interface used, such as membranes, spheres, cocoons (i.e. large 3D hydrogels), and tubes [27-33]. The purity and biocompatibility of BC makes it an ideal material in biomedical applications. For example, biosynthesized cellulose tubes (BCTs) have been studied mainly as blood vessel substitutes, i.e. vascular grafts [34-38], but not extensively for other applications such as urinary reconstruction [39], bone

regeneration [40], biofiltration [41], and nerve regeneration [42-44]. Other researchers have analysed the BCTs properties without addressing specific applications [45-48]. However, none of the mentioned publications have thoroughly analysed the BCTs produced at several cultivation times and/or explored the potential of BCTs as nerve guidance drug delivery system to promote neurite outgrowth.

Thus, the aim of this chapter was to build a bioreactor, to produce BCTs at different cultivation times, and to characterize the physical, morphological, and mechanical properties of these potential nerve guidance tubes. In addition, the BCT was loaded with NGF and its release characteristics and efficacy were studied to determine if BCTs could be suitable as SCI graft.

4.1. Materials and Methods

4.1.1. Materials

Both *Gluconacetobacter hansenii* (*G. hansenii)* (ATCC® 53582™) and rat pheochromocytoma cell line, PC12 (ATCC® CRL-1721™) were purchased from American Type Culture Collection (Manassas, VA). Recombinant human β-nerve growth factor (NGF) and ELISA detection kit for the NGF were obtained from PeproTech Inc. (Rocky Hill, NJ). All other chemicals were purchased from Sigma-Aldrich (St. Louis, MO) and used as received unless indicated otherwise.

4.1.2. Production of Biosynthesized Cellulose Tubes (BCTs)

For the formation of BCTs, *G. hansenii* cells were cultivated in a special bioreactor (**Figure 4.1**). More specifically, the bioreactor was consisted of a 250 mL glass bottle with two pieces of silicone tubing (2.52 mm inner diameter; 3.53 mm outside diameter; 0.51 mm wall thickness) (HelixMark®, Freudenberg Medical, Gloucester, MA) connected by a U-shaped stainless steel tubing, which was used to keep the silicone tubing straight and secured in place. At both ends of the silicone tubing, additional metal tubing was attached -- one was connected to an oxygen tank while the other was connected to the next bioreactor (**Figure 4.1**). Pure oxygen was injected at 50 kPa into the silicone tubing, allowing the production of BCTs with 3.53 mm of inner diameter. The bioreactors were sterilized by autoclaving and filled with an average of 1.3×10^5 CFU·mL^{-1} (Day 0) in a modified Hestrin-Schramm culture media containing glucose (20.0 g·L^{-1}), peptone (5.0 g·L^{-1}), yeast extract (5.0 g·L^{-1}), disodium phosphate (2.7 g·L^{-1}), and citric acid (1.5 g·L^{-1}) [28]. The filled bottles were kept under static condition at 26 °C for a pre-determined period of time, after which the resulting BCTs were removed from the silicone tubing and treated with 0.1 M of NaOH at 50 °C for 24 h. The purified tubes were subsequently washed with distilled water until neutral pH and stored at 4 °C. When required, the processed tubes were further freeze-dried and autoclaved. To investigate the characteristics of BCT samples, 7 different cultivation times were used to obtain 7 different samples, named BCT3, BCT6, BCT9, BCT12, BCT16, BCT18 and BCT 22, e.g. the BCT produced after 3 days of cultivation was named BCT3.

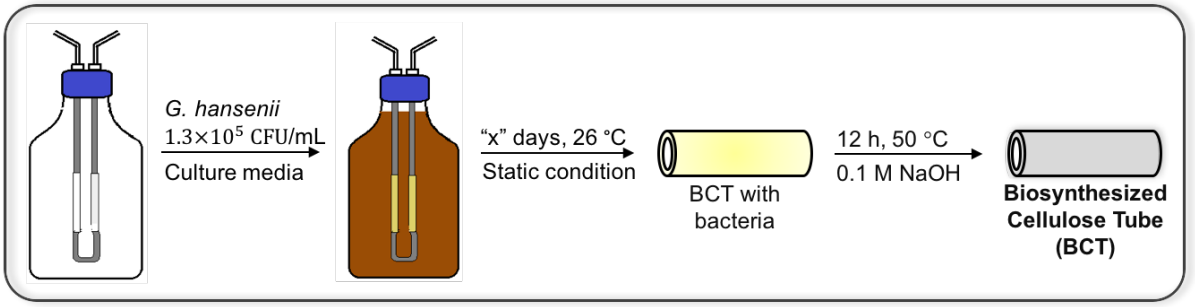

Figure 4.1 – Schematic representation for the biosynthesized cellulose tubes (BCTs) production. 1.3×10^5 CFU·mL^{-1} of *G. hansenii* cells were cultivated inside the bioreactor in a glucose-based media for "x" days (x = 3, 6, 9, 12, 16, 18 and 22 days), then cellulose tubes were collected, the silicone tubing removed and purified to obtain purified BCTs.

4.1.2.1. Number of Free Cells and Media pH

To determine the cell number in the cell culture media during the BCT production over time (characterized by colony forming unit per milliliter of media, CFU·mL^{-1}), at pre-determined cultivation time points, aliquots of the cell culture media were collected and diluted in sterile growth media (pH 5.5), and 100 µL of the diluted solution was carefully-plated on agar media for 3 days at 26 °C. Subsequently, the number of colonies that had grown on each plate were counted. To provide an accurate representation of the bacterial titer, only plates containing between 25 and 250 colonies were considered. In addition, the pH of the cell culture media was monitored over time using an Oakton™ PC 700 pH/Conductivity Meter (Oakton Instruments, Vernon Hills, IL).

4.1.3. Characterization of Biosynthesized Cellulose Tubes (BCTs)

4.1.3.1. Rehydration Ratio (RR)

The rehydration ratio (RR) of BCTs was determined by a gravimetric method using the equation below:

$$RR\ (\%) = \frac{W_{reh} - W_{dry}}{W_{wet} - W_{dry}} \times 100$$

where W_{wet}, W_{dry}, W_{reh} are the mass of the original wet, lyophilized and rehydrated BCT samples, respectively.

4.1.3.2. Mechanical Properties

To characterize the mechanical properties of the prepared BCTs, rehydrated BCT samples were subjected to tensile tests. Specifically, rehydrated BCT specimens (15 mm long and individual thickness), were stretched lengthwise with a crosshead speed at 5 $mm \cdot min^{-1}$ [49]. The measurements were carried out at 25 ± 2 °C and relative humidity of 45 ± 5 % on an Instron ElectroPuls™ E3000 mechanical tester (Norwood, MA) equipped with Instron® Bluehill® Software (Norwood, MA). The samples were tested for Young's modulus, ultimate tensile strength (UTS) and elongation-at-break.

4.1.3.3. Scanning Electron Microscopy (SEM) Analysis

To compare the microstructures of the resulting BCTs a Phenom Pro SEM (Phoenix, AZ) was used. Images of inner, outer and cross-section views of the BCTs obtained after 6 and 22 days of cultivation (i.e. BCT6 and BCT22, respectively) were investigated for comparison. The samples were produced, froze and freeze-dried before the SEM analyses.

4.1.4. Drug Delivery Study

NGF was used as a model drug to be delivered, and BCT22 was studied as a nerve guidance drug delivery tube. Briefly, freeze-dried BCT22 tubes were cut into 1 cm in length. Subsequently the tubes were autoclaved and individually placed into the wells of a 24-well plate. To each of the tubes, 50 µL of 7000 $ng \cdot mL^{-1}$ NGF sterile solution was added (hereinafter

referred to as NGF-BCT22). The NGF-loaded tubes were allowed to be air dried for ~2 hours until the NGF solution was completely absorbed by the tubes. To study the drug delivery performance of the NGF loaded tubes, the NGF-BCT22 was completely submerged in 2 mL of PBS (pH 7.4) at 37 °C; at pre-determined time points, 0.32 mL of the buffer was collected and replenished with the same volume of fresh buffer. The released amount of NGF from the collected samples were determined by NGF ELISA using vendor's protocol.

4.1.5. Bioactivity Assessment of Released NGF

PC12 cells, which differentiate into a neuronal phenotype in the presence of bioactive NGF [50], were used to test whether the NGF delivered from the NGF-BCT22 samples were bioactive by stimulating the differentiation of PC12 [51]. PC12 cells were routinely maintained in growth media that consisted of 84 % RPMI 1460 (Gibco Waltham, MA), 10 % heat-inactivated horse serum (HS), 5 % fetal bovine serum (FBS) and 1 % penicillin/streptomycin solution (P/S). Cells were incubated at 37 °C in 5 % of CO_2 in air. All the PC12 cells used in the bioactivity studies were less than 12 passages and were primed for one week before the experiment with 50 $ng \cdot ml^{-1}$ of NGF in serum-reduced media (93 % RPMI 1460, 1 % HS, 5 % FBS and 1 % P/S) as reported previously [52].

To investigate the bioactivity of the released NGF from the BCTs, PC12 cells were co-cultured with NGF releasing BCTs. Specifically, NGF primed PC12 cells were gently washed with PBS (pH 7.4) for three times and seeded into the wells of a high adhesion 12-well plate ($Cell^{+}$, Sarstedt, North Rhine-Westphalia, Nümbrecht) at a concentration of 1.7×10^5 $cells \cdot well^{-1}$. To deliver the NGF to the cell culture, NGF-BCT22 samples were co-cultured with the PC12 cells using PET inserts (1 μm pore size, Sarstedt, North Rhine-Westphalia, Nümbrecht), in a

total of 2.0 mL·well^{-1} of cell culture. Every 4 days, a partial cell media change (1 mL) was performed. In parallel, cell culture media supplemented with 50 ng·ml^{-1} of NGF (NGF media) was used as a positive control while cell cultures with cell culture media only (Media) and blank BCT (Nude BCT) were both used as negative controls.

After 2, 4, and 7 days in culture, the morphology of the PC12 cells were observed and documented using phase-contrast microscopy, and the cell images were analyzed using Image-Pro Plus 6 software (Media Cybernetics, Inc., Rockville, MD). More than 100 cells from 5 random (and different) fields from each samples were analyzed, and only cells bearing neurites longer than or equal to one cell body length were considered positive for neurite outgrowth. MTT assays were also carried out for all the samples. In addition, at Day 4 in culture, the PC12 cells were fluorescently stained for F-actin. In brief, PC12 cells were rinsed with PBS and fixed with 3.7 % formaldehyde in PBS (pH 7.4) for 30 min, after which the cells were permeabilized with 0.1 % Triton X-100 solution and blocked with 1 % w/v BSA blocking solution for 30 min. Finally the preparations were incubated with 0.1 μg·ml^{-1} FTIC-phalloidin to stain for F-actin in the cytoskeleton of the cells and counterstained for 20 min with 1 μg·ml^{-1} DAPI. The stained PC12 cells were observed with an Olympus IX81 inverted fluorescent microscope (Mississauga, ON).

4.1.6. Statistical Analysis

All statistical analyses were carried out using one-way and two-way ANOVA, followed by post hoc Tukey's analysis, using GraphPad Prism 6 Data (GraphPad Software, La Jolla, CA). P values < 0.05 were considered statistically significant.

4.2. Results and Discussion

4.2.1. Preparation and Characterization of Biosynthesized Cellulose Tubes (BCTs)

This study investigated the potential of BCTs as drug delivery system to stimulate spinal cord regeneration after SCI. For the BCTs production, a special vertical bioreactor was designed, where silicone tubing was used as mold and oxygen-semipermeable material to allow *G. hansenii* to grow and synthesize BC fibers around the outer surface of the silicone tubing into a tube shape (**Figure 4.2A** and **Figure 4.2B**). The silicone tubing with outside diameter of 3.53 mm was chosen to give a BCT with the inside diameter of 3.53 mm, which corresponds to the average size of rat spinal cord [53]. It is recognized that culture conditions such as bacteria concentration, pH of media, cultivation time, carbon source, and the concentration of oxygen could significantly affect the formation and properties of BC [54-57]. In this study, glucose was chosen as the sole carbon source, because it has shown high cellulose productivity by *Gluconacetobacter* genus [58, 59]. It has also been reported by Watanabe and Yamanaka [55] and Bodin et al. [36] that a high concentration of oxygen during static cultivation increases the cellulose yield, density and, subsequently, the toughness of BC. Therefore, 100 % oxygen was used in this study to increase the amount of cellulose produced around the silicone tubing.

G. hansenii cells are aerobic bacteria and were kept in static culture for different period of time. The number of free cells in the culture media (**Figure 4.2C**) and the pH of the media were measured over time (**Figure 4.2D**). There was a significant increase in the number of free bacterial cells in the first 3 days of the culture ($p < 0.0001$) and that number decreased till Day 9 ($p < 0.0001$), after which remained constant for the rest of the study. The changes of the cell number in the culture media over time was expected since it is known that the aerobic *G. hansenii* cells allocate in areas with higher concentration of oxygen as possible (i.e. around silicone tubing) [60, 61]. As result, the cell number showed an initial increase in the first 3

days; however, as the cells started to produce and accumulate cellulose biomass around the silicone tubing over time, the cells likely got trapped inside of the cellulose network, thereby resulting in a reduced number of free cells in the culture media. In addition, the pH of the media at different time points was analyzed (**Figure 4.2D**). The pH is an essential factor in the bacteria growth, because it can affect the cell membrane's permeability and structure, thereby influencing the microorganism biochemistry activities including the cellulose production [62]. The initial pH of the glucose-based media was 5.5, when *G. hansenii* solution was added, the pH decreased to 5.2 ± 0.1, which after 22 days of cultivation decreased to 4.8 ± 0.1 ($p < 0.0001$), likely due to the side production of organic acids because of the metabolic activities of the cells [63].

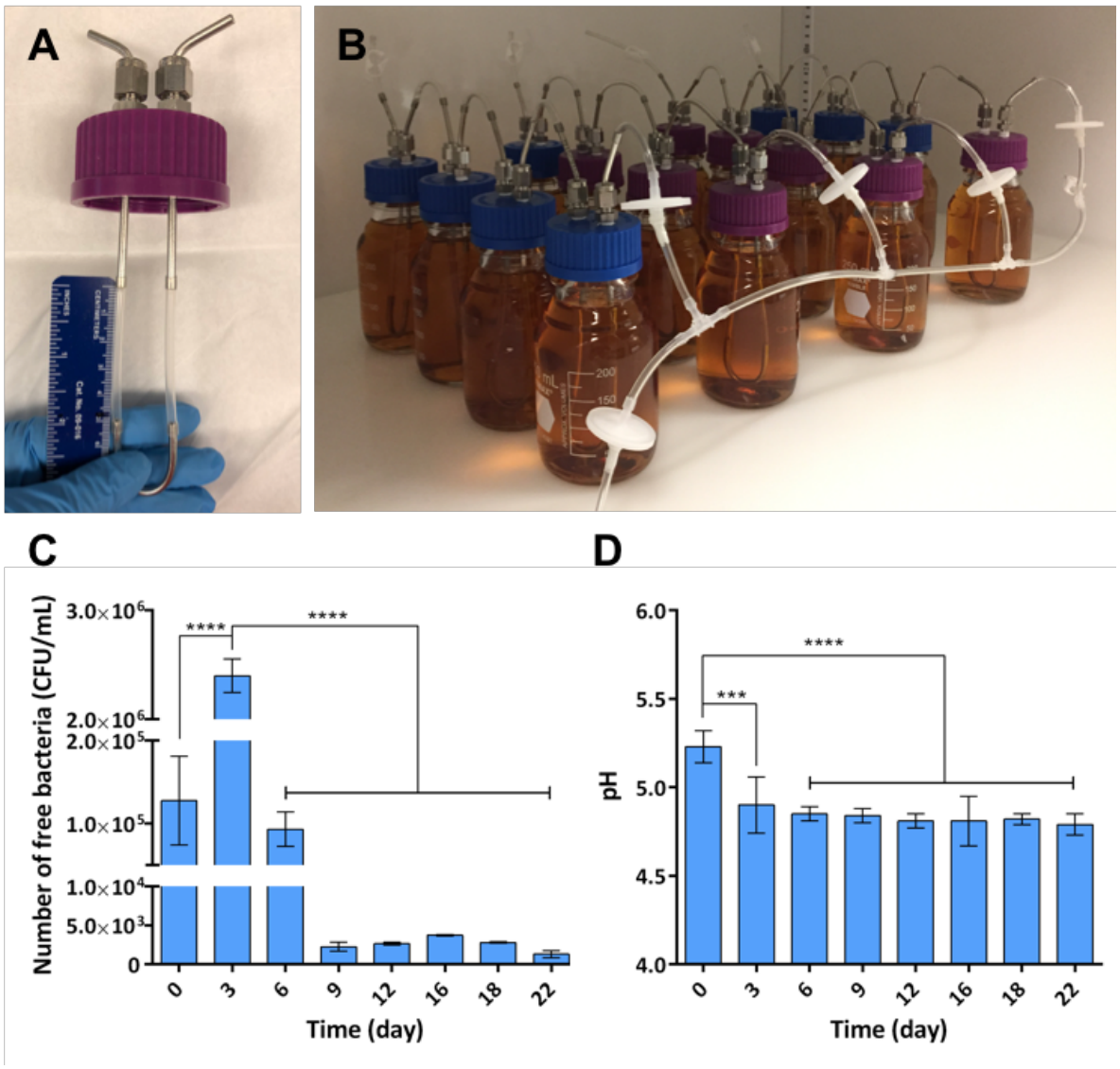

Figure 4.2 – Biosynthesized cellulose tubes (BCTs) production and cultivation conditions. **A)** Bioreactor cap where a stainless steel tubing was used as oxygen inlet and outlet, and in which a silicone tubing was attached as a mold for the BCT production. **B)** BCTs bioreactors containing *G. hansenii* in a glucose-based media at Day 0 and 26 °C. **C)** Number of free bacteria as colony formed units per milliliter ($CFU \cdot mL^{-1}$) in the media and the pH (**D**) of the media at different time points. *(One-way ANOVA followed by multiple-comparisons test (Tukey's) were performed for statistical analysis. Data obtained from at least two independent experiments and presented as mean ± sd; n = 4; ***p < 0.001; ****p < 0.0001).*

BCTs were produced by culturing *G. hansenii* around oxygen permeable silicone tubing inside of a bioreactor (**Figure 4.3A**). The original BCTs directly produced from the cell culture were removed from the bioreactor (**Figure 4.3B**) and were subsequently washed to obtain white translucent cellulose hydrogel tubes (**Figure 4.3C**). **Figure 4.3F** shows the different

dry cellulose mass and wall thickness for the produced BCTs over time**.** While it is evident that increasing the cultivation time inside of the bioreactor would increase the amount of dry cellulose, significant increase in the tube wall thickness took place only after 12 days of cultivation. Overall, BCT22 presented the highest mass of dry cellulose (15.5 ± 2.8 mg) and wall thickness (0.55 ± 0.07 mm). Few studies have shown the relation between the cultivation time and wall thickness. However, Putra et al. produced BC tubes with orientated cellulose fibers for 10 days, which had the wall thickness increased with an increase in the cultivation time [45], similar to the results showed here.

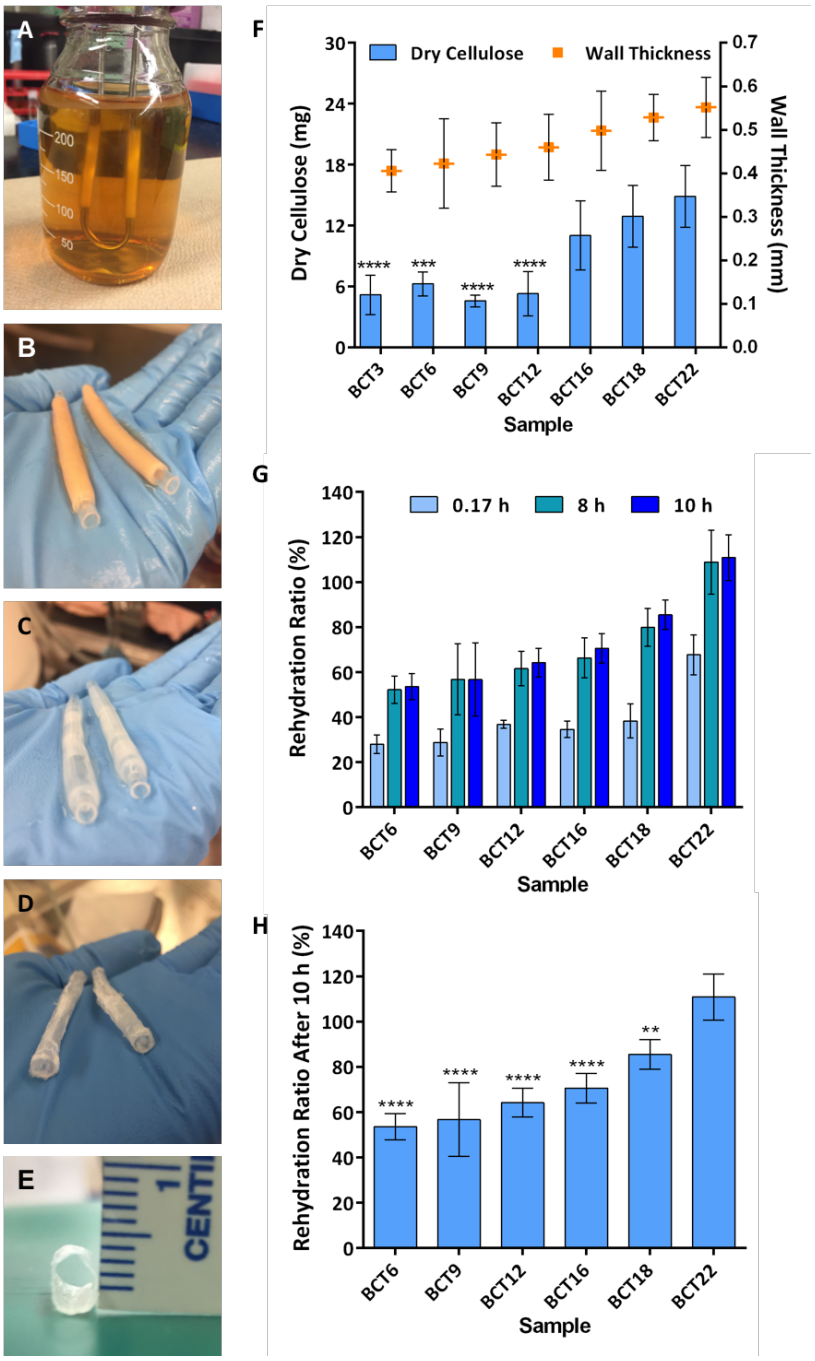

Figure 4.3 – Production and physical characteristics of biosynthesized cellulose tubes (BCTs). **A)** Flask of *G. hansenii* inoculum containing BCTs after 22 days of cultivation (named BCT22) in static condition at 26 °C. BCT22 around silicone tubing before **(B)** and after purification **(C)**. **D)** BCT22 without silicone tubing, after purification and lyophilization. **E)** Cross-section view of BCT22 showing tube format. **F)** Graph showing the wall thickness and the dry cellulose mass of the different BCTs samples (BCT3, BCT 6, BCT 9, BCT12, BCT16, BCT18 and BCT22), e.g. the BCT produced after 3 days of cultivation was named BCT3. **G)** Rehydration ratio of BCT6-22 in PBS at 37 °C in different time points. **H)** Rehydration ratio from (G) after 10 hours. *(One-way ANOVA followed by multiple-comparisons test (Tukey's) were performed for statistical analysis. Data obtained from two independent experiments and presented as mean ± sd; n = 8; **p < 0.01; ***p < 0.001; ****p < 0.0001 from BCT22).*

Figure 4.3G and **Figure 4.3H** show the rehydration ratio (RR) of BCT6 to BCT22 samples. There was an ascending trend for RR, where BCT22 showed the highest RR while BCT6 demonstrated the lowest RR among the samples. The RRs for all BCTs increased within the first 8 hours after which they remained roughly constant. The interaction between the BC network and the water molecules mostly depends on the organization of the BC fiber network. Increasing the porosity and the pore size increases the amount of water that can penetrate and be adsorb onto the BC [56]. Therefore, the difference in RR may be caused by the variances in the fiber network and porosity of BCT samples. The cellulose fibers when arranged in a looser way interact to the water molecules more strongly due to hydrogen bonding (as in BCT22) as compared to the tighter fibers structure, what results in a denser cellulose arrangement with less space to absorb water (as in BCT6). The density and arrangement of BC fibers varies with the cultivation time due to the secretion of more fibrils. This in turn explains why the RR of BCTs change along its production time.

The study of BCT microstructures by SEM supports the RR results. SEM images show that increasing the cultivation time, e.g. 6 to 22 days of cultivation, and cellulose content resulted in a less dense fiber network and more porous microstructure on the outside of the tubes. Visually, the outside of BCT22 was more porous with plenty gaps between the cellulose fibers, as shown in **Figure 4.4**, which led to a higher RR. On the other hand, BCT6 was denser with the fibers closer compared to BCT22, this meant a lower ability to reabsorb water, which resulted in a lower RR. Besides, BCT6 was a weaker tube, not standing its own weight and, as can be seen in the SEM images, presented fractures in its inner side (**Figure 4.4**).

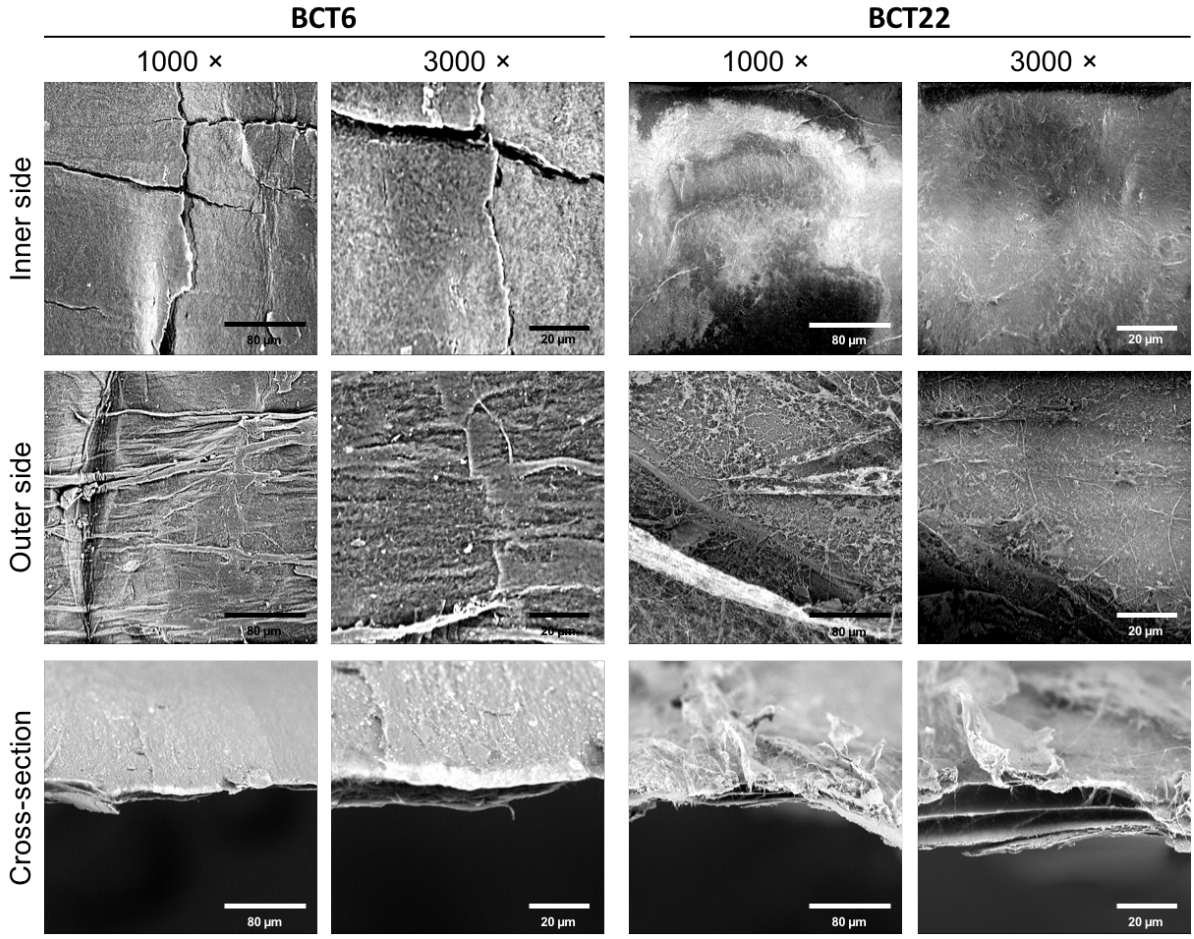

Figure 4.4 – Scanning electron microscopy (SEM) micrographs of freeze-dried biosynthesized cellulose tubes after 6 (BCT6) and 22 (BCT22) days of cultivation: inner side (silicone contact), outer side (liquid contact), and cross-sectional views with 1000 and 3000× magnification. *Three samples were assayed in duplicate by SEM analysis for each condition.*

When the cellulose-producing bacteria is statically cultured in a flask, they produce BC biomass as a heterogeneous and layered membrane at the air-liquid interface [64]. This biomass membrane is composed of highly entangled cellulose fiber networks, which are denser at the membrane/air interface than at the membrane/liquid interface on the opposite side. This same phenomena happened when the BC biomass was produced around the silicone tubing; the inner side of the BCTs that are in contact with the silicone, where there is more oxygen, was denser than the outer side of the BCTs – in contact with the media, as shown in **Figure**

4.4. In addition, BCT22 was composed of a layered structure similar in morphology to BC membranes produced statically, as seen in the SEM images of the cross-section of BCT22 in **Figure 4.4**. BCTs have a high hydrophilicity, being BCT22 more porous and with a higher RR, what increases its application as drug delivery system in biomedicine [65].

In addition, the mechanical properties of the BCTs were studied. Mechanical properties are essential for determining the performance of spinal cord grafts [66]. Two of the essential requirements for a BCT to function as a nerve in the human body are stiffness and mechanical strength. BCT must not only resist mechanical strain in surgical preparation and the anastomosis but also be able to withstand the biomechanical forces in the body without collapsing [34, 67]. In other words, it is important that the biomaterial match the mechanical properties to that of the spinal cord at the injury site for the effective integration of the biomaterial into the surrounding tissue [13, 67]. The mismatch of mechanical properties between the soft spinal cord tissue and the implant may further damage the neural tissue by compressing the surrounding tissue. Consequently, delaying the tissue repair because of the formation of cysts or fibrotic tissue between the implant and the surrounding spinal cord tissue [68, 69]. BCT22 can stand by itself (see **Figure 4.3D** and **Figure 4.3E**), demonstrating that it can support its own weight, without collapsing.

Figure 4.5 shows the results for the rehydrated tubes' tensile properties. The ultimate tensile strength (UTS) of BCTs was affected by cultivation time. BCT22, the tube cultivated for 22 days and with the highest cellulose content, exhibited greater UTS (1.43 ± 0.29 MPa) when compared to those cultivated for less time (i.e. BCT3-18) (**Figure 4.5A**). It would be expected that the Young's modulus (i.e. elastic modulus) would increase with increasing cultivation time and consequently cellulose mass. There was, however, no specific trend among the samples as a result of an increase in the cultivation time; the Young's modulus was

approximately 1.6 MPa for all tubes. The layered structure mentioned above makes it difficult to directly correlate the Young's modulus among the samples, similar to the observations made by Bodin et al. [36]. Among all samples, BCT22 demonstrated the lowest Young's modulus (1.24 ± 0.07 MPa) (**Figure 4.5B**), matching the Young's modulus of human spinal cord (0.2 to 1.9 MPa) [70-72]. The value of BCT22 elongation-at-break was 55.1 ± 5.5 %, which was significantly different from BCT6 ($p < 0.001$), BCT12 ($p < 0.001$) and BCT16 ($p < 0.01$) (**Figure 4.5C**).

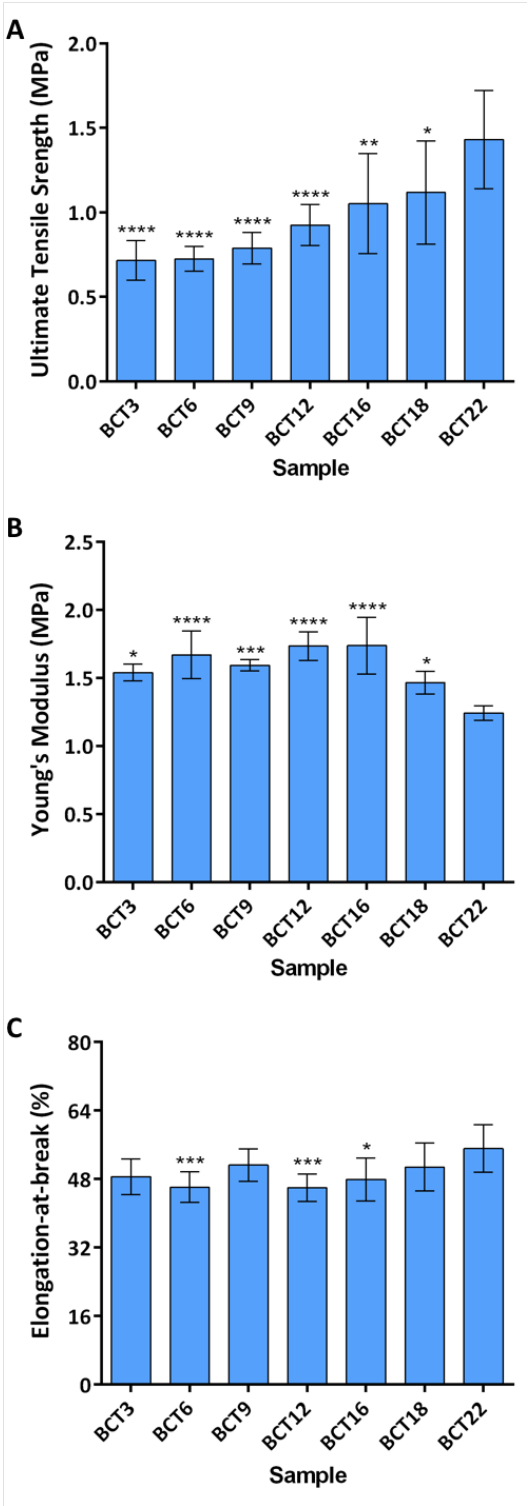

Figure 4.5 – Mechanical properties of biosynthesized cellulose tubes (BCTs) produced at different cultivation times. **A)** Ultimate tensile strength (UTS); **B)** Young's Modulus; **C)** Elongation-at-break. *(One-way ANOVA followed by a multiple-comparisons test (Tukey's) were used for statistical analysis. Data obtained from two independent experiments (n = 10) and is presented as mean ± s.d. *p < 0.05; **p < 0.01; ***p < 0.001; ****p < 0.0001 from BCT22).*

4.2.2. Drug Delivery Study

To improve cell regeneration, BCT was designed as a nerve guidance system to deliver NGF to the SCI site. Because of the structural and mechanical properties of BCT22 described here, combined with the various studies that showed the superior mechanical properties of BC over many synthetic biomaterials [73], BCT22 was the only tube used for the rest of the studies unless indicated otherwise. **Figure 4.6A** shows the physical characteristics of BCT22, which was cut into 1 cm length (inner diameter of 3.53 mm and wall thickness of 0.55 ± 0.07 mm) and presented a dry cellulose mass of 3.1 ± 0.6 mg. It is also noted that 350 ng of NGF was successfully loaded into BCT22, being the average NGF entrapment efficiency of 91.3 %. **Figure 4.6B** exhibits the release profile of NGF from NGF-BCT22 over 1 week. The NGF-BCT22 presented a burst release at the first day, then a not pronounced linear increase trend in the NGF released until 5 days, after the release profile appeared to level off (**Figure 4.6B**). After 7 days of release, the cumulative amount released of NGF was 295.3 ± 24.2 ng, representing 92.4 ± 7.6 % of initial NGF loaded into NGF-BCT22.

A

Masses	
Dry mass (mg)	3.1 ± 0.6
Wet mass (mg)	19.0 ± 3.3
Dimensions	
Wall thickness (mm)	0.55 ± 0.07
Inner diameter (mm)	3.53
Length (mm)	100 ± 0.1
Drug Release Characteristics	
Loaded NGF (ng)	350.2
Entrapment efficiency (%)	91.3 ± 2.5
Cumulative NGF released (%)	92.4 ± 7.6

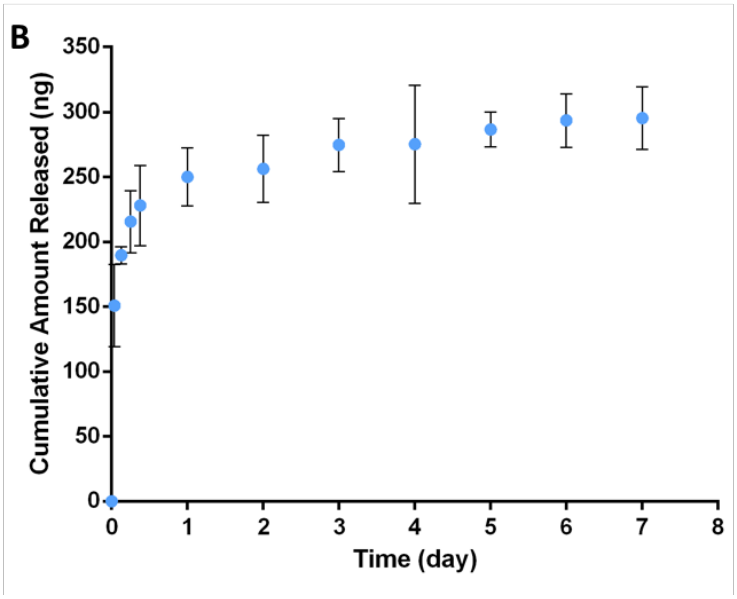

Figure 4.6 – Nerve growth factor (NGF) release profile from biosynthesized cellulose tubes after 22 days of cultivation (NGF-BCT22). **A)** Table of physical and drug release characteristics of NGF-BCT22. **B)** ELISA assessment of cumulative amount of NGF over 7 days. *Values are presented as mean ± s.d., n = 5.*

4.2.3. Bioactivity of Released NGF

The bioactivity of the NGF-BCT22 was studied by the differentiation of PC12 cells into neurons like cells, in the presence of the directly delivered-NGF from the NGF-BCT22. PC12 cells are frequently used in *in vitro* studies to assess neuronal differentiation [16, 74]. After NGF exposure, PC12 cells change phenotype and develop characteristics associated with

sympathetic neuron-like cells, which involves the reduction of proliferation and outgrowth of neurites [75, 76]. To assess how NGF delivered from NGF-BCT22 affected neural cell growth, PC12 cells were co-cultured in serum-reduced culture media with NGF-BCT22. PC12 cells in nude serum-reduced culture media with (Nude BCT) or without BCT (Media) had fewer cells, with a spherically-shape, and with a few visible neurites (**Figure 4.7**). Compared to the other groups, NGF media was the most beneficial to PC12 cells growth as evidenced by the increased cell number. Importantly, the treatment with NGF-BCT22 significantly promoted PC12 cells growth, and the elaboration of an extensive network of neurites when compared to the negative controls after 4 and 7 days (**Figure 4.7**; $p < 0.0001$).

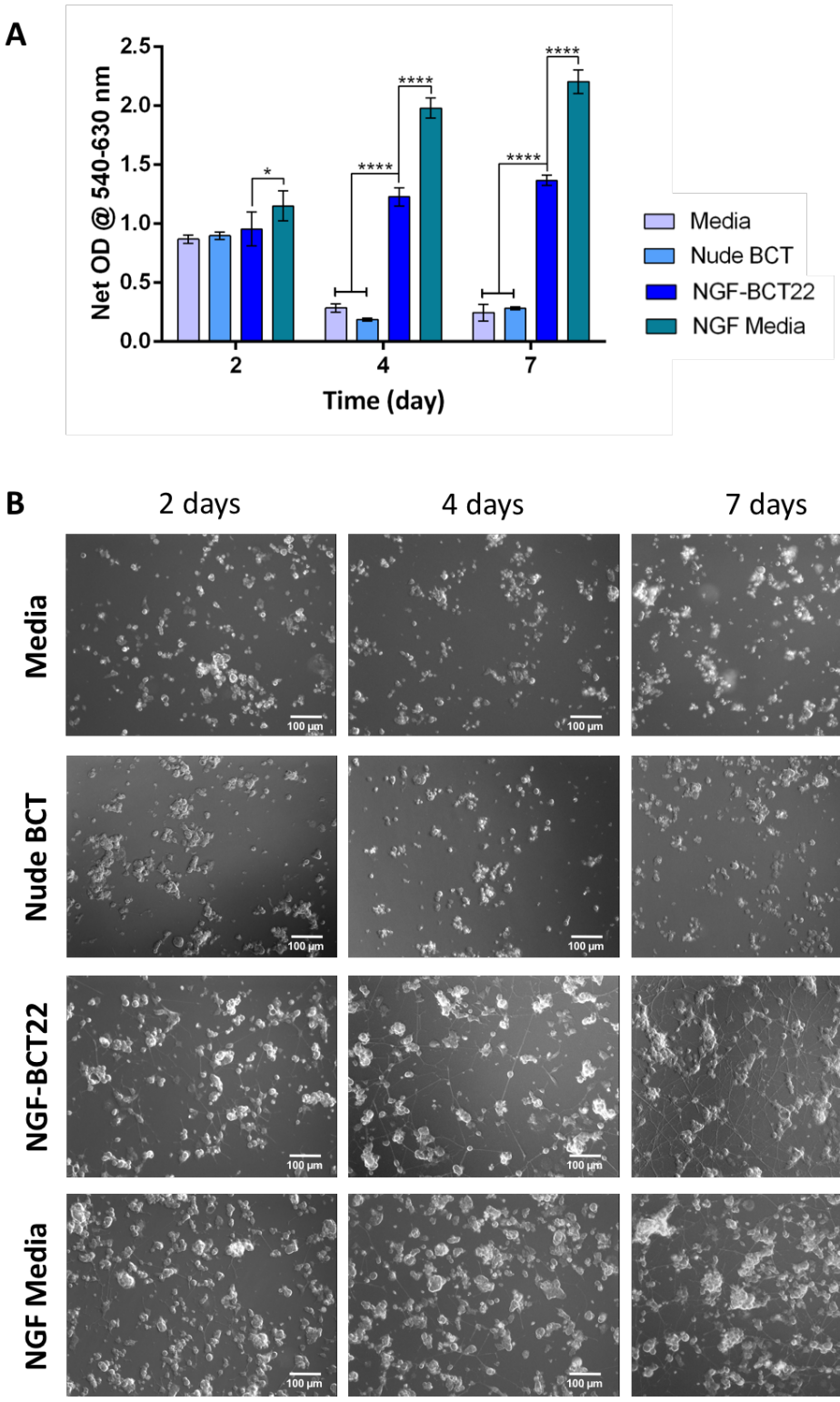

Figure 4.7 – NGF-BCT22 promotes the cell growth of PC12 cells. **A)** Quantitative analysis of the number of PC12 cells by MTT assay. **B)** The morphology of PC12 cells after 2, 4 and 7 days of treatment: negative controls (Media and Nude BCT); sample (NGF-BCT22); and positive control (NGF media). *(One-way ANOVA followed by a multiple-comparisons test (Tukey's) were used for statistical analysis. Data are expressed as mean ± s.d (n = 5). *p < 0.05; ****p < 0.0001 from NGF-BCT22).*

In the presence of NGF, PC12 cells undertake a distinctive change in which they reduce the proliferation and start to extend neurites [76]. To quantify PC12 cell differentiation, the neurites length and the percentage of cells bearing neurites more than one cell body length were measured, as shown in **Figure 4.8**. In the absence of NGF, the cells are reasonably more round, smaller and have few noticeable neurites after 2 days and close to zero after 4 and 7 days of cultivation (**Figure 4.8A** and **Figure 4.8C**; Media and Nude BCT). Although, there was no significantly difference for the neurite length among treatments at Day 2, the differentiation percentage was significantly lower for the negative controls (~4 %, Nude BCT and Nude BCT) and positive control (~20 %, NGF media), compared to ~40 % for NGF-BCT22, $p < 0.0001$ and $p < 0.05$, respectively (**Figure 4.8A** and **Figure 4.8B**). For the culture condition containing NGF, the neurite length and cell differentiation were time-dependently increased. The treatment with NGF-BCT22 for 7 days resulted in larger cell bodies and the formation of a wider network of neurites (**Figure 4.8B** and **Figure 4.8C**).

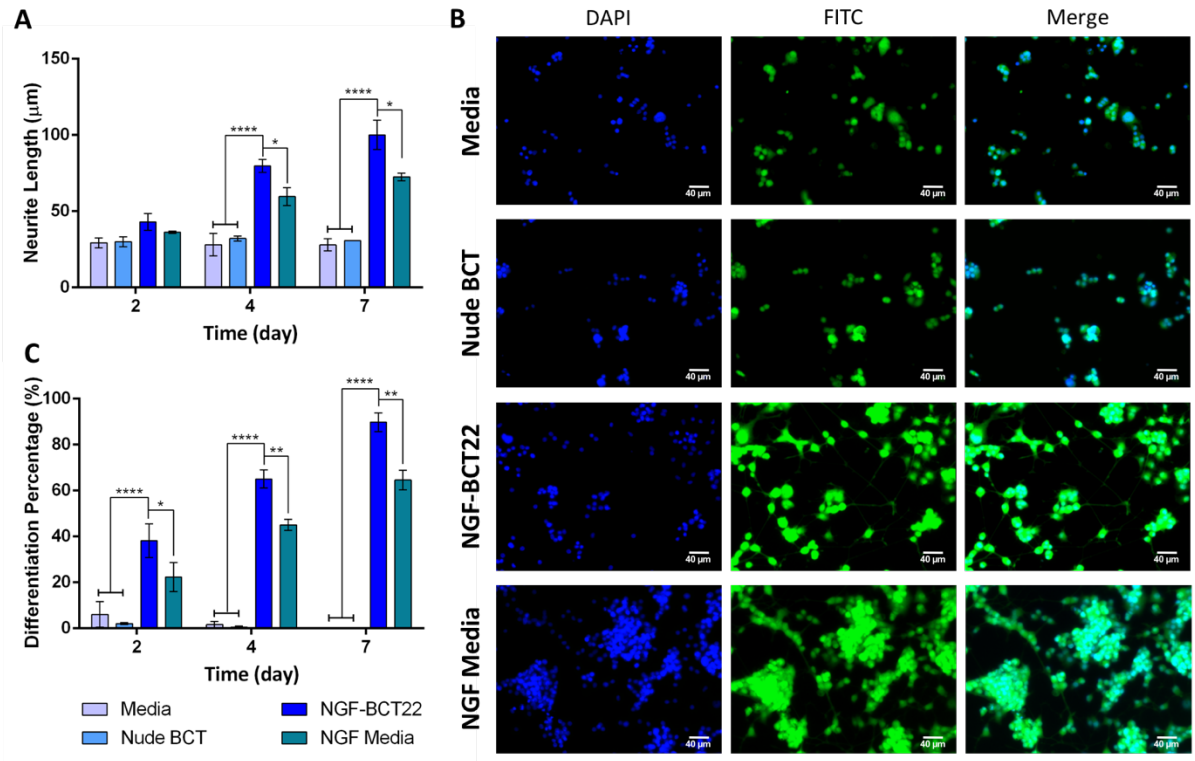

Figure 4.8 – Directly delivered-NGF from the NGF-BCT22 was bioactive, inducing PC12 cells differentiation and neurite outgrowth. **A)** Comparison of the neurite length of PC12 cells among the treatment groups. **B)** Differentiation percentage of cells bearing neurites more than one cell body length. **C)** Differentiation of PC12 cells based on morphology; fluorescence images of PC12 cells cultured on Day 4. Green fluorescence, FTIC for actin cytoskeleton; blue fluorescence, DAPI DNA stain for cell nuclei. Treatment groups: negative controls (Media and Nude BCT), sample (NGF-BCT22), and positive control (NGF media). *(One-way ANOVA followed by a multiple-comparisons test (Tukey's) were used for statistical analysis. Data are presented as mean ± s.d (n = 5). *p < 0.05; **p < 0.01; ****p < 0.0001 from NGF-BCT22).*

The neurite length gradually increased with passing time after exposure to NGF delivered from NGF-BCT22, with the maximal extent of neurite outgrowth achieved by Day 7, 100.1 ± 9.7 μm. This was statistically different from the negative and positive controls, $p < 0.0001$ and $p < 0.05$, respectively (**Figure 4.8A**). Similarly, the number of differentiated cells for the NGF-BCT22 treatment gradually increased, with greater than 90 % of the cells differentiated by Day 7 (**Figure 4.8B**). The differentiation of PC12 cells is dependent of the NGF dose [77]. There was a burst release of NGF from NGF-BCT22 of ~130 $ng{\cdot}ml^{-1}$ until Day 2, as determined by ELISA. The amount of released NGF added to the PC12 culture at

the time points 4 and 7 days was around 8 and 11 ng·ml^{-1}, respectively. These amounts were enough to stimulate and keep more PC12 differentiated and reduce the cell proliferation compared to the positive control containing fresh NGF. NGF media (50 ng·ml^{-1}) was able to differentiate 65 % (**Figure 4.8C**) of the cells and demonstrated greater cell growth after 7days (**Figure 4.7A**), similar to the observations made by others [52, 74, 77]. In summary, this study indicated that the NGF released from the NGF-BCT22 preserved excellent bioactivity for at least 7 days. Such release of NGF is useful for drug delivery applications, as NGF is known to promote an appropriate environment for nerve regeneration as well as stem cells neurogenesis [15, 78].

4.3. Conclusion

Biosynthesized cellulose hydrogels were produced in a special bioreactor in tube-shape (BCTs) and nerve growth factor (NGF) was incorporated into the tubes as a potential nerve guidance drug delivery tube to assist with the reconnection of nerve tissues across the spinal cord lesion. The physical and mechanical properties of the BCTs changed with the passage of time. Among the tubes, BCT formed at Day 22 of cultivation (BCT22) presented the highest amount of cellulose and the highest rehydration ratio. Besides, BCT22 showed appropriate mechanical properties with an ultimate tensile strength of 1.43 ± 0.29 MPa and Young' Modulus of 1.24 ± 0.07 MPa, value similar to the human spinal cord. In addition, NGF was incorporated into the BCT22 nerve guidance tube in an effective way while ensuring sterility. The dosage of NGF released from the BCT22 was bioactive and proved to be sufficient to stimulate PC12 cell differentiation *in vitro* for a period of one week. Overall, this study

explored the use of BCTs as drug releasing systems, which are relevant strategies to enhance nerve regeneration for many patients facing physical strains due to SCI.

4.4. References

[1] R.C. Assuncao-Silva, E.D. Gomes, N. Sousa, N.A. Silva, A.J. Salgado, Hydrogels and Cell Based Therapies in Spinal Cord Injury Regeneration, Stem Cells Int (2015).

[2] M.B. Bracken, M.J. Shepard, W.F. Collins, T.R. Holford, W. Young, J. Piepmeier, L. Leosummers, D.S. Baskin, H.M. Eisenberg, E. Flamm, L.F. Marshall, J. Maroon, J. Wilberger, P.L. Perot, V.K.H. Sonntag, F.C. Wagner, H.R. Winn, A Randomized, Controlled Trial of Methylprednisolone or Naloxone in the Treatment of Acute Spinal-Cord Injury, New Engl J Med 323(17) (1990) 1209-1209.

[3] Y.D. Teng, W.L. Liao, H. Choi, D. Konya, S. Sabbarwal, R. Langer, R.L. Sidman, E.Y. Synder, W.R. Frontera, Physical activity-mediated functional recovery after spinal cord injury: potential roles of neural stem cells, Regenerative Medicine 1(6) (2006) 763-776.

[4] K. Fouad, L. Schnell, M.B. Bunge, M.E. Schwab, T. Liebscher, D.D. Pearse, Combining Schwann cell bridges and olfactory-ensheathing glia grafts with chondroitinase promotes locomotor recovery after complete transection of the spinal cord, Journal of Neuroscience 25(5) (2005) 1169-1178.

[5] S.W. Liu, T. Schackel, N. Weidner, R. Puttagunta, Biomaterial-Supported Cell Transplantation Treatments for Spinal Cord Injury: Challenges and Perspectives, Frontiers in Cellular Neuroscience 11 (2018).

[6] W.C. Ji, S.Y. Hu, J. Zhou, G. Wang, K.Z. Wang, Y.L. Zhang, Tissue engineering is a promising method for the repair of spinal cord injuries (Review), Exp Ther Med 7(3) (2014) 523-528.

[7] S. Kubinova, New trends in spinal cord tissue engineering, Futur Neurol 10(2) (2015) 129-145.

[8] A.J. Wang, Q. Ao, W.L. Cao, M.Z. Yu, Q. He, L.J. Kong, L. Zhang, Y.D. Gong, X.F. Zhang, Porous chitosan tubular scaffolds with knitted outer wall and controllable inner structure for nerve tissue engineering, J Biomed Mater Res A 79a(1) (2006) 36-46.

[9] B. Lanfer, A. Hermann, M. Kirsch, U. Freudenberg, U. Reuner, C. Werner, A. Storch, Directed Growth of Adult Human White Matter Stem Cell-Derived Neurons on Aligned Fibrillar Collagen, Tissue Eng Pt A 16(4) (2010) 1103-1113.

[10] S. Gnavi, B.E. Fornasari, C. Tonda-Turo, R. Laurano, M. Zanetti, G. Ciardelli, S. Geuna, In vitro evaluation of gelatin and chitosan electrospun fibres as an artificial guide in peripheral nerve repair: a comparative study, J Tissue Eng Regen M 12(2) (2018) E679-E694.

[11] E.C. Tsai, P.D. Dalton, M.S. Shoichet, C.H. Tator, Matrix inclusion within synthetic hydrogel guidance channels improves specific supraspinal and local axonal regeneration after complete spinal cord transection, Biomaterials 27(3) (2006) 519-533.

[12] V. Chiono, C. Tonda-Turo, Trends in the design of nerve guidance channels in peripheral nerve tissue engineering, Prog Neurobiol 131 (2015) 87-104.

[13] M.D. Wang, P. Zhai, X.B. Chen, D.J. Schreyer, X.D. Sun, F.Z. Cui, Bioengineered Scaffolds for Spinal Cord Repair, Tissue Eng Part B-Re 17(3) (2011) 177-194.

[14] E.G. Fine, I. Decosterd, M. Papaloizos, A.D. Zurn, P. Aebischer, GDNF and NGF released by synthetic guidance channels support sciatic nerve regeneration across a long gap, Eur J Neurosci 15(4) (2002) 589-601.

[15] I.P. Clements, J.M. Munson, R.V. Bellamkonda, Chapter II.6.14 - Neuronal Tissue Engineering, in: B.D. Ratner, A.S. Hoffman, F.J. Schoen, J.E. Lemons (Eds.), Biomaterials Science (Third Edition), Academic Press2013, pp. 1291-1306.

[16] Y.Q. Wu, Z.G. Wang, P.T. Cai, T. Jiang, Y.Y. Li, Y. Yuan, R. Li, Y.F. Lu, J. Wang, D.Q. Chen, Q.Q. Zeng, S.N. Khor, R.S. Zhong, H.Y. Zhang, Y. Lin, X.K. Li, J. Xiao, Dual Delivery of bFGF-and NGF-Binding Coacervate Confers Neuroprotection by Promoting Neuronal Proliferation, Cellular Physiology and Biochemistry 47(3) (2018) 948-956.

[17] X. Cao, M.S. Shoichet, Investigating the synergistic effect of combined neurotrophic factor concentration gradients to guide axonal growth, Neuroscience 122(2) (2003) 381-389.

[18] A. Singh, S. Asikainen, A.K. Teotia, P.A. Shiekh, E. Huotilainen, I. Qayoom, J. Partanen, J. Seppala, A. Kumar, Biomimetic Photocurable Three-Dimensional Printed Nerve Guidance Channels with Aligned Cryomatrix Lumen for Peripheral Nerve Regeneration, Acs Appl Mater Inter 10(50) (2018) 43327-43342.

[19] S.H. Hsu, S.H. Chan, C.T. Weng, S.H. Yang, C.F. Jiang, Long-Term Regeneration and Functional Recovery of a 15mm Critical Nerve Gap Bridged by Tremella fuciformis Polysaccharide-Immobilized Polylactide Conduits, Evid-Based Compl Alt (2013).

[20] T. Liu, J.D. Houle, J.Y. Xu, B.P. Chan, S.Y. Chew, Nanofibrous Collagen Nerve Conduits for Spinal Cord Repair, Tissue Eng Pt A 18(9-10) (2012) 1057-1066.

[21] E. Masaeli, M. Morshed, M.H. Nasr-Esfahani, S. Sadri, J. Hilderink, A. van Apeldoorn, C.A. van Blitterswijk, L. Moroni, Fabrication, Characterization and Cellular Compatibility of Poly(Hydroxy Alkanoate) Composite Nanofibrous Scaffolds for Nerve Tissue Engineering, Plos One 8(2) (2013).

[22] S.F. Wang, L. Cai, Polymers for Fabricating Nerve Conduits, Int J Polym Sci (2010).

[23] S. Kehoe, X.F. Zhang, D. Boyd, FDA approved guidance conduits and wraps for peripheral nerve injury: A review of materials and efficacy, Injury 43(5) (2012) 553-572.

[24] S.F. Yang, K.F. Leong, Z.H. Du, C.K. Chua, The design of scaffolds for use in tissue engineering. Part 1. Traditional factors, Tissue Eng 7(6) (2001) 679-689.

[25] A. Svensson, E. Nicklasson, T. Harrah, B. Panilaitis, D.L. Kaplan, M. Brittberg, P. Gatenholm, Bacterial cellulose as a potential scaffold for tissue engineering of cartilage, Biomaterials 26(4) (2005) 419-431.

[26] T.R. Stumpf, X.Y. Yang, J.C. Zhang, X.D. Cao, In situ and ex situ modifications of bacterial cellulose for applications in tissue engineering, Mat Sci Eng C-Mater 82 (2018) 372-383.

[27] W.F. Dudman, Cellulose production by Acetobacter actigenum in defined medium, J Gen Microbiol 21 (1959) 327-37.

[28] M. Schramm, S. Hestrin, Factors Affecting Production of Cellulose at the Air Liquid Interface of a Culture of Acetobacter-Xylinum, Journal of General Microbiology 11(1) (1954) 123-&.

[29] F. Yoshinaga, N. Tonouchi, K. Watanabe, Research progress in production of bacterial cellulose by aeration and agitation culture and its application as a new industrial material, Biosci Biotech Bioch 61(2) (1997) 219-224.

[30] H.X. Zhu, S.R. Jia, H.J. Yang, Y.Y. Jia, L. Yan, J. Li, Preparation and Application of Bacterial Cellulose Sphere: A Novel Biomaterial, Biotechnol Biotec Eq 25(1) (2011) 2233-2236.

[31] W. Czaja, D. Romanovicz, R.M. Brown, Structural investigations of microbial cellulose produced in stationary and agitated culture, Cellulose 11(3-4) (2004) 403-411.

[32] D.O.S. Recouvreux, C.R. Rambo, F.V. Berti, C.A. Carminatti, R.V. Antonio, L.M. Porto, Novel three-dimensional cocoon-like hydrogels for soft tissue regeneration, Mat Sci Eng C-Mater 31(2) (2011) 151-157.

[33] D.O.S. Recouvreux, Desenvolvimento de novos biomateriais baseados em celulose bacteriana para aplicações biomédicas e de engenharia de tecidos, Programa de Pós-Graduação em Engenharia Química, Universidade Federal de Santa Catarina, Florianópolis, 2008, p. 124.

[34] D. Klemm, D. Schumann, U. Udhardt, S. Marsch, Bacterial synthesized cellulose - artificial blood vessels for microsurgery, Prog Polym Sci 26(9) (2001) 1561-1603.

[35] M. Scherner, S. Reutter, D. Klemm, A. Sterner-Kock, M. Guschlbauer, T. Richter, G. Langebartels, N. Madershahian, T. Wahlers, J. Wippermann, In vivo application of tissue-engineered blood vessels of bacterial cellulose as small arterial substitutes: proof of concept?, J Surg Res 189(2) (2014) 340-347.

[36] A. Bodin, H. Backdahl, H. Fink, L. Gustafsson, B. Risberg, P. Gatenholm, Influence of cultivation conditions on mechanical and morphological properties of bacterial cellulose tubes, Biotechnol Bioeng 97(2) (2007) 425-434.

[37] H. Backdahl, B. Risberg, P. Gatenholm, Observations on bacterial cellulose tube formation for application as vascular graft, Mat Sci Eng C-Mater 31(1) (2011) 14-21.

[38] Y. Li, K. Jiang, J. Feng, J.Z. Liu, R. Huang, Z.J. Chen, J.C. Yang, Z.H. Dai, Y. Chen, N.X. Wang, W.J. Zhang, W.F. Zheng, G. Yang, X.Y. Jiang, Construction of Small-Diameter Vascular Graft by Shape-Memory and Self-Rolling Bacterial Cellulose Membrane, Adv Healthc Mater 6(11) (2017).

[39] A. Bodin, S. Bharadwaj, S.F. Wu, P. Gatenholm, A. Atala, Y.Y. Zhang, Tissue-engineered conduit using urine-derived stem cells seeded bacterial cellulose polymer in urinary reconstruction and diversion, Biomaterials 31(34) (2010) 8889-8901.

[40] K.A. Zimmermann, J.M. LeBlanc, K.T. Sheets, R.W. Fox, P. Gatenholm, Biomimetic design of a bacterial cellulose/hydroxyapatite nanocomposite for bone healing applications, Mat Sci Eng C-Mater 31(1) (2011) 43-49.

[41] H. Orelma, L.O. Morales, L.S. Johansson, I.C. Hoeger, I. Filpponen, C. Castro, O.J. Rojas, J. Laine, Affibody conjugation onto bacterial cellulose tubes and bioseparation of human serum albumin, Rsc Adv 4(93) (2014) 51440-51450.

[42] D. Klemm, B. Heublein, H.P. Fink, A. Bohn, Cellulose: Fascinating biopolymer and sustainable raw material, Angew Chem Int Edit 44(22) (2005) 3358-3393.

[43] K. Kowalska-Ludwicka, J. Cala, B. Grobelski, D. Sygut, D. Jesionek-Kupnicka, M. Kolodziejczyk, S. Bielecki, Z. Pasieka, Modified bacterial cellulose tubes for regeneration of damaged peripheral nerves, Arch Med Sci 9(3) (2013) 527-534.

[44] C.L. Zhu, F. Li, X.Y. Zhou, L. Lin, T.Y. Zhang, Kombucha-synthesized bacterial cellulose: Preparation, characterization, and biocompatibility evaluation, J Biomed Mater Res A 102(5) (2014) 1548-1557.

[45] A. Putra, A. Kakugo, H. Furukawa, J.P. Gong, Y. Osada, Tubular bacterial cellulose gel with oriented fibrils on the curved surface, Polymer 49(7) (2008) 1885-1891.

[46] S.R. Jia, W.H. Tang, H.J. Yang, Y.Y. Jia, H.X. Zhu, Preparation and Characterization of Bacterial Cellulose Tube, 2009 3rd International Conference on Bioinformatics and Biomedical Engineering, Vols 1-11 (2009) 1051-1054.

[47] K. Hirayama, T. Okitsu, H. Teramae, D. Kiriya, H. Onoe, S. Takeuchi, Cellular building unit integrated with microstrand-shaped bacterial cellulose, Biomaterials 34(10) (2013) 2421-2427.

[48] J.Y. Tang, X. Li, L.H. Bao, L. Chen, F.F. Hong, Comparison of two types of bioreactors for synthesis of bacterial nanocellulose tubes as potential medical prostheses including artificial blood vessels, J Chem Technol Biot 92(6) (2017) 1218-1228.

[49] S.S. Zang, R. Zhang, H. Chen, Y.D. Lu, J.H. Zhou, X. Chang, G.X. Qiu, Z.H. Wu, G. Yang, Investigation on artificial blood vessels prepared from bacterial cellulose, Mat Sci Eng C-Mater 46 (2015) 111-117.

[50] T.T. Puck, S.J. Cieciura, H.W. Fisher, Clonal growth in vitro of human cells with fibroblastic morphology; comparison of growth and genetic characteristics of single epithelioid and fibroblast-like cells from a variety of human organs, J Exp Med 106(1) (1957) 145-58.

[51] X.D. Cao, M.S. Shoichet, Delivering neuroactive molecules from biodegradable microspheres for application in central nervous system disorders, Biomaterials 20(4) (1999) 329-339.

[52] K.K. Teng, J.M. Angelastro, M.E. Cunningham, L.A. Greene, Chapter 21 - Cultured PC12 Cells: A Model for Neuronal Function, Differentiation, and Survival, in: J.E. Celis (Ed.), Cell Biology (Third Edition), Academic Press, Burlington, 2006, pp. 171-176.

[53] N.V. Jaumard, J. Leung, A.J. Gokhale, B.B. Guarino, W.C. Welch, B.A. Winkelstein, Relevant Anatomic and Morphological Measurements of the Rat Spine, Spine 40(20) (2015) E1084-E1092.

[54] W.H. Tang, S.R. Jia, Y.Y. Jia, H.J. Yang, The influence of fermentation conditions and post-treatment methods on porosity of bacterial cellulose membrane, World J Microb Biot 26(1) (2010) 125-131.

[55] K. Watanabe, S. Yamanaka, Effects of Oxygen-Tension in the Gaseous-Phase on Production and Physical-Properties of Bacterial Cellulose Formed under Static Culture Conditions, Biosci Biotech Bioch 59(1) (1995) 65-68.

[56] O. Shezad, S. Khan, T. Khan, J.K. Park, Physicochemical and mechanical characterization of bacterial cellulose produced with an excellent productivity in static conditions using a simple fed-batch cultivation strategy, Carbohyd Polym 82(1) (2010) 173-180.

[57] A. Suwanposri, P. Yukphan, Y. Yamada, D. Ochaikul, Identification and biocellulose production of Gluconacetobacter strains isolated from tropical fruits in Thailand, Maejo Int J Sci Tech 7(1) (2013) 70-82.

[58] S.A. Hutchens, R.V. Leon, H.M. O'Neill, B.R. Evans, Statistical analysis of optimal culture conditions for Gluconacetobacter hansenii cellulose production, Lett Appl Microbiol 44(2) (2007) 175-180.

[59] K.V. Ramana, A. Tomar, L. Singh, Effect of various carbon and nitrogen sources on cellulose synthesis by Acetobacter xylinum, World J Microb Biot 16(3) (2000) 245-248.

[60] M. Marx-Figini, B.G. Pion, Kinetic invetigations of biosynthesis of cellulose by Actobacter xylinum, Biochimica et Biophysica Acta (BBA) - General Subjects 338(2) (1974) 382-393.

[61] S. Kawano, K. Tajima, Y. Uemori, H. Yamashita, T. Erata, M. Munekata, M. Takai, Cloning of cellulose synthesis related genes from Acetobacter xylinum ATCC23769 and ATCC53582: comparison of cellulose synthetic ability between strains, DNA Res 9(5) (2002) 149-56.

[62] M.E. Embuscado, J.S. Marks, J.N. Bemiller, Bacterial Cellulose .1. Factors Affecting the Production of Cellulose by Acetobacter-Xylinum, Food Hydrocolloid 8(5) (1994) 407-418.

[63] A. Budhiono, B. Rosidi, H. Taher, M. Iguchi, Kinetic aspects of bacterial cellulose formation in nata-de-coco culture system, Carbohyd Polym 40(2) (1999) 137-143.

[64] H. Backdahl, G. Helenius, A. Bodin, U. Nannmark, B.R. Johansson, B. Risberg, P. Gatenholm, Mechanical properties of bacterial cellulose and interactions with smooth muscle cells, Biomaterials 27(9) (2006) 2141-2149.

[65] A.M. Sokolnicki, R.J. Fisher, T.P. Harrah, D.L. Kaplan, Permeability of bacterial cellulose membranes, J Membrane Sci 272(1-2) (2006) 15-27.

[66] S. Kubinova, D. Horak, A. Hejcl, Z. Plichta, J. Kotek, V. Proks, S. Forostyak, E. Sykova, SIKVAV-modified highly superporous PHEMA scaffolds with oriented pores for spinal cord injury repair, J Tissue Eng Regen M 9(11) (2015) 1298-1309.

[67] M. Tsintou, K. Dalamagkas, A.M. Seifalian, Advances in regenerative therapies for spinal cord injury: a biomaterials approach, Neural Regen Res 10(5) (2015) 726-742.

[68] B.K.K. Chen, A.M. Knight, N.N. Madigan, L. Gross, M. Dadsetan, J.J. Nesbitt, G.E. Rooney, B.L. Currier, M.J. Yaszemski, R.J. Spinner, A.J. Windebank, Comparison of polymer scaffolds in rat spinal cord: A step toward quantitative assessment of combinatorial approaches to spinal cord repair, Biomaterials 32(32) (2011) 8077-8086.

[69] R.H. Cholas, H.P. Hsu, M. Spector, The reparative response to cross-linked collagen-based scaffolds in a rat spinal cord gap model, Biomaterials 33(7) (2012) 2050-2059.

[70] P.D. Dalton, L. Flynn, M.S. Shoichet, Manufacture of poly(2-hydroxyethyl methacrylate-co-methyl methacrylate) hydrogel tubes for use as nerve guidance channels, Biomaterials 23(18) (2002) 3843-51.

[71] S.J. Nagel, C.G. Reddy, L.A. Frizon, M.K. Chardon, M. Holland, A.G. Machado, G.T. Gillies, M.A. Howard, 3rd, S. Wilson, Spinal dura mater: biophysical characteristics relevant to medical device development, J Med Eng Technol 42(2) (2018) 128-139.

[72] L.E. Bilston, L.E. Thibault, The mechanical properties of the human cervical spinal cord in vitro, Ann Biomed Eng 24(1) (1996) 67-74.

[73] H. Ullah, F. Wahid, H.A. Santos, T. Khan, Advances in biomedical and pharmaceutical applications of functional bacterial cellulose-based nanocomposites, Carbohydr Polym 150 (2016) 330-52.

[74] K.P. Das, T.M. Freudenrich, W.R. Mundy, Assessment of PC12 cell differentiation and neurite growth: a comparison of morphological and neurochemical measures, Neurotoxicol Teratol 26(3) (2004) 397-406.

[75] M. Wigerius, N. Asghar, W. Melik, M. Johansson, Scribble controls NGF-mediated neurite outgrowth in PC12 cells, Eur J Cell Biol 92(6-7) (2013) 213-221.

[76] L.A. Greene, A.S. Tischler, Establishment of a noradrenergic clonal line of rat adrenal pheochromocytoma cells which respond to nerve growth factor, Proc Natl Acad Sci U S A 73(7) (1976) 2424-8.

[77] R.D. Hu, Q.Y. Cao, Z.Q. Sun, J.Y. Chen, Q. Zheng, F. Xiao, A novel method of neural differentiation of PC12 cells by using Opti-MEM as a basic induction medium, Int J Mol Med 41(1) (2018) 195-201.

[78] D. Otto, K. Unsicker, C. Grothe, Pharmacological Effects of Nerve Growth-Factor and Fibroblast Growth-Factor Applied to the Transectioned Sciatic-Nerve on Neuron Death in Adult-Rat Dorsal-Root Ganglia, Neurosci Lett 83(1-2) (1987) 156-160.

CHAPTER 5 – SYNTHESIS, OPTIMIZATION AND CHARACTERIZATION OF RGDS-PEPTIDES

5.1. Introduction

Peptides are a key component on transmitting the cell signal, targeting the deliver and translation of the biochemical "message" that activates molecular, structural, cellular, and biological outcomes [1]. Synthetic peptides can be used to mimic the biological functions of natural peptides. The peptide conformation is fundamental to its binding to the corresponding integrin receptor. The engineering of multi-substituted chemical identities (branched peptides) has attracted interest in modern biomedicine [2]. Branched peptides mimic the conformational features of functional protein domains involved in biological molecular detection, such as antigen–antibody, ligand–receptor, substrate–enzyme, and others protein–protein interactions. Thus, branched peptides have been developed as new therapeutic agents, such as vaccines, antibodies, and antimicrobial and antitumor drugs [3-8].

Currently, most branched peptides are based on the multiple antigen peptide (MAP) system, which is a cascade-type peptide dendrimer with a wide size distribution [9, 10]. MAPs are well-defined, hyper branched polymers with a high density of functional binding sites. They consist of a central core with surface functional groups and branching units that link these together [11]. A variety of synthetic approaches have been reported for the preparation of MPAs [12, 13]. The most used strategy is based on the combination of temporary and permanent protecting groups as well as the employment of efficient coupling reagents for the controlled formation of peptide chains [14]. One standard method used is called Solid Phase Peptide Synthesis (SPPS), where the peptide is synthesized in two phases, an insoluble solid support and liquid soluble reagents [15].

MAPs have shown great promise compared to their similar linear peptides in different biomedical fields, such as hepatitis A [16], antimicrobial activity [17, 18], and antigenicity

[19]. In addition, multi-branched peptides have shown higher cellular uptake compared to their parent monomers [20-27]. Due to the improved uptake of the branched designs, much lower concentrations can be used [20]. MAP systems can present a specific chemical functionality with spatial selectivity. Known bioactive sequences such as arginine-glycine-aspartic acid (RGD) or arginine-glycine-aspartic acid-serine (RGDS) have been used in these systems to act as identifiable epitopes to influence cell behavior [28-33]. The RGD sequence and its peptide-mimics (i.e. RGDS) are, consequently, considered as the minimum recognizable biomolecular segments in peptides [34].

The tetrapeptide RGDS is particularly well known to stimulate cell adhesion on biomaterials surfaces [32, 35]. This is due to its widespread distribution and use throughout the organism, its ability to address more than one cell adhesion receptor, and its biological impact on cell anchoring, behavior and survival [36]. Thus, the development of hybrid biomaterials equipped with RGDS has been an attractive research avenue to optimize cellular interactions in tissue engineering [35, 37-40]. For example, Silva et al. functionalized a modified gellan gum hydrogel with the GRGDS peptide, which demonstrated superior cell adhesion and viability of NSPCs [41]. Similarly, RGD was immobilized into elastin hydrogels and showed increased neurite outgrowth in dorsal root ganglia [42]. Therefore, producing MAPs containing the RGDS sequence is significant for several structural/biological activity relationships and drug design considerations.

In such context, the aim of this study was to synthesize and optimize the synthesis of linear and two-branched peptides having in their composition the RGDS sequence as potential bioactive molecules to enhance or create specific cell binding properties in biomaterials.

5.2. Materials and Methods

5.2.1. Materials

The permanent side-chain protecting groups (PPGs) and the temporary protecting groups (TPGs) for the amino acids are listed in **Table 2.2** (Chapter 2). The protected amino acids Fmoc-**βAla**-OH, Fmoc-**Arg**(Pbf)-OH, Fmoc-**Asp**(OtBu)-OH, Fmoc-**Cys**(Acm)-OH, Fmoc-**Adoa,** and the coupling reagent O-(7-Azabenzotriazol-1-yl)-N,N,N',N'-tetramethyluroniumhexafluorophosphate (HATU) were purchased from ChemPep Inc. (Wellington, FL). The remain protected amino acids Fmoc-**Cys**(Trt)-OH, Fmoc-**Lys**(Fmoc)-OH, Fmoc-**Ser**(tBu)-OH, Fmoc-**Gly**-OH, and the coupling reagent O-(Benzotriazol-1-yl)-N,N,N',N'-tetramethyluroniumhexafluorophosphate (HBTU) were ordered from Peptides International, Inc. (Louisville, KY). The tetra-branched MAP resin ($[Fmoc\text{-}Lys(Fmoc)]_2$-Lys-Cys(Acm)-βAla-Wang Resin; mesh size: 100-200 mesh; substitution capacity: 0.42 $mmol \cdot g^{-1}$) was purchased from Advanced Chemtech (Louisville, KY), and the TentaGel amide resin (TG, substitution capacity: 0.24 $mmol \cdot g^{-1}$) was purchased from Intavis Inc. (Chicago, IL). All other chemicals were obtained from Sigma-Aldrich (Oakville, ON) and used as received unless otherwise indicated.

5.2.2. Peptide Synthesis and Optimization

Linear and 2-branched peptides containing the RGDS sequence in their configurations were synthesized. **Figure 5.1** shows the schematic representation for the design of the peptides and the chemical structures for the monomer and dimer peptides. All peptides were synthesized in a 96-well plate Intavis Biochem automatic peptide synthesizer (AG, Germany). The Fmoc (9-fluorenylmethoxycarbonyl) solid phase peptide synthesis (Fmoc-SPPS) protocol was used at 2 μmol scale (per well), with all the side-chain functional groups protected. First, 8.33 mg of TG resin in 833 μL of dimethylformamide (DMF) was added into each well. For the MAP

resin, 4.76 mg in 833 μL of DMF was used when required. After, the peptide syntheses were conducted in three main steps:

i) *Deprotection:* The Fmoc-protected groups were removed by suspending the resins or amino acids in 50 μL of 20 % piperidine in DMF for 5 min.

ii) *Coupling:* For the linear peptide, amino acid couplings were carried out with 5 equivalents excess (10 μmol) of Fmoc-protected amino acid (17.5 μL of 0.6 M of amino acid stock solution) using 17 μL of the coupling agents HBTU or HATU (0.6 M), in the presence of 2 μL of N-methylpyrrolidinone (NMP, 4 M) in DMF for 10 min. The peptide chain was built up from the β-alanine on the resin to the final arginine residue to obtain the desired linear peptide sequence: RGDS-Adoa-CβA. Then, the coupled resin was washed 8 times with 100 μL of DMF. Branching was achieved by the coupling of Fmoc-Lys(Fmoc)-OH at appropriate point, and was followed by incorporation of a derivatizing moiety of each amino acid. For the tetra branched peptide two different resins were tested, the TG resin and the tetra-branched MAP resin.

iii) *Cleavage:* After automated synthesis (~ 20 hours) all peptides were cleaved from the resin. The peptides were treated with a solution of trifluoroacetic acid (TFA), water, phenol and triisopropylsilane (TIPS) (88:5:5:2, named Reagent B**)** for different time periods (for optimization). Then, the excess of Reagent B was removed and the remaining viscous peptide solution was precipitated and washed 3 times with 10 mL of cold ethyl ether (-20° C).

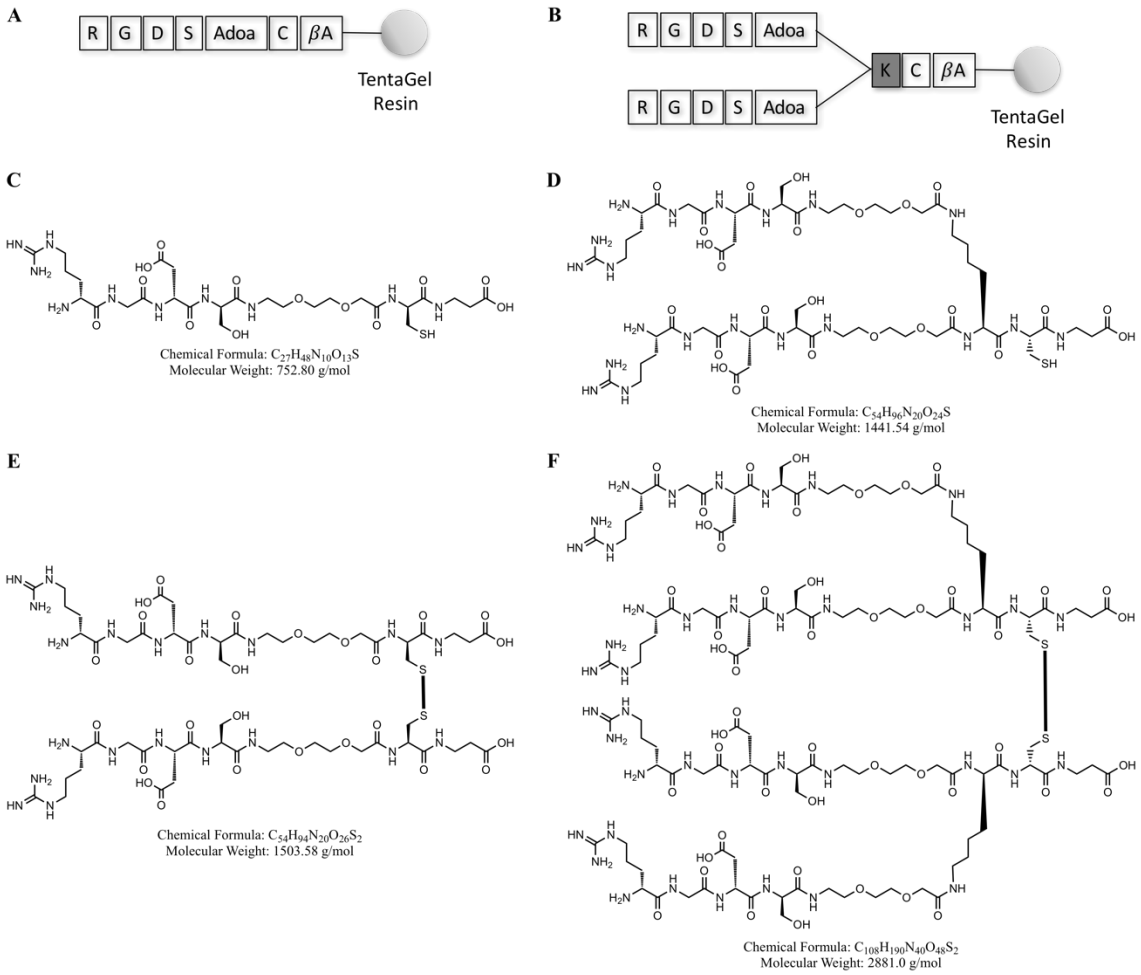

Figure 5.1 – Peptides design. Schematic representation of the (**A)** linear peptide, RGDS-Adoa-C-βA, and **(B)** 2-branched peptide, $[RGDS\text{-}Adoa]_2$-K-C-βA. Chemical structure, formula, and molecular weight of (**C**) linear peptide, (**E**) its dimer form, and (**D**) 2-branched peptide and its (**F**) dimer form. Disulfide bond is showed in bold for the dimeric peptides (E and F).

The resulting products were freeze-dried, purified by high performance liquid chromatography (HPLC, see *Section 5.2.3* below), and analyzed by matrix-assisted laser desorption/ionization mass spectrometry (MALDI-MS, see *Section 5.2.4* below). To ensure the yield and purity of the peptides, the following synthesis parameters were tested: two different coupling reagents; two different protecting groups for cysteine; number of deprotection and coupling repetitions; and the duration of time for the cleavage reaction with Reagent B. **Table 5.1** shows the summary of the parameters evaluated.

Table 5.1 – Parameters evaluated for the optimization of the synthesis protocol of the linear and branched peptides.

Parameter	Description	Optimization options
Resin	Two different solid resins were used to synthesize the 4-branched peptide	TG or MAP
Coupling reagent	Two different coupling reagents were used	HBTU or HATU
Cys PPG	Two different permanent protecting groups (PPG) for the amino acid cysteine were used	Acm or Trt
Deprotection ×	How many times the deprotection step was repeated	3 to 5 times
Coupling ×	How many times the coupling step was repeated	3 to 5 times
Cleavage reaction time	How long the peptides were exposed to the Reagent B	2.5 to 4.5 hours

Abbreviations: TentaGel amide resin (TG); MAP resin ($[Fmoc\text{-}Lys(Fmoc)]_2$-Lys-Cys(Acm)-βAla-Wang Resin); O-(Benzotriazol-1-yl)-N,N,N',N'-tetramethyluroniumhexafluorophosphate (HBTU); O-(7-Azabenzotriazol-1-yl)-N,N,N',N'-tetramethyluroniumhexafluorophosphate (HATU); Cysteine (Cys); permanent protecting groups (PPG); trityl (Trt); acetamidomethyl (Acm).

5.2.3. Reversed-Phase High Performance Liquid Chromatography (RP-HPLC)

The purification of the peptides was accomplished by semi-preparative Reversed-Phase High Performance Liquid Chromatography (RP-HPLC) in a VarianProStar 325 chromatograph (Palo Alto, CA). A Phenomenex Gemini® C-18 column (250 × 10 mm, particle size of 10 μm; pore size of 110 Å) was used in a gradient of solvent A (0.1% TFA in water, v/v) and solvent B (0.1% TFA in acetonitrile, v/v), from 10% to 60% of solvent B in 55 min, and then up to 90% in 66 min. The flow rate applied was 2 $mL \cdot min^{-1}$ and the UV detection wavelength was fixed at 260 nm. Then, the fractions were collected, freeze-dried and analyzed by MS.

5.2.4. Mass Spectrometry (MS)

To confirm the chemical structure of the products matrix-assisted laser desorption/ionization mass spectrometry (MALDI-MS, Bruker MALDI Microflex) was performed, using 2,5-dihydroxybenzoic acid (DHB) matrix.

5.2.5. Three Dimensional (3D) Molecular Structure

The theoretical 3D model of the energy-minimized peptide structures in vacuum was computed using HyperChem software, version 11.0 from Hypercube Inc. (Gainesville, FL). The following parameters were used:

- Algorithm: Polak-Ribiere
- Termination Condition
    - Root mean square (RMS) gradient of: 0.1 Kcal/(Åmol) or 1485 maximum cycles
- AMBER, OPLS on Biotforce field
    - Dielectric: distance dependent
    - Scale factor: 1
    - Eletrostatic: 0.833
    - Van der Waals: 0.5

5.3. Results and Discussion

Recently, there has been significant interest to apply tissue regeneration concepts for treatment of damaged tissues and organs [43]. These approaches normally involve biomaterials that can serve as scaffolds to release cells or recruit them [44]. The purpose of scaffolds may range

from physically supporting cells to actually signaling cells at the level of receptors to promote cell proliferation and cell survival [44]. One of the approaches to improve scaffolds biofunctionality has been the incorporation of peptides that are involved in the cell signaling [45]. Several studies have previously shown that attaching the RGDS sequence to the surface of biomaterial scaffolds improve cell adhesion and promote cell proliferation [34, 46, 47]. In addition, the RGDS sequence is found in several proteins and it is reasonable easy to be synthesized [48]. For the peptide design, the RGDS sequence was selected to be incorporated in all the peptides.

The syntheses of linear and branched peptides were accomplished in an automatic peptide synthesizer running Fmoc-SPPS protocol. The amino acid cysteine (C) was chosen because its reactive free thiol group can be used to chemically modify different biomaterials or to generate dimers [49]. In addition, the cysteine lateral thiol group is important for the stabilization of tertiary structures due to its ability to form disulfide bonds, which can be formed intra- and intermolecularly by oxidation. The protection of this very reactive group during the peptide synthesis is mandatory. In SPPS, thiol protection has to be compatible with the chosen strategy: trityl (Trt) group has become the most frequently used PPG in Fmoc-SPPS and Acm is usually removed in a separate step [49]. To further improve the applicability of the peptides, it was chosen to use the Trt PPG for cysteine instead of Acm, since Trt can be cleaved easily using TFA scavengers compared to Acm that requires Ag(I) or Hg(I) solutions [50].

Yield and purity can be further improved if flexible spacer amino acids such as Adoa, which adds PEG-like moiety, are inserted at all branching points [51]. It is hypothesized that the flexibility provoked by Adoa helps maintaining the peptides properly solvated during synthesis, preventing aggregation and consequently improving the success of growing peptide sequences. This approach has been verified by Kowalczyk et al. [51], which synthesized

branched peptides using two different spacers, Adoa and Ahx (6-aminohexanoic acid, residue). They demonstrated that Adoa besides improving the peptide flexibility, added solubility-enhancing features to the branched peptides, what resulted in an increased peptide yield [51]. The amino acid alanine was used to mimic the sequence provided by the MAP resin. Finally, the amino acid lysine (K) was added to form branching on the peptide sequence, altering the structural presentation of the bioactive peptide sequence after synthesis. The number of branching is proportional to the number of lysine residues coupled.

5.3.1. Linear Peptide

Linear peptide was successfully synthesized on TentaGel amide resin (TG) by solid phase Fmoc chemistry after optimization. It was desired to optimize the synthesis protocol since an efficient synthesis procedure can increase yield and make more viable the use of these molecules to enrich biomaterials. **Table 5.2** shows all the tested parameters for the synthesis of the linear peptide. After several attempts, the best yield was achieved for the linear peptide 8 (L8, 92.9%) using TG resin, the HATU as coupling reagent, 4 repetitions of the deprotection step and 5 repetitions of the coupling step. In addition, keeping the peptide in Reagent B for 3.5 hours showed better results for cleaving the peptide from the resin. After synthesis, linear peptides were purified by HPLC and their chemical structures were confirmed by MS. As an example, only the results for the sample L8 are presented.

Table 5.2 – Tested parameters to synthesize the linear peptide, RGDS-Adoa-C-βA, and their respective percentage yield (Yield %). Synthesis repetitions for the linear peptide (L1-L12) using TentaGel amide resin (TG), two different coupling reagents, two permanent protecting groups (PPG) for cysteine (Cys), different numbers of deprotection (deprotection ×) and coupling (Coupling ×) cycles, and time length for the cleavage reaction using Reagent B are presented.

Peptide	Resin	Coupling Reagent	Cys PPG	Deprotection ×	Coupling ×	Reagent B (h)	Yield (%)

L1	TG	HBTU	Acm	3	4	4.5	49.7
L2[1]	TG	HBTU	Acm	3	4	3.5	3.15
L3	TG	HBTU	Acm	3	4	3.5	84.7
L4	TG	HATU	Acm	3	4	3	73.4
L5	TG	HATU	Acm	3	4	4.5	46.3
L6	TG	HATU	Trt	4	4	2.5	70.3
L7	TG	HATU	Trt	5	5	3	48.9
L8	TG	HATU	Trt	4	5	3.5	**92.9**
L9	TG	HATU	Trt	4	5	3.5	64.1
L10	TG	HATU	Trt	4	5	3.5	81.9
L11[2]	TG	HATU	Trt	4	5	3.5	0
L12[3]	TG	HATU	Trt	4	5	3.5	20.1

[1,3]Problem with the resin. [2]Equipment failed. Abbreviations: O-(Benzotriazol-1-yl)-N,N,N',N'-tetramethyluroniumhexafluorophosphate (HBTU); O-(7-Azabenzotriazol-1-yl)-N,N,N',N'-tetramethyluroniumhexafluorophosphate (HATU); trityl (Trt); acetamidomethyl (Acm).

The MALDI-MS was recorded for the crude linear peptide, RGDS-Adoa-C-βA (L8), to confirm its identity, which showed two main peaks (**Figure 5.2A**). The first peak at m/z 752.1 $[M+H]^+$ (indicated by *****) corresponds to the calculated molecular weight (752.8 $g \cdot mol^{-1}$) for the linear peptide. The second peak was observed at m/z 1500.3 $[M+H]^+$ (indicated by ******) likely being the dimer form of the peptide, which has a calculated molecular weight of 1503.6 $g \cdot mol^{-1}$. The free thiol group (–SH) in the peptide composition allowed the formation of a dimer, where a disulfide bond was formed between two cysteine residues of two peptide chains (showed in bold in **Figure 5.1B**). The small difference between the theoretical and experimental values may be due equipment calibration. The peaks at low m/z region are correspondent to the matrix used for the MS analysis. The crude peptide L8 was purified by RP-HPLC using a C_{18} semi-preparative column. The chromatogram shows two major peaks,

one intense peak eluting at 30.6 min (indicated by **1**), and another at 34.4 min (indicated by **2**) in **Figure 5.2B**. Most likely, peak **1** corresponds to the linear monomer peptide and peak **2** to its dimer form.

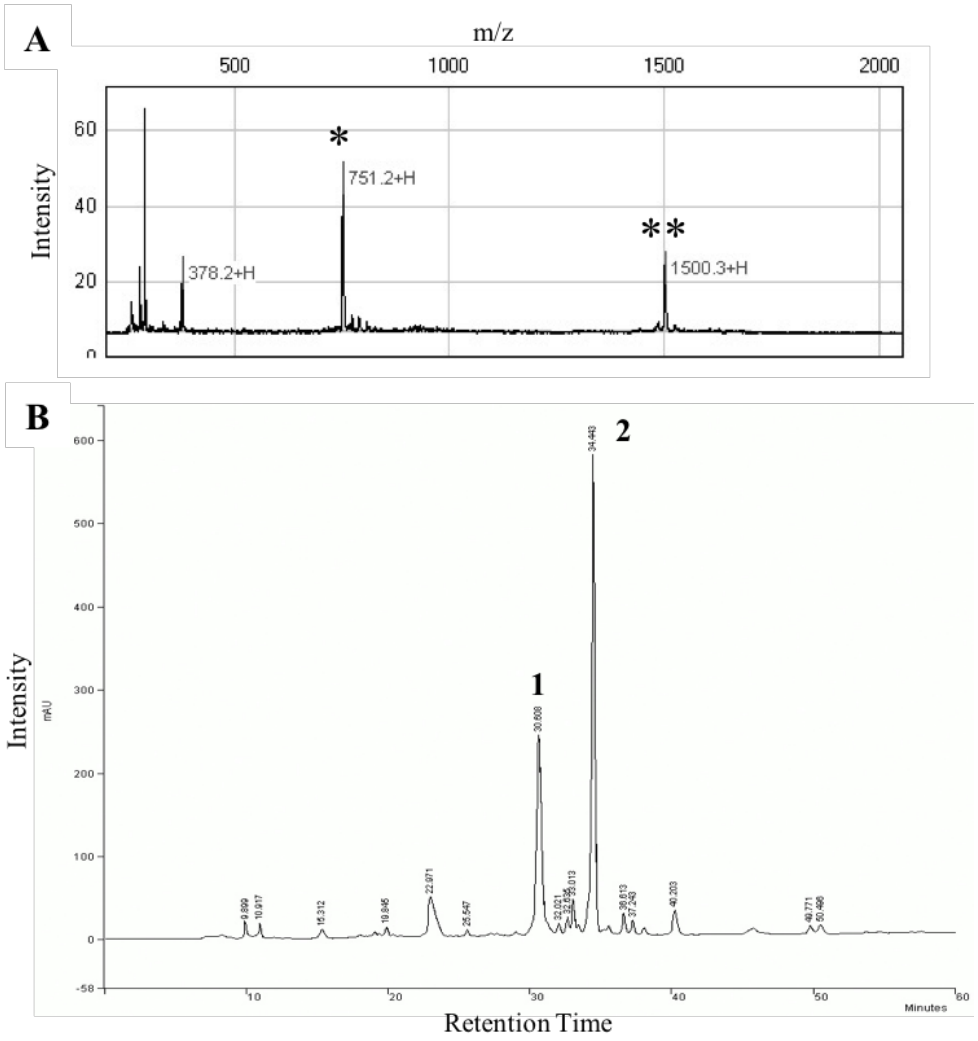

Figure 5.2 – Characterization of the crude linear peptide (L8), RGDS-Adoa-C-βA. **A)** MALDI-MS spectrum showing the two major peaks at m/z 751.2 and 1500.3 $[M+H]^+$ for monomer (*) and dimer peptide (**), respectively. **B)** RP-HPLC chromatogram of the crude linear peptide with the detection wavelength at 260 nm.

The portions correspondent to the two peaks showed in **Figure 5.2B** were separately collected and analyzed by a second HPLC-injection. **Figure 5.3A** shows the chromatogram for the re-injection of peak **1**, that eluted at ~34.3 min, and **Figure 5.3B** shows the

chromatogram for the peak **2**, which still eluted at around 34.8 min. These findings were in agreement with what has been proposed, peak **1** may be the monomer peptide, which after storage and a second injection becomes the dimeric peptide, and peak **2** is the original dimer peptide.

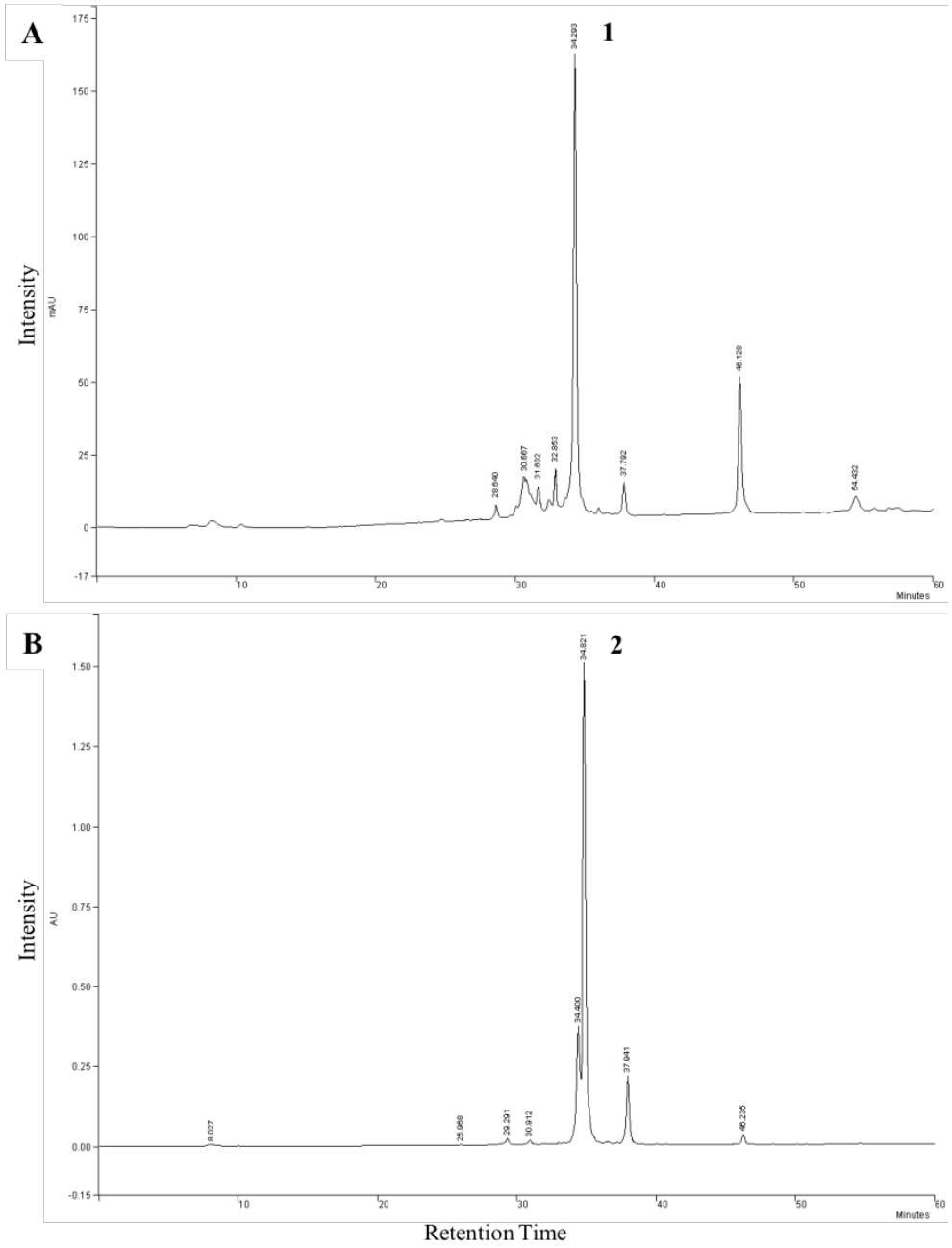

Figure 5.3 – RP-HPLC chromatograms for the linear peptide (RGDS-Adoa-C-βA) after the second HPLC-injection, with the detection wavelength at 260 nm. **A**) Reinjection of the solution correspondent to the peak **1** at 30 min in the first HPLC-run. **B**) Reinjection of the solution correspondent to the peak **2** at 34 min in the first HPLC-run.

5.3.2. Two-Branched Peptide

Two-branched peptide was also synthesized on the solid TentaGel amide resin (TG). To synthesize the branch peptide, the SPPS protocol was adapted by adding the MAP (multiple-antigen peptide) system established by Tam et al. [11]. Multiple peptide chains can be bound to the MAP branching core depending on the number of double Fmoc-protected lysines are used as branching units. The resulting MAP peptide is usually a large molecule with a 3D configuration. Two-branched peptide containing the epitope RGDS, which is known to promote cell adhesion and proliferation [39] was synthesized and the optimizated parameters are listed in **Table 5.3**. The best synthesis conditions, related to the yield, obtained for the liner peptide were also the best set of conditions for the 2-branched peptide, being the maximum peptide yield of 81.3% for 2-branched peptide number 4 (2B4), which characterization is shown here.

Table 5.3 – Evaluated parameters to synthesize the 2-branched peptide, $[RGDS\text{-}Adoa]_2$-K-C-βA, and the percentage yield (Yield %) for each synthesis. Synthesis repetitions for the 2-branched peptide (2B1-2B7) using TentaGel amide resin (TG), two different coupling reagents, two permanent protecting groups (PPG) for cysteine (Cys), different numbers of deprotection (deprotection ×) and coupling (Coupling ×) cycles, and time length for the cleavage reaction using Reagent B are shown.

Peptide	Resin	Coupling Reagent	Cys PPG	Deprotection ×	Coupling ×	Reagent B (h)	Yield (%)
2B1	TG	HBTU	Acm	3	4	3.5	75.1
2B2	TG	HATU	Acm	3	4	3.5	56.5
2B3	TG	HATU	Acm	4	4	3.5	68.7
2B4	TG	HATU	Trt	4	5	3.5	**81.3**
2B5	TG	HATU	Trt	4	5	3.5	75.1
2B6[1]	TG	HATU	Trt	4	5	3.5	-
2B7	TG	HATU	Trt	4	5	3.5	70.0

[1]Didn't precipitated. Abbreviations: O-(Benzotriazol-1-yl)-N,N,N’,N’-tetramethyluroniumhexafluorophosphate (HBTU); O-(7-Azabenzotriazol-1-yl)-N,N,N’,N’-tetramethyluroniumhexafluorophosphate (HATU); trityl (Trt); acetamidomethyl (Acm); high performance liquid chromatography (HPLC); mass spectroscopy (MS).

The calculated molecular weight for the 2-branched peptide, $[RGDS\text{-}Adoa]_2$-K-C-βA, and its dimer are 1441.5 $g \cdot mol^{-1}$ and 2881.0 $g \cdot mol^{-1}$, respectively. The mass spectrum for the crude 2-branched peptide (2B4, **Figure 5.4A**) shows one main peak at m/z 1440.0 $[M+H]^+$ (indicated by *****) correspondent to the monomeric 2-branched peptide, and three smaller peaks. The peak at m/z 2877.9 $[M+H]^+$ (indicated by ******) corresponds to the 2-branched dimer peptide. The other two peaks are most likely by-products. The chemical structures and molecular weights of the suggested by-products are illustrated in **Figure D.1** (Appendix D). The peak at m/z 1618.1 $[M+H]^+$ may be corresponding to the 2-branched peptide linked to the amino acids cysteine and alanine, but in this case the thiol group attacked the carboxyl group of alanine; calculated molecular weight of 1615.7 $g \cdot mol^{-1}$. Finally, the peak at m/z 2074.8 $[M+Na]^+$ may be the 2-branched peptide attached by a disulfide bond to a piece of another 2-branched peptide, in this case without the RGDS sequence in both branches, plus a sodium; calculated molecular weight of 2050.2 $g \cdot mol^{-1}$+Na. In comparison to the linear peptide, the synthesis of the 2-branched peptide was found to be much less clean as demonstrated by the presence of multiple peaks in the RP-HPLC chromatogram (**Figure 5.4B**). The major peak **1** at 30.5 min was attributed to the dimeric 2-branched peptide.

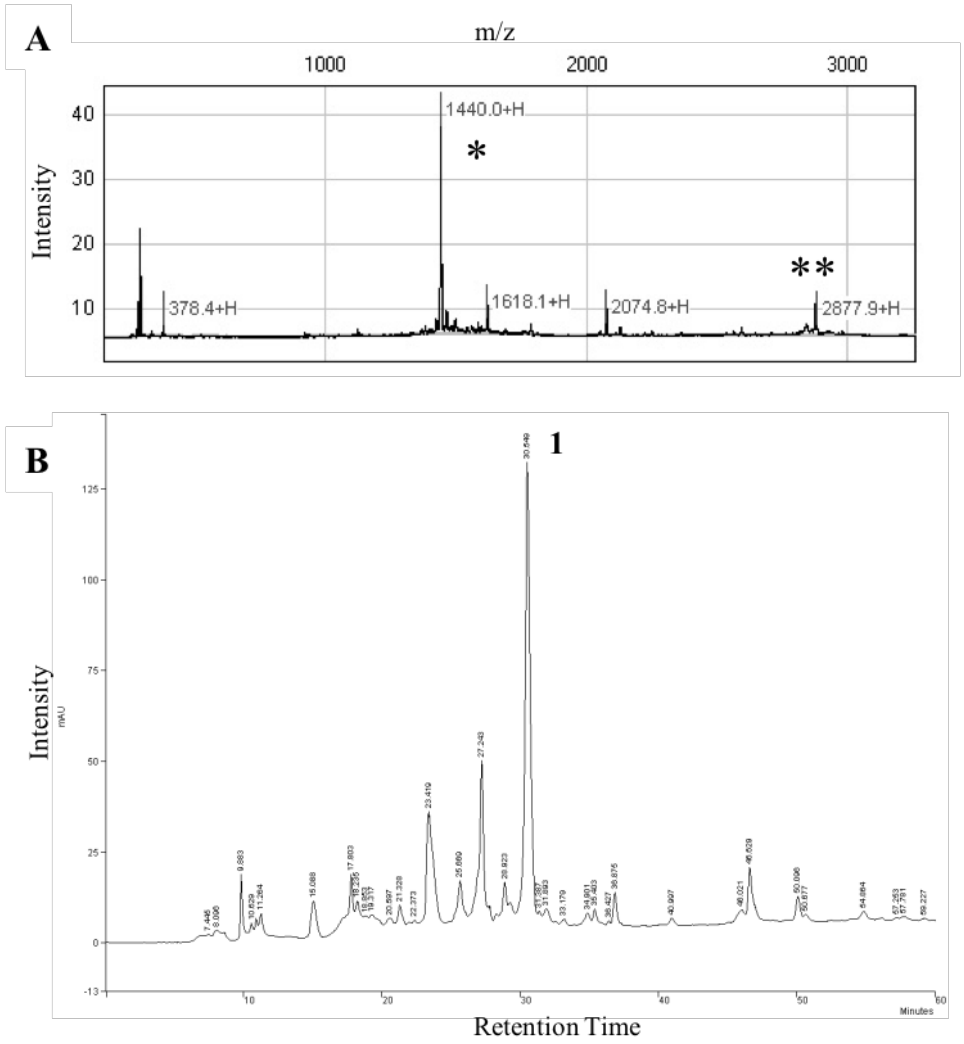

Figure 5.4 – MS and HPLC analyses for the crude 2-branched peptide (2B4), $[RGDS\text{-}Adoa]_2$-K-C-βA. **A)** MALDI-MS spectrum. *Indicates the peak at m/z 1440.0 $[M+H]^+$ correspondent to the monomer peptide; ** indicates the peak at m/z 2877.9 $[M+H]^+$ correspondent to the dimer form. **B)** RP-HPLC chromatogram of the crude 2-branched peptide (2B4) with the detection wavelength at 260 nm.

5.3.1. Energy-minimized 3D model structures

Though completely theoretical and generated under vacuum condition, understanding the stable structure conformation of a peptide is significant because it allows to comprehend properties and behaviors based upon structural considerations [52]. Optimized structures often correspond to a substance as it is found in nature and the geometry of such structures can be used in a variety of experimental and theoretical investigations. These theoretically derived structures often provide, at least in part, the explanation for the different cell behaviors in

presence of different peptide molecular structures. **Figure 5.5** and **Figure 5.6** shows the 3D theoretical model structures of the linear and 2-branched peptides, and their dimer forms in their lowest possible energy state. Hydrogen bonds were displayed and named in figures as dotted bonds in order to differentiate them. It was observed that there were no hydrogen bonds formed in the monomeric linear peptide structure (RGDS-Adoa-C-βA, **Figure 5.5A**), however there were three potential hydrogen bonds formed in the dimeric linear peptide (**Figure 5.5B**), which likely participated in the stabilization of the obtained structure. Otherwise, in the 3D model structures for the monomeric and dimeric 2-branched peptide ($[RGDS\text{-}Adoa]_2$-K-C-βA, **Figure 5.6**) several hydrogen bonds were observed, 3 and 5, respectively, which possibly contributed to the stability and conformation of the molecules.

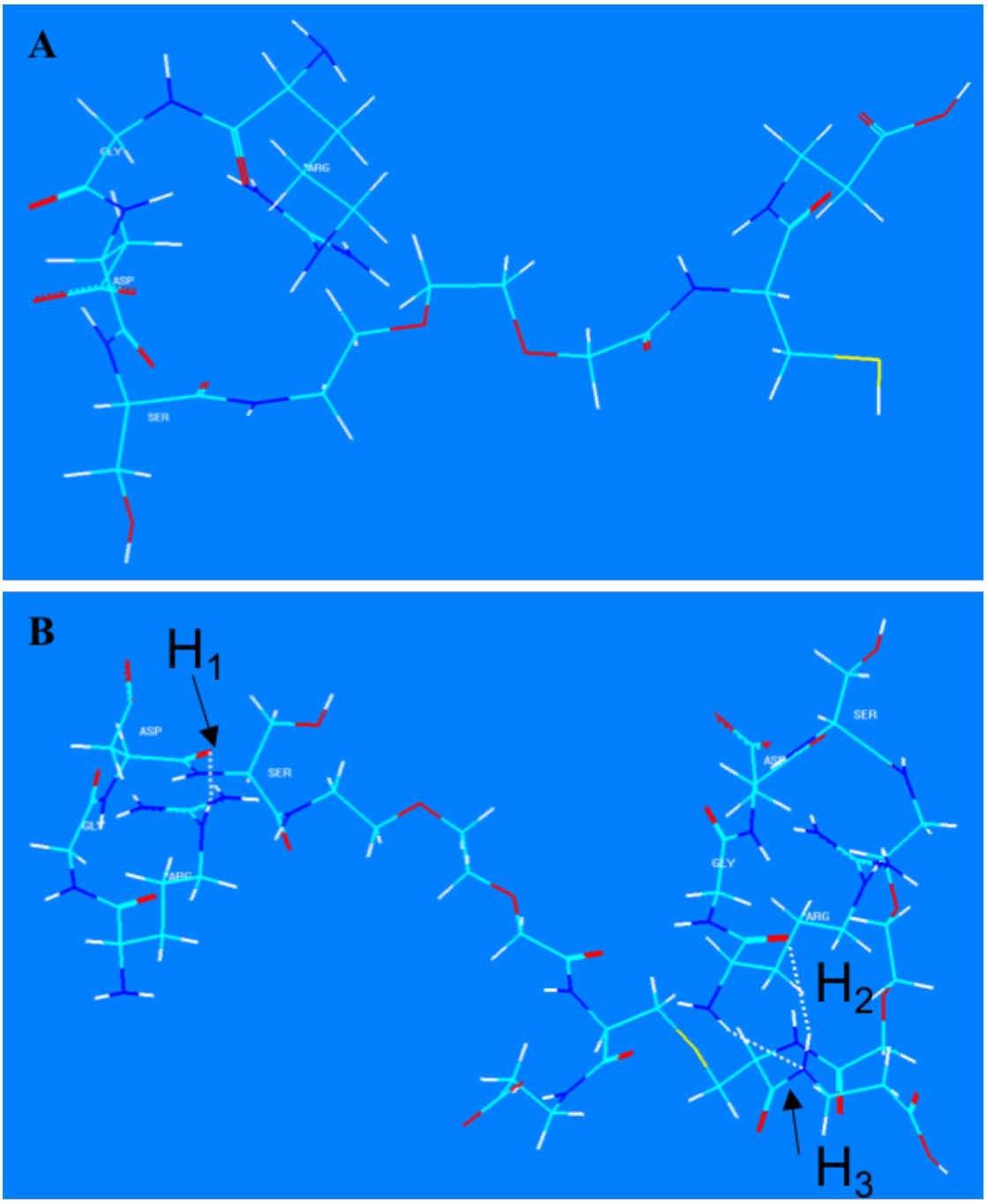

Figure 5.5 – Energy-minimized theoretical 3D model structures in vacuum of liner peptide and its dimer form generated using HyperChem software. **A**) Monomer structure (RGDS-Adoa-C-βA) and **B**) its correspondent dimer structure and hydrogen bonds (**H1-H3**).

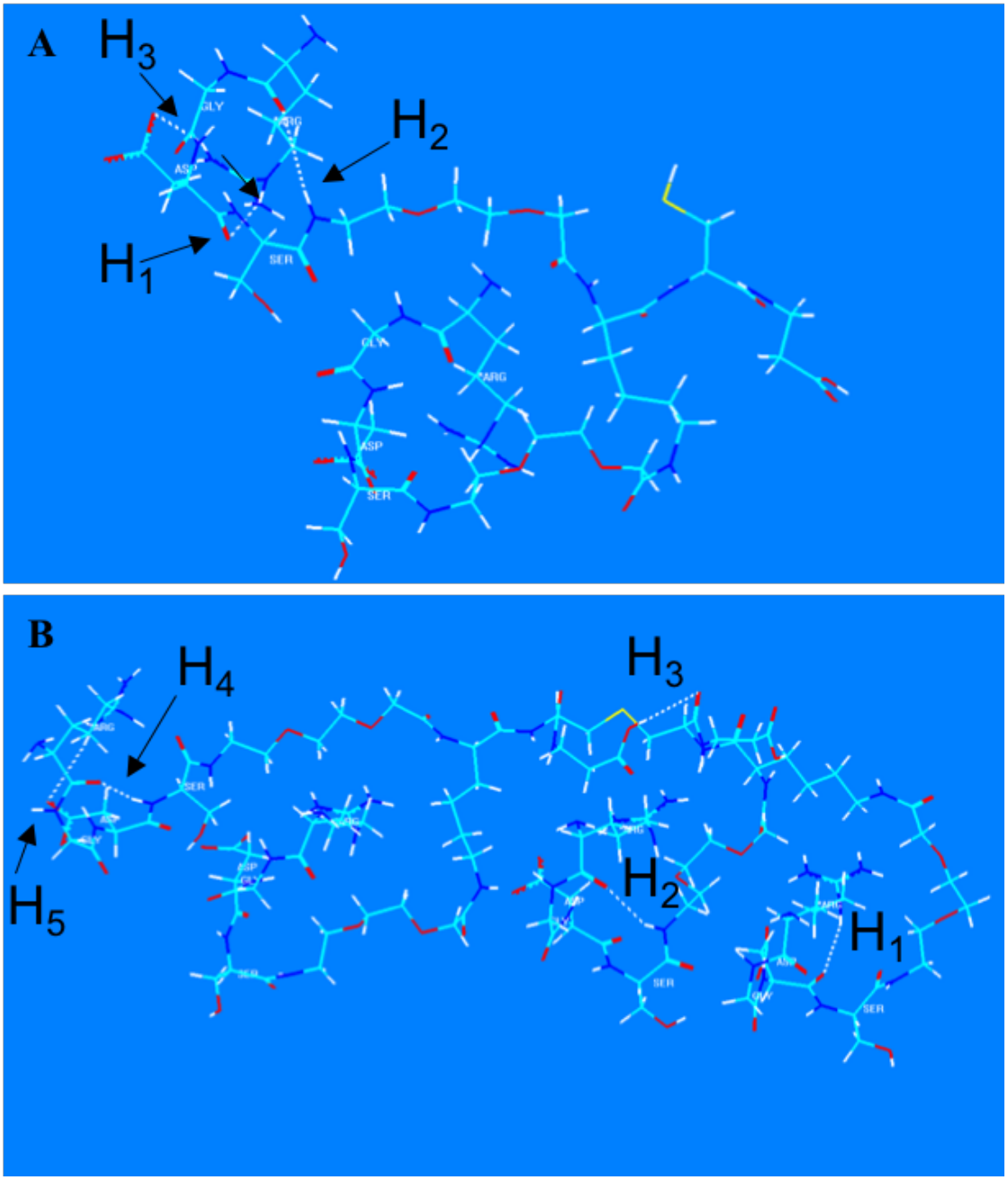

Figure 5.6 – Energy-minimized theoretical 3D model structures in vacuum of 2-branched peptide ([RGDS-Adoa]$_2$-K-C-βA) generated using HyperChem software. **A**) Monomer structure and and hydrogen bonds (**H1-H3**). **B**) Dimer structure and hydrogen bonds (**H1-H5**).

It is important to mention that similar Fmoc-SPPS protocol can be used to increase the number of branches in a peptide. For example, 4-branched peptides can be synthesized similarly as 2-branced peptides. Data obtained for the optimization of the 4-branced peptide (RGDS-Adoa]$_4$-K$_2$-K-C-βA) are presented in **Table D.1** (Appendix D). In addition, **Figure**

D.2 shows the RP-HPLC chromatogram for the crude peptide. **Figure D.3** shows the chemical structure and molecular weight and **Figure D.4** shows the energy-minimized theoretical 3D model structures of the 4-branched peptide and its dimer form.

5.4. Conclusion

We have reported the synthesis optimization of linear and branched peptides, which presented different densities of bioactive peptide sequences on their structures. The Fmoc-SPPS chemistry provided a reasonable approach to prepare RGDS peptides in different configurations. The RGDS cell adhesion epitope was incorporated into the peptides for potential use as bioactive molecules to be incorporated into biomaterials for tissue engineering applications. The linear architecture was modified using a MAP strategy for appropriate introduction of branching. This branched architecture enabled the presentation of several bioactive groups on the same molecule. Linear and 2-branched peptides were successfully synthesized and their structures were confirmed by HPLC and MALDI. In addition, their energy-minimized theoretical 3D model structures were presented. In summary, the best conditions for the peptide synthesis were:

- TentaGel resin for linear and branched peptides;
- HATU as coupling reagent;
- Trt as the cysteine protecting group;
- 4 repetitions for the deprotection step;
- 5 repetitions for the coupling step;
- 3.5 h in Reagent B for the cleavage reaction.

5.5. References

[1] D.J. Craik, D.P. Fairlie, S. Liras, D. Price, The Future of Peptide-based Drugs, Chem Biol Drug Des 81(1) (2013) 136-147.

[2] T. Uhlig, T. Kyprianou, F.G. Martinelli, C.A. Oppici, D. Heiligers, D. Hills, X.R. Calvo, P. Verhaert, The emergence of peptides in the pharmaceutical business: From exploration to exploitation, EuPA Open Proteomics 4 (2014) 58-69.

[3] J.D. Fontana, A.M. Desouza, C.K. Fontana, I.L. Torriani, J.C. Moreschi, B.J. Gallotti, S.J. Desouza, G.P. Narcisco, J.A. Bichara, L.F.X. Farah, Acetobacter Cellulose Pellicle as a Temporary Skin Substitute, Appl Biochem Biotech 24-5 (1990) 253-264.

[4] F. Yoshinaga, N. Tonouchi, K. Watanabe, Research progress in production of bacterial cellulose by aeration and agitation culture and its application as a new industrial material, Biosci Biotech Bioch 61(2) (1997) 219-224.

[5] L.R. Mello, L.T. Feltrin, P.T.F. Neto, F.A.P. Ferraz, Duraplasty with biosynthetic cellulose: An experimental study, J Neurosurg 86(1) (1997) 143-150.

[6] M. Scherner, S. Reutter, D. Klemm, A. Sterner-Kock, M. Guschlbauer, T. Richter, G. Langebartels, N. Madershahian, T. Wahlers, J. Wippermann, In vivo application of tissue-engineered blood vessels of bacterial cellulose as small arterial substitutes: proof of concept?, J Surg Res 189(2) (2014) 340-347.

[7] D.A. Schumann, J. Wippermann, D.O. Klemm, F. Kramer, D. Koth, H. Kosmehl, T. Wahlers, S. Salehi-Gelani, Artificial vascular implants from bacterial cellulose: preliminary results of small arterial substitutes, Cellulose 16(5) (2009) 877-885.

[8] V. Haridas, S. Sadanandan, P.Y. Collart-Dutilleul, S. Gronthos, N.H. Voelcker, Lysine-Appended Polydiacetylene Scaffolds for Human Mesenchymal Stem Cells, Biomacromolecules 15(2) (2014) 582-590.

[9] S. Ramesh, P. Cherkupally, T. Govender, H.G. Kruger, F. Albericio, B.G. de la Torre, 6-(Bromomaleimido)hexanoic Acid as a Connector for the Construction of Multiple Branched Peptide Platforms, Org Lett 17(3) (2015) 464-467.

[10] K. Sadler, J.P. Tam, Peptide dendrimers: applications and synthesis, J Biotechnol 90(3-4) (2002) 195-229.

[11] J.P. Tam, Recent advances in multiple antigen peptides, J Immunol Methods 196(1) (1996) 17-32.

[12] W. Chan, P. White, Fmoc Solid Phase Peptide Synthesis: A Practical Approach, OUP Oxford2000.

[13] S.S. Zang, R. Zhang, H. Chen, Y.D. Lu, J.H. Zhou, X. Chang, G.X. Qiu, Z.H. Wu, G. Yang, Investigation on artificial blood vessels prepared from bacterial cellulose, Mat Sci Eng C-Mater 46 (2015) 111-117.

[14] R.B. Merrifield, Solid-Phase Synthesis (Nobel Lecture), Angewandte Chemie-International Edition in English 24(10) (1985) 799-810.

[15] R.B. Merrifield, Solid Phase Peptide Synthesis. I. The Synthesis of a Tetrapeptide, Journal of the American Chemical Society 85(14) (1963) 2149-2154.

[16] M.J. Gomara, S. Riedemann, I. Vega, H. Ibarra, G. Ercilla, I. Haro, Use of linear and multiple antigenic peptides in the immunodiagnosis of acute hepatitis A virus infection, J Immunol Methods 234(1-2) (2000) 23-34.

[17] I. Kim, H.H. Jeong, Y.J. Kim, N.E. Lee, K.M. Huh, C.S. Lee, G.H. Kim, E. Lee, A "Light-up" 1D supramolecular nanoprobe for silver ions based on assembly of pyrene-labeled peptide amphiphiles: cell-imaging and antimicrobial activity, J Mater Chem B 2(38) (2014) 6478-6486.

[18] J.G. Li, S.P. Liu, R. Lakshminarayanan, Y. Bai, K. Pervushin, C. Verma, R.W. Beuerman, Molecular simulations suggest how a branched antimicrobial peptide perturbs a bacterial membrane and enhances permeability, Bba-Biomembranes 1828(3) (2013) 1112-1121.

[19] P. Kim, C.P. Pau, Comparing tandem repeats and multiple antigenic peptides as the antigens to detect antibodies by enzyme immunoassay, J Immunol Methods 257(1-2) (2001) 51-54.

[20] I.A. Monreal, Q. Liu, K. Tyson, T. Bland, D.S. Dalisay, E.V. Adams, G.A. Wayman, H.C. Aguilar, J.P. Saludes, Branched dimerization of Tat peptide improves permeability to HeLa and hippocampal neuronal cells, Chem Commun 51(25) (2015) 5463-5466.

[21] W.L. Zhu, S.Y. Shin, Effects of dimerization of the cell-penetrating peptide Tat analog on antimicrobial activity and mechanism of bactericidal action, J Pept Sci 15(5) (2009) 345-352.

[22] F.S. Hassane, G.D. Ivanova, E. Bolewska-Pedyczak, R. Abes, A.A. Arzumanov, M.J. Gait, B. Lebleu, J. Gariepy, A Peptide-Based Dendrimer That Enhances the Splice-Redirecting Activity of PNA Conjugates in Cells, Bioconjugate Chem 20(8) (2009) 1523-1530.

[23] A.M. Angeles-Boza, A. Erazo-Oliveras, Y.J. Lee, J.P. Pellois, Generation of Endosomolytic Reagents by Branching of Cell-Penetrating Peptides: Tools for the Delivery of Bioactive Compounds to Live Cells in Cis or Trans, Bioconjugate Chem 21(12) (2010) 2164-2167.

[24] G.A. Eggimann, S. Buschor, T. Darbre, J.L. Reymond, Convergent synthesis and cellular uptake of multivalent cell penetrating peptides derived from Tat, Antp, pVEC, TP10 and SAP, Org Biomol Chem 11(39) (2013) 6717-6733.

[25] G.A. Eggimann, E. Blattes, S. Buschor, R. Biswas, S.M. Kammer, T. Darbre, J.L. Reymond, Designed cell penetrating peptide dendrimers efficiently internalize cargo into cells, Chem Commun 50(55) (2014) 7254-7257.

[26] S.H. Park, J. Doh, S.I. Park, J.Y. Lim, S.M. Kim, J.I. Youn, H.T. Jin, S.H. Seo, M.Y. Song, S.Y. Sung, M. Kim, S.J. Hwang, J.M. Choi, S.K. Lee, H.Y. Lee, C.L. Lim, Y.J. Chung, D. Yang, H.N. Kim, Z.H. Lee, K.Y. Choi, S.S. Jeun, Y.C. Sung, Branched oligomerization of cell-permeable peptides markedly enhances the transduction efficiency of adenovirus into mesenchymal stem cells, Gene Ther 17(8) (2010) 1052-1061.

[27] J. Hoyer, U. Schatzschneider, M. Schulz-Siegmund, I. Neundorf, Dimerization of a cell-penetrating peptide leads to enhanced cellular uptake and drug delivery, Beilstein J Org Chem 8 (2012) 1788-1797.

[28] K.L. Niece, J.D. Hartgerink, J.J.J.M. Donners, S.I. Stupp, Self-assembly combining two bioactive peptide-amphiphile molecules into nanofibers by electrostatic attraction, Journal of the American Chemical Society 125(24) (2003) 7146-7147.

[29] S.R. Bull, M.O. Guler, R.E. Bras, T.J. Meade, S.I. Stupp, Self-assembled peptide amphiphile nanofibers conjugated to MRI contrast agents, Nano Letters 5(1) (2005) 1-4.

[30] P. Simpson, B.C. Merrifield, Real-Time Signal-Processing Applications of a Distributed Array Processor, Comput Phys Commun 37(1-3) (1985) 133-140.

[31] D.A. Harrington, E.Y. Cheng, M.O. Guler, L.K. Lee, J.L. Donovan, R.C. Claussen, S.I. Stupp, Branched peptide-amphiphiles as self-assembling coatings for tissue engineering scaffolds, J Biomed Mater Res A 78A(1) (2006) 157-167.

[32] M.O. Guler, L. Hsu, S. Soukasene, D.A. Harrington, J.F. Hulvat, S.I. Stupp, Presentation of RGDS epitopes on self-assembled nanofibers of branched peptide amphiphiles, Biomacromolecules 7(6) (2006) 1855-1863.

[33] H. Storrie, M.O. Guler, S.N. Abu-Amara, T. Volberg, M. Rao, B. Geiger, S.I. Stupp, Supramolecular crafting of cell adhesion, Biomaterials 28(31) (2007) 4608-4618.

[34] R.A. Plenderleith, C.J. Pateman, C. Rodenburg, J.W. Haycock, F. Claeyssens, C. Sammond, S. Rimmer, Arginine-glycine-aspartic acid functional branched semi-interpenetrating hydrogels, Soft Matter 11(38) (2015) 7567-7578.

[35] C.A. Goubko, A. Basak, S. Majumdar, H. Jarrell, N.H. Khieu, X.D. Cao, Comparative analysis of photocaged RGDS peptides for cell patterning, J Biomed Mater Res A 101(3) (2013) 787-796.

[36] F.K. Andrade, S.M.G. Moreira, L. Domingues, F.M.P. Gama, Improving the affinity of fibroblasts for bacterial cellulose using carbohydrate-binding modules fused to RGD, J Biomed Mater Res A 92A(1) (2010) 9-17.

[37] J.H. Collier, Modular self-assembling biomaterials for directing cellular responses, Soft Matter 4(12) (2008) 2310-2315.

[38] M. Zhou, A.M. Smith, A.K. Das, N.W. Hodson, R.F. Collins, R.V. Ulijn, J.E. Gough, Self-assembled peptide-based hydrogels as scaffolds for anchorage-dependent cells, Biomaterials 30(13) (2009) 2523-2530.

[39] C.A. Goubko, S. Majumdar, A. Basak, X.D. Cao, Hydrogel cell patterning incorporating photocaged RGDS peptides, Biomed Microdevices 12(3) (2010) 555-568.

[40] C.A. Goubko, A. Basak, S. Majumdar, X.D. Cao, Dynamic cell patterning of photoresponsive hyaluronic acid hydrogels, J Biomed Mater Res A 102(2) (2014) 381-391.

[41] N.A. Silva, M.J. Cooke, R.Y. Tam, N. Sousa, A.J. Salgado, R.L. Reis, M.S. Shoichet, The effects of peptide modified gellan gum and olfactory ensheathing glia cells on neural stem/progenitor cell fate, Biomaterials 33(27) (2012) 6345-6354.

[42] K.J. Lampe, A.L. Antaris, S.C. Heilshorn, Design of three-dimensional engineered protein hydrogels for tailored control of neurite growth, Acta Biomater 9(3) (2013) 5590-5599.

[43] R. Patel, M. Santhosh, J.K. Dash, R. Karpoormath, A. Jha, J. Kwak, M. Patel, J.H. Kim, Ile-Lys-Val-ala-Val (IKVAV) peptide for neuronal tissue engineering, Polym Advan Technol 30(1) (2019) 4-12.

[44] P. Sensharma, G. Madhumathi, R.D. Jayant, A.K. Jaiswal, Biomaterials and cells for neural tissue engineering: Current choices, Mater Sci Eng C Mater Biol Appl 77 (2017) 1302-1315.

[45] J. Nikolovski, D.J. Mooney, Smooth muscle cell adhesion to tissue engineering scaffolds, Biomaterials 21(20) (2000) 2025-2032.

[46] D.J. Irvine, A.V.G. Ruzette, A.M. Mayes, L.G. Griffith, Nanoscale clustering of RGD peptides at surfaces using comb polymers. 2. Surface segregation of comb polymers in polylactide, Biomacromolecules 2(2) (2001) 545-556.

[47] C.H. Zhao, J.S. Yu, R.H. Peng, M.Y. Rao, M.Z. Hu, Biodegradable dendritic copolymers consisting of poly(L-lactide) and cRGDfK peptide: synthesis, characterization, and regulation of MC3T3-E1 cell functions, Des Monomers Polym 18(6) (2015) 557-566.

[48] U. Hersel, C. Dahmen, H. Kessler, RGD modified polymers: biomaterials for stimulated cell adhesion and beyond, Biomaterials 24(24) (2003) 4385-4415.

[49] R. Behrendt, P. White, J. Offer, Advances in Fmoc solid-phase peptide synthesis, J Pept Sci 22(1) (2016) 4-27.

[50] V. Made, S. Els-Heindl, A.G. Beck-Sickinger, Automated solid-phase peptide synthesis to obtain therapeutic peptides, Beilstein J Org Chem 10 (2014) 1197-1212.

[51] W. Kowalczyk, M. Monso, B.G. de la Torre, D. Andreu, Synthesis of multiple antigenic peptides (MAPs) - strategies and limitations, J Pept Sci 17(4) (2011) 247-251.

[52] A. Basak, A.M. Khatib, D. Mohottalage, S. Basak, M. Kolajova, S.S. Bag, A. Basak, A Novel Enediynyl Peptide Inhibitor of Furin That Blocks Processing of proPDGF-A, B and proVEGF-C, Plos One 4(11) (2009).

CHAPTER 6 – GENERAL DISCUSSION

The motivation for the development of the projects presented in this thesis was to investigate the use of biosynthesized cellulose (BC) and arginine-glycine-aspartic acid-serine (RGDS) peptides in treating central nervous system (CNS) disorders. The studies performed towards that end provided insights into the production, physical and mechanical properties of BC-based drug release systems, besides the investigation of their *in vitro* and *in vivo* behavior, as well as, into the synthesis and characterization of linear and branched peptides containing the RGDS peptide moiety as potential therapeutic drugs for CNS disorders. The main aspects about these projects are presented and discussed here.

6.1. Biosynthesized Cellulose (BC)-Based Drug Releasing Systems for Treatment of CNS Disorders

Treatment options for CNS disorders are very limited. The development of new biomaterial approaches could generate new paths for CNS treatment. Therefore, in Chapter 3 and 4 of this thesis, two different drug releasing systems were produced. Specifically, in Chapter 3 a duraplasty membrane based on BC was developed to treat stroke. The purpose was to take advantage of the already standard procedure to decrease intracranial pressure after stroke, the decompressive craniectomy (DC) [1, 2], to add a new "possibility" of regenerative outcomes, which otherwise do not exist. In Chapter 4 a drug delivery system in tube shape was produced to promote cell proliferation and differentiation and hopefully guide axon regeneration of the spinal cord after a spinal cord injury (SCI). The production of BC tubes has already been described in the literature; however, these reports are often limited, showing BC tubes produced in only one-time point of cultivation and the physical and mechanical characterization are poorly studied [3-7]. In addition, to the best of our knowledge, no previous

publication suggested the application of BC tubes as nerve guidance drug delivery systems for SCI treatment.

6.2. Production and Modification of Biosynthesized Cellulose (BC)-Based Drug Releasing Systems

BC is produced by several genus of bacteria, such as *Gluconacetobacter hansenii (G. hansenii),* at the air/liquid interface [8, 9]. The asymmetrical BC membranes are normally denser on the side in contact with air and more porous on the liquid side due to the difference in the availability of oxygen [7, 10, 11]. Scanning electron microscopy (SEM) images showed this same behavior for the native BC membrane produced here (Chapter 3). This characteristic of the BC bacteria, to produce more cellulose where there is more oxygen, can be used to produce different shapes of BC hydrogels through *in situ* modification [12, 13].

In situ modification is achieved during bacterial cell culture [14], and it was performed in Chapter 4 by cultivating *G. hansenii* cells in static condition for several time points in a home-made cultivation bioreactor. In the bioreactor a silicone tubing was used as a tempalte and since it is permeable to oxygen, it allowed for the production of BC fibers into a tube shape, named biosynthesized cellulose tubes (BCTs) (Appendix C: **Figure C.1**). Similar to the native BC membranes, SEM images in Chapter 4 showed that the inner side of the BCTs (in contact with the silicone) was denser than the outer side of the BCTs (in contact with the media). The SEM images of the cross-sectioned BCTs revealed that the BCTs were composed of a layered structure similarly to the native BC membranes, see Appendix C: **Figure C.2** for additional SEM images. Other researchers have studied the production of BC tubes [6, 7, 15-22]. For example, Bodin et al. studied the influence of oxygen concentration used for the

production of BC tubes at Day 5 of cultivation [5, 23], and they concluded that the number of layers, cellulose yield and wall thickness increased with increasing the oxygen concentration injected into the mold tube [5, 23].

Ex situ modification of BC is performed after the production of original BC membrane, and it can be performed by either chemical or physical methods [14]. Chapter 3 of this thesis demonstrated an *ex situ* approach to physically modify BC. **Figure B.3** in Appendix B shows the schematic representation of the blending method to produce blended BC (BBC) membranes containing different amounts of dry cellulose. To produce BBC membranes, no organic solvents were required [24]. The resulting BBC was highly pure (**Figure B.4**) and maintained the original biocompatibility of the BC. This fabrication method provided the possibility to modify the physical and mechanical properties of BC, as shown in Chapter 3. Using the blending protocol a more uniform duraplasty membrane was created, which is important for a more consistent and predictable drug release [25, 26].

BBC was sterilized by autoclaving, what did not have any extensive effect on the fiber morphology as can be seen by the SEM comparison of BBC before and after autoclaving in **Figure B.5**. In addition, BBC production technique allowed a much easier incorporation of growth factors (GFs) into the membranes while maintaining sterility. This is of note because the sterilization process is frequently a challenge for the design of biomaterials, as it is difficult to find a sterilization technique that maintains the original properties of the biomaterial and does not affect the activity of molecules [14, 27].

6.3. Physical and Mechanical Properties of Biosynthesized Cellulose (BC)-Based Drug Releasing Systems

When designing a biomaterial for tissue engineering applications it is important to consider the nature of the native tissue. Even though the material has intrinsic properties that need to be considered, such as thickness, microstructure, water-related and mechanical properties, the design of the biomaterial needs to take in account the therapeutic approach [28, 29]. Finding a biomaterial with all the desired properties is challenging, therefore engineered biomaterials represent a promising approach to adjust the biomaterial properties. The main properties investigated in this thesis are discussed below.

In Chapter 3, the thickness of the BBC membranes was investigated because of the limited space of the skull. The aim of the BBC membrane is to act as a duraplasty that is implanted into the brain during a DC procedure after stroke. Thus, it is important for the biomaterial to fit into the restricted space without causing further damage to the area. Although the thickness of the BBC membranes doubled after rehydration they were still within the thickness range of human dura mater [30]. Therefore, the BBC thickness likely would not cause any problems when implanted. This was confirmed by the *in vivo* biocompatibility test performed. In Chapter 4, bacteria cultivation was completed for seven different cultivation times to obtain seven different BCT samples to investigate and compare their physical and mechanical properties. Our data suggested that increasing the cultivation time increased the amount of cellulose, as expected. However, the substantial increase in wall tube thickness took place only after 12 days of cultivation.

The water-related properties of the BBC and BCT samples were analyzed using the swelling ratio (SR) and rehydration ratio (RR), respectively. The SR and RR of biomaterials were dependent largely on the fibers organization and the formation of hydrogen bonds between the cellulose fibers and water molecules [31]. The water absorbing property is influenced by how porous the material is, i.e. increasing the porosity increases the volume of

water that could penetrate into the sample [31, 32]. Thus, the fiber network arrangement and porosity of the cellulose in the BBC and BCT samples are what will dictate the SR and RR behavior. The SEM was used to characterize the microstructure and understand the RR/SR behavior of both drug delivery systems.

In the case of the BBC samples, because of the production method, more cellulose resulted in more rigid and denser samples as shown by SEM images (**Figure B.6**), resulting in a lower SR (Chapter 3). On the other hand, for the BCTs with a longer cultivation time more cellulose was produced, but as the bacteria excrete the BC fibers in layers, the outer surface of the BCTs were more porous as shown by the SEM images in Chapter 4 and **Figure C.2**. This explains the increase in the RR for the samples cultivated for longer periods of time. In addition, BCTs cultivated for shorter periods of time tended to be weaker tubes, not standing their own weight and presenting ruptures in their inner side.

To ensure that the BBC and BCT had the potential to perform the role of duraplasty and nerve guidance tube, respectively, the Young's Modulus and the ultimate tensile strength (UTS) of the materials were evaluated. For stroke applications (Chapter 3), it is important that the biomaterial presents similar mechanical properties to the brain tissue, where stiffer biomaterials can result in gliosis, while softer ones can impact the material stability [33, 34]. In addition, an ideal biomaterial to be implanted onto the brain should be able to conform to the brain shape [35]. For a biomaterial to successfully substitute the spinal cord (Chapter 4), its stiffness should match the mechanical properties of the spinal cord at the injury site [36, 37]. Additionally, the biomaterial should be strong enough to withstand the biomechanical forces in the body without collapsing [7, 37].

In Chapter 3, our data suggested that the increase in cellulose mass increased the UTS and Young's Modulus. This can be explained by the BBC production method, where an

increased amount of cellulose meant a more compact and dense membrane and that resulted in higher strength and stiffness. For the BCT samples, the changes in the amount of cellulose were proportional to the UTS, similar to the BBC samples. However, that was not the case for the Young's Modulus of the BCTs, which varied among the samples. This can be explained because of the BCTs layered structure which makes it difficult to directly correlate the Young's modulus with the change in cellulose mass, similar to the observations made by Bodin et al. [5]. Nevertheless the average Young's modulus of the produced BCTs matched the Young's modulus of the human spinal cord [38-40].

Because of the structural and mechanical properties of the BBC and BCTs, combined with the various studies that showed the superior mechanical properties of BC over many other synthetic biomaterials [41], our platforms – BBC and BCT – were further studied as drug delivery systems.

6.4. Biosynthesized Cellulose (BC) as Drug Releasing Systems

Hydrogels can be useful vehicles to directly deliver bioactive molecules, such as GFs, into the damaged CNS site [42-44]. However, their potential has been impeded by two challenges: the production of hydrogels with suitable mechanical properties [29, 43, 45] and the sterilization of the hydrogels without altering their properties or the bioactivity of the incorporated molecules [27]. In this thesis, both drug releasing systems were successfully loaded with GFs at high entrapment efficiencies. It was demonstrated that GFs (e.g. FGF2, EGF and NGF) can be sterilely loaded into the BBC and BCT samples without compromising their physical and mechanical characteristics and mostly important without affecting the bioactivity of the GFs. It is noted that 93 % of the total amount of GFs that was initially loaded into both drug delivery systems was detected by ELISA. However, the *in vitro* drug release profiles were slightly

different for the BBC and BCT samples. While both presented a burst release at the first hours, normally due to the presence of GFs on the surface of the samples, BBC membranes had ~61 % of GFs released at 8 hours, while BCT presented ~75 % of NGF released at 9 hours. At Day 1, BBC released ~64 % and BCT ~82 %. This difference in release performance is likely due to the difference in microstructure and water-related properties of the samples. The BCT swelled faster and allowed more liquid into its cellulose matrix than BBC membranes, meaning that the drug can diffuse out of the BCT faster [46].

The various release kinetic models developed are supposed to reason different release mechanisms [47]. Therefore, in the current study, the zero-order, Higuchi, and Korsemyer-Peppas models were used to analyze the *in vitro* released data. The adjusted correlation coefficients of Zero-order, Higuchi equation, and Korsemyer-Peppas kinetic models used in the BBC and BCT studies are shown in **Table B.1** (Appendix B) and **Table C.1** (Appendix C), respectively. The delivery of FGF2 and EGF from BBC were similar, presenting no statistical difference. Both drug delivery systems, BBC and BCT, presented a poor correlation with the Zero-order model. For the Higuchi mechanism the correlation was better, ~0.89 for BBC and ~0.80 for BCT, but still considered low. However, the *in vitro* drug release profiles of BBC and BCT were well-fitted with Korsemyer-Peppas kinetic model, being R^2 0.9905 for FGF2 (**Figure B.7A**), 0.9847 for EGF (**Figure B.7.B**), and 0.9954 for NGF from BCT (**Figure C.3**). According to this model, a value of $n<0.5/0.45/0.43$ for a slab/cylinder/sphere indicates a diffusion controlled drug release. When $n>1/0.89/0.85$ for a slab/cylinder/sphere, the drug release behavior is called case-II transport. In contrast, when $0.5/0.45/0.43<n<1/0.89/0.85$, the drug release behavior is classified as a combination of both phenomenon and is referred to anomalous transport. In the current study, BBC samples were prepared in the slab shape while BCT samples were cylinders. The drug delivery systems presented n-values lower than 0.5

and 0.45. The results in **Table B.1** and **Table C.1** suggest that NGF released from BCT was slightly more diffusion-based (n = 0.113) than FGF2 and EGF released from BBC (n = 0.147 and 0.140, respectively). The releases were more likely to be Fickan diffusion without impeding or driving forces.

6.5. Bioactivity Studies of the Growth Factors

The desired outcome of differentiation and proliferation of cells can be achieved by stimulating the cells with GFs to direct cellular activities [48]. GFs can be integrated into biomaterials to promote cellular viability and adhesion and stimulation of neurite growth [49, 50]. The *in vitro* GFs delivery success of BBC duraplasty and BCT nerve guidance tube was tested using endogenous neural stem/progenitor cells (NSPCs) and PC12 cells, respectively. NSPCs are multipotent CNS cells capable of differentiating into neurons, oligodendrocytes, and astrocytes [51]. PC12 cells are well known cells used for *in vitro* tests to assess neural differentiation [48, 52], since they change phenotype and develop characteristics of neuron-like cells after exposure to NGF [53, 54].

After stroke, commonly, NSPCs proliferate more in the subventricular zone (SVZ), and some precursor cells are directed to the injury site [55, 56]. Thus, it is important to evaluate the proliferative behavior of NSPCs when co-cultured with the GFs-enriched BBC membranes. In Chapter 3 of this thesis, *in vitro* experiments showed that the GFs (EGF and FGF2) delivered from the BBC membranes were able to stimulate rodent and porcine brain NSPC **(**Figure B.1) and human spinal cord NSPC **(**Figure B.2) proliferation. It was observed that NSPCs co-cultured with the GFs-enriched BBC membranes maintained their differentiation capacity and presented a dominant astrocyte phenotype. Furthermore, in Chapter 3, the biocompatibility of the BBC membranes was shown *in vivo* in rats through post-

decompression implantation.

Chapter 4 of this thesis showed the bioactivity of the NGF delivered directly from the BCTs by studying their influence on the differentiation of PC12 cells. The NGF delivered from the BCTs promoted PC12 cells growth. It is known that in the presence of a sufficient amount of NGF, PC12 cells stop proliferating and start differentiating and therefore spreading neurites [54]. In fact, the neurite length and the percentage of differentiated cells increased with the passing of time for the groups containing NGF. Importantly, those were greater for the group co-cultured with the NGF-enriched BCT than for the positive control. The percentage of differentiated PC12 cells is dependent on the NGF dose [57]. This explains why more cells differentiated with the passing of time for the BCTs samples, since higher concentration of bioactive NGF was presented. The delivered NGF concentration proved sufficient to cease proliferation and stimulate differentiation. Such NGF release is known to be useful for nerve regeneration as well as stem NSPC neurogenesis [50, 58].

6.6. Peptides Synthesis, Optimization and Characterization

Recently, tissue regeneration approaches have been used for the treatment of damaged tissues and organs [59]. These approaches normally involve biomaterials that can serve not only as scaffold to physically support cells, but also to signal cells at the level of receptors to promote cell proliferation [29]. Therefore, the incorporation of peptides that are involved in the cell signaling can improve the scaffold biofunctionality [60]. In Chapter 5, linear and two-branched peptides, containing in their composition the arginine-glycine-aspartic acid-serine (RGDS) sequence, were synthesize as potential therapeutic molecules to improve cell binding properties in biomaterials. The syntheses of linear and branched peptides was performed in an automatic peptide synthesizer running 9-fluorenylmethoxycarbonyl (Fmoc) - Solid Phase

Peptide Synthesis (SPPS) protocol. For the peptide design in Chapter 5, the following sequence and amino acids were selected:

- *RGDS sequence:* It is well known for promoting cell adhesion and proliferation [61]. Additionally, many studies have shown the tissue engineering applications of biomaterials containing the RGDS sequence [62-64].
- *8-Amino-3,6-dioxaoctanoic acid (Adoa*): To improve the yield and purity of the peptide by providing flexibility and enhancing the solubility features of the peptides [65].
- *Cysteine*: To incorporate a free thiol group (-SH) that can be used to chemically modify different biomaterials or to generate dimers [66].
- *Lysine*: To form branching on the peptide sequence [67].
- *Alanine*: Spacer, since first amino acid coupling is more difficult.

It was important to optimize the peptide synthesis protocols since an efficient synthesis procedure can increase yield and purity, making the peptides more attractive for tissue engineering applications. In Chapter 5 of this thesis several synthesis parameters were tested including: two different coupling reagents, two different protecting groups for cysteine, the number of deprotection and coupling repetitions, and the duration of time for the cleavage reaction with Reagent B. Using the optimized protocol, linear and 2-branched peptides were successfully synthesized. Then they were characterized by matrix-assisted laser desorption/ionization mass spectrometry (MALDI-MS) and purified by high performance liquid chromatography (HPLC). It was demonstrated that both peptides presented a mixture of their respective monomer and dimer forms. The free –SH group in the peptide allowed for the

formation of a dimer, where a disulfide bond was formed between two cysteine residues of two peptide chains.

The best yield for the linear peptide and the 2-branched peptide were 92.9% and 81.3%, respectively. The synthesis of the 2-branched peptide was found to be less clean than the linear one, as demonstrated by the presence of additional peaks in the HPLC and MADI-MS analyses (Chapter 5). A similar Fmoc-SPPS protocol can be used for increasing the number of branches in a peptide. For example, 4-branched peptides can be synthesized similarly to the 2-branched peptides as demonstrated by the preliminary results show in Appendix D. Theoretical 3D molecular structure studies, such as the one employed in this work for the study of the energy-minimized peptide structures in vacuum, can be useful for understanding the properties and behaviors of peptides based upon the stable structure conformation [68]. In Chapter 5, it was observed that there were no hydrogen bonds formed in the monomeric linear peptide structure; however, there were several hydrogen bonds formed in the dimeric linear peptide, and in the monomeric and dimeric 2-branched peptide. Those hydrogen bonds possibly contributed to the stability of the molecules. Overall, the results showed that linear and branched RGDS peptides can be successfully synthesized.

6.7. References

[1] O.M. Arnaout, S.G. Aoun, H.H. Batjer, B.R. Bendok, Decompressive hemicraniectomy after malignant middle cerebral artery infarction: rationale and controversies, Neurosurg Focus 30(6) (2011) E18.

[2] E. Juttler, A. Unterberg, J. Woitzik, J. Bosel, H. Amiri, O.W. Sakowitz, M. Gondan, P. Schiller, R. Limprecht, S. Luntz, H. Schneider, T. Pinzer, C. Hobohm, J. Meixensberger, W. Hacke, D.I. Investigators, Hemicraniectomy in older patients with extensive middle-cerebral-artery stroke, N Engl J Med 370(12) (2014) 1091-100.

[3] H. Zahedmanesh, J.N. Mackle, A. Sellborn, K. Drotz, A. Bodin, P. Gatenholm, C. Lally, Bacterial cellulose as a potential vascular graft: Mechanical characterization and constitutive model development, J Biomed Mater Res B 97B(1) (2011) 105-113.

[4] K.A. Zimmermann, J.M. LeBlanc, K.T. Sheets, R.W. Fox, P. Gatenholm, Biomimetic design of a bacterial cellulose/hydroxyapatite nanocomposite for bone healing applications, Mat Sci Eng C-Mater 31(1) (2011) 43-49.

[5] A. Bodin, H. Backdahl, H. Fink, L. Gustafsson, B. Risberg, P. Gatenholm, Influence of cultivation conditions on mechanical and morphological properties of bacterial cellulose tubes, Biotechnol Bioeng 97(2) (2007) 425-434.

[6] S.S. Zang, R. Zhang, H. Chen, Y.D. Lu, J.H. Zhou, X. Chang, G.X. Qiu, Z.H. Wu, G. Yang, Investigation on artificial blood vessels prepared from bacterial cellulose, Mat Sci Eng C-Mater 46 (2015) 111-117.

[7] D. Klemm, D. Schumann, U. Udhardt, S. Marsch, Bacterial synthesized cellulose - artificial blood vessels for microsurgery, Prog Polym Sci 26(9) (2001) 1561-1603.

[8] H. El-Saied, A.H. Basta, R.H. Gobran, Research progress in friendly environmental technology for the production of cellulose products (bacterial cellulose and its application), Polym-Plast Technol 43(3) (2004) 797-820.

[9] A.F. Jozala, L.C. de Lencastre-Novaes, A.M. Lopes, V.D. Santos-Ebinuma, P.G. Mazzola, A. Pessoa, D. Grotto, M. Gerenutti, M.V. Chaud, Bacterial nanocellulose production and application: a 10-year overview, Appl Microbiol Biot 100(5) (2016) 2063-2072.

[10] H. Backdahl, G. Helenius, A. Bodin, U. Nannmark, B.R. Johansson, B. Risberg, P. Gatenholm, Mechanical properties of bacterial cellulose and interactions with smooth muscle cells, Biomaterials 27(9) (2006) 2141-2149.

[11] F.V. Berti, C.R. Rambo, P.F. Dias, L.M. Porto, Nanofiber density determines endothelial cell behavior on hydrogel matrix, Materials Science and Engineering: C 33(8) (2013) 4684-4691.

[12] D.O.S. Recouvreux, C.R. Rambo, F.V. Berti, C.A. Carminatti, R.V. Antonio, L.M. Porto, Novel three-dimensional cocoon-like hydrogels for soft tissue regeneration, Mat Sci Eng C-Mater 31(2) (2011) 151-157.

[13] T.R. Stumpf, R.A.N. Pertile, C.R. Rambo, L.M. Porto, Enriched glucose and dextrin mannitol-based media modulates fibroblast behavior on bacterial cellulose membranes, Mat Sci Eng C-Mater 33(8) (2013) 4739-4745.

[14] T.R. Stumpf, X.Y. Yang, J.C. Zhang, X.D. Cao, In situ and ex situ modifications of bacterial cellulose for applications in tissue engineering, Mat Sci Eng C-Mater 82 (2018) 372-383.

[15] M. Scherner, S. Reutter, D. Klemm, A. Sterner-Kock, M. Guschlbauer, T. Richter, G. Langebartels, N. Madershahian, T. Wahlers, J. Wippermann, In vivo application of tissue-engineered blood vessels of bacterial cellulose as small arterial substitutes: proof of concept?, J Surg Res 189(2) (2014) 340-347.

[16] D.A. Schumann, J. Wippermann, D.O. Klemm, F. Kramer, D. Koth, H. Kosmehl, T. Wahlers, S. Salehi-Gelani, Artificial vascular implants from bacterial cellulose: preliminary results of small arterial substitutes, Cellulose 16(5) (2009) 877-885.

[17] J. Wippermann, D. Schumann, D. Klemm, H. Kosmehl, S. Satehi-Gelani, T. Wahlers, Preliminary Results of Small Arterial Substitute Performed with a New Cylindrical Biomaterial Composed of Bacterial Cellulose, Eur J Vasc Endovasc 37(5) (2009) 592-596.

[18] H. Backdahl, B. Risberg, P. Gatenholm, Observations on bacterial cellulose tube formation for application as vascular graft, Mat Sci Eng C-Mater 31(1) (2011) 14-21.

[19] F. Hong, B. Wei, L. Chen, Preliminary Study on Biosynthesis of Bacterial Nanocellulose Tubes in a Novel Double-Silicone-Tube Bioreactor for Potential Vascular Prosthesis, Biomed Res Int (2015).

[20] H. Orelma, L.O. Morales, L.S. Johansson, I.C. Hoeger, I. Filpponen, C. Castro, O.J. Rojas, J. Laine, Affibody conjugation onto bacterial cellulose tubes and bioseparation of human serum albumin, Rsc Adv 4(93) (2014) 51440-51450.

[21] K. Kowalska-Ludwicka, J. Cala, B. Grobelski, D. Sygut, D. Jesionek-Kupnicka, M. Kolodziejczyk, S. Bielecki, Z. Pasieka, Modified bacterial cellulose tubes for regeneration of damaged peripheral nerves, Arch Med Sci 9(3) (2013) 527-534.

[22] C.L. Zhu, F. Li, X.Y. Zhou, L. Lin, T.Y. Zhang, Kombucha-synthesized bacterial cellulose: Preparation, characterization, and biocompatibility evaluation, J Biomed Mater Res A 102(5) (2014) 1548-1557.

[23] A. Bodin, H. BÄCKDAHL, P. Gatenholm, L. Gustafsson, B. Risberg, Bacterial cellulose tubes, Google Patents, 2012.

[24] E.M. Ahmed, Hydrogel: Preparation, characterization, and applications: A review, J Adv Res 6(2) (2015) 105-121.

[25] J. Li, D.J. Mooney, Designing hydrogels for controlled drug delivery, Nat Rev Mater 1(12) (2016).

[26] Z.M. Wang, Z.F. Wang, W.W. Lu, W.X. Zhen, D.Z. Yang, S.L. Peng, Novel biomaterial strategies for controlled growth factor delivery for biomedical applications, Npg Asia Mater 9 (2017).

[27] Z. Dai, J. Ronholm, Y. Tian, B. Sethi, X. Cao, Sterilization techniques for biodegradable scaffolds in tissue engineering applications, J Tissue Eng 7 (2016) 2041731416648810.

[28] K.S. Straley, C.W.P. Foo, S.C. Heilshorn, Biomaterial Design Strategies for the Treatment of Spinal Cord Injuries, J Neurotraum 27(1) (2010) 1-19.

[29] P. Sensharma, G. Madhumathi, R.D. Jayant, A.K. Jaiswal, Biomaterials and cells for neural tissue engineering: Current choices, Mater Sci Eng C Mater Biol Appl 77 (2017) 1302-1315.

[30] D. De Kegel, J. Vastmans, H. Fehervary, B. Depreitere, J. Vander Sloten, N. Famaey, Biomechanical characterization of human dura mater, J Mech Behav Biomed 79 (2018) 122-134.

[31] M. Ul-Islam, T. Khan, J.K. Park, Water holding and release properties of bacterial cellulose obtained by in situ and ex situ modification, Carbohyd Polym 88(2) (2012) 596-603.

[32] O. Shezad, S. Khan, T. Khan, J.K. Park, Physicochemical and mechanical characterization of bacterial cellulose produced with an excellent productivity in static conditions using a simple fed-batch cultivation strategy, Carbohyd Polym 82(1) (2010) 173-180.

[33] P. Moshayedi, L.R. Nih, I.L. Llorente, A.R. Berg, J. Cinkornpumin, W.E. Lowry, T. Segura, S.T. Carmichael, Systematic optimization of an engineered hydrogel allows for selective control of human neural stem cell survival and differentiation after transplantation in the stroke brain, Biomaterials 105 (2016) 145-55.

[34] K.C. Spencer, J.C. Sy, K.B. Ramadi, A.M. Graybiel, R. Langer, M.J. Cima, Characterization of Mechanically Matched Hydrogel Coatings to Improve the Biocompatibility of Neural Implants (vol 7, 1952, 2017), Sci Rep-Uk 7 (2017).

[35] S.F. Danish, A. Samdani, A. Hanna, P. Storm, L. Sutton, Experience with acellular human dura and bovine collagen matrix for duraplasty after posterior fossa decompression for Chiari malformations, J Neurosurg 104(1) (2006) 16-20.

[36] M.D. Wang, P. Zhai, X.B. Chen, D.J. Schreyer, X.D. Sun, F.Z. Cui, Bioengineered Scaffolds for Spinal Cord Repair, Tissue Eng Part B-Re 17(3) (2011) 177-194.

[37] M. Tsintou, K. Dalamagkas, A.M. Seifalian, Advances in regenerative therapies for spinal cord injury: a biomaterials approach, Neural Regen Res 10(5) (2015) 726-742.

[38] P.D. Dalton, L. Flynn, M.S. Shoichet, Manufacture of poly(2-hydroxyethyl methacrylate-co-methyl methacrylate) hydrogel tubes for use as nerve guidance channels, Biomaterials 23(18) (2002) 3843-51.

[39] S.J. Nagel, C.G. Reddy, L.A. Frizon, M.K. Chardon, M. Holland, A.G. Machado, G.T. Gillies, M.A. Howard, 3rd, S. Wilson, Spinal dura mater: biophysical characteristics relevant to medical device development, J Med Eng Technol 42(2) (2018) 128-139.

[40] L.E. Bilston, L.E. Thibault, The mechanical properties of the human cervical spinal cord in vitro, Ann Biomed Eng 24(1) (1996) 67-74.

[41] H. Ullah, F. Wahid, H.A. Santos, T. Khan, Advances in biomedical and pharmaceutical applications of functional bacterial cellulose-based nanocomposites, Carbohydr Polym 150 (2016) 330-52.

[42] Z.Z. Khaing, R.C. Thomas, S.A. Geissler, C.E. Schmidt, Advanced biomaterials for repairing the nervous system: what can hydrogels do for the brain?, Materials Today 17(7) (2014) 332-340.

[43] R.Y. Tam, T. Fuehrmann, N. Mitrousis, M.S. Shoichet, Regenerative therapies for central nervous system diseases: a biomaterials approach, Neuropsychopharmacology 39(1) (2014) 169-88.

[44] O.A. Carballo-Molina, I. Velasco, Hydrogels as scaffolds and delivery systems to enhance axonal regeneration after injuries, Front Cell Neurosci 9 (2015) 13.

[45] S. Yao, X. Liu, X. Wang, A. Merolli, X. Chen, F. Cui, Directing neural stem cell fate with biomaterial parameters for injured brain regeneration, Progress in Natural Science: Materials International 23(2) (2013) 103-112.

[46] R. Zarzycki, Z. Modrzejewska, K. Nawrotek, Drug Release from Hydrogel Matrices, Ecol Chem Eng S 17(2) (2010) 9-28.

[47] R. Langer, Polymeric Delivery Systems for Controlled Drug Release, Chem Eng Commun 6(1-3) (1980) 1-48.

[48] Y.Q. Wu, Z.G. Wang, P.T. Cai, T. Jiang, Y.Y. Li, Y. Yuan, R. Li, Y.F. Lu, J. Wang, D.Q. Chen, Q.Q. Zeng, S.N. Khor, R.S. Zhong, H.Y. Zhang, Y. Lin, X.K. Li, J. Xiao, Dual Delivery of bFGF-and NGF-Binding Coacervate Confers Neuroprotection by Promoting Neuronal Proliferation, Cellular Physiology and Biochemistry 47(3) (2018) 948-956.

[49] E.G. Fine, I. Decosterd, M. Papaloizos, A.D. Zurn, P. Aebischer, GDNF and NGF released by synthetic guidance channels support sciatic nerve regeneration across a long gap, Eur J Neurosci 15(4) (2002) 589-601.

[50] I.P. Clements, J.M. Munson, R.V. Bellamkonda, Chapter II.6.14 - Neuronal Tissue Engineering, in: B.D. Ratner, A.S. Hoffman, F.J. Schoen, J.E. Lemons (Eds.), Biomaterials Science (Third Edition), Academic Press2013, pp. 1291-1306.

[51] T. Zahir, Y.F. Chen, J.F. MacDonald, N. Leipzig, C.H. Tator, M.S. Shoichet, Neural Stem/Progenitor Cells Differentiate In Vitro to Neurons by the Combined Action of Dibutyryl cAMP and Interferon-gamma, Stem Cells Dev 18(10) (2009) 1423-1432.

[52] K.P. Das, T.M. Freudenrich, W.R. Mundy, Assessment of PC12 cell differentiation and neurite growth: a comparison of morphological and neurochemical measures, Neurotoxicol Teratol 26(3) (2004) 397-406.

[53] M. Wigerius, N. Asghar, W. Melik, M. Johansson, Scribble controls NGF-mediated neurite outgrowth in PC12 cells, Eur J Cell Biol 92(6-7) (2013) 213-221.

[54] L.A. Greene, A.S. Tischler, Establishment of a noradrenergic clonal line of rat adrenal pheochromocytoma cells which respond to nerve growth factor, Proc Natl Acad Sci U S A 73(7) (1976) 2424-8.

[55] V. Pencea, K.D. Bingaman, L.J. Freedman, M.B. Luskin, Neurogenesis in the subventricular zone and rostral migratory stream of the neonatal and adult primate forebrain, Exp Neurol 172(1) (2001) 1-16.

[56] S.G. Kernie, J.M. Parent, Forebrain neurogenesis after focal Ischemic and traumatic brain injury, Neurobiol Dis 37(2) (2010) 267-74.

[57] R.D. Hu, Q.Y. Cao, Z.Q. Sun, J.Y. Chen, Q. Zheng, F. Xiao, A novel method of neural differentiation of PC12 cells by using Opti-MEM as a basic induction medium, Int J Mol Med 41(1) (2018) 195-201.

[58] D. Otto, K. Unsicker, C. Grothe, Pharmacological Effects of Nerve Growth-Factor and Fibroblast Growth-Factor Applied to the Transectioned Sciatic-Nerve on Neuron Death in Adult-Rat Dorsal-Root Ganglia, Neurosci Lett 83(1-2) (1987) 156-160.

[59] R. Patel, M. Santhosh, J.K. Dash, R. Karpoormath, A. Jha, J. Kwak, M. Patel, J.H. Kim, Ile-Lys-Val-ala-Val (IKVAV) peptide for neuronal tissue engineering, Polym Advan Technol 30(1) (2019) 4-12.

[60] J. Nikolovski, D.J. Mooney, Smooth muscle cell adhesion to tissue engineering scaffolds, Biomaterials 21(20) (2000) 2025-2032.

[61] C.A. Goubko, S. Majumdar, A. Basak, X.D. Cao, Hydrogel cell patterning incorporating photocaged RGDS peptides, Biomedical Microdevices 12(3) (2010) 555-568.

[62] D.J. Irvine, A.V.G. Ruzette, A.M. Mayes, L.G. Griffith, Nanoscale clustering of RGD peptides at surfaces using comb polymers. 2. Surface segregation of comb polymers in polylactide, Biomacromolecules 2(2) (2001) 545-556.

[63] C.H. Zhao, J.S. Yu, R.H. Peng, M.Y. Rao, M.Z. Hu, Biodegradable dendritic copolymers consisting of poly(L-lactide) and cRGDfK peptide: synthesis, characterization, and regulation of MC3T3-E1 cell functions, Des Monomers Polym 18(6) (2015) 557-566.

[64] R.A. Plenderleith, C.J. Pateman, C. Rodenburg, J.W. Haycock, F. Claeyssens, C. Sammond, S. Rimmer, Arginine-glycine-aspartic acid functional branched semi-interpenetrating hydrogels, Soft Matter 11(38) (2015) 7567-7578.

[65] W. Kowalczyk, M. Monso, B.G. de la Torre, D. Andreu, Synthesis of multiple antigenic peptides (MAPs) - strategies and limitations, J Pept Sci 17(4) (2011) 247-251.

[66] R. Behrendt, P. White, J. Offer, Advances in Fmoc solid-phase peptide synthesis, J Pept Sci 22(1) (2016) 4-27.

[67] J.P. Tam, Recent advances in multiple antigen peptides, J Immunol Methods 196(1) (1996) 17-32.

[68] A. Basak, A.M. Khatib, D. Mohottalage, S. Basak, M. Kolajova, S.S. Bag, A. Basak, A Novel Enediynyl Peptide Inhibitor of Furin That Blocks Processing of proPDGF-A, B and proVEGF-C, Plos One 4(11) (2009).

CHAPTER 7 – CONCLUSION

Results based on the aims of this thesis are summarized below:

i. A novel drug releasing duraplasty was designed and produced using a sustainable *ex situ* approach to physically modify biosynthesized cellulose (BC). Using the blending protocol, uniform blended biosynthesized cellulose (BBC) membranes that can be applied after the decompression craniectomy procedure in patients with stroke to stimulate neural stem cell proliferation were successfully prepared.

ii. Several BC hydrogels were produced using an *in situ* approach, using a special bioreactor to form BC in tube-shape (i.e. biosynthesized cellulose tubes - BCTs) with varying cultivation times. BCTs were proposed as a potential nerve guidance drug delivery system to assist with the reconnection of nerve tissues after a spinal cord injury (SCI).

iii. Both drug delivery systems (BBC and BCT) were characterized. The BBC fabrication method provided the possibility to build BBC membranes with different cellulose contents and to modify the properties of the duraplasty. The BBC membrane composed with the highest cellulose mass was the densest, strongest and most homogenous membrane and it had the lowest swelling ratio, making it a promising candidate as a drug releasing duraplasty. The physical and mechanical properties of the BCTs varied with the increase of cultivation time. Indeed, the BCT formed after 22 days of cultivation showed the highest cellulose mass and the highest rehydration ratio. It also presented suitable mechanical properties with a Young's Modulus similar to the human spinal cord.

iv. Growth factors (GFs) were used to load both systems and their *in vitro* drug delivery profiles were analysed. The GFs were sterilely loaded into the BBC and BCTs samples with high entrapment efficiencies and without compromising their bioactivity. While

both BBC and BCT samples showed a release profile featured with an initial burst release at the first day, BBCs showed a slower and more linear release (until 10 days) in comparison with BCTs.

v. The BBC and BCT samples were able to fulfill their intended purpose after sterilization and incorporations of GFs. The dosage of GFs was bioactive and proved to be sufficient to stimulate primary rodent neural stem/progenitor cells (NSPC) and PC12 cells proliferation *in vitro* for a period of one week. In addition, the GFs-enriched BBC drug releasing duraplasty were able to stimulate proliferation of porcine brain-derived and human spinal cord NSPCs. In fact, the rodent NSPCs were multipotent and displayed a dominant astrocyte phenotype upon differentiation for one and two weeks. Therefore, these studies suggest that the GFs-enriched BBC and BCT could be exploited as delivery systems for protein-based drugs to enhance nerve regeneration in the central nervous system.

vi. The resulting BBC duraplasty was highly pure and biocompatible. This was confirmed by the *in vivo* post-decompression implantation of BBC membranes loaded with GFs in adult rats. These findings indicated that the GFs-enriched BBC membranes are a promising and clinically relevant drug releasing duraplasty option for the treatment of stroke.

vii. The solid-phase peptide synthesis (SPPS) chemistry was used to synthesize peptides containing the arginine-glycine-aspartic acid-serine (RGDS) sequence in different configurations, i.e. linear and 2-branched. The peptide syntheses were optimized and the linear and 2-branched peptides were successfully synthesized. The peptide structures were confirmed by HPLC and MS, and their 3D energy-minimized molecular structure were analysed. In addition, it was demonstrated that similar

synthesis protocol could be used to synthesize peptides containing a higher number of branches, such as 4-branched peptides.

CHAPTER 8 – RECOMMENDATIONS AND LIMITATIONS

8.1. Design and evaluation of a biosynthesized cellulose duraplasty to stimulate neural stem cell proliferation

While the experiments presented in **Chapter 3** serving as proof-of-concept for the clinical applicability of blended biosynthesized cellulose (BBC) duraplasty, there were some limitations:

- If indeed the growth factor-enriched BBC duraplasty is efficient in stimulating human neural stem/progenitor cells (NSPCs), given that the *in vitro* tests of human spinal cord cells were performed with the cells from a single donor.
    - Recommendation: Further test *in vitro* the BBC duraplasty with human brain cells.
- If the concentration and duration of the growth factors released from the enriched BBC duraplasty are sufficient to penetrate the post-stroke area and stimulate NSPC proliferation.
    - Recommendation: Test *in vivo* the penetration of the drugs released from BBC duraplasty; if necessary improve the drug release profile by encapsulating the drugs to have a more sustained delivery.
- If BBC duraplasty can improve the post-stroke neurological function of rats following decompressive craniectomy.
    - Recommendation: Test growth factor-enriched BBC duraplasty in rodent stroke models.

The ability to test BBC *in vitro* on porcine brain and human spinal cord cells strengthens the potential clinical applicability of BBC duraplasty. However, future studies should address these previously mentioned points.

8.2. Production and evaluation of biosynthesized cellulose tube (BCT) as promising nerve guidance delivery system for spinal cord injuries treatment

In **Chapter 4** of this thesis biosynthesized cellulose tubes (BCTs) were proposed as nerve guidance drug delivery systems for SCI. Although the experiments demonstrated the potential of this platform, some aspects still need to be addressed:

- If the concentration and duration of the nerve growth factor released from the loaded-BCT nerve guidance are sufficient to stimulate axonal growth
    - Recommendation: Test *in vivo* the effect of the drugs released from BCTs.
- If necessary, improve the drug release profile of the BCTs.
    - Recommendation: Incorporate dual drug delivery systems into the BCTs to provide a more prolonged release.
- If the nerve guidance BCTs are able to localize and promote cell regeneration in the injury site without causing gliosis.
    - Recommendation: Test BCTs *in vivo* SCI animal models.

8.3. Synthesis, optimization and characterization of RGDS-peptides

While the results in **Chapter 5** provided some insights on the syntheses of linear and branched peptides containing the RGDS peptide sequence, some remained points should be improved:

- Further purification of the synthesized linear and 2-branched peptides;
- Fully synthesize and characterize the 4-branched peptide;
- Test the *in vitro* bioactivity of the produced peptides;
- Incorporate the synthesized peptides into the biomaterials and test their cell–biomaterial interactions.

8.4. Limitations on Mechanical Tests

Mechanical testing on hydrogels involves several practical challenges, such as the clamping of the samples, the effect of the rehydration, the measurement of the samples and the strain quantification.

8.4.1. Clamping the Samples

Clamping hydrogel samples for a correct tensile testing presents many difficulties, as it is necessary to ensure a firm grip between the sample and the clamps. The specimens tested in Chapter 3 were membranes made of blended biosynthesized cellulose (BBC). For mechanical testing the samples were cut in rectangular shaped samples. Testing the rectangular specimens was proved to induce good results in the experiments, as the tested samples often presented fractures in the middle of the free-length region between the clamps. In addition, it made easier the calculation of the extension to failure, as it was easily measured from the grip-to-grip separation. After studying from literature the best solutions for clamping polymer hydrogels and soft biological tissues, the best interface was characterized by the presence of a fine sandpaper or filter paper adherent onto the jaw faces. For our BBC samples, the filter paper showed to be efficient to hold the samples avoiding slip. The same technique was used to test the biosynthesized cellulose tubes (BCTs), however the limitation for these analyses was to keep the cylinder shape of the samples.

8.4.2. Effect of the Rehydration

For the mechanical tests of BBC and BCTs it was chosen to analyse the samples in their rehydration form. The main challenge was to perform the tests while keeping the samples in the same hydration condition during all the test. It was decided to test the samples in normal conditions, i.e. in air using normal metal jaw faces. In fact, the samples left in air undergo a slow drying, and the time between the sample preparation and the end of the experiment was considered enough short to avoid any sensible drying of the specimen.

8.4.3. Measurement of the Samples

To calculate the mechanical properties of the BC membranes, as the tensile stress, it is critical to measure accurately the cross sectional area of the samples. In literature many techniques for cross sectional area have been used, as ultrasonography, gravimetric methodologies and area micrometers. In this work the cross sectional area of the samples was calculated with the use of a caliper. The width and thickness of the BBC samples was not the most critical because cutting adequately the rectangular specimens (with a plastic mold) permitted to obtain samples with uniform width. In addition, using our blended procedure to produce the membranes the thickness was uniform along the membrane, and since the BBC are compacted cellulose membranes was easier to measure the thickness with a caliper. On the other hand, for the BCTs the measurements of wall thickness were more challenging since the tubes were made of the original BC hydrogel (soft and malleable). To make sure about the BCTs thickness along the tubes several local measurements were taken, with a digital caliper, but still high errors were obtained among the samples.

Another limitation of the mechanical test is the strain quantification. Testing rectangular and cylinder-shaped specimens permitted the calculation of the strain from the

grip-to-grip displacement. It could be also possible to calculate local strains through the use of a video-extensometer and dog-bone shaped specimens, whose shape leads to a better defined point of fracture in the specimen. One of the practical challenge for the use of video extensometer on BC samples is to draw markers on the hydrogel.

APPENDIX A – SUPPLEMENTAL INFORMATION FOR CHAPTER 2

Table A.1 – Summary of the tissue engineering (TE) applications of unmodified biosynthesized cellulose (BC).

Application	Experiment Description	Results	References
Scaffold Material	▪ Biocompatibility of BC evaluated by MTT assay using human vein endothelial cells grown on BC surfaces	▪ No evidence of BC toxicity *in vitro* after 3 days Cells proliferated and migrated vertically into BC matrix after 7 days	[1]
	▪ Subcutaneous implantation of BC at the back of Wistar rats for *in vivo* cytotoxicity evaluation	▪ No evidence of inflammation or cytotoxicity was observed, and the BC membrane was fully integrated with the host tissue after 12 weeks	[2]
Bone Tissue Engineering	▪ *In vitro* biocompatibility, osteogenic differentiation, and gene expression studies using human adipose-derived mesenchymal stem cells (HASCs) *In vivo* cytotoxicity study in ulna defects of rabbits	▪ Cells differentiated into osteoblasts after 4 weeks of culture on BC surface Significant mineralization without any signs of inflammation responses 8 weeks after HASCs loaded BC scaffold implanted into ulna defects of rabbits	[3]
Nerve Regeneration	▪ *In vitro* assessment by MTT assay, flow cytometry, RT-PCR and Schwann cell culture *In vivo* biocompatibility in rat sciatic nerve injury model	▪ Good biocompatibility No toxic effects on nerve tissues after 6 weeks *In vivo*	[4]
	▪ Animal study using rat peripheral nerve injury model	▪ Good biocompatibility, no formation of neuroma, and proper guidance of axons after 6 months	[5]
Blood Vessel Replacement	▪ *In vivo* biocompatibility in carotid arteries of sheep	▪ No evidence of graft dilatation, dehiscence, or aneurysm formation, and no inflammatory signs after 12 weeks	[6]

Table A.2 – List of additional examples of biosynthesized cellulose (BC) applications in tissue engineering (TE).

	TE applications	References
BIOSYNTHESIZED CELLULOSE	Urethra	[7]
	Cornea	[8]
	Cartilage	[9, 10]
	Meniscus	[11]
	Ear auricle	[9, 10, 12]
	Heart valve	[13, 14]
	Blood vessel	[15-17]
	Bone	[18-21]
	Skin	[22-26]
	Gum	[27, 28]
	Nasal	[29]

Appendix A. References

[1] D.O.S. Recouvreux, C.R. Rambo, F.V. Berti, C.A. Carminatti, R.V. Antonio, L.M. Porto, Novel three-dimensional cocoon-like hydrogels for soft tissue regeneration, Mat Sci Eng C-Mater 31(2) (2011) 151-157.

[2] G. Helenius, H. Backdahl, A. Bodin, U. Nannmark, P. Gatenholm, B. Risberg, In vivo biocompatibility of bacterial cellulose, J Biomed Mater Res A 76A(2) (2006) 431-438.

[3] S.S. Zang, Q. Zhuo, X. Chang, G.X. Qiu, Z.H. Wu, G. Yang, Study of osteogenic differentiation of human adipose-derived stem cells (HASCs) on bacterial cellulose, Carbohyd Polym 104 (2014) 158-165.

[4] C.L. Zhu, F. Li, X.Y. Zhou, L. Lin, T.Y. Zhang, Kombucha-synthesized bacterial cellulose: Preparation, characterization, and biocompatibility evaluation, J Biomed Mater Res A 102(5) (2014) 1548-1557.

[5] K. Kowalska-Ludwicka, J. Cala, B. Grobelski, D. Sygut, D. Jesionek-Kupnicka, M. Kolodziejczyk, S. Bielecki, Z. Pasieka, Modified bacterial cellulose tubes for regeneration of damaged peripheral nerves, Arch Med Sci 9(3) (2013) 527-534.

[6] M. Scherner, S. Reutter, D. Klemm, A. Sterner-Kock, M. Guschlbauer, T. Richter, G. Langebartels, N. Madershahian, T. Wahlers, J. Wippermann, In vivo application of tissue-

engineered blood vessels of bacterial cellulose as small arterial substitutes: proof of concept?, J Surg Res 189(2) (2014) 340-347.

[7] A. Bodin, S. Bharadwaj, S.F. Wu, P. Gatenholm, A. Atala, Y.Y. Zhang, Tissue-engineered conduit using urine-derived stem cells seeded bacterial cellulose polymer in urinary reconstruction and diversion, Biomaterials 31(34) (2010) 8889-8901.

[8] J.H. Wang, C. Gao, Y.S. Zhang, Y.Z. Wan, Preparation and in vitro characterization of BC/PVA hydrogel composite for its potential use as artificial cornea biomaterial, Mat Sci Eng C-Mater 30(1) (2010) 214-218.

[9] A. Svensson, E. Nicklasson, T. Harrah, B. Panilaitis, D.L. Kaplan, M. Brittberg, P. Gatenholm, Bacterial cellulose as a potential scaffold for tissue engineering of cartilage, Biomaterials 26(4) (2005) 419-431.

[10] E.M. Feldmann, J.F. Sundberg, B. Bobbili, S. Schwarz, P. Gatenholm, N. Rotter, Description of a novel approach to engineer cartilage with porous bacterial nanocellulose for reconstruction of a human auricle, Journal of Biomaterials Applications 28(4) (2013) 626-640.

[11] A. Bodin, S. Concaro, M. Brittberg, P. Gatenholm, Bacterial cellulose as a potential meniscus implant, J Tissue Eng Regen M 1(5) (2007) 406-408.

[12] L. Nimeskern, H. Martínez Ávila, J. Sundberg, P. Gatenholm, R. Müller, K.S. Stok, Mechanical evaluation of bacterial nanocellulose as an implant material for ear cartilage replacement, J Mech Behav Biomed 22 (2013) 12-21.

[13] H. Mohammadi, D. Boughner, L.E. Millon, W.K. Wan, Design and simulation of a poly(vinyl alcohol)-bacterial cellulose nanocomposite mechanical aortic heart valve prosthesis, Proc Inst Mech Eng H 223(6) (2009) 697-711.

[14] L.E. Millon, G. Guhados, W. Wan, Anisotropic polyvinyl alcohol-Bacterial cellulose nanocomposite for biomedical applications, J Biomed Mater Res B Appl Biomater 86(2) (2008) 444-52.

[15] D. Klemm, D. Schumann, U. Udhardt, S. Marsch, Bacterial synthesized cellulose - artificial blood vessels for microsurgery, Prog Polym Sci 26(9) (2001) 1561-1603.

[16] H. Backdahl, G. Helenius, A. Bodin, U. Nannmark, B.R. Johansson, B. Risberg, P. Gatenholm, Mechanical properties of bacterial cellulose and interactions with smooth muscle cells, Biomaterials 27(9) (2006) 2141-2149.

[17] Y.Z. Wan, C. Gao, M. Han, H. Liang, K.J. Ren, Y.L. Wang, H.L. Luo, Preparation and characterization of bacterial cellulose/heparin hybrid nanofiber for potential vascular tissue engineering scaffolds, Polym Advan Technol 22(12) (2011) 2643-2648.

[18] M. Zaborowska, A. Bodin, H. Backdahl, J. Popp, A. Goldstein, P. Gatenholm, Microporous bacterial cellulose as a potential scaffold for bone regeneration, Acta Biomater 6(7) (2010) 2540-2547.

[19] R. Mori, T. Nakai, K. Enomoto, Y. Uchio, K. Yoshino, Increased Antibiotic Release from a Bone Cement Containing Bacterial Cellulose, Clinical Orthopaedics and Related Research 469(2) (2011) 600-606.

[20] S. Saska, H.S. Barud, A.M. Gaspar, R. Marchetto, S.J. Ribeiro, Y. Messaddeq, Bacterial cellulose-hydroxyapatite nanocomposites for bone regeneration, Int J Biomater 2011 (2011) 175362.

[21] S. Saska, R.M. Scarel-Caminaga, L.N. Teixeira, L.P. Franchi, R.A. dos Santos, A. Gaspar, P.T. de Oliveira, A. Rosa, C. Takahashi, Y. Messaddeq, S.J.L. Ribeiro, R. Marchetto, Characterization and in vitro evaluation of bacterial cellulose membranes functionalized with osteogenic growth peptide for bone tissue engineering, J Mater Sci-Mater M 23(9) (2012) 2253-2266.

[22] J. Kucińska-Lipka, I. Gubanska, H. Janik, Bacterial cellulose in the field of wound healing and regenerative medicine of skin: recent trends and future prospectives, Polymer Bulletin 72(9) (2015) 2399-2419.

[23] W. Czaja, A. Krystynowicz, S. Bielecki, R.M. Brown, Microbial cellulose - the natural power to heal wounds, Biomaterials 27(2) (2006) 145-151.

[24] M.H. Kwak, J.E. Kim, J. Go, E.K. Koh, S.H. Song, H.J. Son, H.S. Kim, Y.H. Yun, Y.J. Jung, D.Y. Hwang, Bacterial cellulose membrane produced by Acetobacter sp. A10 for burn wound dressing applications, Carbohyd Polym 122 (2015) 387-398.

[25] L.N. Fu, J. Zhang, G. Yang, Present status and applications of bacterial cellulose-based materials for skin tissue repair, Carbohyd Polym 92(2) (2013) 1432-1442.

[26] J.D. Fontana, A.M. Desouza, C.K. Fontana, I.L. Torriani, J.C. Moreschi, B.J. Gallotti, S.J. Desouza, G.P. Narcisco, J.A. Bichara, L.F.X. Farah, Acetobacter Cellulose Pellicle as a Temporary Skin Substitute, Appl Biochem Biotech 24-5 (1990) 253-264.

[27] A. Yoshino, M. Tabuchi, M. Uo, H. Tatsumi, K. Hideshima, S. Kondo, J. Sekine, Applicability of bacterial cellulose as an alternative to paper points in endodontic treatment, Acta Biomater 9(4) (2013) 6116-6122.

[28] L.A. Salata, G.T. Craig, I.M. Brook, In-Vivo Evaluation of a New Membrane (Gengiflex(R)) for Guided Bone Regeneration (Gbr), J Dent Res 74(3) (1995) 825-825.

[29] E.E.M. Neto, J.E.L. Dolci, Nasal Septal Perforation closure with bacterial cellulose in rabbits, Braz J Otorhinolar 76(4) (2010) 442-449.

APPENDIX B – SUPPLEMENTAL INFORMATION FOR CHAPTER 3

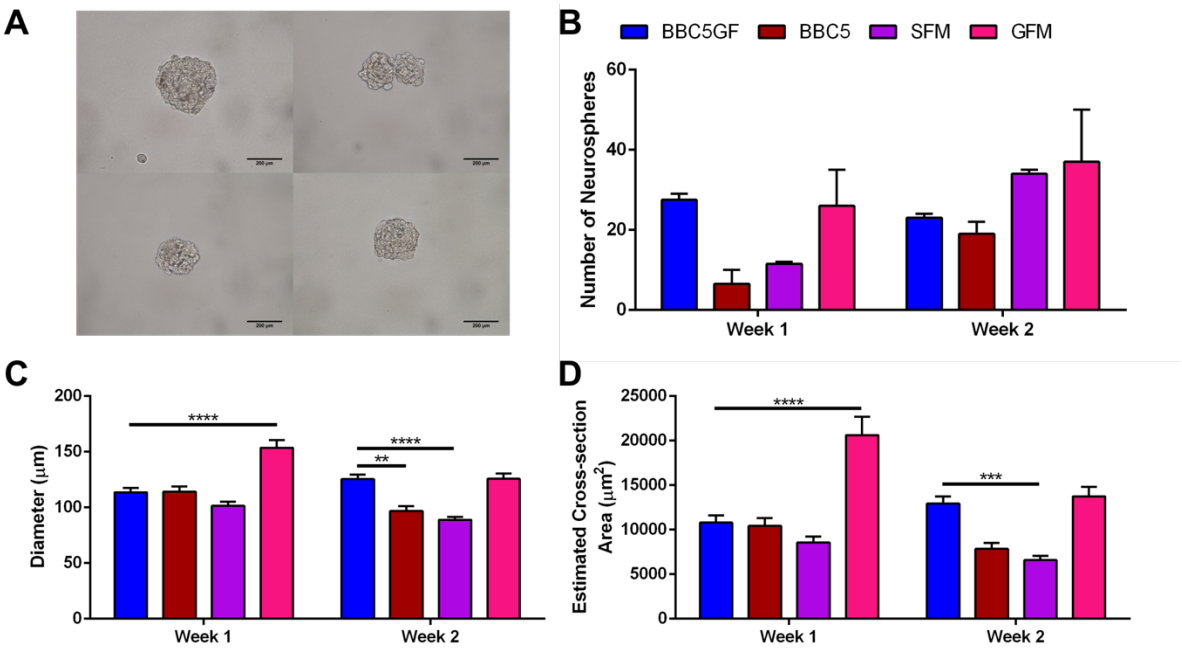

Figure B.1 – BBC5GF moderately stimulates porcine SVZ neural stem/progenitor cell proliferation. **(A)** Images of porcine neurospheres taken at 20× magnification; top row images: BBC5GF neurospheres; bottom row images: GFM neurospheres; after 2 weeks. **(B)** Number of porcine neurospheres were assessed after one or two weeks of culturing. **(C)** Diameter and **(D)** estimated cross-section area of porcine neurospheres were assessed from previous experiment (A). Cross-section area of porcine neurospheres was estimated using measured diameter (A). *(Two-way ANOVA followed by a multiple-comparisons test (Tukey's) in (B), (C) and (D) were used for statistical analysis. Values are presented as mean ± s.e.m; n =2. Only comparisons related to BBC5GF are shown, **p<0.01, ****p<0.0001).*

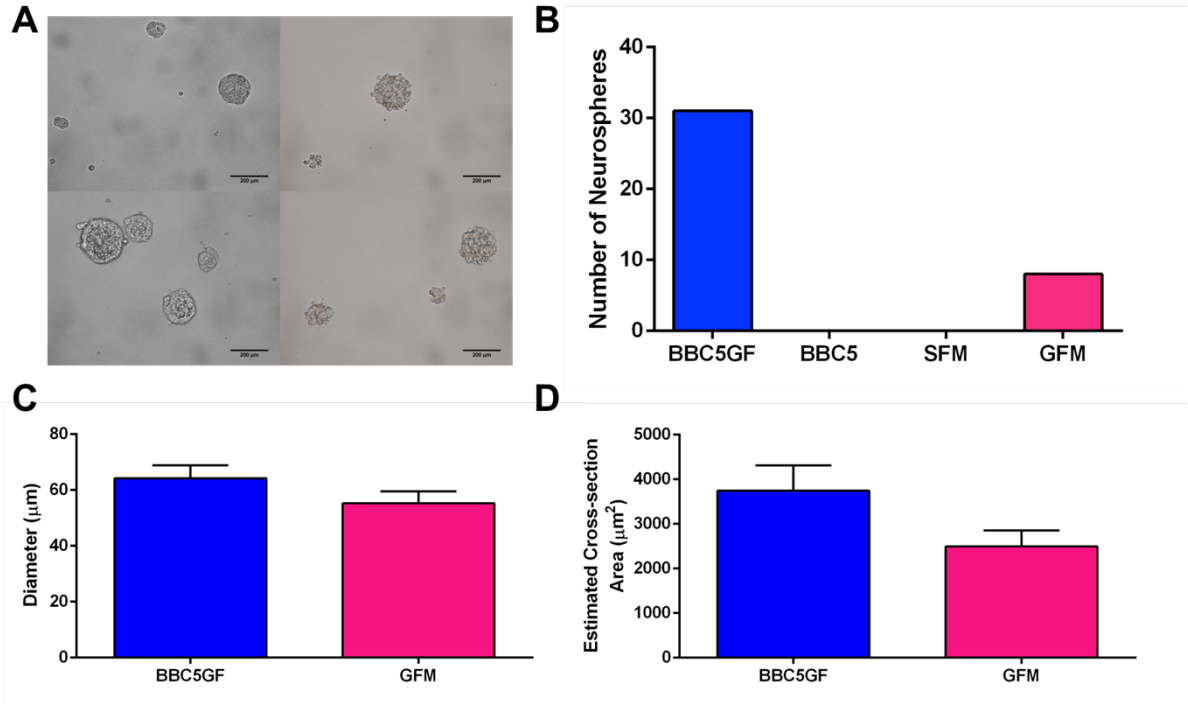

Figure B.2 – BBC5GF stimulates human spinal cord neural stem/progenitor cell proliferation obtained from an 18-year-old male. **(A)** Images of human neurospheres taken at 20× magnification; top row images: BBC5GF neurospheres; bottom row images: GFM neurospheres; after 1 week. **(B)** Number of human neurospheres were assessed after one or two weeks of culturing. **(C)** Diameter and **(D)** estimated cross-section area of human neurospheres were assessed from previous experiment (A). Cross-section area of human neurospheres was estimated using measured diameter. *(Welch's t-test in (C) and (D)was used for statistical analysis, no statistical difference was observed. Values are presented as mean ± s.e.m).*

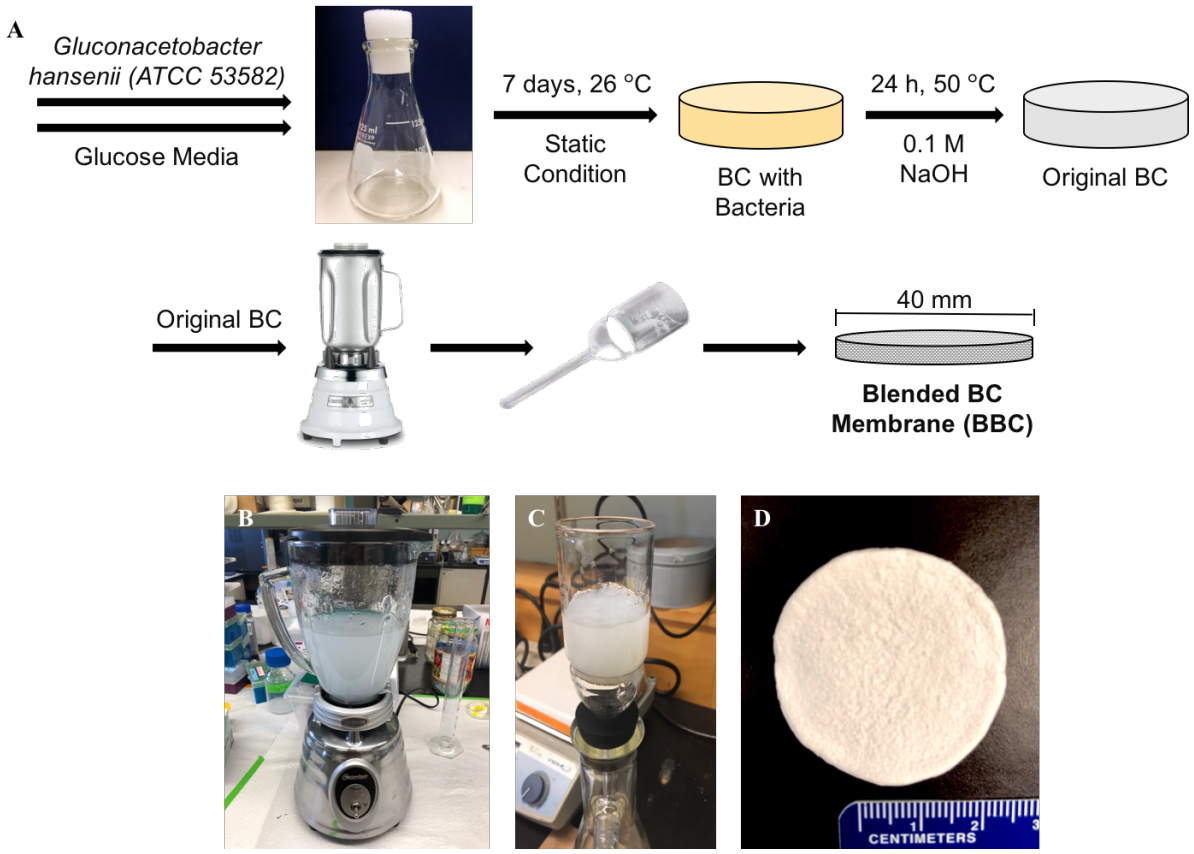

Figure B.3 – Blended biosynthesized cellulose (BBC) production. **A)** Steps of blending method to produce BBC membranes. **B)** Original BC membrane is blended a homogenous pulp is achieved. **C)** Pulp obtained in (C) is filter until a paper-like membrane is achieved. **D)** Final BBC membrane after filtration and lyophilisation.

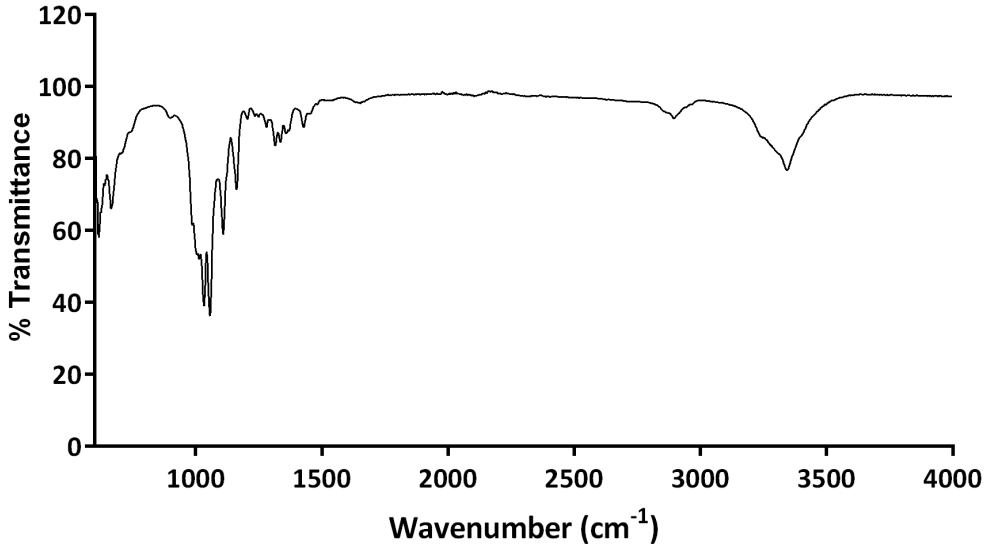

Figure B.4 – Fourier-transform infrared spectroscopy (FTIR) spectrum for freeze-dried blended biosynthesized cellulose 5 (BBC5, membrane with highest dry cellulose mass).

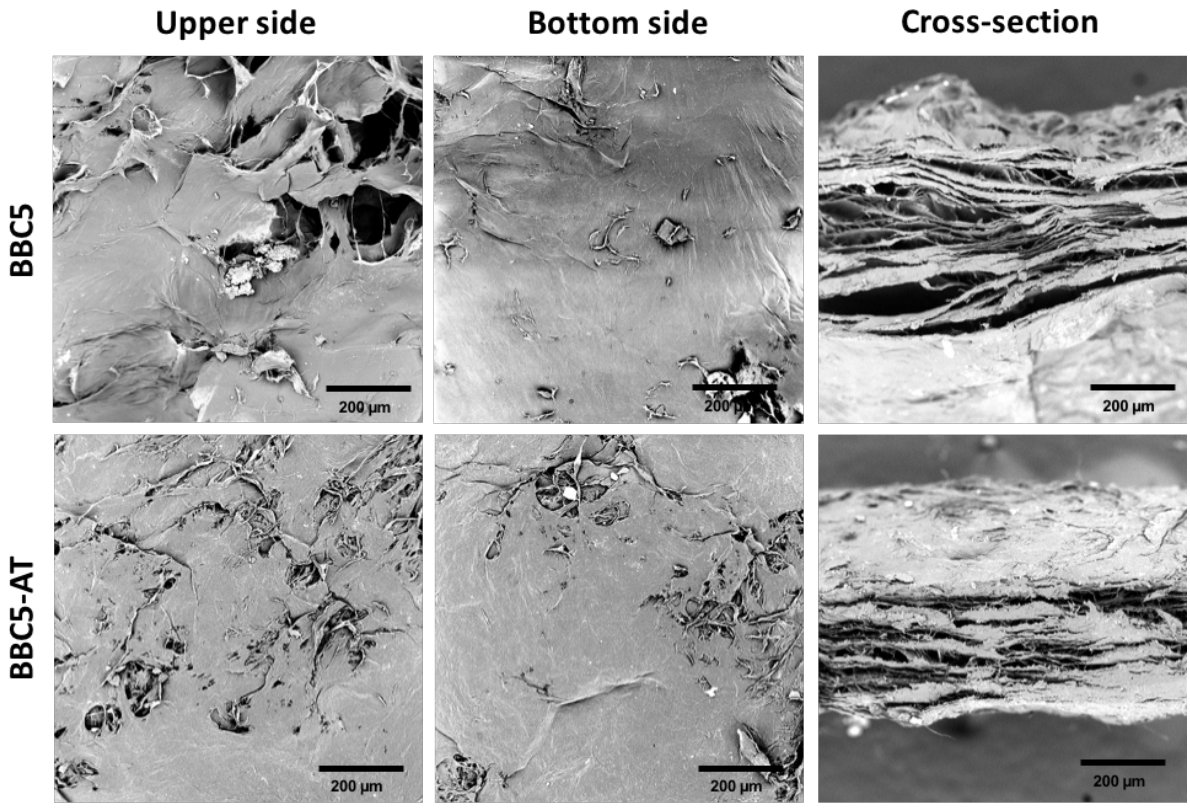

Figure B.5 – Scanning electron microscopy micrographs of freeze-dried blended biosynthesized cellulose 5 (BBC5, membrane with highest dry cellulose mass), and BBC5-AT (BBC5 after sterilization by autoclave): upper side (air contact), bottom side (filter contact) and cross-section views in 300× magnification.

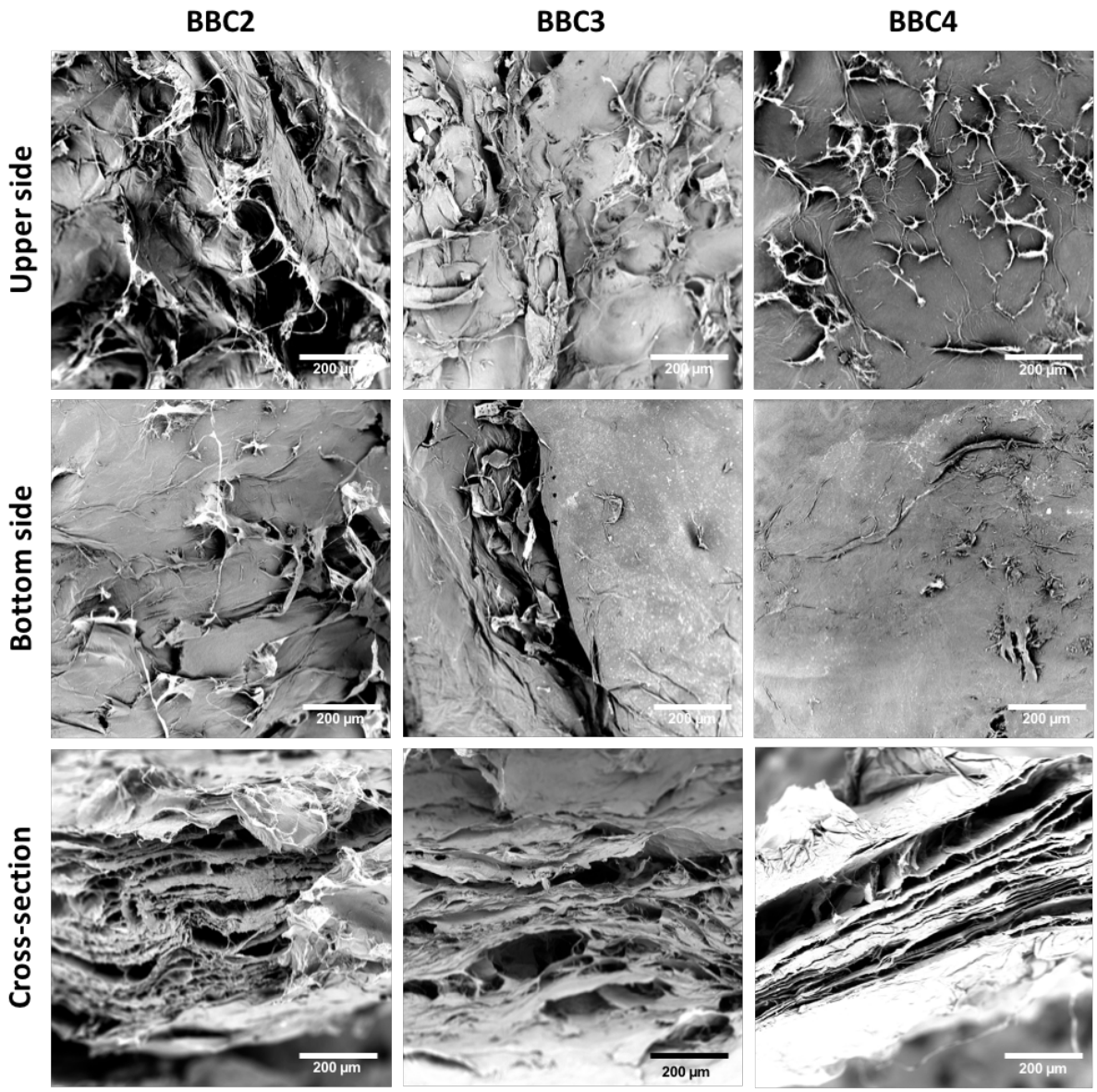

Figure B.6 – Scanning electron microscopy images of additional samples of blended biosynthesized cellulose (BBC). Freeze-dried BBC2-BBC4 membranes in crescent order of dry cellulose mass: upper side (air contact), bottom side (filter contact) and cross-section views, 300× magnification.

Table B.1 – The adjusted correlation coefficients of Zero-order, Higuchi equation, and Korsemyer-Peppas kinetic models for fibroblast growth factor 2 (FGF2) and endothelial growth factor (EGF) released from blended biosynthesized cellulose 5 (BBC5, membrane with highest dry cellulose mass).

Model	K		n		R^2	
	FGF2	EGF	FGF2	EGF	FGF2	EGF
Zero order	0.11	0.43	N/A	N/A	0.7997	0.7789
Higuchi	6.91	6.77	N/A	N/A	0.8959	0.8789
Korsmeyer-Peppas	40.24	40.96	0.147	0.140	0.9905	0.9847

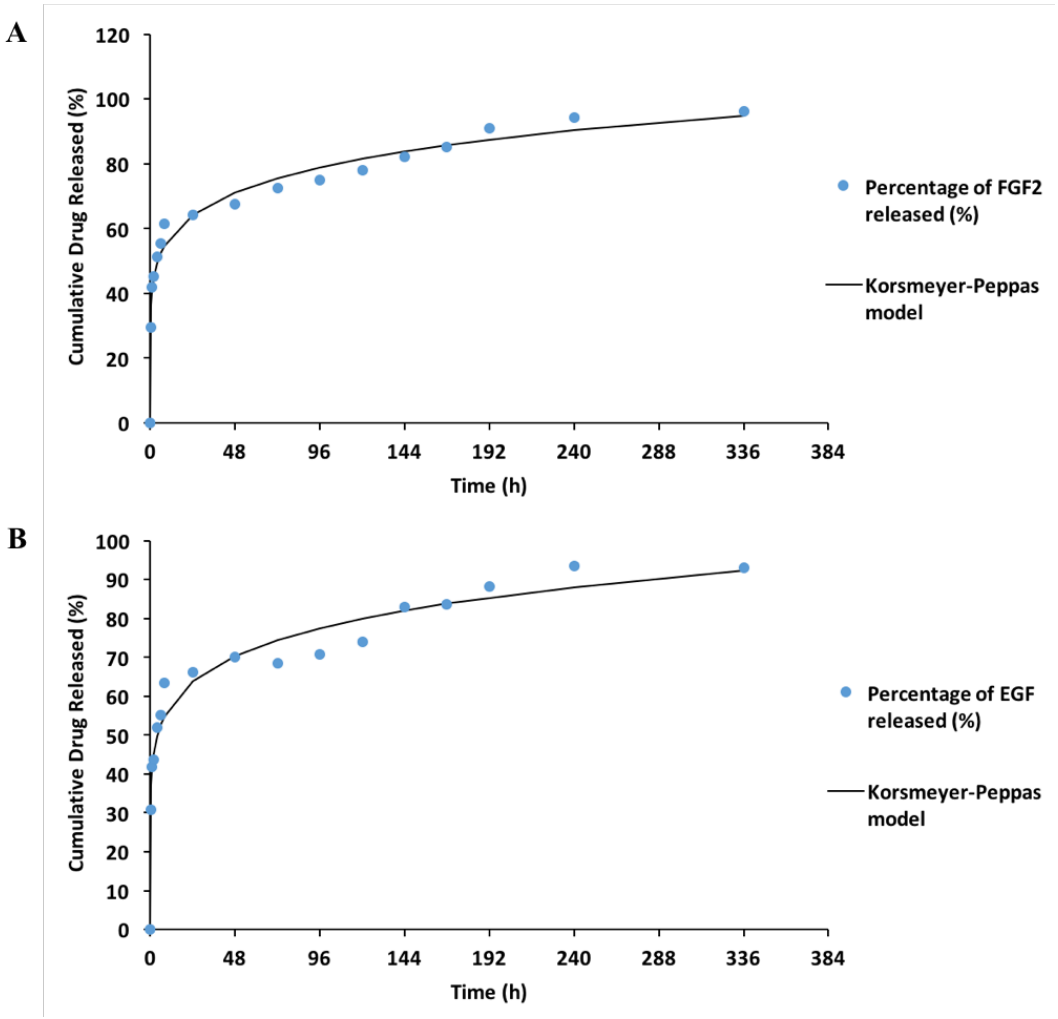

Figure B.7 – Release profile and kinetic model for fibroblast growth factor 2 (FGF2) and endothelial growth factor (EGF) released from blended biosynthesized cellulose 5 (BBC5, membrane with highest dry cellulose mass). **A)** Release profile and kinetic model for FGF2. **B)** Release profile and kinetic model for EGF. Blue dots: ELISA assessment of cumulative amount of growth factors over 7 days. Continuous black line: fit of Korsmeyer-peppas kinetic model.

APPENDIX C – SUPPLEMENTAL INFORMATION FOR CHAPTER 4

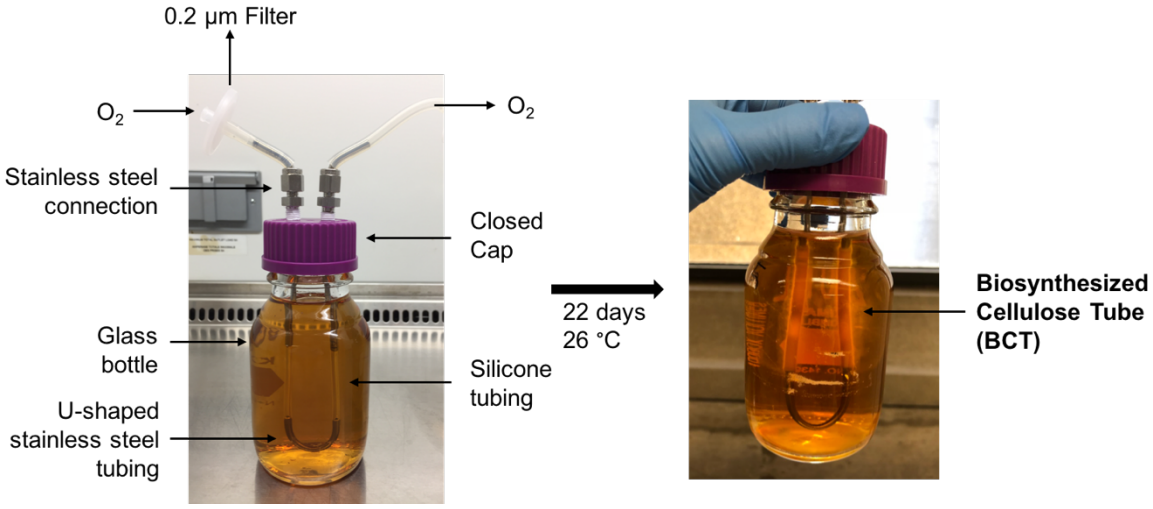

Figure C.1 – Bioreactor assembly containing bacteria in glucose-based media to produce biosynthesized cellulose tubes (BCTs). After 22 days in static culture at 26 °C BCT22 was produced.

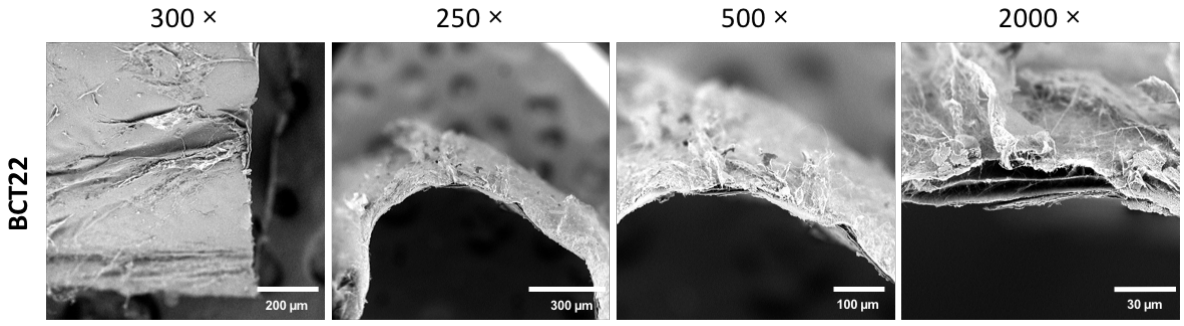

Figure C.2 – Scanning electron microscopy images of biosynthesized cellulose tube produced after 22 days of cultivation (BCT22). First image on left shows the upper view of a BCT22 in horizontal, 300× magnification. Three other images show the cross section view of a BCT22 in vertical in several magnifications: 250×, 500× and 2000×.

Table C.1 – The adjusted correlation coefficients of Zero-order, Higuchi equation, and Korsemyer-Peppas kinetic models for nerve growth factor (NGF) released from biosynthesized cellulose tubes after 22 days of cultivation (NGF-BCT22).

Model	K	n	R2
Zero order	0.79	N/A	0.6826
Higuchi	9.63	N/A	0.8053
Korsmeyer-Peppas	55.65	0.113	0.9954

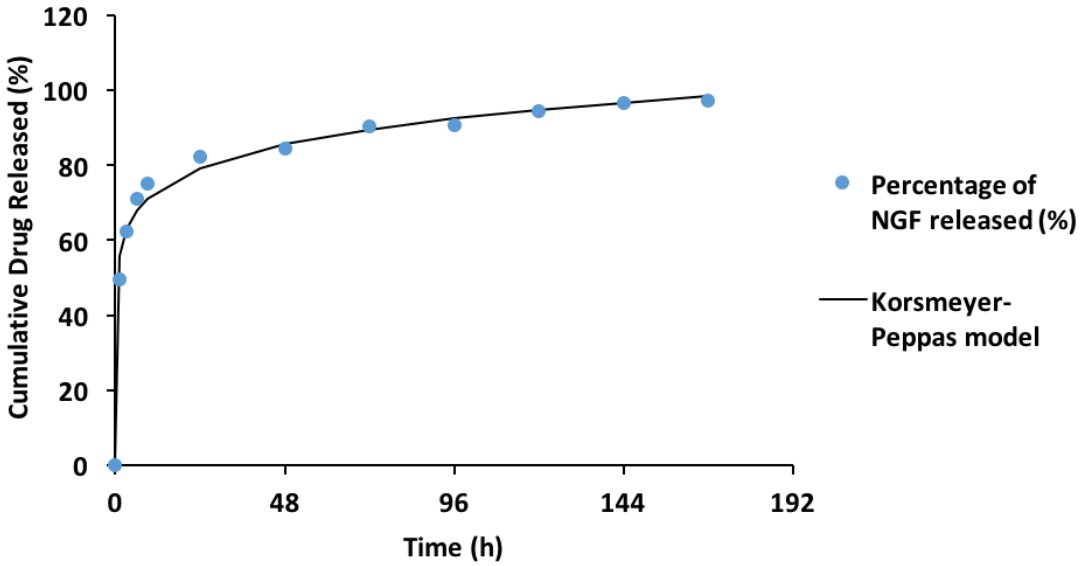

Figure C.3 – Release profile and kinetic model for nerve growth factor (NGF) released from biosynthesized cellulose tubes after 22 days of cultivation (NGF-BCT22). Blue dots: ELISA assessment of cumulative amount of NGF over 7 days. Continuous black line: fit of Korsmeyer-peppas kinetic model.

APPENDIX D – SUPPLEMENTAL INFORMATION FOR CHAPTER 5

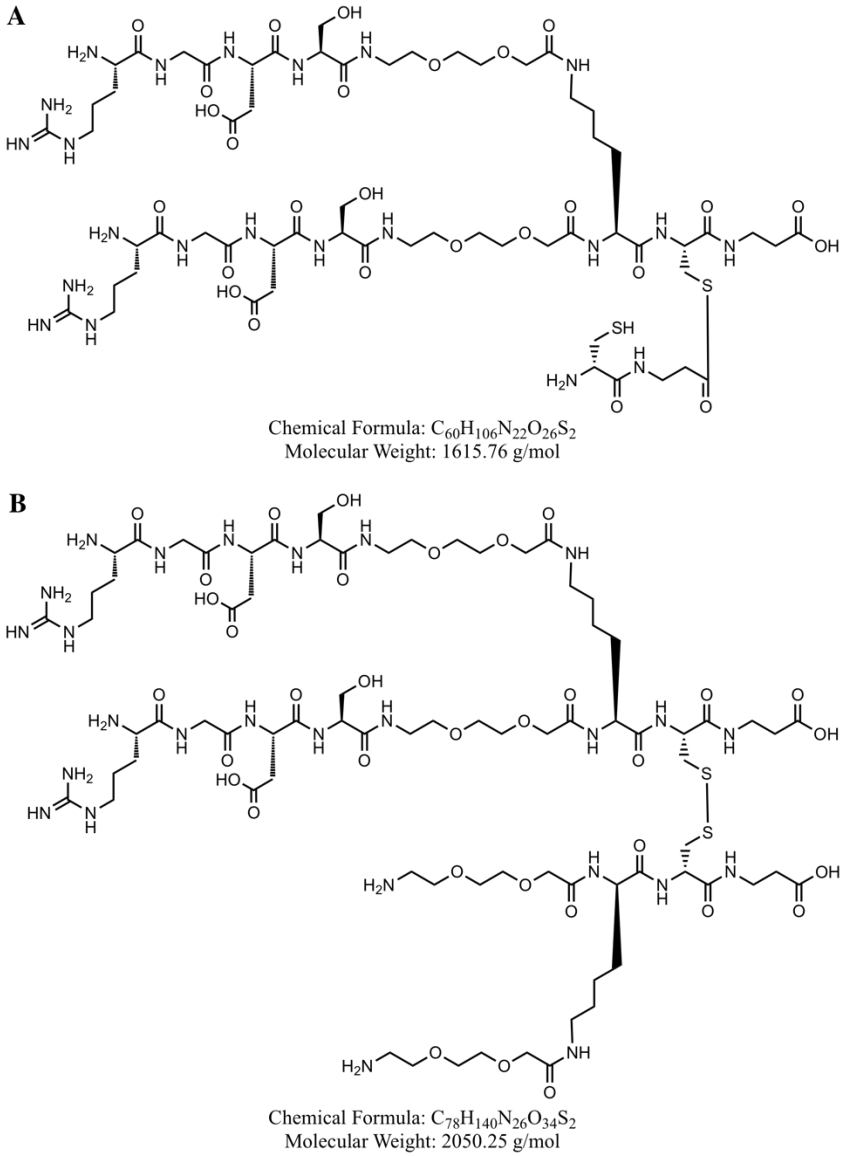

Figure D.1 – Chemical structures and molecular weights of the suggested by-products of the 2-branched peptide synthesis.

Table D.1 – Parameters optimized to synthesize the 4-branched peptide, [RGDS-Adoa]$_4$-K$_2$-K-C-βA, and the percentage yield (Yield %) for each synthesis. Synthesis repetitions for the 4-branced peptide (4B1-4B4) using MAP resin or TentaGel amide resin (TG), two different coupling reagents, two permanent protecting groups (PPG) for cysteine (Cys), different numbers of deprotection steps(deprotection ×) and coupling (Coupling ×) steps, and time length for the cleavage reaction using Reagent B.

Peptide	Resin	Coupling Reagent	Cys PPG	Deprotection ×	Coupling ×	Reagent B (h)	Yield (%)
4B1	MAP	HBTU	Acm	3	4	4	41.6
4B2	MAP	HATU	Acm	3	4	4	33.1
4B3	TG	HATU	Acm	3	4	4	59.8
4B4	TG	HATU	Trt	4	5	3.5	32.3

Abbreviations: O-(Benzotriazol-1-yl)-N,N,N’,N’-tetramethyluroniumhexafluorophosphate (HBTU); O-(7-Azabenzotriazol-1-yl)-N,N,N’,N’-tetramethyluroniumhexafluorophosphate (HATU); acetamidomethyl (Acm); high performance liquid chromatography (HPLC); mass spectroscopy (MS).

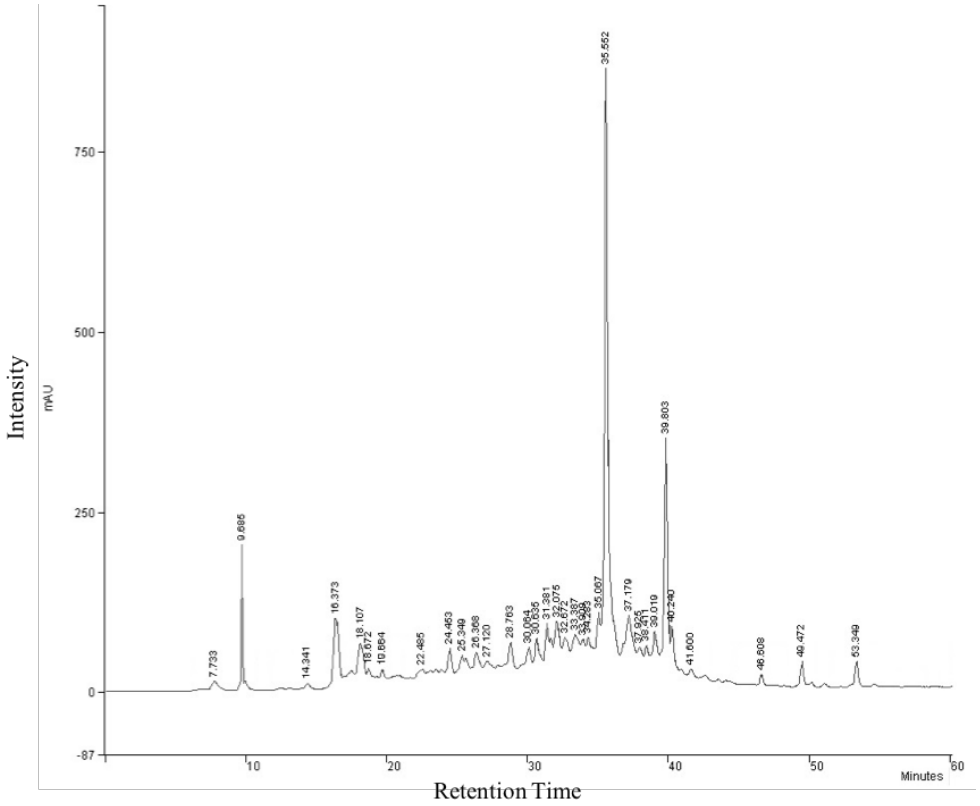

Figure D.2 – RP-HPLC chromatograms for the crude 4-branched peptide ([RGDS-Adoa]$_4$-K$_2$-K-C-βA) with the detection wavelength at 260 nm.

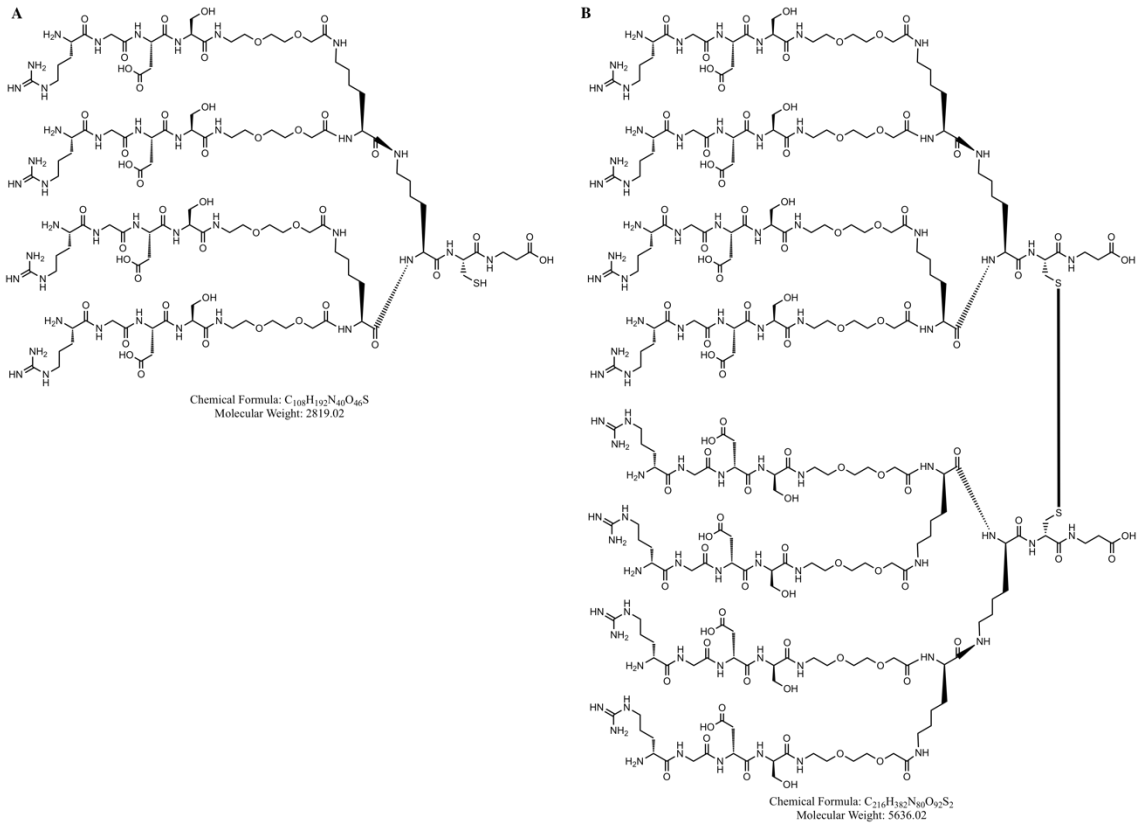

Figure D.3 – Chemical structure and formula and molecular weight (g/mol) of (**A**) monomer ([RGDS-Adoa]$_4$-K$_2$-K-C-βA) and (**B**) dimer of 4-branched peptide.

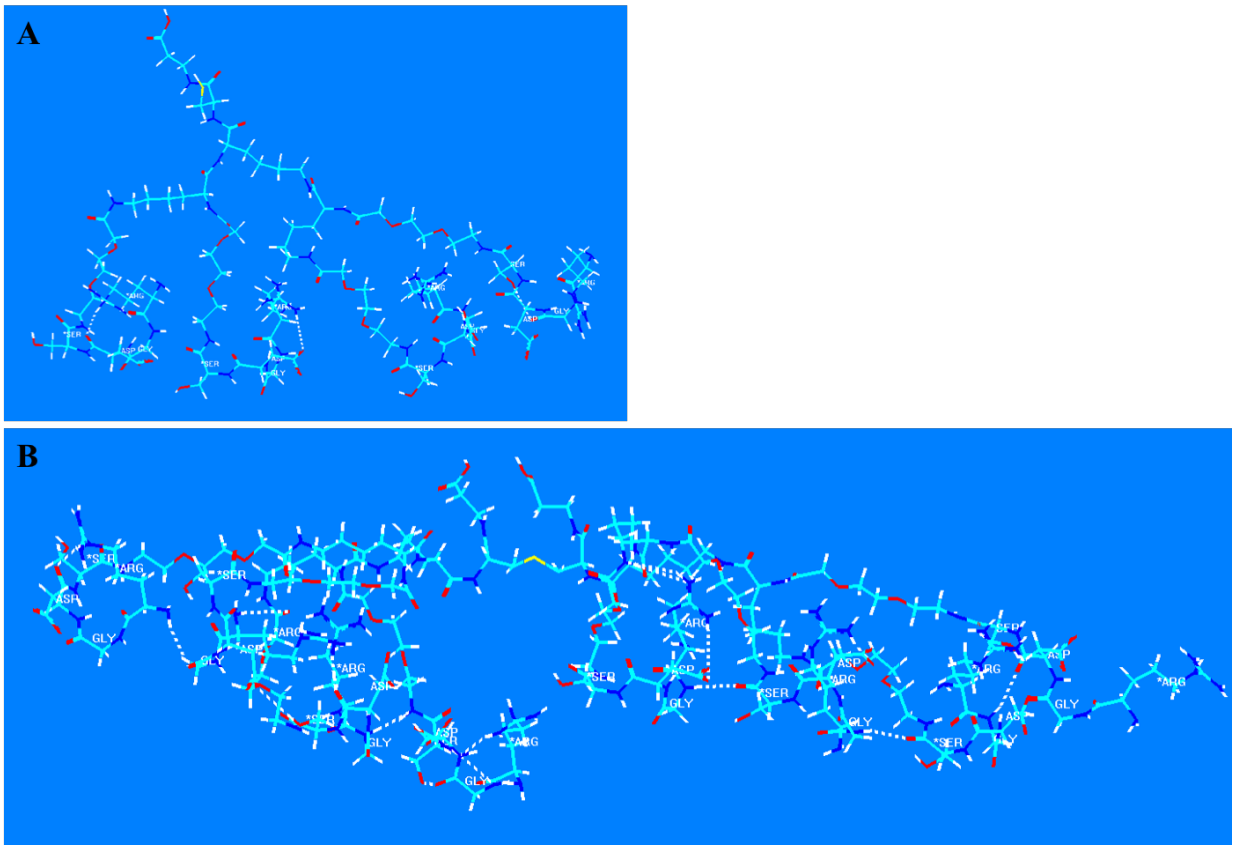

Figure D.4 – Energy-minimized 3D model structures in vacuum of 4-branched peptide. (A) Monomer and (B) dimer.